DISSECTING THE CONSEQUENCES OF PD-1 BLOCKADE ON THE FUNCTIONAL ADAPTATIONS OF REGULATORY T CELLS IN MELANOMA

Mikhaël Attias

Department of Microbiology & Immunology

McGill University

Montréal, Québec

September 2023

A thesis submitted to McGill University in partial fulfillment of the requirements of the degree of Doctor in Philosophy

Table of contents

Abstract

Immune checkpoint inhibitors targeting PD-1 have been a breakthrough in the treatment of advanced melanoma. This pharmacological class was designed to target specifically tumor-infiltrating $CD8^+$ T cells and counteract their exhaustion. While they induce durable remissions in a subset of patients, >50% of patients do not experience a clinically significant benefit. Regulatory T (T_{reg}) cells, a specialized subset of $CD4^+$ T cells whose main function is to suppress self-reactive T cells and prevent the development of autoimmunity, also express PD-1 in and outside of the tumor. Furthermore, tumor cells, whose antigens are often derived from self-peptides, are adept at hijacking the numerous suppressive mechanisms of T_{reg} cells to inhibit the development of anti-tumor responses and promote the establishment of an immunosuppressive microenvironment that supports their growth and metastatic potential. However, it remains unclear how PD-1 blockade affects T_{reg} cell function and fate and how T_{reg} cells impact the outcome of tumor immunotherapy.

In this work, we describe the impact of anti-PD-1 on T_{reg} cell homeostasis at the systemic level and its consequences on T_{reg} cell fate in tumors that respond or fail to respond to anti-PD-1 monotherapy. First, using a melanoma model that is poorly responsive to checkpoint inhibition, we demonstrate that anti-PD-1 downregulates PD-1 expression on T_{reg} cells locally and systemically, resulting in increased T_{reg} cell activation that may constitute an acquired mechanism of resistance to treatment. Second, we demonstrate using a highly immunogenic melanoma model that successful response to anti-PD-1 is associated with a functional adaptation of regulatory T cells in response to inflammatory signals within the tumor microenvironment which alleviates their local suppressive capacity. Finally, we identify IL-18 signaling on T cells as a key mediator of inflammation in the tumor, required for the successful response to PD-1 blockade.

Résumé

Les inhibiteurs de point de contrôle ont entrainé une révolution dans la prise en charge des mélanomes avancés. Cette classe de médicaments est conçue pour cibler spécifiquement les lymphocytes T tumoraux et prévenir leur épuisement. Bien qu'ils induisent des rémissions durables dans un nombre important de cas, plus de la moitié des patients n'obtiennent pas de bénéfice clinique significatif. Les lymphocytes T régulateurs (T_{regs}), une population de lymphocytes T $CD4^+$ dont la fonction est de supprimer les lymphocytes auto-réactifs et prévenir le développement de maladies auto-immunes, expriment aussi PD-1 dans la tumeur, et même en périphérie. De plus, les tumeurs, dont les antigènes sont souvent dérivés du soi, sont capables de détourner les mécanismes de suppression des T_{regs} pour établir un environnement immunosuppressif et ainsi promouvoir leur croissance et leur capacité métastatique. Toutefois, les conséquences des anti-PD-1 sur la fonction et la destinée des T_{regs}, ainsi que le rôle des T_{regs} dans le succès ou l'échec de l'immunothérapie restent à définir.

Dans ce corpus, nous décrivons l'impact d'un anti-PD-1 sur l'homéostase des T_{regs} et ses conséquences sur la destinée des T_{regs} dans des tumeurs qui répondent ou résistent au traitement par anti-PD-1 en monothérapie. Dans un premier temps, nous mettons en évidence dans un modèle de mélanome résistant à l'immunothérapie, que l'anti-PD-1 module le niveau d'expression de PD-1 à la surface des T_{regs} au niveau systémique et dans la tumeur, ce qui conduit à une augmentation de leur niveau d'activation et pourrait constituer un mécanisme de résistance secondaire au traitement. Dans un second temps, nous démontrons à l'aide d'un modèle de mélanome murin hautement immunogénique que la réponse à l'anti-PD-1 est associée à une adaptation fonctionnelle des T_{regs} en réponse à des signaux inflammatoires dans l'environnement tumoral, qui atténue leur capacité suppressive localement. Enfin, nous identifions la réponse des lymphocytes T à

l’interleukine-18 comme un déterminant majeur de l’établissement d’un environnement tumoral inflammé et nécessaire à la réponse à l’anti-PD-1.

Acknowledgements

Science is a collaborative effort and whilst this thesis bears my name, it owes its existence to the support of countless people throughout this journey.

First, I would like to thank my supervisor Dr. Ciriaco Piccirillo and my co-supervisor Dr. Constantin Polychronakos for their scientific mentorship, for granting me the opportunity to work on such an exciting project, for giving me the autonomy to gear the research in my direction and for inspiring me to broaden my scientific knowledge and give my best effort. I would also like to thank my advisory committee members, Dr. Christopher Rudd, Dr. Martin Richer, and Dr. Woong-Kyung Suh for their guidance and contributions in shaping this project's milestones.

Of course, I also must thank past mentors without whom I would not have built my path to Montréal. First, Dr. Roland Gueret who was the first to spark my interest in biology. Then Dr. Dominique Bellet who ignited my passion for immunology and guided me throughout my PharmD up to directing my thesis. I would also like to think Dr. Alberto Pugliese who recruited me to his lab and initiated me to T_{reg} cell biology during my master's degree. But foremost, I would like to thank Dr. Roberto Mallone who gave me my first opportunity to train and work on a scientific project, who guides me on my career path and whose exemplary character decided me to pursue a career in research, surrounded with like-minded people.

I found the same qualities of curiosity, altruism and empathy cultivated in our laboratory. My first thank you goes to Dr. Fernando Alvarez who mentored me day to day, fostered my scientific curiosity and inspired many ideas throughout this project through constant exchange. Tho-Alfakar Al-Aubodah and Roman Istomine were also instrumental in teaching me skills, helping me develop this project and raising the bar I'd set for myself. I would also like to thank all

my friends in the Piccirillo Lab family and particularly: Helen Mason, Harry Yang, Geneviève Genest, Mina Ayoub, Ngoc Mai Nathalie Van, Laura Widawski, Jia Min Huang, Zhiyang Liu, Abrahim Sleiman, Marie-Ashley Ste-Croix, Sebastian Grocott, Céleste Pilon, and Dr. Eva Michaud who all generously lent a helping hand at some point and made it a joy to come to the lab every day. This extends to our collaborators: Drs. Fan Huang and Sonia Del Rincon who provided us our tumor models and helped with the spatial analysis, Drs. Ali Mehdi and Shafaat Rabbani with whom we confirmed some of our findings in other tumor models; Tamiko Nishimura and Dr. Yasser Riazalhosseini for their support with the development of the spatial proteomics assay and the RI-MUHC flow cytometry core: Marie-Hélène Lacombe, Ekaterina Yurchenko, and Hélène Pagé-Veillette, without whom most of this work would not have been possible.

Finally, the conditions to flourish scientifically would not be met without the love, support and inspiration of family and friends. I grew a lot during these six years in Montreal and made wonderful memories. For that I'd like to give a special thanks to my brother Raphaël, who made me feel at home in Montreal since day one; our adored little cat Shalom who left her imprint on this manuscript; my parents Nadine and Maurice, my grandmother Monique and my uncle Georges, and all my friends in France thanks to whom I never felt uprooted; Marie Mauriès whose loving gaze was a source of happiness, laughter, pride and motivation; as well as David Cloud Berman, Will Oldham, Javier Pastore, Marco Verratti, Neymar Jr and Jimmy Butler, all artists in their own rights and sources of inspiration and joy along the ride.

Merci à tous!

Author contributions

The core of this thesis is the collection of three original manuscripts, two of which are in submission, and one is under review. The author contribution for the work presented in this thesis is as follows:

Chapter 1: General Introduction

Authors: I was responsible for researching the literature and wrote the review in close supervision with Dr. Ciriaco Piccirillo who contributed to the elaboration of the structure and reviewed the manuscript.

Chapter 2: PD-1 signaling dampens Helios^{+} T_{reg} cell activation levels in cold and hot murine models of melanoma.

Authors: Mikhaël Attias, Fernando Alvarez, Tho-Alfakar Al-Aubodah, Roman Istomine, Yujian Yang, Abrahim Sleiman, Laura Widawski, Constantin Polychronakos, Ciriaco Piccirillo.

I was responsible for the design of all the experiments described, in collaboration with my supervisor Dr. Ciriaco Piccirillo and co-supervisor Dr. Constantin Polychronakos. My colleagues, Dr. Fernando Alvarez, Tho-Alfakar Al-Aubodah, Roman Istomine, Yujian Yang and Laura Widawski contributed to the *in vivo* D4M.3A melanoma experiments and contributed their input on the interpretation of the data. Abrahim Sleiman performed the PD-L1-Fc *in vitro* experiments. All authors provided valuable input throughout the study. I wrote the manuscript under the supervision of Dr. Ciriaco Piccirillo.

Chapter 3: Anti-PD-1 promotes a T_h1-like functional adaptation of melanoma-infiltrating regulatory T cells to alleviate immunosuppression locally.

Authors: Mikhaël Attias, Fernando Alvarez, Tho-Alfakar Al-Aubodah, Roman Istomine, Paige McCallum, Fan Huang, Abrahim Sleiman, Tamiko Nishimura, Constantin Polychronakos, Sonia Del Rincon, Yasser Riazalhosseini, Ciriaco Piccirillo.

I was responsible for the design of all the experiments described, in collaboration with my supervisor Dr. Ciriaco Piccirillo and co-supervior Dr. Constantin Polychronakos. My colleagues, Tho-Alfakar Al-Aubodah, Dr. Fernando Alvarez and Roman Istomine contributed to the *in vivo* tumor experiments and contributed their input on the interpretation of the data. Dr. Fan Huang performed the immunofluorescence stainings. Paige McCallum contributed to the study design, acquired the immunofluorescence images, and performed preliminary analyses. Dr. Sonia Del Rincon collaborated on the immunofluorescence studies. Abrahim Sleiman performed the PD-L1-Fc *in vitro* experiments. Tamiko Nishimura and Dr. Yasser Riazalhosseini contributed to the design of the spatial proteomics experiment. All authors provided valuable input throughout the study. I wrote the manuscript in close supervision with Dr. Ciriaco Piccirillo.

Chapter 4: T cell responses to IL-18 promote the establishment of an inflamed melanoma environment and are required for successful response to anti-PD-1.

Authors: Mikhaël Attias, Fernando Alvarez, Tho-Alfakar Al-Aubodah, Constantin Polychronakos, Ciriaco Piccirillo.

I was responsible for the design of all the experiments described, in collaboration with my supervisor Dr. Ciriaco Piccirillo and co-supervisor Dr. Constantin Polychronakos. My colleagues, Dr. Fernando Alvarez and Tho-Alfakar Al-Aubodah contributed to the *in vivo* tumor experiments

and contributed their input on the interpretation of the data. All authors provided valuable input throughout the study. I wrote the manuscript under the supervision of Dr. Ciriaco Piccirillo.

I have also co-authored the following reviews:

Attias M*, *Al-Aubodah TA*, Piccirillo CA.* Mechanisms of human Foxp3$^+$ T_{reg} cell development and function in health and disease. *Clinical and Experimental Immunology 2019 Jul;197(1):36-51. *These authors have contributed equally.*

Attias M, *Piccirillo CA.* The impact of Foxp3$^+$ Regulatory T cells on CD8$^+$ T cell dysfunction in tumor microenvironments and responses to immune checkpoint inhibitors. *British Journal of Pharmacology 2023 (in revision).*

I have also contributed to the following articles:

Mehdi A, ***Attias M,*** *Mahmood N, Arakelian A, Mihalcioiu C, Piccirillo CA, Szyf M, Rabbani SA.* Enhanced Anticancer Effect of a Combination of S-adenosylmethionine (SAM) and Immune Checkpoint Inhibitor (ICPi) in a Syngeneic Mouse Model of Advanced Melanoma. Frontiers in Oncology. 2020 Sep 2;10:1361

Huang F, Gonçalves C, Bartish M, Rémy-Sarrazin J, Issa ME, Cordeiro B, Guo Q, Emond A, ***Attias M,*** *Yang W, Plourde D, Su J, Gimeno MG, Zhan Y, Galán A, Rzymski T, Mazan M, Masiejczyk M, Faber J, Khoury E, Benoit A, Gagnon N, Dankort D, Journe F, Ghanem GE, Krawczyk CM, Saragovi HU, Piccirillo CA, Sonenberg N, Topisirovic I, Rudd CE, Miller WH Jr, Del Rincón SV.* Inhibiting the MNK1/2-eIF4E axis impairs melanoma phenotype switching and potentiates antitumor immune responses. Journal of Clinical Investigation. *2021 Apr 15;131(8)*

Mehdi A, ***Attias M,*** *Arakelian A, Piccirillo CA, Szyf M, Rabbani SA.* Co-Targeting Luminal B Breast Cancer with S-Adenosylmethionine and Immune Checkpoint Inhibitor Reduces Primary Tumor Growth and Progression, and Metastasis to Lungs and Bone. *Cancers (Basel). 2022 Dec 22;15(1):48*

Mehdi A, ***Attias M****, Arakelian A, Szyf M, Piccirillo CA, Rabbani SA.* S-adenosylmethionine blocks tumorigenesis and with immune checkpoint inhibitor enhances anti-cancer efficacy against BRAF mutant and wildtype melanomas. Neoplasia. 2023 Feb;36:100874.

List of figures

List of abbreviations

ADCC	Antibody-dependent cellular cytotoxicity
Ag	Antigen
AICD	Activation-induced cell death
Akt	(Rho family)-alpha serine/threonine-protein kinase
ANOVA	Analysis of variance
APC	Antigen-presenting cells
ATP	Adenosine tri-phosphate
Braf	V-Raf murine sarcoma viral oncogene homolog B
CAF	Cancer-associated fibroblasts
cAMP	Cyclic adenosine mono-phosphate
CD	Cluster of Differentiation
CDKN2A	Cyclin-dependent kinase inhibitor 2A
CFSE	Carboxyfluorescein succinimidyl ester
CI	Confidence Interval
CNS	Conserved non-coding sequences
Cre	C-recombinase
CTLA-4	Cytotoxic T-lymphocyte-associated protein 4
CTV	Cell trace violet
D4M	Dartmouth Murine Mutant Malignant Melanoma
DC	Dendritic cell
DNA	Deoxyribonucleic acid
eIF4E	Eukaryotic translation initiation factor 4E
ERBB2	Erb-b2 receptor tyrosine kinase 2
ERT2	Estrogen receptor T2
FACS	Fluorescence assisted cell sorting
FasL	Fas ligand
FBS	Fetal bovine serum
FDA	Food and drug administration
FOXP3	Forkhead winged helix protein 3
GFP	Green fluorescent protein
GITR	Tumor necrosis factor receptor superfamily, member 18
GM-CSF	Granulocyte Macrophage - Colony Stimulating Factor
gp	Glycoprotein
GRZB	Granzyme B
GVHD	Graft versus host disease
HER2	Human epidermal growth factor receptor 2
HIF-1a	Hypoxia-inducible factor 1-alpha
IAV	Influenza A virus
ICI	Immune Checkpoint Inhibitor

ICOS	Inducible T cell co-stimulator
IDO	Indoleamine 2, 3-dioxygenase
IFN	Interferon
IKZF2	Ikaros zing-finger family 2
IL-18R1	Interleukin 18 receptor 1
IL-18RBP	Interleukin 18 binding protein
IL-1R1	Interleukin 1 receptor 1
IL-2Rα	Interleukin 2 receptor alpha
IL-6R	Interleukin 6 receptor
ILC	Innate-like lymphoid cell
INK4	Inhibitors of CDK4
IPEX	Immuno-deficiency, Polyendocrinopathy, enteropathy, X-linked
irAEs	Immune-related adverse events
iRECIST	Immunotherapy response evaluation criteria in solid tumors
IRES	Internal ribosome entry sequence
ITAM	Immunoreceptor tyrosine-based activation motif
ITIM	Immunoreceptor tyrosine-based inhibition motif
iT_{reg}	*In vitro* induced regulatory T cells
JAK	Janus Kinase
Kras	V-Ki-ras2 Kirsten rat sarcoma viral oncogene homolog
LAG	Lymphocyte-activation gene
LCMV	Lymphocytic Choriomeningitis Virus
Log	Logarithm
mAb	Monoclonal antibody
MACS	Magnetic bead assisted cell sorting
MAGE	Melanoma-associated antigen
MAPK	Mitogen-activated protein kinase
Mart1	Melanoma antigen recognized by T cells 1
MDSC	Myeloid-derived suppressor cell
MFI	Mean fluorescence intensity
MHC	Major histocompatibility complex
MHCII	Type II major histocompatibility complex
MITF	Microphthalmia-associated Transcription Factor
MNK1/2	MAP Kinase Interacting serine/threonine-protein kinase 1 and 2
mRNA	Messenger RNA
MS	Multiple sclerosis
mTOR	Mammalian target of rapamycin
mTORC1/2	Mammalian target of rapamycin complex 1/2
NET	Neutrophil extracellular traps
NFAT	Nuclear factor of activation in T cells
NFkB	Nuclear factor kappa B

NGFR	Nerve Growth Factor Receptor
NK	Natural killer
NO	Nitric oxide
Nras	Neuroblastoma RAS viral oncogene homolog
Nrp-1	Neuropilin-1
NY-ESO-1	Cancer/Testis Antigen 1
ORR	Overall response rate
OS	Overall survival
OVA	Ovalbumin
PBMC	Peripheral blood mononuclear cells
PD-1	Programmed cell death 1
PD-L1/2	Programmed-death ligand 1/2
PFS	Progression-free survival
PI3K	Phosphatidylinositol 3-kinase
PMA	Phorbol 12-myristate 13-acetate
Pmel	Premelanosome protein
PTEN	Phosphatase and tensin homolog
pT_{reg}	Peripherally-induced Treg cell
RA	Rheumatoid arthritis
RECIST	Response evaluation criteria in solid tumors
RFP	Red Fluorescent protein
rhIL-2	Recombinant human IL-2
ROR	RAR-related orphan receptor
SAM	S-adenosylmethionine
SCID	Severe combined immune deficiency
SD	Standard deviation
SLE	Systemic lupus erythematosus
SMAD	Small body size and mothers against decapentaplegic homolog
SNP	Single nucleotide polymorphism
ST2	Interleukin 1 receptor-like 1
STAT	Signal-transducer and activator of transcription protein
T1D	Type-1-diabetes
TAM	Tumor-associated macrophage
T-bet	T-cell-specific T-box transcription factor
Tcf-1	Transcription factor 1
T_{conv}	Conventional (non-Foxp3) T cells
TCR	T-cell receptor
T_{eff}	Effector T cells
TERT	Telomerase Reverse Transcriptase
TGFβ	Transforming growth factor beta
Th	T helper cell

TIGIT	T cell immunoreceptor with Ig and ITIM domains
TIL	Tumor-infiltrating lymphocyte
Tim-3	T-cell immunoglobulin and mucin-domain containing-3
TLR	Toll-like receptor
TLS	Tertiary lymphoid structure
TME	Tumor microenvironment
TNF	Tumour necrosis factor
TNM	Tumor Number of Lymph Nodes Metastasized
Tox	Thymocyte selection-associated high mobility group box protein
T_{reg}	Regulatory T cells
TSDR	Treg-specific demethylated region
tT_{reg}	Thymic-derived Treg cell
UV	Ultraviolet
VEGF	Vascular Endothelial Growth factor
WT	Wild Type
YUMM	Yale University Mouse Melanoma
YUMMER	Yale University Mouse Melanoma Exposed to Radiation
ZF	Zinc Finger

I, Mikhaël Attias, have read, understood, and abided by all norms and regulations of academic integrity of McGill University

Chapter 1 – General Introduction

1. Melanoma

1.1. The deadliest form of skin cancer

Cancer is defined as the uncontrolled growth of some progenitor cells. It originates from a primary tumor, which first gains malignancy and can further invade nearby tissues and migrate to unconnected parts of the body. Skin cancers are the most frequently diagnosed cancers in Canada (1). According to the American Academy of Dermatology Association, the three major subsets are: (*i*) basal cell carcinoma, which commonly affects the inside layer of the epidermis of the head, neck, and face, (*ii*) squamous cell carcinoma which affects cells in the outside layer of the epidermis upon sun exposure, and (*iii*) melanoma, which affects melanocytes, a cell type specialized in producing melanin found in cutaneous, acral, mucosal and uveal skin. While most skin cancers are diagnosed early and readily treatable in a dermatology clinic, melanoma represents the most highly aggressive and metastatic form, accounting for 75% of deaths related to skin cancer (2) and 1200 deaths per year in Canada (3). The prognosis of advanced metastatic melanoma had a median survival of 6-12 months until the 2010s (4), but the advent of immune checkpoint inhibitors (ICIs) has considerably increased the survival rates (5). Furthermore, melanoma is the first indication for which ICIs received marketing authorization, as early as 2011, and is considered a poster child for the success of tumor immunotherapy (6).

1.2. Biology and function of melanocytes in human and mice

Melanoma is a malignant cancer of melanocytes. While these cells originate from the neural crest, they populate the epithelia of the skin, iris and rectum, where they account for 1 to 5% of cells (7). As such, they do not express epithelial cell markers that allow for the histological identification of certain tumor tissues. In humans, skin melanocytes are present at the

dermal/epidermal layer. However, despite mouse skin also being structured in an epidermal, a dermal and a hypodermal layer, mouse dorsal skin is unpigmented, and as such melanocytes are mostly found in the hair follicles, the mice' fur (8).

The role of melanocytes is to produce melanin which protects from UV exposure and color tissues. Melanin production is triggered by activation of the Microphthalmia-associated Transcription Factor (MITF), downstream the activation of the melanocortin-1 receptor by the release of α-melanocyte-stimulating hormones by DNA-damaged keratinocytes. This melanin is produced in specialized organelles called melanosomes, which are released into the neighbouring layer of keratinocytes to limit DNA damage. However, excessive sun exposure leads to a UV damage signature characteristic of melanoma, with mutations in the Telomerase Reverse Transcriptase (TERT) promoter region being the most frequent genetic alteration, found in 70% of patients (9). Thus, sun exposure represents the major risk factor for cutaneous melanoma. As such, 90% of melanoma cases are sporadic.

1.3. Types of melanoma and stages of disease

Melanoma is further classified into 4 main types: (*i*) superficial spreading melanoma is the most frequent, it is flat, displays radial or vertical growth and usually develops on the trunk, arms or legs; (*ii*) nodular melanoma grows vertically in a polypoid shape, on the chest, face or back; (*iii*) *lentigo maligna* melanoma develops from an early flat brown *lentigo maligna* lesion on the face, ears or arms, (iv) acral lentiginous melanoma presents as a discoloured patch of acral skin (soles, palms, under nails) and is not related to sun exposition. Furthermore, rarer types of melanomas include mucosal lentiginous and intraocular melanomas, which target mucosal and uveal skin.

In the clinic, melanoma is commonly graded using the TNM system which defines 5 main stages of disease. At early stages of disease (0-2c), the melanoma lesion is localized to the skin; at stage 3, melanoma is locoregional, i.e., has metastasized to sentinel lymph nodes. At stage 4, melanoma has distant metastases and is usually non-resectable.

1.4. Molecular mechanisms of melanomagenesis and immune evasion

1.4.1. General mechanisms of tumorigenesis

Tumor immunity develops concomitantly to tumorigenesis and is classically described as following three stages: elimination, equilibrium, and evasion, which are not reflected in the clinical pathology staging of tumors. At the elimination stage, the immune system recognizes and destroys tumor cells. Along this course, cancer immunoediting occurs through which tumors acquire enough protective mutations to survive selective pressure from the immune system recognizing and destroying tumor cells, reaching an equilibrium. Finally, the escape phase is characterized by tumor cells evading anti-tumor immunity and becoming clinically detectable. Reaching the escape phase requires the genetic alteration of an oncogene, a gene that is altered dominantly by a gain of function alteration and stimulates the synthesis of a protein controlling cell growth and division (e.g. Kras, Nras, Braf, ERBB2), and a tumor-suppressor gene that encodes a protein that inhibits cell proliferation (e.g., p53, INK4, PTEN, CDKN2A). In the case of melanoma, the important role of UV damage in tumorigenesis confers to melanoma the highest mutational burden amongst human tumors (10). Nonetheless, while the target lesions initiating melanoma-genesis vary, they typically target up to 3 major signalling pathways: MAPK, PI3K and CDKN2A which are key controllers of cell cycle progression, proliferation, survival, and melanin secretion and favor immune evasion.

1.4.2. Braf is the most frequently altered oncogenic pathway in melanoma.

The most common of these oncogenic mutations is the *Braf*^{T1799A} point mutation which is found in 65% of patients (11). It encodes the constitutively activated BRAF^{V600E} kinase, and thus sustains MAPK signaling in melanocytes. A murine model of inducible activation of this mutation revealed that mutation of this oncogene triggers melanocyte hyperplasia and pigmented lesions, but is insufficient to progress towards malignancy (12). While other oncogenes such as *Nras* can be mutated, these alterations rarely coexist (13), as their effects are not synergistic.

1.4.3. Loss of the tumor suppressor PTEN induces metastatic potential.

Indeed, melanomagenesis requires the deletion of a tumor-suppressor gene, such as PTEN, a negative regulator of the PI3K/Akt pathway. As such, Braf^{V600E} and PTEN loss is the most common combination of genetic alterations, found in around 20% of patients and 44% of *Braf*-mutated tumors (13), reducing their sensitivity to Braf inhibitors (14). Furthermore, this constitutive activation of the PI3K pathway can be amplified by stabilizing mutations in exon 3 of *Bcat*, which stabilize β-catenin signaling, and accelerate melanomagenesis and metastatic potential (15).

1.4.4. Inactivation of cell cycle control genes promotes melanoma cell division.

Furthermore, germline inactivating mutations in *Cdkn2a*, which encodes p16INK4A and p14ARF, promote tumorigenesis by constitutively promoting G1-S cell cycle transition and inhibiting the degradation of p53 respectively; and are found in both sporadic and hereditary melanomas (2).

1.4.5. Melanoma genetic alterations promote a phenotype switch through convergent activation of eiF4E.

Constitutive Braf^{V600E} expression leads to activation of MAP Kinase Interacting serine/threonine-protein kinase 1 and 2 (MNK1 and MNK2) and phosphorylation of the initiator of translation eIF4E. Furthermore, the eIF4E pathway is also synergistically amplified by increased mTOR signaling consecutive to PTEN loss (16). Phosphorylation of eIF4E leads to the translation of proteins involved in melanocyte survival, proliferation and metastatic potential (17). Furthermore, it regulates the translation of NGFR (18), a receptor which acts as a molecular switch for melanoma phenotype switching, a process of dedifferentiation through which the expression of most melanoma antigens, expressed in the melanosomes of terminally differentiated cells, is thus reduced (19). Therefore, in addition to their increased invasiveness, phenotype switched melanoma cells display reduced immunogenicity which limits T cell infiltration and favors the chemoattraction of myeloid-derived suppressor cell (MDSC) populations (20) (**Figure 1**).

1.5. Murine models allow to study the anti-melanoma immune response.

1.5.1. The B16 cell lines

Murine models have allowed to study the key features of melanoma biology and the anti-melanoma immune response. One of the earliest is the B16 melanoma model, which has been the gold standard for the preclinical development of anti-melanoma therapeutics. This cell line was derived from a spontaneous melanoma in a C57Bl/6 mouse in the 1930s. However, it does not recapitulate some of the key oncogenic mutations found in human pathology, thus tumor-intrinsic immunogenicity and low mutational burden limit the diversity of antigens available for T cell recognition, allowing for aggressive tumor growth and limited lymphocyte infiltration (21).

1.5.2. Oncogene-driven models

In order to study the individual roles of each of the commonly identified melanoma oncogenic pathways, a series of cell lines recapitulating these mutations were generated, the Yale University Mouse Melanoma (22) and the Dartmouth Murine Mutant Malignant Melanoma (23), derived from inducible knockout systems. These models have successfully contributed to the development of targeted therapies, a class of drugs that directly target specific oncogenic pathways, including Braf inhibitors (dabrafenib, vemurafenib) and MEK inhibitors (trametinib, cobimetinib). However, while $Braf^{V600E}$ and $PTEN^{-/-}$ are found in a large frequency of tumor lesions, the D4M and YUMM cell lines do not present the high somatic mutational burden characteristic of most human melanomas (24). As such, most of these preclinical models respond poorly to immunotherapies that have proven their efficacy in the clinic (22).

Paucity of tumor-antigens is hypothesized to contribute to ineffective priming of anti-tumor responses. However, UV signature mutations can produce neoantigens that increase overall immunogenicity. Following this rationale, Wang and colleagues irradiated $Braf^{V600E}$ $PTEN^{-/-}$ $Cdkn2a^{-/-}$ cells and expanded a single clone bearing additional somatic mutations. At low inoculum numbers, the resulting highly immunogenic YUMMER1.7 tumor spontaneously regresses following a strong T-cell response. Furthermore, established tumors respond fully to ICI (25). However, in depth characterization of the immune response to these tumors is still lacking.

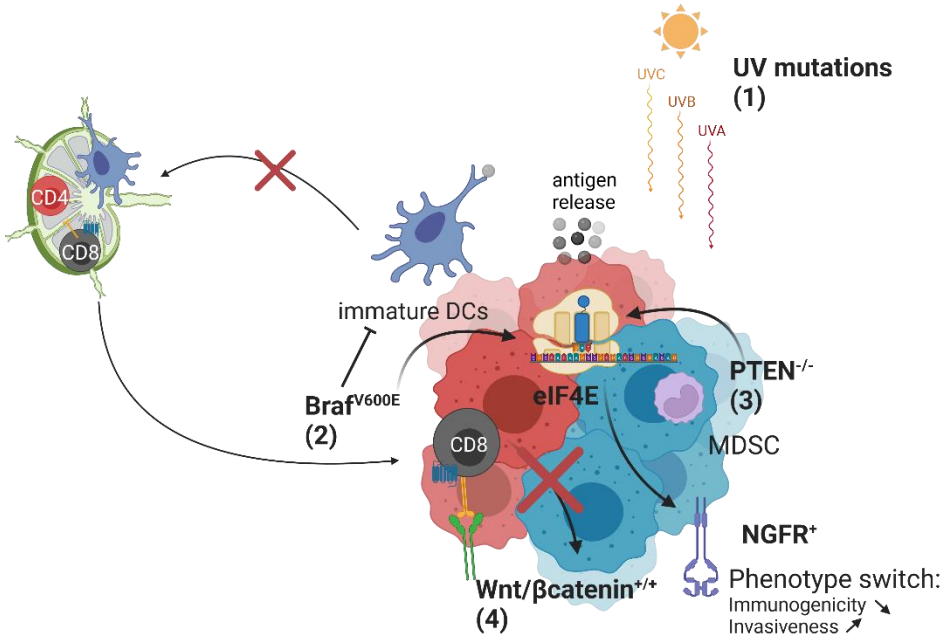

Figure 1. Molecular mechanisms leading to melanoma phenotype switching. (1) UV mutations induce DNA damage, thereby releasing neoantigens captured by migratory dendritic cells. (2) Constitutive Braf expression initiates melanocyte hyperplasia and leads to phosphorylation of eIF4E. (3) Loss of PTEN induces malignancy and reinforces eIF4E expression which induces NGFR expression which acts as phenotypic switch for melanoma dedifferentiation. (4) Constitutive β-catenin signaling further inhibits T cell exclusion. Created with biorender.com®

2. Mechanisms of tumor immunity

2.1. Tumor antigens

Tumors are identified by the immune system through their expression of tumor antigens, presented on MHC molecules in the context of an adaptive T cell response. These tumor antigens are classified in different categories depending on their nature. Tumor-specific antigens are found on cancer cells only, and result from point mutations or rearrangements of a protein. Such antigens are by-products of the genetic alteration of an oncogene, a tumor-suppressor gene, or a point mutation in a normal self-protein that generates a change in amino acids and binding of this neoepitope to an MHC-I molecule. A second family of tumor antigens are cancer-testis antigens, generated through aberrant expression of proteins normally expressed exclusively in male germ cells (e.g., MAGE, NY-ESO-1). These two classes encompass non-self-antigens, in contrast to the family of tumor-associated antigens which are found at elevated levels on tumor cells but are expressed at lower levels by healthy cells. TAAs include differentiation antigens (e.g., Tyrosinase, Mart-1, Pmel, CD19), proteins normally only expressed at a specific phase of a cell type's differentiation; and antigens resulting from overexpression of a particular gene (e.g., HER-2, WT1), abnormal post-transcriptional, or post-translational modifications. Finally, proteins expressed following the incorporation of a viral oncogene are a source of tumor antigens.

2.2. Tumor-infiltrating lymphocytes mediate tumor cytotoxicity.

Tumor-infiltrating lymphocytes (TILs) are major effectors of anti-tumor immunity (26) and most of the hallmarks of the anti-tumor T cell response have been established or confirmed in the setting of melanoma. Indeed, the recruitment of TILs to primary melanomas is dependent on CXCR3 chemokine receptor signaling following their priming in the draining lymph node. Both these processes are orchestrated by migratory $CD103^{+}$ dendritic cells (DCs (27)) which capture

the cognate antigen and establish an early type 1 interferon (IFN) response that leads to the secretion of CXCL9 and 10 (28). Upon T cell recruitment, local production of IL-12 by tumoral antigen-presenting cells (APCs) allows for the establishment of a type 1 adaptive immune response, with recruitment of $CD8^+$ and $CD4^+$ T_h1 cells and production of IFNγ, a dominant mediator of antitumor responses through inhibition of tumor cell proliferation, induction of tumor cell apoptosis and necroptosis, facilitating antigen presentation through upregulation of MHC-I expression, and enhancing $CD8^+$ T cell cytotoxicity (29).

2.3. Multiple primary mechanisms of immune-evasion limit T cell recruitment.

2.3.1. Lack of immunogenicity

Tumors evade immune responses using a large variety of mechanisms which enable it to reach malignancy. Lack of immunogenicity, through low mutational burden, limits the amount of recognizable tumor antigens, and thus restrains T cell infiltration in the tumor, especially in the early phases of tumor growth. While melanoma is a highly immunogenic solid tumor type, as described earlier, it undergoes phenotype switching which represents an example of antigenic modulation. Indeed, during the cancer equilibrium phase, escape variants with low levels of antigen expression are selected. Loss of expression of MHC-I molecules further diminishes melanoma immunogenicity and represents a secondary mechanism of evasion to avoid CD8-mediated tumor cytotoxicity (30). Moreover, melanoma-associated antigens (e.g., NY-ESO-1, Mart1, Pmel) are expressed at low levels by normal melanocytes, and thus considered self-antigens. Thus, they are recognized in the absence of co-stimulation, leading to T cell anergy and tolerization of APCs.

2.3.2. Modulation of the tumor microenvironment limits T cell infiltration and fitness.

In addition to limiting tumor immunogenicity, tumors can modulate the tumor microenvironment (TME) to avoid immune recognition and inhibit T cell activation and migration. By secreting factors such as collagen, tumors create physical barriers that render them an immune-privileged site. In melanoma, aberrant Wnt-β-catenin signaling inhibits T cell trafficking by modulating cancer-associated fibroblasts (31). Furthermore, tumor cells also outcompete T cells for nutrients such as glucose and amino acids, especially in hypoxic environments, though expression of HIF-1α. Anaerobic glycolysis leads to the production of lactate by tumor cells, which is then exported in the TME and in turn, alters the extracellular lactate gradient which inhibits T cell glycolysis and acidifies the pH which hinders T cell effector functions (reviewed in (32)). Tumor cells also modulate the local metabolic activity of T cells by inducing indoleamine 2,3-dioxygenase (IDO) expression, an enzyme that diminishes tryptophan availability and produces metabolites that induce T_{eff} cell apoptosis (33).

2.3.3. Recruitment of immunosuppressive leucocytes drives T cell exclusion.

Tumors induce immunosuppression through the secretion of anti-inflammatory cytokines (IL-10, TGFβ), and recruitment of a wide variety of suppressive myeloid cells such TAMs, neutrophils, tolerogenic dendritic cells and MDSCs. TAMs usually adopt a pro-tumorigenic M2 profile, through their interplay with cancer-associated fibroblasts, which contributes to T cell exclusion through densification of the extracellular matrix and altering the composition of the chemokine milieu (34). They inhibit T cell responses by producing reactive oxygen species, inducing NO synthesis, depriving arginine locally, and secreting anti-inflammatory cytokines such as TGFβ and IL-10. Furthermore, they inhibit T cell migration by inducing vascular dysfunction and promoting local hypoxia (35). Neutrophils also infiltrate tumors where they produce reactive

oxygen species and contribute to T cell exclusion through the formation of extracellular traps (36) (NETs), all the while promoting metastasis by seeding trapped circulating tumor cells (37), and are thus associated with worse prognosis (38). In addition, tumors inhibit the terminal differentiation of macrophages and neutrophils by producing factors such as GM-CSF and VEGF, giving rise to immature populations of MDSCs (39) which share some of their suppressive mechanisms with TAMs and neutrophils. In melanoma, the common key oncogenic pathways synergize to induce the recruitment of these immunosuppressive populations. For example, constitutive Braf expression polarizes dendritic cells towards a tolerogenic phenotype and induces PD-L1 expression (40); and PTEN loss promotes the recruitment of MDSCs and TAMs which contributes to T cell exclusion (41, 42).

2.4. Immunological classifications of tumors

In the clinic, tumors are staged using the TNM system, which aggregates primary tumor size, number of metastatic lymph nodes and distant metastases. However, tumors are not solely comprised of tumor cells and their phenotype and clinical properties also rely on the composition of their stromal cells, vascularization and infiltrating immune cells. Alongside the development of tumor immunotherapies, immunological classifications of tumors were developed (43). They categorize tumor microenvironments (TMEs) along a gradient from cold (scarcity of T cells), excluded (T cells sequestered in the margin), immunosuppressed (low infiltration in the core) to hot (high infiltration in the core and/or tertiary lymphoid structure). Overall, this degree of inflammation predicts treatment outcome better than cancer-based classifications (44, 45).

2.4.1. Hallmarks of the cold tumor immune phenotype

The progressive establishment of a cold TME results from a feedback loop from poorly immunogenic tumor cells that promote the activation of immunosuppressive pathways that further inhibit T cell responses. It is characterized by defective homing of APCs and T cells to the primary tumor and low CD8:CD4 ratios (43). On the other hand, cold TMEs are dominated by the various myeloid populations previously described that contribute to dampening local inflammation (**Figure 2**). Immunogenicity is the main determinant of the tumor immune phenotype (46). As such, melanoma and its high mutational burden is often considered a prototypical hot tumor. However, tumor immune phenotype is not set in time. As previously outlined, immunogenicity is tightly linked to cancer genotype (47), and the melanoma oncogenic pathways confer it a colder phenotype in advanced disease stages. On the other hand, a tumor's immune phenotype can be manipulated through clinical intervention. Indeed, new tumoral antigens are released upon treatment with either chemotherapy (48) or radiotherapy (28), which contributes to their therapeutic efficacy.

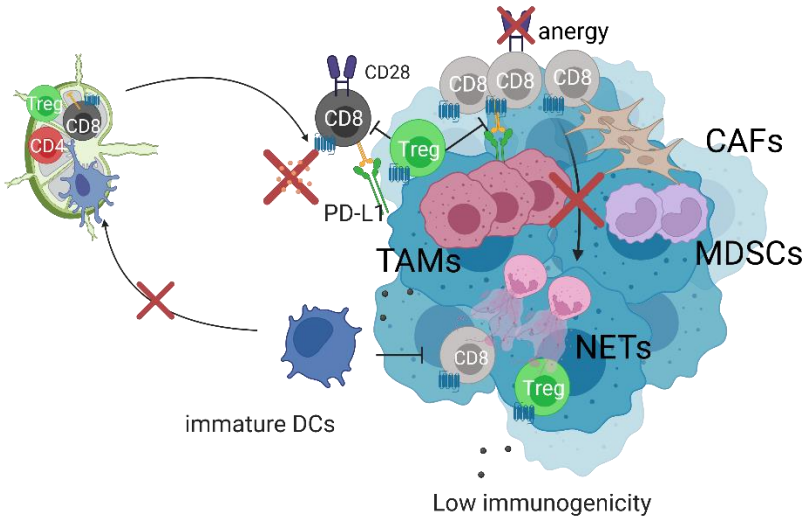

Figure 2. Mechanisms of immune evasion in cold tumor microenvironments. Adapted from Attias and Piccirillo, BJP, 2023 (in revision). Low immunogenicity limits T cell recruitment. Presentation of tumor self-antigen by immature DCs in the absence of CD28 co-stimulation leads to T cell anergy. Tumor-associated macrophages (TAMs) and myeloid-derived suppressor cells (MDSCs) further inhibit T cell responses by secretion of anti-inflammatory cytokines and reactive oxygen species. Cancer-associated fibroblasts (CAFs) and neutrophil extracellular traps (NETs) create physical barriers that prevent T cell infiltration of the tumor core. Created with Biorender.com®

2.4.2. Establishment of hot tumor microenvironments

In tumors with higher mutational burden, such as melanoma, higher antigen uptake allows for stronger early type 1 IFN responses and establishment of a hot TME, which is characterized by its abundance of T cell-recruiting chemokines, antigen-presenting cells, and lymphocytes. Furthermore, melanoma immunogenicity can be increased by the formation of tertiary lymphoid structures (TLS) (49). Indeed, secretion of CXCL13 by stromal cells induces the recruitment of

lymphoid tissue inducer cells such as T_h17, B cells or M1 macrophages. These cells then interact with the stromal cell through Lymphotoxin α1β2 which triggers the production of VEGF, thus high endothelial venule formation (50). Meanwhile, chemokines and adhesion molecules attract B and T cells to the TLS. In the context of anti-tumor responses, this is a net positive, as it allows for better antigen-presentation and the coordinated actions of $CD8^+$ cytotoxic effector T cells and B cells generated in TLSs. This enables *in situ* tumour destruction via direct tumor cell killing, antibody-dependent cellular cytotoxicity (ADCC) mediated by macrophages and/or natural killer cells and local complement activation (51). Furthermore, central memory T and B cells generated in TLSs circulate and protect against metastasis. As such, presence of TLS is associated with better prognosis and response to treatment (52). However, they are not associated with melanoma stage, probably because they don't appear from the beginning of tumor growth.

As a result, hot tumors are abundantly infiltrated by $CD8^+$ and $CD4^+$ T_h1 cells, whose production of IFNγ also contributes to the polarization of TAMs toward an M1 phenotype, which is associated with the gain of anti-tumor functions such as antigen-presentation through induction of MHC-II (53) and reinforces the hot immune phenotype.

2.5. Acquired mechanisms of immune evasion dampen inflammation in hot tumors.

However, tumors develop mechanisms to escape the antitumor effects of IFNγ, such as the acquisition of loss of function mutations in *JAK1* and *JAK2* to resist the induction of apoptosis (54). Furthermore, while early type 1 IFN responses are necessary for T cell recruitment to the tumor, sustained signaling leads to IL-10 secretion by APCs, as well as regulatory T (T_{reg}) cell and MDSC accumulation (55), thereby diminishing IFNγ signaling throughout the TME and inhibiting the polarization of TAMs towards an anti-tumor phenotype (**Figure 3**) (56).

2.5.1. Role of checkpoint molecules in modulating T cell activation

IFNγ signaling also promotes the upregulation of co-inhibitory ligands such as PD-L1, PD-L2, galectin-9, CEACAM-1 and CD155 which provide an inhibitory feedback loop on TCR activation and promote T cell dysfunction (57). As such, high amounts of PD-L1 expression is a feature of hot TMEs which renders them sensitive to immunotherapies targeting immune checkpoint molecules (44). Engagement of their TCR by a peptide-MHC complex is not sufficient to transduce a fully activating signal in T cells. This process requires the formation of an immune synapse with the antigen-presenting cell, grouping CD3 to maintain the TCR at the surface and transduce additional signals through Immunoreceptor Tyrosine-based Activating Motifs (ITAMs); CD4 or CD8 co-receptors to stabilize TCR/pMHC interactions and phosphorylating ITAMs; and engagement of the co-stimulatory receptor CD28 by CD80 or CD86 to induce signaling through the Phosphoinositide 3-kinase (PI3K)/Akt pathway, which ultimately promotes T cell proliferation, effector functions, cytokine production and survival.

Immune checkpoint molecules are a family of either co-inhibitory or co-activating ligands and receptors that act as secondary signals to modulate various components of the PI3K/Akt pathway, thus governing T cell fate. Indeed, the expression of co-inhibitory receptors is induced upon acute productive TCR activation to provide an inhibitory feedback loop on T cell activation. CTLA-4 inhibits T cell activation by competing with CD28 for binding to CD80 and CD86 on the surface of APCs, thus inducing self-tolerance (58). On the other hand, interaction of PD-1 with any of its ligands leads to activation of its immunoreceptor tyrosine-based switch motif, which recruits Shp-2 phosphatases that dephosphorylate CD3ζ, Zap70 and CD28 (59), leading to inhibition of Bcl-2 and Ras, and downstream inactivation of PI3K/Akt signaling (60). As such, CTLA-4 and PD-1 play a role in functions such as maintaining immune tolerance and contraction of physiological

immune responses, to minimize tissue damage by mediating apoptosis of mature T cells in peripheral tissues.

2.5.2. Chronic TCR stimulation induces states of T cell dysfunction in melanoma.

However, prolonged TCR stimulation induces chronically high expression of PD-1 through FoxO1, and other checkpoint receptors such as TIGIT, Tim-3 and LAG-3, in contexts such as LCMV infection or anti-tumor responses (61). Signaling through these pathways converge around inhibiting PI3K/Akt/mTOR signaling and ultimately lead to the establishment of an exhausted phenotype, with diminished proliferation and protein synthesis and metabolic consequences that render the cell dysfunctional.

While T cell exhaustion also affects $CD4^+$ T cells, its hallmarks have mostly been studied in $CD8^+$ T cells. T cell exhaustion is defined by high expression of multiple inhibitory checkpoint receptors through chronic antigen stimulation, progressive loss of proliferative capacity and capacity to secrete pro-inflammatory cytokines IFNγ, TNFα and IL-2, reduced cytotoxic activity because of a metabolic shift towards fatty acid oxidation, leading to eventual apoptosis. As opposed to anergy, it is not a transient state that can be readily rescued by certain cytokines (62), but results from a stable form of differentiation driven by the transcription factor Tox (63). As such, two main subsets of exhausted cells have been described: progenitor-exhauster cells and terminally exhausted cells.

Progenitor exhausted cells are memory cells that express intermediate levels of PD-1 and differ from effector $CD8^+$ T cells by their expression of the transcription factor Tcf-1, which endows them with stem-like properties (64). Ontogenically, they derive from effector cells that escape the initial contraction of the immune response to become long-lived. Their differentiation into

terminally exhausted cells is associated with a loss of Tcf-1 and high levels of PD-1 and Tim-3 expression (65).

Terminal exhaustion was initially described in chronic viral infections, where it is hypothesized to alleviate immunopathology all the while maintaining partial control of pathogen replication. In tumor microenvironments, PD-1^{High} CD8^{+} T cells share a large part of their transcriptional signature with LCMV gp-33 specific terminally exhausted cells (64), but often completely lack effector functions and are thus referred to as dysfunctional rather than exhausted by some groups (66). Indeed, tumor-associated antigen-specific dysfunctional CD8^{+} TILs originate from anergic cells that did not differentiate in an effector phenotype like is seen in chronic viral infections (67). Thus, the dysfunctional phenotype is associated with tumor-reactive rather than bystander TCR specificity (68). As such, while surface expression of PD-1 is a useful biomarker of exhaustion and therapeutic target, it does not fully capture the heterogeneity of exhausted cell subsets and is also observed in effector populations. Furthermore, while exhaustion is readily induced by removing CD4^{+} T cell help (69) and T_{reg} cells suppress the effector functions of both CD4^{+} and CD8^{+} T cells, the role of T_{reg} cells in promoting immune exhaustion remains ill-defined.

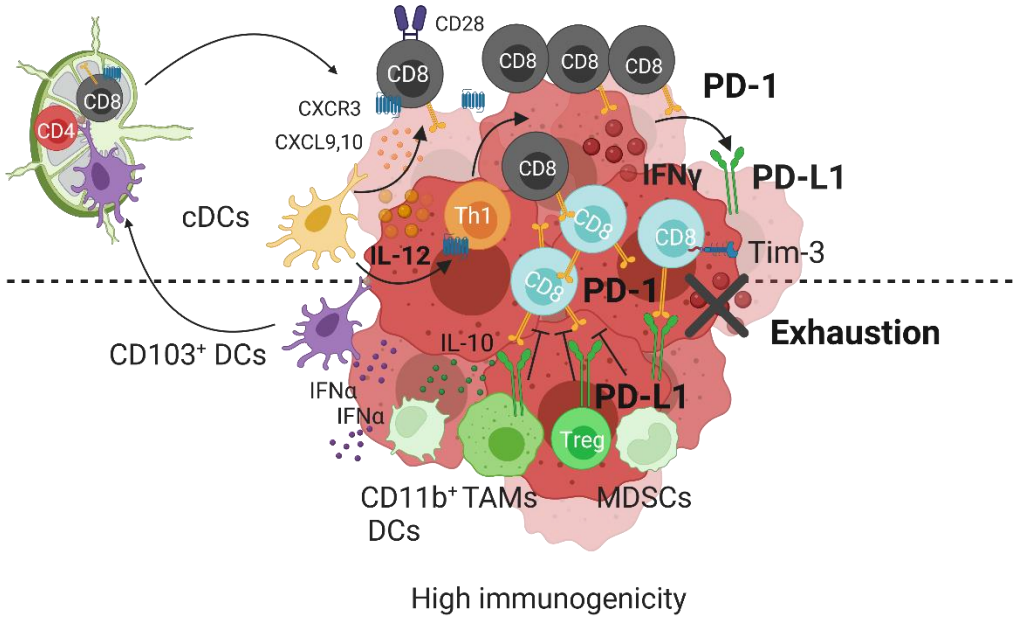

Figure 3. Establishment of a hot tumor microenvironment and subsequent immune exhaustion.

Adapted from Attias and Piccirillo, BJP, 2023 (in revision). Early type 1 interferon responses induce the migration of $CD103^+$ DCs to the tumor-draining lymph nodes where they prime T cell responses. Local T cell re-activation by IL-12-secreting DCs promotes $CD4^+$ T_h1 and $CD8^+$ T_{eff} cell differentiation, PD-1 expression, and production of IFNγ, which in turn induces PD-L1 expression by tumor cells and APCs. $CD11b^+$ DCs, TAMs, T_{reg} cells and MDSCs secrete IL-10 with inhibits T cell function. If the antigen is not cleared, PD-1 expression persists and signaling through PD-L1 and Tim-3 induces T cell exhaustion. Created with Biorender.com®

3. T_{reg} cells play a dominant role in tumor-induced immunosuppression.

3.1. T_{reg} cells are essential mediators of peripheral tolerance.

Whether hot or cold, tumors are adept at hijacking the numerous suppressive mechanisms of T_{reg} cells to dampen the proliferation and effector functions of anti-tumor T_{eff} cells. T_{reg} cells are a specialized subset of $CD4^+$ T cells whose major function is to prevent the development of autoimmunity by inhibiting autoreactive T cells and are essential mediators of peripheral tolerance (70). They are defined by their expression of their master transcription factor Foxp3 which endows them with their unique immunosuppressive transcriptome (71). Indeed, Foxp3 represses the expression of key genes that play a role in T cell activation, proliferation and acquisition of pro-inflammatory effector functions (IL-2, IFNγ, IL-4, IL-17) (72). As such, genetic alterations of Foxp3 expression lead to a catastrophic lethal multi-organ autoimmune disease called IPEX syndrome in humans (73) and scurfy in mice (74). Another defining feature of T_{reg} cells is their constitutive high expression of the IL-2Rα (CD25) which allows them to readily capture the IL-2 they can't produce and supports their proliferation and survival in the periphery (75, 76).

3.2. Developmental origins of melanoma-infiltrating T_{reg} cells

T_{reg} cells can arise from two separate developmental pathways: (*i*) natural-occurring or thymic T_{reg} (tT_{reg}) cells stem from single positive $CD4^+$ thymocytes expressing Foxp3 following TCR engagement of self-antigen (77). In mice, expression of the zinc-finger transcription factor Helios is associated with these tT_{reg} cells (78). On the other hand, (*ii*) peripherally-induced T_{reg} (pT_{reg}) cells arise in the periphery from naïve $CD4^+$ T cells activated in the presence of Foxp3-inducing factors such as TGF-β and IL-2 (79) which are readily found in tumor microenvironments (80), and often lack Helios expression (78). Thus, it has long been hypothesized that local induction is an important source of T_{reg} cells in TMEs (81).

To this date, it remains unclear which of these subsets dominates melanoma tumor microenvironments. Some reports indicate that a majority of T_{reg} TILs are Helios$^+$ in human breast (82) and colorectal (83) cancers. However, Helios is not a perfectly reliable marker of T_{reg} cell ontogeny as Helios expression can be acquired by pT_{reg} cells induced upon antigen-specific challenge of TCR-transgenic CD4$^+$ T cells (84). While pT_{reg} cells are readily detected in TMEs upon adoptive transfer of purified polyclonal T_{conv} splenocytes (80), it remains to be determined if these cells are tumor antigen-specific. Indeed, there is no pT_{reg} induction observed when transferring OT-II cells into OVA-expressing murine melanomas (85). Furthermore, in B16 murine melanoma, single-cell sequencing of purified T_{reg} cells revealed that local skin and melanoma-infiltrating T_{reg} cells share genetic signatures of tissue adaptation, suggesting an active migration of circulating T_{reg} cells (86). Finally, TCR sequencing analyses have found limited overlap between the repertoires of T_{conv} and T_{reg} TILs in preclinical models of lung cancer (87), and in patients with colorectal carcinoma (88) metastatic melanoma, gastrointestinal and ovarian cancers (89), despite shared antigen-specificity (90). Taken together, these data suggest that in melanoma, the establishment of the tumoral T_{reg} cell niche is highly dependent on the local proliferation of thymic-derived Helios$^+$ T_{reg} cells recruited from the lymph node rather than a local induction of pT_{reg} cells.

3.3. Suppressive mechanisms of T_{reg} cells within melanoma microenvironments

Melanomas co-opt the multiple T_{reg} cell suppressive mechanisms to induce local immunosuppression and favor their own growth. Indeed, T_{reg} cells (*i*) mediate the deletion of melanoma-infiltrating T_{eff} cells through direct cell contact, by secreting cytotoxic granules containing Granzyme B and Perforin (91); (*ii*) secrete anti-inflammatory cytokines TGFβ, IL-10 and IL-35 (92) which inhibit the effector functions of T_{eff} cells and increase tumor cell survival,

proliferation and metastatic potential (93); (*iii*) establish inhibitory interactions with dendritic cells via LAG-3 which suppresses DC maturation (94) and via CTLA-4 which induces the endocytosis of its ligands CD80 and CD86 (95), polarizes dendritic cells towards a tolerogenic phenotype, limits the availability of co-activating signals to T_{eff} cells (96) and induces secretion of IDO which mediates T_{eff} apoptosis (97); (*iv*) increase the availability of inhibitory adenosine metabolites by inducing local adenosine secretion via surface expression of CD39 (98), by releasing adenosine during their own apoptosis in conditions of oxidative stress in melanoma TMEs (99) and by transferring cyclic AMP to target T_{eff} cells (100) which leads to inhibition of their proliferation and cytokine production; and (v) compete for nutrients with T_{eff} cells and act as an IL-2 sink through their constitutive expression of the trimeric high affinity form of IL-2R, which limits T_{eff} cell activity and ultimately leads to their apoptosis by cytokine-deprivation (101). As such, abundant T_{reg} cell infiltration correlates with worse prognosis, metastatic potential, and resistance to treatment (102).

3.4. Accumulation of T_{reg} cells in tumor microenvironments

In addition to the direct suppression of T_{eff} cells, multiple mechanisms concur to the establishment of large T_{reg} cell niches within TMEs. First, the tT_{reg} cell TCR repertoire is skewed towards self-antigens and distinct from T_{conv} cells. Thus, T_{reg} TILs are reactive to tumor self-antigens and neoantigens in melanoma (89). Furthermore, tT_{reg} cells are preferentially recruited to certain tumor types through chemokines that are secreted directly or induced by tumor cells. For example, production of CCL22 by tumor cells and TAMs drives the recruitment of $CCR4^{+}$ T_{reg} cells in ovarian carcinoma, where they suppress Her-2 specific T cells (102).

Multiple pathways confer T_{reg} cells a competitive advantage over T_{eff} cells in melanoma TMEs. (*i*) Secretion of Foxp3-inducing factors such as TGFβ promote T_{reg} cell homeostasis locally and can trigger the conversion of T_{conv} cells into pT_{regs} in the TME (80). (*ii*) PD-L1 signaling synergizes with TGFβ to stabilize Foxp3 expression epigenetically and promote T_{reg} cell fitness (103). (*iii*) Secretion of IDO by melanoma cells and APCs promote T_{reg} cell survival and expansion, all the while inducing T_{eff} cell apoptosis (104). (*iv*) T_{reg} cells have higher rates of fatty acid synthesis and glycolysis which confer them a proliferative advantage over T_{eff} cells in low-glucose environments such as the melanoma TME (105). (*v*) In hypoxic conditions, HIF-1α binds to the Foxp3 promoter and favors T_{reg} cell migration and proliferation, at the detriment of their suppressive potency. Nonetheless, they retain some suppressive capacity through oxidative phosphorylation of free fatty acids (106).

3.5. Dominant role of T_{reg} cells in establishing a cold melanoma immune phenotype

Through their suppressive mechanisms and competitive advantages, T_{reg} cells play a dominant-role in establishing tumor-induced immunosuppression. Indeed, temporal depletion of T_{reg} cells, either through the use of anti-CD25 antibodies or administration of diphtheria toxin to $Foxp3^{DTR}$ mice, leads to the clearance of established tumors in a variety of cancer types, including melanoma (107–110). Furthermore, subtle alterations to the canonical T_{reg} cell phenotype in the TME are sufficient to render poorly immunogenic melanoma models hot, and delay tumor growth (111). As such, the role of Helios in promoting T_{reg} cell fitness is crucial in melanoma. Indeed, the constitutive deletion of Helios in $Foxp3^{+}$ cells enhances anti-tumor responses as reflected by a reduced frequency of tumor-infiltrating T_{reg} cells and delayed B16 tumor growth (112). Functionally, while it does not directly bind of Foxp3 or its promoter (113), Helios plays a crucial role in T_{reg} cell fitness by stabilizing the canonical T_{reg} cell phenotype upon priming through Stat5

signaling (114). Furthermore, Helios promotes cycling and survival by preserving Bcl-2 expression in these activated T_{reg} cells. As such Helios$^{-/-}$ T_{reg} cells are outcompeted by their WT counterparts upon adoptive transfer and fail to control T_h1 and T_{fh} responses (115). Furthermore, the remaining tumor-infiltrating Helios$^{-/-}$ T_{reg} cells display impaired lineage stability, characterized by reduced expression of Foxp3 and CD25, secretion of otherwise-repressed cytokines such as IFNγ (112), and increased expression of genes associated with T_h1 and T_h2 differentiation (116). However, it remains unclear if this delay in melanoma growth is a consequence of reduced T_{reg} cell survival or suppressive capacity.

3.6. Functional specialization of T_{reg} cells in tumor microenvironments

3.6.1. Role of Helios in orchestrating the tissue-specialization of T_{reg} cells

Foxp3 is the master transcription factor of T_{reg} cells and its sustained expression stabilizes T_{reg} cell suppressive function in time (117). However, T_{reg} cells demonstrate functional plasticity and adopt other master transcription factors associated with conventional CD4$^+$ (T_{conv}) T helper linages in response to local inflammatory cues (**Figure 4**). Furthermore, in addition to promoting T_{reg} cell fitness in melanoma TMEs, emerging data links the expression of the transcription factor Helios to these functional adaptations of T_{reg} cells. Functionally, circulating Helios$^+$ and Helios$^-$ T_{reg} cells have similar capacity to control effector cell proliferation *in vitro* and in a model of T cell-mediated colitis. However, they harbor distinct transcriptional profiles which suggests they are differentially susceptible to polarizing and inflammatory signals. Indeed, circulating Helios$^+$ T_{reg} cells express higher levels of genes associated with a T_h1-profile compared to their Helios$^-$ counterparts (118). Furthermore, our lab confirmed that Helios$^-$ T_{reg} cells express higher levels of RORγt (119), and preferentially adopt a T_h17 phenotype (84). Accordingly, TCR sequencing of circulating Helios$^+$ and Helios$^-$ T_{reg} cells isolated from Foxp3-Helios dual reporter mice revealed

very little overlap between the two repertoires, suggesting these two subsets represent different T_{reg} lineages (118). Nonetheless, Helios is not a reliable marker of tT_{reg} cells as recent data from our lab and others indicates that Helios expression can be modulated both *in vitro* and *in vivo* (84, 118, 119).

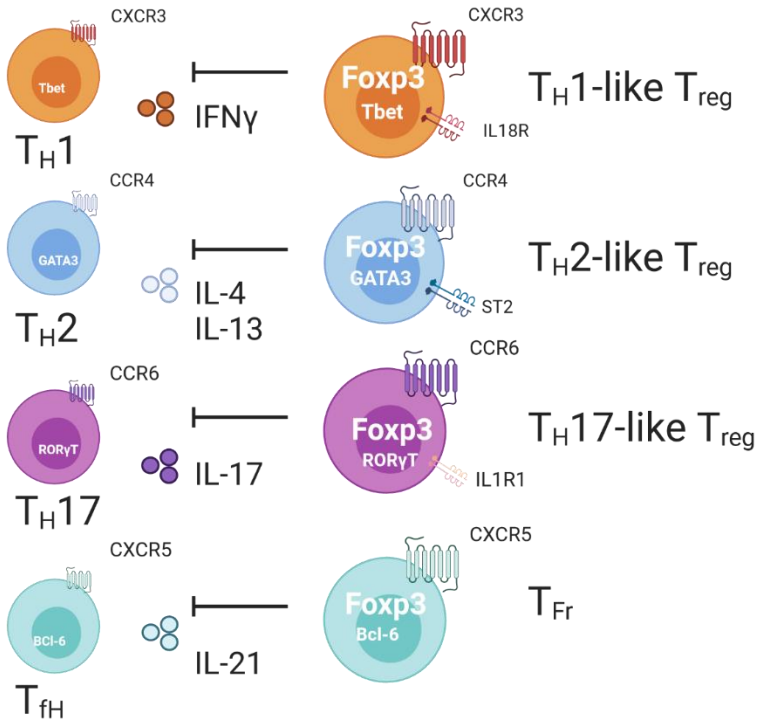

Figure 4. Functional adaptation of regulatory T cells in response to inflammatory cues.

In response to distinct polarizing signals, T_{reg} cells gain the expression of the respective T helper master transcription factor. In turn, they gain the expression of chemokine receptors and alarmin receptors which allow them to co-localize with T_{eff} cells at the site of inflammation and proliferate and survive in tissues. As such, they are hypothesized to be functionally specialized in the control of a subtype of inflammatory response. Yet, the role of this adaptation in TMEs is ill-defined. Created with Biorender.com®

3.6.2. Acquisition of T_h1-like characteristics

Expression of T-bet allows T_h1-like T_{reg} cells to colocalize with infiltrating T_{eff} cells through CXCR3 (120, 121). In the context of mucosal infections, this T_h1 specialization is believed to be required for their local survival, proliferation and suppressive ability, and to promote the temporal control of type 1 immune responses and return to homeostasis (122). T_h1-like T_{reg} cells have been identified in human ovarian carcinoma and oropharyngeal cancer (123, 124). However, the consequences of this adaptation on T_{reg} cell function and fate remain to be determined in the context of anti-tumor immunity. Indeed, while CXCR3$^+$ T_{reg} TILs appeared to suppress T cell proliferation *in vitro* (123), and promote dendritic cell tolerization *in situ* (125), they are associated with stronger IFNγ secretion by T_{conv} cells *in vivo* (124). Furthermore, IL-12-induced upregulation of T-bet drives the secretion of low levels of IFNγ by T_{reg} cells (126), which has been associated with strong anti-tumor responses and delayed tumor growth (111), suggesting such functional plasticity could render these cells susceptible to a dysregulation of the canonical T_{reg} cell phenotype.

3.6.3. Reprogramming towards an effector phenotype

T_{reg} cells can ultimately reprogram into inflammatory T_{conv} cells contributing to anti-tumor immunity. Loss of Foxp3 expression results in abrogated T_{reg} cell suppressive capacity and unleashes their inflammatory potential (127). These reprogrammed cells are thus called "*ex*Foxp3$^+$" and were first observed upon adoptive transfer of purified T_{reg} cells into lymphopenic mice. Emerging *ex*Foxp3$^+$ cells produce cytokines normally repressed in T_{reg} cells, like IL-2, IL-4, IL-17A and IFNγ (72, 127, 128). Our laboratory showed that *ex*Foxp3$^+$ cells mediate potent inflammatory, effector functions in the gut microenvironment or sites of parasitic infection (128). In melanoma, these reprogrammed T_{reg} cells contribute to anti-tumor immunity by acting as

conventional helper T cells and licensing DCs to mount $CD8^+$ T cell responses to a cross-presented antigen (129). However, this process is inhibited by expression of IDO which suppresses IL-6 secretion in dendritic cells and in $Foxp3^+$ cells through the GCN2 kinase pathway (130).

3.6.4. Role of IL-18 in the specialization of T_{reg} cells during T_h1 responses

One of the most highly upregulated genes by *ex*Foxp3 cells is *IL18R1* which encodes the IL-18 receptor (131). IL-18 is a member of the IL-1 family of alarmins which is secreted by tumor cells and by infected cells during type 1 immune responses. It was first described as an IFNγ-inducing factor and synergizes with IL-12 to promote the differentiation of $CD4^+$ T cells into T_h1 cells, despite being insufficient to induce T_h1 development by itself (132). Another mechanism through which IL-18 potentiates the establishment of T_h1 responses is by promoting the expansion and survival of effector-like $CD8^+$ T cells (133). Importantly, T_{reg} cells also sense IL-18 through expression of the IL-18 receptor in cancer and during viral infections (131, 134).

Our lab has shown that IL-18R expression by tissue-infiltrating T_{reg} cells is associated with their acquisition of T_h1-like characteristics. Indeed, IL-18 potentiates IL-12-induced IFNγ secretion by T_{reg} cells *in vitro*, and IL-18 promotes T_{resp} cell evasion from suppression without impairing T_{reg} cell suppressive capacity (135). Furthermore, through a T_{reg}-specific conditional deletion of IL-18R1 expression, we demonstrated that T_{reg} cell responsiveness to IL-18 is required for the specialized suppression of T_h17 cells during T_h1-biasing infections such as Influenza A Virus and Leishmania (135). In addition, $IL\text{-}18R^+$ T_{reg} cells display promote tissue-repair mechanisms by secreting amphiregulin (136). Taken together, these results are coherent with a model whereby IL-18 allows T_{reg} cells to expand and survive without impairing the effector functions of T_h1 cells during the initiation of a type 1 immune response, before favoring the effective contraction of the immune response and return to tissue homeostasis after pathogen

clearance (122). However, numerous knowledge gaps remain on the role of IL-18 sensing by T_{reg} cells in the context of anti-tumor responses. Administration of exogenous IL-18 decreased T_{reg} cell accumulation and improved survival in a model of metastatic melanoma treated with either anti-PD-L1 or anti-CTLA-4 (137), suggesting that IL-18 may potentiate T_{eff} evasion from T_{reg} cell suppression. However, IL-18 also has pro-tumor effects, such as inducing the exhaustion of $CD8^+$ TILs (138), thus it remains to be determined how IL-18 impacts the fate of T_{reg} TILs. Taken together, these data suggest that IL-18 may promote the acquisition of T_h1-like characteristics and T_{reg} cell reprogramming in inflamed TMEs.

3.6.5. Acquisition of T_h2-like characteristics

On the other hand, the acquisition of T_h2-like features, is associated with a more stable T_{reg} cell phenotype. Indeed, GATA-3 promotes Foxp3 expression through direct binding to the Foxp3 locus (139). In addition, it drives their upregulation of CCR4 (140), which has been identified as mechanism of preferential recruitment of T_{reg} cells to the tumor bed (102). GATA-3 expression is associated with tissue-resident T_{reg} cells (86) and T_h2-like T_{reg} cells are enriched in melanoma compared to healthy skin (141). However, the direct role of GATA-3 in regulating the functional fate of T_{reg} cells, and their capacity to selectively inhibit T_h1 or T_h2 responses remains to be determined. Nonetheless, recent data supports the notion that the T_h2-adaptation of T_{reg} cells favors tumor-induced immunosuppression. GATA-3^+ T_{reg} cells co-express the IL-33 receptor ST2 (142), allowing them to fine-tune their function in response to inflammation. Our lab has shown that cells that expression of ST2 was increased in the stable T_{reg} cells that maintain Foxp3 expression upon adoptive transfer in lymphopenic (131). Indeed, $ST2^+$ T_{reg} cells are highly suppressive through high secretion of IL-10 and TGFβ (143). Furthermore, $ST2^+$ T_{reg} cells were found to predominate at advanced disease stages in a model of lung adenocarcinoma, in which conditional deletion of

ST2 in T_{reg} cells delays tumor growth (144). Moreover, ST2-deficient T_{reg} cells displayed diminished suppressive capacity and adopted a T_h1-like phenotype in B16 melanoma (145).

3.6.6. Acquisition of T_h17-like characteristics

Polarization of T_{reg} cells towards a Th17 phenotype is driven by TGFβ and IL-6 signaling and drives their upregulation of RORγt and CCR6 (119). These cells are found predominantly in tissues such as the gut and the kidney, alongside T_h17 responses (146). Our lab has shown that this phenotype is associated with increased rate of Foxp3 loss in lymphopenic mice (131). Nonetheless, RORγt$^+$ T_{reg} cells are potent suppressors of gut inflammation (147). T_h17-like T_{reg} cells are found at high frequencies in colon cancer (148). However, T_{reg} cells play paradoxical roles in the control of colon cancer development. In established primary lesions, T_{reg} TILs dampen anti-tumor T cell responses (149) and a specific subset of CD45RA$^-$ memory T_{reg} cells is correlated with worse prognosis (150). However, multiple reports correlate high T_{reg} frequencies with positive clinical outcomes (151–153). Indeed, the onset of colon cancer is linked to persistent gut inflammation, thus T_{reg} cells can protect from cancer through local IL-10 production (154). In this context, RORγt$^+$ T_{reg} cells were shown to play a pro-tumorigenic role by failing to control IL-6 production by DCs (155). However, the role of T_h17-like T_{reg} cells remains to be established in melanoma.

Thus, while T_{reg} cell play a key role in tumor-induced immunosuppression, numerous knowledge gaps remain regarding the relationship between stages of tumor growth and T_{reg} cell specialization, the factors that promote distinct T_{reg} cell adaptations in melanoma, their consequence on T_{reg} cell localization within hot and cold tumor microenvironments and the contribution of T_{reg} cells to primary and acquired resistance to treatment.

4. Place of immune checkpoint inhibitors in the therapeutic arsenal against melanoma

4.1. Place of immune checkpoint inhibitors in the treatment of solid cancers

While T_{reg} cell depletion induces tumor regression in preclinical models of melanoma, this potent anti-tumor efficacy comes at the cost of severe systemic autoimmunity (110). Thus, while T_{reg} cells represent an extremely attractive therapeutic target for the development of tumor immunotherapies, they have yet to be successfully harnessed for the safe and efficacious treatment of cancer in the clinic (156). Nonetheless, immunotherapy is at the forefront of therapeutic guidelines for the treatment of multiple metastatic cancers. ICIs are FDA-approved in a variety of tumors such as Hodgkin's lymphoma, melanoma, head and neck squamous cell carcinoma, renal cell carcinoma, non-small cell lung cancer and urothelial carcinoma. The three main cellular targets of these drugs are CTLA-4 (ipilimumab, tremelimumab), PD-1 (nivolumab, pembrolizumab, cemiplimab, tislelizumab, dostarlimab), and PD-L1 (atezolizumab, avelumab, durvalumab). ICIs are monoclonal antibodies (mAbs) that alleviate inhibitory signaling on T_{eff} and cytotoxic T cells by competing with their targets' natural binding partners. The rationale behind developing this pharmacological class was to increase TCR signal strength and activation of the effector and cytotoxic T cell compartments to amplify the anti-tumor response. The clinical efficacy of ICIs depends on the solid tumor type and is maximal in melanoma (157), which was the first indication for which these molecules received marketing authorization.

4.2. Therapeutic strategy in melanoma

If diagnosed at an early stage, the gold standard treatment is surgical resection. However, if a patient is at risk of local recurrence, pembrolizumab can be used as an adjuvant treatment to prevent relapse (158). At stage 3, surgical excision of the primary tumor and neighbouring lymph nodes is the standard of care. For patients presenting with $Braf^{V600E/K}$ mutations, a combination of

targeted therapies (signal transduction inhibitors: dabrafenib and trametinib) is indicated as adjuvant strategy (159). For patients with Braf-negative tumors, 3 immune checkpoint inhibitors have been approved: pembrolizumab, nivolumab (160) (anti-PD-1) and ipilimumab (161) (anti-CTLA-4). At stage 4, the primary lesion is usually non-resectable and metastasized distally. For patients with Braf-negative advanced melanoma, anti-PD-1 antibodies demonstrated superiority to chemotherapy (162) and are thus the recommended first line of treatment (163). Furthermore, combination of nivolumab and ipilimumab has shown to increase overall survival in advanced melanoma patients (5). Finally, recent phase II and III clinical trials indicate a benefit to using immunotherapy in a neoadjuvant setting, prior to surgical resection (164, 165).

4.3. The variable outcomes of immune checkpoint inhibition

4.3.1. Clinical assessment of responses

Checkpoint inhibitors have been a breakthrough in cancer immunotherapy, inducing durable remissions which can persist after treatment interruption in responding patients. Nonetheless, many patients do not experience a clinically significant response, defined by RECIST criteria as a reduction in the sum of the area of target lesions. These include partial responses, a >30% reduction of tumor burden compared to baseline with no appearance of new metastatic lesions, and complete responses which are defined as the disappearance of the primary tumor and distant metastatic nodules. While Overall Survival (OS) is the gold standard to assess efficacy in the clinic, it is usually considered too lengthy in the context of evaluation in clinical trials (166). Instead, Overall Response Rates (ORR), the percentage of patients whose cancer shrinks or disappears after treatment, and Progression-Free Survival (PFS), the average length of time after the start of treatment in which a person is alive and their cancer does not grow or spread, are the FDA-recommended primary endpoints to assess efficacy in phase III clinical trials.

Checkpoint inhibitors improve patient outcomes regardless of the clinical endpoint used: in the case of advanced melanoma, in a phase III-controlled study, the overall survival rate at one year was 72.9% in the nivolumab group compared to 42.9% with dacarbazine (162). The overall response rate of nivolumab is estimated around 44% at 6.5 years of follow-up (167). The median progression-free survival of melanoma patients receiving nivolumab in monotherapy is 6.9 months, and goes up to 11.5 months in combination with ipilimumab (168).

4.3.2. Pseudo- and hyper-progressions

Progression is defined as an increase in the size of lesions or the appearance of new lesions. While nivolumab and pembrolizumab display clinical superiority to chemotherapy and radiotherapy in a variety of solid tumors (169), they can be slower to induce tumor regression. Indeed, contrary to other treatment alternatives such as chemotherapy and radiotherapy, they rely on the induction of an adaptive anti-tumor response and do not induce direct cancer cytotoxicity and the immediate shrinkage that correlates with survival with these agents (170). As such, new criteria, such as iRECIST had to be established to account for the delayed efficacy of ICI (171) when defining the appropriate time points to assess primary endpoint in clinical trials. Indeed, pseudo-progressions are described in ~10% of patients treated with ICI, whereby patients undergo a response after an initial disease progression (172). Thus, it is recommended to confirm initial progression at least 4 weeks after initial assessment (171), and continuation of immunotherapy can be considered in patients that do not experience severe toxicity and whose disease-related symptoms improved (173). However, in another ~10% of patients, treatment with ICI induces cancer hyper-progression, a catastrophic outcome associated with higher mortality (174, 175) and an expansion of T_{reg} cells post-treatment (176). While the criteria diverge between studies, it is broadly defined as an increase in tumor growth rate following the initiation of ICI. The concept of

hyper-progression remains controversial as it is not defined against a control arm. Nonetheless, it is recommended to discontinue ICI in such outcomes (177).

4.3.3. Onset of immune-related adverse events

Treatment-induced toxicities are the other outcome that may require treatment discontinuation. Due to their absence of direct cellular toxicity, ICIs present with a much better safety profile than chemotherapy and radiotherapy (169). Indeed, no maximal tolerated dose was reached during phase I trials for nivolumab (178). Notably, most frequent toxicities associated with ICIs are immune-mediated and dubbed immune-related adverse events (irAEs). They are classified into early (skin, gastrointestinal, hepatic) and late (endocrine, renal, pulmonary) toxicities, based on median time of onset (179). Early toxicities are the most common forms of irAEs, including symptoms of diarrhea and colitis (10%), pruritus and skin rashes and occur within the first few weeks of treatment initiation (178). Most of these adverse events are mild, yet 10% of patients treated with nivolumab develop grade 3-4 adverse events (180). As such, fatal cases of colitis, pneumonitis, hepatitis and myocarditis have been reported (181). In the case of melanoma, the incidence of vitiligo is notably increased, up to 25% of patients during pembrolizumab treatment. Indeed, vitiligo is a pathology mediated by the infiltration of healthy skin by autoreactive Melan-A specific $CD8^+$ T cells, which indeed share antigen-specificity with melanoma cells (182). As such, heavy infiltrates of resident $CD8^+$ T cells are found in ICI-induced vitiligo lesions (183), and the onset of vitiligo is associated with tumor clearance (184), suggesting that this irAEs is mediated by tumor-specific T cells breaching peripheral tolerance in healthy tissue. Nonetheless, given the wide range of clinical manifestations, and their varying immunological nature (autoimmune, inflammatory, allergic), it is unlikely a single causal mechanism is at play.

Considering the critical role of T_{reg} cells in maintaining peripheral tolerance to self and non-

self-antigens, and the diversity of tissues affected, the question of T_{reg} dysregulation induced by checkpoint inhibitors is raised. Indeed, CTLA-4 and PD-1 are both expressed at steady state by T_{reg} cells. Thus, a prevalent hypothesis is that unintended effects of ICIs on T_{reg} cells could lead to a breach in tolerance. However, to date, the strongest statistical association with onset of irAEs is treatment efficacy (185). Thus, a better understanding of the factors that influence response to treatment, primary and acquired resistance and onset of irAEs is warranted to better identify patients that are susceptible to the development of these toxicities and to guide clinical practice regarding the discontinuation of ICI therapy and the timely assessment of treatment efficacy.

4.4. Hallmarks of response to immune checkpoint inhibitors

PD-1^+ cells are a highly heterogeneous population, spanning multiple cell types ($CD8^+$, $CD4^+$ T_{conv} and T_{reg}, but also B cells, macrophages, and dendritic cells), tissue types (tissue-resident, tumor-infiltrating, lymph-node dwelling, circulating) and functional states (recently primed, follicular helper cells, effector memory, progenitor exhausted, terminally exhausted). Thus, understanding of the differential consequences of checkpoint blockade on these different subsets is needed and the subject of intense research within the field.

4.4.1. Confirmed mechanisms of action of PD-1 blockade.

Increased infiltration of $CD8^+$ T cells is a major hallmark of response to treatment (186), and the presence of tumor-infiltrating lymphocytes pre-treatment is a pre-requisite of a successful response (45, 187). However, studies in preclinical models show that the efficacy of PD-1 blockade is maintained when inhibiting T cell egress from lymph nodes after tumor implantation, suggesting that anti-PD-1 does not increase infiltration through enhancing the migration of lymph-node dwelling cells to the tumor bed (188), but through increasing PD-1^+ TIL proliferation instead.

However, contrary to their stated rationale, anti-PD-1 mAbs do not reactivate anti-tumor responses by rescuing terminally dysfunctional $CD8^+$ TILs (189). Indeed, upon reaching a threshold of PD-1 signaling, exhausted cells become unresponsive to PD-1 blockade (190). Indeed, exhaustion represents a terminal differentiation state, with epigenetic reconfiguration of chromatin accessibility that prevents rescue of its effector functions by cytokines *in vitro* (62). Instead, anti-PD-1 provides a proliferative burst to progenitor exhausted $CD8^+$ T cells and prevents their differentiation into terminally exhausted cells (189).

The efficacy of anti-PD-1 antibodies is dependent on a CD28-mediated increase of PI3K/Akt signaling in these progenitor cells (191), which restores their effector functions, mainly the secretion of pro-inflammatory cytokines IFNγ, TNFα, and IL-2 (192, 193). Indeed, these polyfunctional $CD8^+$ cells have been shown to be the main effectors of tumor cytotoxicity *in vivo* (194), whereas terminally exhausted cells continue to produce large amounts of Granzyme B (64). In line with increased $CD8^+$ T cell function, increased $CD8:T_{reg}$ ratios have been associated with successful response to PD-1 blockade (195, 196), suggesting that $CD8^+$ T cells evade T_{reg} cell suppression locally. However, the mechanisms by which this ratio is modulated remain unclear.

Recently, analyses of immune cell topography identified that the spatial distribution of $CD8^+$ T cells in close proximity to tumor predicts response to PD-1 blockade (197, 198), a process tightly controlled by intra-tumoral chemokines. Indeed, the efficacy of anti-PD-1 is abrogated upon deletion of CXCR3 in preclinical models (188). As such, $CD8^+$ T cells preferentially localize in the vicinity of CXCL9/10-secreting macrophages within immune "hubs" of the TME, and progenitor exhausted cells co-localize with $CCR7^+$ DCs (199). Thus, during a successful response, anti-PD-1 increases the proliferation and function (200) of tumor-specific (180) $CD8^+$ T cells

which infiltrate the tumor core (43) and provide a positive feedback loop on inflammation by inducing the expression of interferon-stimulated genes in neighboring myeloid cells (199).

Importantly, anti-PD-1 and anti-PD-L1 antibodies differ by design from anti-CTLA-4 mAbs in their pharmacological mechanism of action, through the choice of their IgG subunit. Nivolumab, pembrolizumab (both humanized IgG4) and their murine counterpart used to evaluate preclinical efficacy, RMP1-14 (rat IgG2a), were designed to solely inhibit ligand binding, and not engage Fcγ receptors susceptible of inducing antibody-dependent cellular cytotoxicity (ADCC) (201). Indeed, RMP1-14 only binds with low affinity to mouse activating Fcγ receptors IIb, and switching its isotype to a mouse IgG1, diminished its efficacy by inducing ADCC of $CD8^+$ TILs (202). Interestingly, while atezolizumab (humanized IgG1) was also designed to minimize ADCC of PD-$L1^+$ T_{eff} cells, and increase $CD8^+$ T cell activation, murine data suggests that optimal efficacy of anti-PD-L1 is achieved through FcγR-induced deletion of PD-$L1^+$ macrophages (202).

4.4.2. Mechanisms of action of anti-CTLA-4 antibodies

On the other hand, anti-CTLA-4's efficacy relies on binding to activating Fcγ receptors (203). Indeed, in preclinical models, anti-CTLA-4 induces T_{reg} TIL depletion by tumor-infiltrating FcγRIV$^+$ macrophages *in vivo* (204). While ipilimumab induces human T_{reg} cell depletion *ex vivo* in the presence of $CD16^+$ Monocytes (205), and *in vivo* in humanized mouse models (206), it remains to be determined if this mechanism plays a role in the success of ipilimumab in the clinic. Indeed, while activation of NK cells, another effector of ADCC, has been linked with successful response to ipilimumab in patients (207), NK cell depletion did not affect the efficacy of anti-CTLA-4 in mice (204). Furthermore, some studies have failed to show significant T_{reg} cell depletion in melanoma patients (104, 208). Moreover, the murine anti-CTLA-4 clone 4F10 induced T_{reg} TIL expansion through CD28 (209), and ipilimumab expands suppressive T_{reg} cells

in the blood of melanoma patients (210). Furthermore, maximal efficacy of anti-CTLA-4 requires blocking CTLA-4 on both the T_{reg} and the T_{eff} compartment (211). As such, its T_{reg}-depleting effect remains controversial and expansion of $ICOS^+$ $CD4^+$ T_{eff} cells is the consensus hallmark of response to anti-CTLA-4 (212).

4.5. Proposed biomarkers of response to treatment

Despite retrospective data spanning over 10 years of use in the clinic, and active research, there is still no robust one-size-fits-all validated predictive biomarker of response to any ICI. This is partly due to non-immunological considerations such as availability of biopsy samples, variable choice of the time of sampling, heterogeneity between tumor lesions, use of cost-effective and readily available technology in a clinical laboratory setting, need for robust tests that withstand inter-operator variability and the difficulty to identify clear cut-off positivity thresholds. For example, PD-L1 expression by tumor cells, which can routinely be identified by immunohistochemistry and is an obvious candidate given the mechanism of action of anti-PD-1, is an FDA-approved companion test. Nonetheless, its use is only recommended for treatment with pembrolizumab in non-small cell lung carcinoma patients (213). Indeed, while PD-L1 positivity identifies a population with a higher response rate to PD-1 blockade (180), its negative predictive value is only 58% for nivolumab, as 20% of patients with PD-L1 negative tumors experience a successful response (5).

Nonetheless, immunological classifications of tumors, designed to support the clinical development of ICIs, proved to be a useful tool in research settings to better understand the features that correlate with beneficial outcomes. Indeed, features associated with hot TMEs, such as abundance of lymphocyte infiltration, localization of $CD8^+$ T cells within the tumor, presence of TLS, and M1 macrophage phenotypes all correlate with response (214), whereas cold tumor

features correlate with resistance to treatment (47). One of the main determinants of tumor immune phenotype is tumor type itself. As such, overall response rates vary depending on the nature of the solid tumor. In monotherapy, they are lower in non-small cell lung cancer (17% for nivolumab), and maximal in metastatic melanoma (44% for nivolumab) (reviewed in (157)). Furthermore, mismatch-repair deficiencies, which lead to considerable increase in DNA replication errors and thus generation of neoantigens in a variety of tumor types, increase the ORR to 40% in colorectal cancer patients (compared to 0% in mismatch-repair proficient tumors). Given its remarkable efficacy in this setting (215), pembrolizumab is now FDA-approved for the treatment of mismatch-repair deficient solid tumors, regardless of tumor site or histology, a first in oncology. This illustrates that tumor immunogenicity is a major driver of response to treatment, irrespective of tumor type.

Finally, Kumagai *et al.* proposed that the clinical outcome of immunotherapy is dictated by the T_{reg}:T_{eff} balance within PD-1 expressing TILs at treatment onset (216). Despite limited sample size, this simple ratio provided remarkable predictive value in metastatic melanoma, non-small cell lung cancer and gastric cancer, highlighting a potential role of T_{reg} cells in determining the variable outcomes of tumor immunotherapy.

5. Impact of immune checkpoint inhibition on regulatory T cells

5.1. Expression of checkpoint molecules identifies highly suppressive T_{reg} cells in circulation.

Despite ICIs being designed to target preferentially tumor-infiltrating T_{eff} cells, CTLA-4, PD-1, and a multitude of other checkpoint molecules are expressed by T_{reg} cells, even at steady state. As previously described, CTLA-4 is indeed one of the major suppressive mechanisms deployed by T_{reg} cells to tolerize DCs and limit the availability of co-stimulatory molecules to T_{eff} cells. As such, high levels of CTLA-4 expression denotes highly suppressive T_{reg} cells and increased rates of CTLA-4 internalization cripple T_{reg} cell function (217). LAG-3 is another checkpoint molecule that is constitutively expressed by T_{reg} cells and allows them to bind antigen-presenting cells through MHC-II and transduce inhibitory signals for dendritic cell maturation (94).

While they are not directly implicated in T_{reg} cell suppression, expression of ICOS and TIGIT also identify highly suppressive T_{reg} cells. Our lab and others have shown that ICOS co-stimulation plays a crucial role in the homeostasis of tissue-infiltrating T_{reg} cells at sites of inflammation (218). TIGIT expression identifies stably suppressive memory T_{reg} cells in humans (219). Furthermore, both ICOS and TIGIT-expressing T_{reg} cells are enriched in T_h1-like T_{reg} cells and are expert suppressors of Th1 responses (220, 221).

5.2. Biological roles of PD-1 in T_{reg} cells

On the other hand, despite high expression levels at steady state, the function of PD-1 in T_{reg} cells is not well established. PD-1 is not known to play a role in T_{reg} cell suppression. Indeed, T_{reg} cells from PD-1$^{-/-}$ mice do not display a diminished suppressive capacity and are found at a similar frequency in circulation (222). However, emerging roles are being proposed:

a) Restraining T_{reg} cell proliferation: This role was uncovered through the recent generation of conditional knockout models of PD-1 expression. In 2019, Kamada *et al.* developed a $CD4^{-Cre}$ $PD\text{-}1^{-loxP}$ mouse model and showed in bone marrow chimera experiments that $PD\text{-}1^{-/-}$ T_{regs} have a higher proliferative rate (176). Concurrently, Tan *et al.* generated $Foxp3^{-Cre}PD\text{-}1^{-loxP}$ mice and showed that, in their hands, $PD\text{-}1^{-/-}$ are more suppressive *in vitro* and outcompete WT T_{reg} cells for homing to the pancreas (223).

b) Promoting T_{reg} cell metabolism: PD-1 signaling promotes fatty acid oxidation, a metabolic program which is beneficial for T_{reg} cell development (224). As such, tamoxifen-inducible conditional deletion of PD-1, using $Foxp3^{-GFP\text{-}Cre\text{-}ERT2}$ $PD\text{-}1^{-loxP}$ mice reduced lipid metabolism in T_{reg} cells, leading to reduced survival in a lung cancer model (225).

c) Peripheral induction of T_{reg} cells: PD-1 has been shown to promote Foxp3 induction in naïve T cells by synergizing with TGFβ through Smad3 (103). Indeed, $PD\text{-}1^{-/-}$ $CD4^{+}$ T cells have a diminished capacity to differentiate into pT_{reg} cells when transferred into lymphopenic $RAG2^{-/-}$ mice (222).

d) Stabilization of Foxp3 expression: Foxp3 is the master transcription factor of T_{reg} cells and reduction of its expression is correlated with loss of suppressive activity and secretion of proinflammatory cytokines (117). Sustained activation of the PI3K/Akt pathway is known to destabilize Foxp3 expression (226) but is directly downmodulated by PD-1 signaling (227). Indeed, administration of nivolumab has been shown to downregulate Foxp3 expression *in vitro* (228). Furthermore, PD-1 was shown to inhibit expression of the Foxp3-cleaving asparagine endopeptidase in T-bet^{+} pT_{reg} cells (229).

e) Inhibiting the reprogramming of T_{reg} cells: *ex*$Foxp3^{+}$ cells are potently pro-inflammatory and contribute to $CD8^{+}$ T cell-mediated anti-tumor responses (129) and PD-1 expression affects

the ability of T_{reg} cells to reprogram. Foxp3$^{GFP\text{-}Cre}$ PD-1$^{fl/fl}$ mice, characterized by diminished Foxp3 expression and conditional absence of PD-1 expression, spontaneously develop lethal pancreatitis. However, this phenotype can be rescued by adoptive transfer of T_{reg} cells isolated from PD-1$^{-/-}$ mice. The breeding of FoxP3$^{GFP\text{-}Cre}$ with Rosa26^{RFP} mice, a Cre-reporter strain, allows stable *in vivo* labeling of the cells that once expressed GFP. Fate mapping experiments showed that cells from Foxp3^{GFPCre} PD-1$^{fl/fl}$ mice have an increased tendency to lose Foxp3 expression during their growth, characterized by the Foxp3-GFP^{-} RFP^{+} phenotype (230), suggesting *ex*Foxp3^{+} cells are pathogenic. Nonetheless, it remains to be determined if PD-1 deletion induces T_{reg} cell reprogramming in TMEs and if this contributes to increased anti-tumor responses.

Taken together, these results suggest that PD-1 does not play a role in T_{reg} cell function but regulates their homeostasis, fitness, and lineage stability in tissues, thus contributing to the regulation of the T_{reg}/T_{eff} balance. pT_{reg} cells could be more sensitive to this effect as partial methylation of their demethylated evolutionarily conserved *foxp3* locus renders them more sensitive to loss of Foxp3 expression (231). However, knowledge gaps remain regarding the consequences of PD-1 expression on T_{reg} cells. While T_{reg} TILs express PD-1, it is unclear whether they undergo exhaustion in the same sense than CD8^{+} TILs. Indeed, circulating T_{reg} cells share several defining characteristics of exhausted cells such as high expression of multiple inhibitory checkpoint molecules, inability to secrete pro-inflammatory cytokines and increased rates of fatty acid oxidation. Thus, it has proven difficult to identify a readout for the consequences of PD-1 signaling on T_{reg} cells. Furthermore, exhaustion dampens T_{eff} cell proliferation, hampering our ability to determine intrinsic T_{reg} cell suppressive function in tumor environments *in vivo*. In addition, while lactic acid has been shown to promote PD-1 expression in T_{reg} cells in glycolytic TMEs (232), it remains unknown whether the PD-1 expression profile differs between hot and

cold TMEs, and whether T_{reg} cells express similar levels of PD-1 than their T_{eff} counterparts. Indeed, T_{reg} cells preferentially consume IL-2, and Stat5 signalling has been shown to override PD-1 inhibition upon chronic antigenic exposure (233).

5.3. Functional consequences of PD-1 blockade on T_{reg} cells.

Given their constitutive expression of checkpoint molecules, a prevalent hypothesis is that unintended effects of ICIs on T_{reg} cells could lead to a breach in tolerance. Indeed, T_{reg} cells are depleted by anti-CTLA-4 (205) and anti-TIGIT (234) anti-ICOS antibodies (235), and antibody-mediated inhibition of LAG-3 reduces T_{reg} suppression *in vitro* and *in vivo* (236).

In the case of anti-PD-1 the consequences of PD-1 blockade on T_{reg} cell functional fate are ill-defined (**Figure 5**). Given its role in stabilizing Foxp3 expression, it has long been hypothesized that PD-1 blockade antagonizes T_{reg} functional stability in inflammatory environments. However, in experimental models where only T_{reg} cells can bind the antibody, administration of anti-PD-1 (*i*) increases T_{reg} cell proliferation and overall suppression *in vitro* and (ii) accelerates tumor growth *in vivo* (176). Furthermore, Kamada *et al.* identified increased proliferation of T_{reg} cells post-treatment in patients with gastric cancer experiencing tumor hyper-progression upon ICI (176), highlighting that the functional impact of PD-1 blockade on T_{reg} cells can influence the success of immunotherapy. Yet, it is unclear how to reconcile these findings with the onset of potent anti-tumor responses and irAEs in high responder patients, and by which mechanisms $CD8^+$ T cells evade T_{reg} cell suppression in highly inflamed TMEs. Furthermore, PD-1 blockade could contribute to the induction of *ex*$Foxp3^+$ cells which have been shown to contribute to anti-tumor immunity. Taken together, numerous knowledge gaps persist regarding mechanisms of action of anti-PD-1 mAbs on T_{reg} cells, dynamics of PD-1 expression and T_{reg} cell function throughout

tumor growth and checkpoint inhibition therapy. Therefore, a better understanding of how PD-1 signaling affects the adaptation of T_{reg} cells to inflammatory signals is warranted.

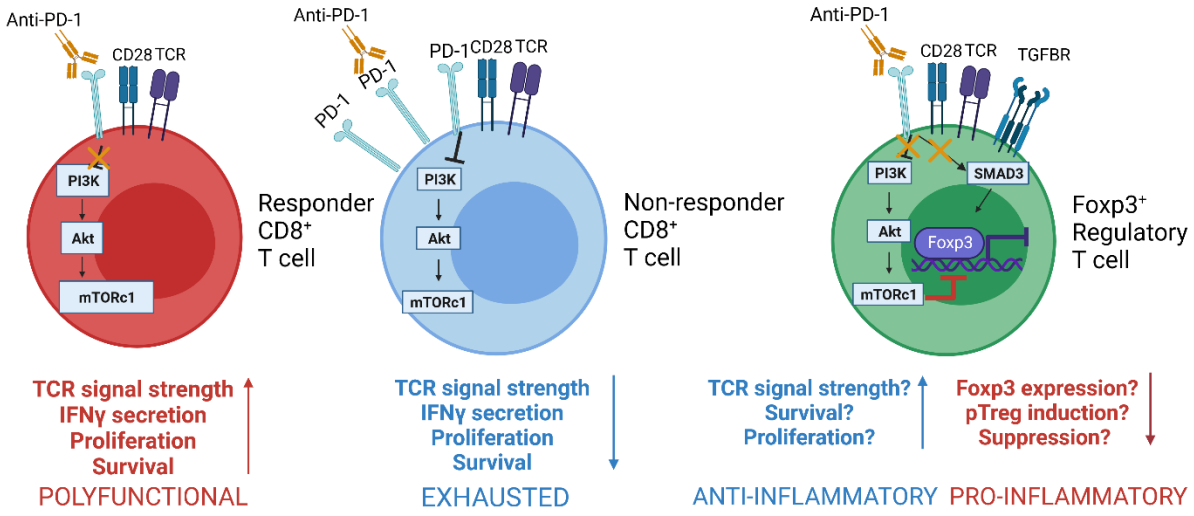

Figure 5. The functional consequences of PD-1 blockade on T_{reg} cells are ill-defined.

Upon PD-1 blockade, responder $CD8^+$ T cells increase their proliferation, survival, IFNγ secretion and do not differentiate in terminally-exhausted cells. Over a threshold of PD-1 inhibitory signaling and terminal differentiation, non-responder $CD8^+$ T cells fail to reactivate in response to anti-PD-1. Increasing T_{reg} cell activation increases their survival, proliferation, and suppressive function in a subset of patients with tumor hyper-progression. However, as high levels of PI3K signaling destabilize Foxp3 expression, it has been hypothesized that anti-PD-1 inhibits pT_{reg} induction and dysregulates T_{reg} cell suppressive function in high responder patients. Created with Biorender.com®

6. Rationale

Although ICIs were designed to target exhausted T_{eff} cells within the tumor microenvironment, anti-PD-1 mAbs have the potential to target T_{reg} cells given their high basal expression of PD-1. This is critical, as T_{reg} cells play important roles in the maintenance of peripheral tolerance and in restraining anti-tumor activity. The onset of irAEs associated with ICI use suggests checkpoint blockade may lead to a systemic dysregulation of T_{reg} cell homeostasis. Incidentally, protection by ipilimumab stems from antibody-dependent cell-mediated cytotoxicity of tumor-infiltrating CTLA-4$^+$ T_{reg} cells by FcγRIIIA$^+$ monocytes (205), demonstrating the potential for T_{reg} dysregulation by some ICIs.

Knowledge gaps remain regarding (*i*) the dynamics of T_{reg} infiltration throughout tumor growth or PD-1 blockade, (*ii*) how CD8$^+$ T cells overcome T_{reg} cell suppression and (*iii*) the mechanisms through which irAEs arise. Furthermore, despite Helios being a putative binding partner to the *PDCD1* promoter, little is known regarding the interplay between Helios and PD-1 expression, and how PD-1 signalling, or blockade affects Helios expression as well as T_{reg} cell fitness, adaptation, and overall functional fate in tumor microenvironments. *Understanding the effect of anti-PD-1 on T_{reg} cell survival, differentiation and function may lead to a better understanding of acquired resistance to treatment, onset of adverse events and lead to the development of preventive therapies for irAEs and novel strategies to enhance anti-tumor immunity.*

While the hallmarks of response to treatment are well characterised for CD8$^+$ T cells, little is known about the effect of anti-PD-1 mAbs on T_{reg} cells. PD-1 signaling impacts PI3K/Akt signaling, a pathway implicated in TCR signaling and activation, which controls T cell metabolism, differentiation, and acquisition of effector functions (227). In the context of an anti-tumor immune response, PD-1 blockade has the potential to impact T cell priming, activation and

migration to and within the tumor, as well as their proliferation and survival. In a T_{reg} cell intrinsic view, these effects would be anti-inflammatory by increasing T_{reg} cell fitness. However, high levels of Akt signaling promote the acquisition of T_h1-like characteristics by T_{reg} cells (237), suggesting that PD-1 blockade might favor this adaptation. Furthermore, it could render these cells T_h1-like cells more sensitive to epigenetic destabilization of Foxp3 expression (103), leading to secretion of IFNγ (117) and possibly loss of Foxp3 expression itself (230), ultimately dysregulating T_{reg} cell phenotype in inflammatory environments. Furthermore, PD-1 blockade could skew the profile of the cytokines and alarmins secreted in the tumor microenvironment towards pro-inflammatory molecules that further destabilize Foxp3 expression and inhibit Foxp3 induction in tumor-infiltrating $CD4^+$ T cells. Moreover, given the synergy between PD-1 and TGFβ, a reduction in peripheral Foxp3 induction following PD-1 blockade could curtail tumor-induced immunosuppression, but also potentially lead to a breach in tolerance in barrier tissues like the gut, where pT_{reg} induction plays a key role in local immune homeostasis (238) (**Figure 6**).

Thus, this work examined the overarching hypothesis that while anti-PD-1 can induce T_{reg} cell activation and proliferation, thereby counterbalancing the increase in T_{eff} cell activation, and mediating resistance to treatment in cold TMEs, it also induces induce phenotypic adaptations that dysregulate T_{reg} cell function and/or fate in hot TMEs, which are required for the success of checkpoint inhibition.

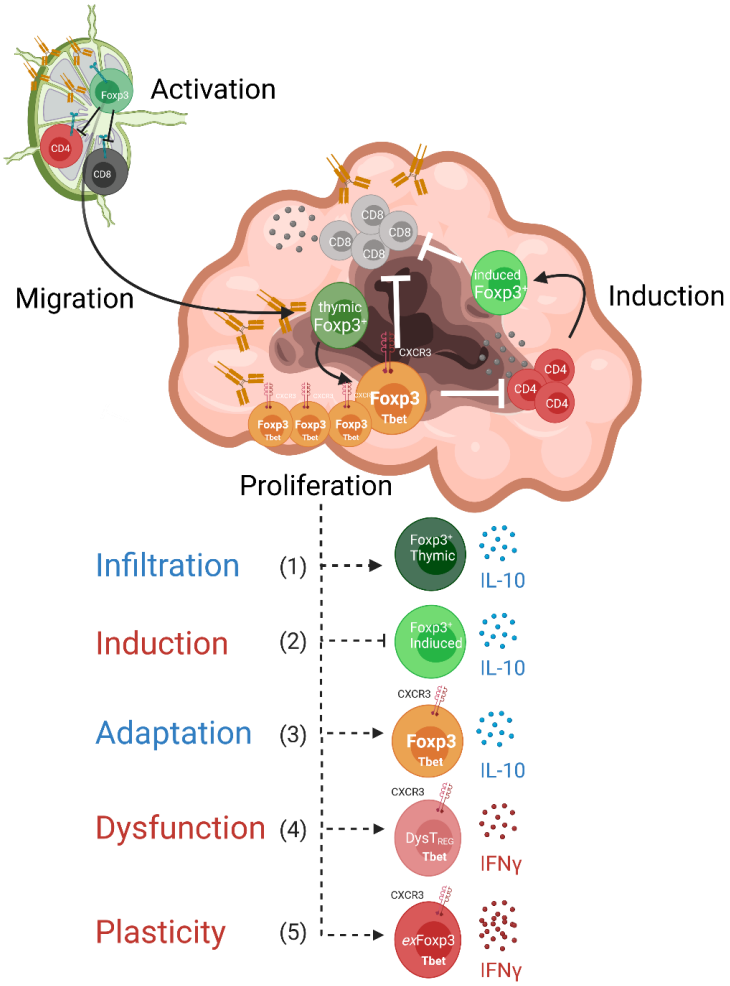

Figure 6. Rationale for assessing the functional consequences of PD-1 blockade on T_{reg} cells.

PD-1 plays a role at numerous stages of the T_{reg} cell life cycle and is expressed not only by tumor-infiltrating T_{reg} cells, but also by effector T_{reg} cells in circulation. (1) PD-1 blockade at the time of T_{reg} cell priming could increase activation and migration to the tumor. (2) Inhibiting PD-L1 ligation on T_{conv} cells could increase the amount of TGFβ signaling required for pT_{reg} cell induction. (3) Increasing $CD8^+$ TIL function could trigger the local production of type 1 inflammatory signals which favor T_{reg} cell functional adaptation to dampen anti-tumor responses. (4) High levels of Akt signaling could trigger IFNγ production by T-bet$^+$ T_{reg} cells and ultimately (5) cause a loss of Fopx3 expression. Created with Biorender.com®.

7. General Objectives

The hypothesis that PD-1 blockade increases T_{reg} cell activation and proliferation but dysregulates their suppressive function in highly inflamed TMEs has been tested by experiments based on the following three objectives:

1) Investigate the consequences of anti-PD-1 on local and systemic T_{reg} cell homeostasis in a melanoma model that is poorly responsive to anti-PD-1 (Chapter 2, manuscript in preparation)
2) Investigate the effects of anti-PD-1 on T_{reg} cell functional fate in a highly immunogenic melanoma model (Chapter 3, manuscript submitted)
3) Investigate the impact of IL-18 signaling on the T_h1-like functional adaptation of T_{reg} cells in melanoma and successful response to anti-PD-1 (Chapter 4, manuscript in submission)

Chapter 2 – PD-1 signaling dampens Helios^{+} T_{reg} cell activation levels in cold and hot murine models of melanoma.

Bridging statement for chapter 2

The use of ICIs has provided a significant amelioration of advanced melanoma prognosis (239). Yet, the majority of patients do not respond to treatment (240), thus preclinical models are needed to better understand the mechanisms underlying primary and acquired resistance to treatment, as well as the conditions that enable successful tumor clearance. The B16 melanoma cell line was the gold standard during the preclinical development of ICIs, yet it does not respond to PD-1 blockade in monotherapy (195, 241, 242). Foxp3$^+$ regulatory T (T_{reg}) cells play a dominant role in preventing the rejection of syngeneic melanomas in preclinical models (107, 110), yet little was known on their contribution to ICI resistance. Specific knowledge gaps concerned (*i*) the impact of PD-1 signaling on their functionality, as T_{reg}-specific knockout models were not generated until 2020 (223), (*ii)* if PD-1 expression levels differ in various tumor environments, and (*iii*) how does this impact their response to PD-1 blockade? We hypothesized that PD-1 blockade on T_{reg} cells could increase their activation and proliferation, counterbalancing the reactivation of CD8$^+$ TILs and causing treatment failure.

In this chapter, we perform the first in depth immune characterization of two novel melanoma models which recapitulate key aspects of human pathogenesis (23, 25) and characterize the different profiles of PD-1 expression by TILs in both models. Through *in vitro* modeling, we establish that PD-L1 restrains T_{reg} cell activation levels and identify features reminiscent of immune exhaustion in T_{reg} cells at tumor endpoint. Furthermore, we characterize the responsiveness of D4M.3A tumors to ICI therapy and identify that anti-PD-1 increases the expansion and activation levels of T_{reg} cells both locally and systemically in a model displaying acquired resistance to treatment.

PD-1 signaling dampens Helios^{+} T_{reg} cell activation levels in cold and hot murine models of melanoma.

Mikhaël Attias[1,2,3], Fernando Alvarez[1,2,3], Tho-Alfakar Al-Aubodah[1,2,3], Roman Istomine[1,2,3], Yujian Yang[1,2,3], Laura Widawski[1,2,3], Abrahim Sleiman[1,2,3], Constantin Polychronakos[4,5], Ciriaco A. Piccirillo[1,2,3]

Affiliations:

[1]Department of Microbiology and Immunology, McGill University, Montréal, Québec, Canada

[2]Program of Infectious Diseases and Immunity in Global Health, Centre for Translation Biology (CTB), The Research Institute of the McGill University Health Centre (RI-MUHC), Montréal, Québec, Canada

[3]Centre of Excellence in Translational Immunology (CETI), McGill University, Montréal, Québec, Canada

[4]Division of Pediatrics, McGill University, Montréal, Québec, Canada

[5]Department of Human Genetics, McGill University, Montréal, Québec, Canada

* Correspondence should be addressed to:

Dr. C.A. Piccirillo
Research Institute of McGill University Health Centre (MUHC)
Centre for Translational Biology, Bloc E, Room E-M2.3248
1001 Boul. Décarie, Montréal, Québec, H4A 3J1
ciro.piccirillo@mcgill.ca
Tel: 514-934-1934 ext. 76143

Keywords: Foxp3+ Treg cells, anti-PD-1, anti-CTLA-4, immuno-oncology, checkpoint inhibitors, melanoma, treatment biomarkers.

Manuscript in preparation

Abstract

Immune checkpoint inhibitors targeting CTLA-4 and PD-1 were designed to counteract the exhaustion of melanoma-infiltrating effector T cells. While they have improved the survival rate of patients with advanced melanoma, most patients do not respond to treatment. To further our understanding of the immunological mechanisms of treatment resistance, new preclinical models that respond to checkpoint blockade in monotherapy are required. Here, we characterized the immune phenotype and T cell responses in two preclinical models of melanoma that harbor Braf and PTEN mutations, the most common combination of genetic alterations found in the clinic. First, we show that the D4M.3A melanoma displays a cold immune phenotype with limited T cell infiltration and a partial response to anti-PD-1 and anti-CTLA-4. Increased inflammation was associated with a local and systemic expansion of Helios^{+} T_{reg} cells displaying reduced PD-1 expression and a more highly activated phenotype, suggesting T_{reg} cells counteract the anti-tumor efficacy of checkpoint blockade. Contrary to D4M.3A, YUMMER1.7 melanomas, which share the same Braf and PTEN mutations, display a potent T cell response that is countered by abundant T_{reg} cell infiltration and robust expression of PD-1, driving CD8^{+} T cell exhaustion, and enabling the tumor to evade immune responses. Importantly, T_{reg} cells also display PD-1 expression and phenotypic signs of exhaustion, denoting that T_{reg} cell fitness decreases with tumor growth and that T_{reg} cell reactivation upon PD-1 blockade contributes to acquired resistance to treatment in cold TMEs.

Introduction

Immune checkpoint inhibitors (ICIs) targeting CTLA-4 and PD-1 have been a breakthrough in the treatment of advanced melanoma. Indeed, the median progression-free survival of melanoma patients receiving nivolumab (anti-PD-1) in monotherapy is 6.9 months and goes up to 11.5 months in combination with ipilimumab (anti-CTLA-4) (1). Nonetheless, most patients do not experience a reduction in the sum of target lesions (2), the threshold used to define an objective response in clinical trials (3). While there is a lack of robust predictive biomarkers of response to treatment (4), the presence of tumor-infiltrating lymphocytes prior to treatment is required for treatment success (5). However, the B16 cell lines which have long been considered a gold standard during the preclinical development of ICIs display low mutational burden and lymphocyte infiltration (6). As such, while ICIs are used in monotherapy in the clinic, seminal papers have relied on adjuvant strategies such as vaccination (7–9) and adoptive transfer of tumor-specific T cells (10) to demonstrate the efficacy of anti-CTLA-4 and anti-PD-1 mAbs in murine models. To better understand the immunological mechanisms of treatment success and failure, it is necessary to develop new melanoma models that recapitulate hallmarks of human melanoma pathophysiology and response to ICI.

Melanoma is the solid tumor type with the highest overall response rates to immunotherapy (11). Indeed, it is considered a “hot” tumor type due to its characteristically high mutational load (12), which generates neoepitopes and thus, increases the diversity of antigens available for T cell recognition. Nonetheless, Braf and PTEN loss, the most common combination of genetic alterations found in melanoma lesions (13), are insufficient to render the melanoma TME immunologically “hot”, in part due to the absence of UV mutations, in a tamoxifen-inducible model of melanoma growth (14). Specifically, these tumors display tolerogenic dendritic cells with

high PD-L1 expression (15), and abundant Myeloid-Derived Suppressor Cells (MDSCs) and Tumor-Associated Macrophages (TAMs) infiltration which contribute to T cell exclusion (16, 17). To better rationalize the processes that occur in poorly immunogenic melanomas, we explored the immune landscape that develops during the expansion of a Dartmouth Murine Mutant Malignant Melanoma (D4M.3A) ($Braf^{V600E}$ $PTEN^{-/-}$), a cell line that was generated for the preclinical development of targeted therapies (18). As such, characterization of their immune phenotype and response to ICI is still lacking.

The high success rate of ICIs suggests that immune exhaustion is a predominant mechanism of immune evasion in melanoma. Nonetheless, it remains to be determined if resistance to treatment is driven by tumor-intrinsic mechanisms such as lack of T cell infiltration (19) or adaptive mechanisms such as tumor-induced immunosuppression. Indeed, $Foxp3^{+}$ regulatory T (T_{reg}) cells, which play a dominant role in promoting an immunosuppressive melanoma tumor microenvironment (TME) (20, 21), also express CTLA-4 and PD-1. In particular, the ratio of intra-tumor CD8:T_{reg} amongst PD-1 expressing cells has been proposed as a predictive biomarker of response to treatment (22). Yet, little is known about the differences in T_{reg} cell infiltration and PD-1 expression levels between responding and non-responding tumors. For example, while a subset of circulating memory $Helios^{+}$ T_{reg} cells expresses PD-1 (23, 24), it is unclear whether T_{reg} tumor-infiltrating leucocytes (TILs) undergo immune exhaustion in tumor micro-environments (TMEs) (25), and whether, akin to $CD8^{+}$ TILs, PD-1 expression levels impact the functional consequences of checkpoint blockade on T_{reg} cells (26). As such, characterizing the differences in PD-1 expression by T_{reg} cells in hot and cold TMEs is key to understanding the variable outcomes of immunotherapy. Successful response to ICIs is associated with the onset of immune-related adverse events (irAEs), suggesting a systemic dysregulation of T_{reg} cell function (27). On the other

hand, anti-PD-1 was shown to promote T_{reg} cell activation and proliferation in a subset of gastric cancer patients that underwent an acceleration of tumor growth upon treatment (28). As PD-1 restrains T_{reg} cell proliferation (29), we hypothesized that increasing the activation of T_{reg} TILs constitutes a mechanism of acquired resistance to PD-1 blockade in cold TMEs.

To study the impact of PD-1 signaling and its blockade on T_{reg} cell functional dynamics in melanoma, we characterized systemic and melanoma-infiltrating T_{reg} cell phenotypes in the D4M.3A preclinical model. We show that D4M.3A tumors display a "cold" immune phenotype and a minor delay in tumor growth in response to anti-PD-1, denoting an acquired resistance to treatment (30). PD-1 blockade reduced PD-1 expression levels by T_{reg} cells, leading to an expansion of highly-activated, Helios^{+} T_{reg} cells, both locally and systemically. While a combination of anti-PD-1 and anti-CTLA-4 showed increased anti-tumor efficacy, it further increased local T_{reg} cell activation and proliferation. When we compared this response to the highly immunogenic YUMMER1.7 melanoma model (31), Helios^{+} T_{reg} cell infiltration was more abundant, and T_{reg} TILs displayed a highly activated phenotype with $T_{h}1$-like features, namely T-bet and IL-18R expression, suggesting a functional specialization that is absent in D4M.3A tumors. Furthermore, PD-L1 signaling dampened their activation levels, indicating that T_{reg} cells undergo a form of immune exhaustion throughout tumor growth. Thus, reactivation of Helios^{+} T_{reg} TILs contributes to the acquired resistance to checkpoint blockade.

Material and Methods

Mice

C57Bl/6.Foxp3$^{IRES\text{-}mRFP}$ reporter knock-in (Foxp3^{RFP}) mice were provided by Jonathan Spicer. C57Bl/6.Foxp3$^{IRES\text{-}mRFP}$.Helios$^{IRES\text{-}GFP}$ dual reporter knock-in (Foxp3^{RFP}-Helios^{GFP}) mice were provided by Ethan Shevach. Wild Type C57Bl/6 mice were purchased from Charles River Laboratories. All mice used were males and 8 to 14 weeks of age, the examiner was blinded to group repartition until the end of the analysis.

Tumor cell lines

The D4M cell lines were derived from the tamoxifen-inducible, Braf/PTEN conditional model of melanoma (14, 18). D4M.3A cells were kindly provided by Dr. Sonia Del Rincon (McGill University) and cultured in Dulbecco's Modified Eagle Medium (DMEM, Wisent), supplemented with 10% FBS (Wisent) and 1% Penicillin/Streptomycin (Wisent). The YUMMER1.7 cell line was generated by Wang and colleagues by irradiating Braf^{V600E} PTEN$^{-/-}$ Cdkn2a$^{-/-}$ cells and expanding a single clone bearing additional somatic mutations (31). YUMMER1.7 cells were kindly provided by Dr. Marcus Bosenberg (Yale University) and cultured in advanced DMEM/F12 supplemented with 10%FBS (Wisent), 1% Penicillin/Streptomycin (Wisent) and 1% MEM Non-essential Amino Acids (Wisent). Tumor cells were tested for mycoplasma and viral contamination by the McGill Comparative Medicine Animal Resources Centre. Cells were expanded in 225 cm^2 tissue culture flasks and $4x10^6$ cells/ml were frozen down and stored in 10% DMSO/FBS in liquid nitrogen. Prior to injection, cells were thawed and passaged twice at 37°C in humidified air with 5% CO_2 and washed twice in cold PBS before preparation of the inoculum.

***In vivo* tumor studies**

D4M.3A cells were resuspended in PBS and then mixed in Corning® Matrigel Basement Membrane HC at a 1:1 PBS to Matrigel ratio. D4M.3A ($1x10^5$) cells were injected subcutaneously in the right flank of male mice, under anesthesia. For evaluation of anti-PD-1 monotherapy, WT C57Bl/6 mice were used. In subsequent experiments, we used $Foxp3^{RFP}$ mice which displayed similar kinetics of tumor growth than WT mice. Mice were monitored thrice weekly. Tumor volumes were measured using an electronic calliper and calculated as: length x $width^2$ x 0.5. Experimental endpoint was defined as the day on which one mouse reached humane endpoint (tumor volume > $1500mm^3$). At necropsy, tumors were harvested, and their weights and volumes were measured post-mortem. Once every tumor had reached palpability (day 8), mice were randomly attributed to a treatment group. They received 5 doses of either 250µg of anti-PD-1 (clone RMP1-14, BioXcell) or isotype control (rat IgG2A, BioXcell) intraperitoneally, thrice weekly. For evaluation of combination ICI, mice received 5 doses of 250µg of anti-PD-1, with or without 5 doses of 200µg of anti-CTLA-4 (clone 9H10, BioXcell). At experimental endpoint, all mice were sacrificed, and we harvested tumors, tumor-draining inguinal lymph nodes, non-tumor draining contralateral lymph nodes, and spleen. All mice were cohoused from birth and the efficacy of ICI did not vary significantly across experiments.

YUMMER1.7 cells were resuspended in PBS and then mixed in Corning® Matrigel Basement Membrane HC at a 1:1 PBS to Matrigel ratio. D4M.3A ($1x10^5$) or YUMMER1.7 cells ($2.5x10^5$) were injected subcutaneously in the right flank of male mice, under anesthesia. Mice were monitored thrice weekly. Experimental endpoint was defined as the day on which one mouse reached humane endpoint (tumor volume > $1500mm^3$). At necropsy, tumors were harvested, and

their weights and volumes were measured post-mortem. At experimental endpoint, all mice were sacrificed, and we harvested tumors, tumor-draining axillary and inguinal lymph nodes, non-tumor draining contralateral lymph nodes. Foxp3^{RFP} and Foxp3^{RFP}-Helios^{GFP} reporter mice displayed the same kinetics of tumor growth as WT C57Bl/6 mice.

Isolation of tumor-infiltrating lymphocytes

After CO_2 euthanasia, tumors were collected in serum-free Hank's Balanced Salt Solution (Wisent), then minced manually in <1mm^3 pieces using razor blades. Tumors were then digested in the presence of collagenase IV (1mg/ml, Gibco) and DNAse I (0.005µM, Sigma-Aldrich) at 37°C for 1 hour. Cells were then pushed through a 21G needle and washed in cold complete RPMI 1640 with 5% FBS. Red blood cells were lysed by incubating the cells for 30 seconds with ACK buffer, washed, resuspended in complete RPMI 1640, and filtered twice through a 70µm mesh.

Purification of immune cell subsets

Prior to FACS-sorting splenocytes and TILs, CD4$^+$ and CD8$^+$ T cells were purified using CD4/CD8 TIL Microbeads (Miltenyi) and an autoMACS (Miltenyi). T_{reg} cells were sorted as CD4$^+$ RFP$^+$, T_{resp} cells were sorted as either CD4$^+$ RFP$^-$ or CD8$^+$ RFP$^-$ cells (purity>99%) using a FACSAria™ (BD Biosciences). Antigen-presenting cells were sorted as live CD45$^+$ MHC-II$^+$ from splenocytes and TILs. Accessory cells were purified from the negative fraction of the CD4/CD8 MACS and mitomycin-C inactivated for 1 hour at 37°C.

***In vitro* T cell assays**

CD4$^+$ RFP$^+$ T_{reg} cells, CD4$^+$ RFP$^-$ T_{conv} and CD8$^+$ T cells were sorted from the splenocytes or endpoint tumors of untreated YUMMER1.7-bearing mice. For comparison of antigen-presenting cell potency, live splenic and tumoral APCs (1x10^5) were co-cultured with splenic T_{conv} or CD8$^+$ T cells (5x10^4) in RPMI 1640 (Wisent) supplemented with 10%FBS in the presence of

soluble αCD3 (0.5µg/mL) for 72 hours at 37°C, in 96-well flat bottom plates (0.2ml). For assessment of $CD8^+$ TIL proliferation, splenic or TIL $CD8^+$ T cells ($5x10^4$) were co-cultured with mitomycin-C inactivated accessory cells ($1x10^5$) in RPMI 1640 (Wisent) supplemented with 10%FBS in the presence of soluble αCD3 (0.5µg/mL) and recombinant human IL-2 (100U/ml) for 72 hours at 37°C, in 96-well flat bottom plates (0.2ml).

***In vitro* activation with PD-L1-Fc**

FACS-sorted $CD4^+$ RFP^+ T_{reg} cells isolated from either the spleen or endpoint tumors. $CD4^+$ RFP^- splenic T_{conv} cells were labelled with CellTrace™ Violet (Thermofisher). T_{conv} cells ($5x10^4$) and T_{reg} cells ($2.5x10^4$) in RPMI 1640 (Wisent) supplemented with 10%FBS were placed in 96-well flat-bottomed (0.2ml) plates previously coated with αCD3 (3µg/ml), αCD28 (1µg/ml) +/- PD-L1-Fc (5µg/ml, R&D systems). Cells were then incubated for 72 hours at 37°C, then washed and stained for flow cytometry analysis.

Flow cytometry analysis

After lymphocyte isolation, the cells were washed in PBS and stained with antiCD16/CD32 (clone 2.4G2, BD) and fixable viability dye eFluor780 or 506 (Thermofisher). Following a wash, cells were marked with extracellular markers. For analysis of Foxp3-reporter protein expression, cells were acquired live within one hour of extracellular staining. For analysis of other transcription factors, cytokine secretion and intracellular markers, cells were fixed and permeabilized with the Foxp3 Transcription Staining Buffer Set (eBioscience™) and then stained for intracellular markers). Samples were acquired on the same day of the intracellular staining using a BD Fortessa LSR-X20 and analyzed using FlowJo v10 (TreeStar and BD). The following anti-mouse antibodies were used: CD45.2 (clone 104), CD19 (clone 1D3), CD11c (clone HL3), I-A[b] (clone AF6-120.1), CD86 (clone GL1), Ly6C (clone AL21), PD-L1 (clone MIH5), CD3 (clone 17A2), CD8a

(clone 53-6.7), CD8b (clone H35-17.2), PD-1 (clone J43), Ki67 (clone B56), KLRG1 (clone 2F1), IFNγ (clone XMG1.2), IL-2 (clone JES6-5H4), TNFα (clone MP6-XT22), RORγt (clone Q31-378) from BD; CD4 (clone RM4-5), CTLA-4 (clone UC-4B9), Helios (clone 22F6), Bcl-2 (clone BCL/10C4), GRZB (clone Q16A02), Ly6G (clone 1A8) from Biolegend; Foxp3 (clone FJK-16S), ICOS (clone C396.4A), T-bet (clone 4B10), TIGIT (clone GIGD7), CD25 (clone PC61.5), CXCR3 (clone CXCR3-173), IL-17A (clone ebio17B7), F4/80 (clone BM8), CD11b (clone M1/70) from eBioscience.

Statistical analysis

Unless otherwise stated, all data is depicted as mean +/- 95%CI. For tumor growth curves, multiple comparisons were made using a mixed-effects analysis with a Geiser-Greenhouse correction for sphericity and a Sidak correction for multiple comparisons. Tumor weights at endpoint were compared using a two-tailed unpaired t-test with Welch's correction.

For flow cytometry data, the normality of each data set's distribution was determined with a Shapiro-Wilk test. Homoscedasticity was tested using Fisher's test. If both conditions were met, when applicable, proportions and MFIs were compared using ordinary One-Way ANOVA with a correction to account for multiple comparisons. If the normality condition was not met, a non-parametric Mann-Whitney test was used. For experiments without treatment, MFI fold changes were calculated by dividing each MFI measurement by the average MFI in the isotype control group for a given experiment. Correlation matrixes were generated by computing Pearson r-correlates with tumor weight at endpoint for each variable and represented as a heatmap. For linear correlation analyses, all data points were pooled to calculate linear correlations. The slope's deviation from zero was evaluated using Fisher's test. All statistical analysis was conducted using GraphPad Prism v10.1.

For *in vitro* experiments, all conditions were realized in triplicates (n=3) and each experiment was repeated three times (N=3). Data is shown from N of 1 representative repeat.

Study approval

All mice were housed and bred in specific pathogen-free conditions in the same facility and used according to the regulations of the Canadian Council of Animal Care Guidelines and Animal Care and Use Committees at McGill University.

Data availability

Numerical data values presented in the graphs are uploaded as supplementary material. FCS files generated by flow cytometry are available upon request from the corresponding author.

Results

T_{reg} cells respond to PD-1 blockade.

While T_{reg} cells express PD-1 and play an important role in melanoma-induced immunosuppression, their response to PD-1 blockade remains ill-defined. Yet, their preferential reactivation over $CD8^+$ T cells in TMEs could contribute to a failure to respond. Thus, we investigated the local and systemic impact of anti-PD-1 monotherapy on T_{reg} cell phenotype in the D4M.3A murine melanoma, a $Braf^{V600E}/PTEN^{-/-}$ cell line that recapitulates key aspects of melanomagenesis (14, 18). Male C57Bl/6 mice were injected s.c. with D4M.3A cells ($1x10^5$) and were treated with either anti-PD-1 or isotype control once tumors reached palpability, at day 8. Mice were sacrificed when control tumors reached humane endpoint, on day 20 (N=5) (**Figure 1A**). While anti-PD-1 treated mice experienced a delay in tumor growth (**Figure 1B**), we did not observe any case of tumor regression, which is used to define an objective clinical response (3). As such, D4M.3A melanomas display an acquired resistance to anti-PD-1 monotherapy (30) and recapitulate the reduced efficacy of ICIs observed in patients carrying $PTEN^{-/-}$ melanomas (16).

A tumor's immune phenotype is a major determinant of its clinical response to ICIs (32). Thus, to determine the immunological parameters that underlie this partial response, we characterized the immune composition of the TME at endpoint and the sources of PD-L1 expression. Anti-PD-1 did not increase immune cell infiltration in the tumor and did not alter the distribution of immune cell types (**Figure 1C**). Indeed, D4M.3A immune TMEs were mostly comprised of $F4/80^+$ TAMs and $CD11b^+$ $Ly6C^+$ monocytes, while B and T cells only represented 5% of the immune infiltrate, characteristic of a cold tumor phenotype (33). Furthermore, non-immune $CD45^-$ cells represented the major source of PD-L1 in the TME (**Figure 1C**), a feature associated with resistance to interferon-mediated cytotoxicity (34).

As high frequencies of PD-1$^+$ T_{reg} cells have been suggested to counteract the efficacy of PD-1 blockade (22), we next characterized the PD-1 expression patterns of CD8$^+$, CD4$^+$ T_{conv} and T_{reg} TILs in both treatment groups. In the isotype control group, while T_{conv} TILs were the predominant T cell subset expressing PD-1, T_{reg} cells expressed PD-1 in higher frequencies and expression levels, as evidenced by MFI (**Figure 1E**), suggesting that T_{reg} cells undergo higher-affinity TCR activation in the D4M.3A TME compared to their CD8$^+$ and T_{conv} counterparts (35). While treatment with anti-PD-1 did not increase the proportion of PD-1 expressing TILs, it resulted in a 60% reduction in PD-1 MFI by all TIL subsets (**Figure 1E**), suggesting that TILs are less susceptible to the co-inhibitory signaling provided by PD-L1 (26).

Given that anti-PD-1 modulated PD-1 expression of TILs and that a subset of memory T_{reg} cells expresses PD-1 in circulation (23), we next asked if PD-1 blockade modulated PD-1 expression systemically. While CD8$^+$ and T_{conv} splenocytes expressed PD-1 at low frequencies (<10%), T_{reg} cells expressed the highest proportion (30%) and expression levels of PD-1 amongst T cell subsets (**Figure 1F**). Furthermore, anti-PD-1 induced a 20% reduction in PD-1 MFI by T_{reg} splenocytes, which was not observed in CD8$^+$ T cells (**Figure 1F**). Taken together, these data indicate that PD-1 blockade modulates PD-1 expression levels and preferentially targets T_{reg} cells both locally and systemically.

PD-1 blockade promotes the accumulation of highly-activated Helios$^+$ T_{reg} cells.

As PD-1 blockade induced a delay in tumor growth and modulated PD-1 expression by T_{reg} cells in D4M.3A-bearing mice, we assessed how local and systemic T cell responses changed in relation to T_{reg} cells. Anti-PD-1 induced a two-fold increase in the density of CD8$^+$ and CD4$^+$ T cell infiltration in the tumor (**Figure 2A**), a hallmark of response to treatment (36, 37). However, anti-PD-1 induced a modest increase in the proportion of IFNγ-secreting CD8$^+$ TILs (6.7% vs

3.8% of $CD8^+$ cells) (**Figure 2B**). Notably, IFNγ production by $CD8^+$ T cells was also increased in the spleen and non-draining lymph nodes (**Figure 2B and Supplementary Figure 1A**), and their relative abundance was higher in the spleen than in the tumor, indicating that the TME remains an immunosuppressed environment despite treatment. On the other hand, there was no increase in the proportion of $IFN\gamma^+$ T_{conv} cells (**Figure 2C**). Rather, anti-PD-1 induced an increase in the frequency of T_{reg} cells amongst $CD4^+$ T cells, both in the tumor and the spleen (**Figure 2D**).

As anti-PD-1 increases the proliferation and effector functions of $CD8^+$ TILs (38), we next asked if PD-1 blockade impacted T_{reg} cells in a similar way, by assessing markers associated with stable T_{reg} cell suppressive activity (CTLA-4, TIGIT, Helios (39–41)) and proliferation (Ki67). Indeed, anti-PD-1 increased the frequency of CTLA-4^+ and $TIGIT^+$ T_{reg} cells, both in TILs and splenocytes (**Figure 2E and Supplementary Figure 1B**). Furthermore, the proportion of $Ki67^+$ T_{reg} splenocytes was increased following PD-1 blockade (**Supplementary Figure 1C**), denoting increased proliferation. As such, the frequency of $Helios^+$ T_{reg} cells, which displayed preferential proliferative capacity in the spleen and the tumor, was increased in the anti-PD-1 group (**Figure 2F**). Furthermore, in the spleen and tumor-draining lymph nodes, PD-1 expression was restricted to the subset of Helios-expressing T_{reg} cells (**Figure 2G**), suggesting they were preferentially targeted. Amongst splenic T_{reg} cells, high expression of Helios was also associated with an absence of CD25 expression, a phenotype associated with dysfunctional T_{reg} cell function in inflamed sites (42); and expression of CXCR3, a chemokine receptor which promotes T_{reg} cell homing (43) but is associated with increased anti-tumor activity (44). Accordingly, anti-PD-1 increased the frequency of $CD25^-$ and $CXCR3^+$ T_{reg} cells at the systemic level (**Supplementary Figure 1D**). However, these cells did not seem to preferentially infiltrate the tumor (**Supplementary Figure 1E**), indicating that T_{reg} TILs retained a stable phenotype. Finally, despite a trend towards increased

IFNγ production by T_{conv} cells in the colon (**Supplementary Figure 1F**), anti-PD-1 treated mice did not display any clinical symptoms of irAEs, suggesting that the systemic effect of PD-1 blockade on T_{reg} cells is insufficient to induce a breach of tolerance. Taken together, these data indicate that in conjunction with the increase of IFNγ$^+$ CD8$^+$ T cells, anti-PD-1 promotes the proliferation and activation of a subset of PD-1$^+$ Helios$^+$ T_{reg} cells.

Combination of anti-PD-1 and anti-CTLA-4 increases anti-tumor responses and T_{reg} cell activation.

While anti-PD-1 monotherapy delayed tumor growth, tumors still underwent immune evasion. As combined use of ICIs increases survival (1), accelerates the onset of irAEs (45), and anti-PD-1 increased the frequency of CTLA-4$^+$ T_{reg} cells, we hypothesized that adding anti-CTLA-4 to our treatment regimen would compromise T_{reg} cell functional fate and drive a more efficacious anti-tumor response. To this end, D4M.3A-bearing mice received either anti-PD-1 alone (n=11) or in combination with anti-CTLA-4 (n=11), using the same administration scheme as previously described (**Figure 3A**, N=3). While anti-CTLA-4 significantly delayed tumor growth in anti-PD-1 treated mice (**Figure 3B**), it was insufficient to induce any tumor regression. Notably, CD45$^-$ cells displayed low expression levels of MHC-I compared to dendritic cells and TAMs (**Figure 3C**), a phenotype that is acquired during treatment resistance phases in the clinic (46), indicating a reduced sensitivity to CD8$^+$ T cell cytotoxicity (47).

Anti-CTLA-4 mediates its anti-tumor effects through different mechanisms of action than anti-PD-1 (48), namely the expansion of ICOS$^+$ T_h1 cells (49) and depletion of T_{reg} TILs through antibody-dependent direct cytotoxicity (10). To investigate the mechanisms for this incomplete response to combination therapy, we characterized T cell responses in both groups. Combination ICI resulted in a modest increase in T cell infiltration compared to anti-PD-1 monotherapy,

although F4/80$^+$ TAMs and CD11b$^+$ Ly6C$^+$ monocytes remained the dominant immune cell subsets in the TME (**Figure 3D**). Despite the maintenance of an immunosuppressive environment, anti-CTLA-4 further increased IFNγ production by CD8$^+$ T cells, all the while inducing TNFα production by CD4$^+$ T_{conv} cells (**Figure 3E**). Nonetheless, combination ICI failed to increase the frequency of ICOS$^+$ T_{conv} cells or a depletion of T_{reg} TILs (**Figure 3F**), hallmarks of a successful response to anti-CTLA-4 (8).

To better characterise the pharmacodynamics of anti-CTLA-4, we assessed CTLA-4 expression on T cells. While surface CTLA-4 expression was not detectable, combination ICI induced an increase in the intracellular levels of CTLA-4 by both T_{conv} and T_{reg} cells, suggesting both subsets internalize CTLA-4 in response to ICI binding (**Supplementary Figure 2A**), which could contribute to the apparent absence of T_{reg} cell depletion. Indeed, the proportion of T_{reg} cells expressing intracellular CTLA-4 was increased both in the spleen and TILs, upon CTLA-4 blockade (**Figure 3G**), highlighting the systemic impact of checkpoint blockade (50). Furthermore, the proportion of actively cycling (Ki67$^+$) T_{reg} TILs was increased in the combination ICI group, as well as the frequency of T_{reg} TILs expressing markers associated with stable T_{reg} cell suppressive function (ICOS, TIGIT, Helios) (**Figure 3H**). Moreover, anti-CTLA-4 did not synergize with anti-PD-1 to further reduce surface PD-1 expression levels on T cells (**Supplementary Figure 2B**). Taken together, these data show that in a poorly responsive TME, combination ICI does not induce T_{reg} TIL depletion *in vivo*, but instead promotes T_{reg} cell activation and proliferation.

YUMMER1.7 tumors display inter-individual variability in tumor growth and a T-cell rich tumor microenvironment.

To determine if the increase in T_{reg} cell activation was due to the specific effect of ICIs or an indirect feature of increased inflammation in the TME, we made use of the highly immunogenic YUMMER1.7 model, which shares the same driver mutations than D4M.3A but was further irradiated to generate additional neoepitopes (31). As this melanoma elicits a potent T cell response that is sufficient to induce tumor clearance at low inoculum numbers (31), we determined an optimal administration scheme that enabled us to harness the inter-individual variability in tumor growth to study T_{reg} cell phenotype in both highly inflamed and immune-evading tumors (**Figure 4A**). As such, male Foxp3-IRES-mRFP ($Foxp3^{RFP}$) reporter mice (n=22) were injected s.c. with YUMMER1.7 cells ($2.5x10^5$) and sacrificed as soon as the first mouse reached humane endpoint, on day 20 (N=4) (**Figure 4B**).

As in-depth characterization of the T cell response to YUMMER1.7 tumors is lacking, we first determined the immune composition of the TME in relation to tumor volume. Immune cell infiltration was increased in tumors with small volume (**Supplementary Figure 3A**). On average, T cells were the most frequent immune cell type in the TME, and their frequency was negatively correlated with tumor volume at endpoint (r^2=0.45, p=0.0009) (**Figure 4C**). On the other hand, tumor growth was associated with higher frequencies of TAMs (r^2=0.52, p<0.0001) (**Supplementary Figure 3B**). Contrary to what we observed in D4M.3A tumors, a large majority of TAMs and $CD11b^+$ $Ly6C^+$ monocytes expressed PD-L1 (**Figure 4D**), a feature associated with high levels of IFNγ signaling in the TME (51), and similar levels of MHC-II than dendritic cells (**Figure 4E**), a feature associated with antigen-presenting capacities (52).

Given the expression of PD-L1 by antigen-presenting cells (APCs) in the TME, we hypothesized that these cells impaired T cell proliferation upon activation. To test this, we isolated MHC-II^+ APCs from the spleen and tumors of YUMMER1.7-bearing mice at tumor endpoint and

cultured them ($1x10^5$) with CTV-labelled splenic $CD4^+$ $Foxp3^-$ or $CD8^+$ T_{resp} cells ($5x10^4$) and anti-CD3. The proliferation of T_{conv} and $CD8^+$ T cells was reduced in the presence of tumoral APCs compared to their splenic counterparts (**Figure 4F**). Notably, tumoral APCs were more potent at suppressing the proliferation of T_{conv} than $CD8^+$ T cells (39.2% vs 16.9% reduction in proliferation index relative to splenic APCs) (**Figure 4F**). Accordingly, the frequency of T_{conv} cells was reduced in TILs compared to the tumor-draining lymph nodes, and $CD8^+$ T cells composed up to 80% of the TIL compartment (**Figure 4G**).

The profile of PD-1 expression by T_{reg} TILs in hot tumors is ill-defined. $CD8^+$, T_{conv} and T_{reg} TILs all upregulated PD-1 compared to their tumor-draining lymph node counterparts. However, contrary to D4M.3A TILs, T_{reg} cells expressed lower levels of PD-1 than their $CD8^+$ and T_{conv} counterparts (**Figure 4H**). Furthermore, while the frequency of PD-1^+ $CD8^+$ was inferior to 5% in the tumor-draining lymph nodes, 80% of $CD8^+$ TILs expressed PD-1 (**Supplementary Figure 3C**), suggesting that most TILs were TCR-activated in the tumor (35) and kept in an exhausted state. Taken together, these data indicate that YUMMER1.7 tumors recapitulate hallmarks of "hot" TMEs (32).

$CD8^+$ TILs are antigen-experienced and display a dysfunctional phenotype at tumor endpoint.

Since IFNγ-secreting $CD8^+$ TILs are potent effectors of anti-tumor immunity, we next investigated $CD8^+$ T cell responses. There was a two-fold increase in the number of $CXCR3^+$ and IFNγ^+ $CD8^+$ T cells in the tumor-draining lymph nodes compared to contralateral lymph nodes (**Figure 5A**), suggesting $CD8^+$ T cells were still primed in the draining lymph nodes, and migrating to the tumor bed (53). Furthermore, 90% of $CD8^+$ TILs displayed an effector memory phenotype ($CD44^+$ $CD62L^-$) (**Figure 5B**), indicating antigen-experience. Accordingly, $CD8^+$ TILs

upregulated their expression of multiple checkpoint molecules (PD-1, CTLA-4, TIGIT), feature of exhausted cells (54). Nonetheless, $CD8^+$ TILs also expressed high levels of T-bet and IL-18R1 compared to their lymph node counterparts (**Figure 5C**), markers that promote T cell expansion, effector functions and counteract T cell exhaustion in TMEs (55–57), suggesting some $CD8^+$ TILs may retain anti-tumor activity.

To assess their functional status, we isolated $CD8^+$ TILs from YUMMER1.7 bearing mice at tumor endpoint and assessed their capacity to proliferate (CTV dilution), secrete pro-inflammatory cytokines (IFNγ) and cytotoxic potential (GRZB) upon *in vitro* restimulation with anti-CD3 and IL-2 (N=3). Here, the majority of $CD8^+$ TILs failed to proliferate upon *in vitro* restimulation (**Figure 5D**), confirming their terminally exhausted differentiation status which cannot be rescued by cytokines (58). However, the $CD8^+$ T cells that proliferated displayed higher expression of IFNγ and GRZB than their splenic counterparts (**Figure 5E**), indicating enhanced effector functions. To investigate the *in vivo* functional status of $CD8^+$ TILs, we characterized their production of IFNγ in relation to PD-1 expression. $IFN\gamma^+$ $CD8^+$ TILs expressed PD-1 in tumors with delayed growth, albeit to lower levels than levels than $CD8^+$ TILs from endpoint tumors which displayed abrogated IFNγ production. Indeed, IFNγ production was negatively correlated with both tumor volume (r=-0.77) and PD-1 MFI (r=-0.45). On the other hand, IFNγ production was strongly associated with the expression of ICOS, IL-18R1 and T-bet (**Figure 5F**). Taken together, these data indicate that migrating $T\text{-}bet^+$ $CD8^+$ TILs are submitted to local immunosuppression and commit to a terminally exhausted phenotype as tumor growth progresses.

Highly-activated $Helios^+$ T_{reg} TILs display signs of immune exhaustion at tumor endpoint.

T_{reg} TILs are potent suppressors of anti-tumor immunity, yet little is known about the consequences of PD-1 signaling on their functional fate. To investigate this, we characterized T_{reg}

cell phenotype in relation to tumor volume and the functional status of $CD8^+$ TILs. First, T_{reg} cells were highly abundant in the TME (**Supplementary Figure 4A**), suggesting strong suppression of T_{conv} cells. In the tumor-draining lymph nodes, antigen-experience (CD44), proliferative capacity (Ki67), and migratory potential (CD62L, CXCR3) were associated with high levels of Helios expression by T_{reg} cells (**Figure 6A**). Accordingly, there was a two-fold increase in the number of $Helios^+$ and $CXCR3^+$ T_{reg} cells in the tumor-draining lymph nodes compared to contralateral lymph nodes (**Figure 6B**), suggesting that, as observed in our model of "cold" tumors, the ongoing anti-tumor immune response promotes the expansion and migration of $Helios^+$ T_{reg} cells. Indeed, 90% of T_{reg} TILs displayed an effector phenotype ($CD44^+$ $CD62L^-$).

Since Helios expression can be downregulated at resting state (59), we injected $Helios^{GFP}$ $Foxp3^{RFP}$ dual reporter mice, in which transcription of IKZF2 triggers the synthesis of a reporter free-floating GFP ($t_{1/2}$=26h) independent of Helios protein expression, with $2.5x10^5$ YUMMER1.7 cells (N=2, n=10). Regardless of tumor volume and tumor type, >97% of T_{reg} TILs expressed Helios and a similar phenotype was observed in D4M.3A TILs (n=2) (**Supplementary Figure 4B**), confirming that the vast majority of T_{reg} TILs originate from $Helios^+$ T_{reg} cells.

Compared to their LN counterparts, T_{reg} TILs upregulated the expression of CTLA-4 and TIGIT (**Figure 6C**), indicative of a strongly activated phenotype (28, 60, 61), as well as T-bet (**Figure 6D**), indicating a T_h1-like functional specialization (62, 63). However, T_{reg} TILs displayed reduced expression of CD25 and Helios, which play key roles in their survival in tissues (42), compared to their draining LN counterparts (**Supplementary Figure 4C**). In fact, the frequency of $CD25^+$ T_{reg} cells decreased in endpoint tumors (**Supplementary Figure 4C**), suggesting some form of cellular exhaustion.

Since T_{reg} TILs upregulated PD-1 expression and $CD8^+$ TILs displayed an exhausted phenotype, we hypothesized that PD-1 signaling also inhibits T_{reg} cell activity. Indeed, high levels of PD-1 expression by T_{reg} cells were strongly associated with increased tumor volume (r=0.83) and reduced expression of CTLA-4 (r=-0.49), ICOS (r=-0.75) and TIGIT (r=-0.52) (**Figure 6E**), markers associated with highly suppressive T_{reg} cells (39, 64, 65). To test the direct impact of PD-1 signaling on T_{reg} cell activation levels, we isolated splenic and TIL RFP^+ T_{reg} cells from tumor-bearing mice and re-stimulated them *in vitro* in the presence of PD-L1-Fc. Engaging PD-1 upon T cell activation reduced the expression levels of CTLA-4 in both T_{reg} TILs and splenocytes (**Figure 6F**). Thus, PD-1 signaling dampens T_{reg} cell activation levels in TMEs.

To assess the consequences of chronic activation on T_{reg} TIL fitness, we isolated RFP^+ T_{reg} cells from YUMMER1.7 bearing mice at tumor endpoint and activated them *in vitro* with plate-bound anti-CD3 and anti-CD28, and splenic T_{conv} cells to provide a source of IL-2. T_{reg} TIL expansion was reduced compared to their splenic counterparts, as evidenced by the reduced number of live T_{reg} cells and the reduced proportion of Ki67 expression (**Figure 6G**). In addition, T_{reg} TILs expressed reduced levels of Bcl-2 compared to splenocytes (**Figure 6H**), indicating an increased susceptibility to apoptosis (66). Furthermore, this phenotype was recapitulated *in vivo*, alongside expression of KLRG1 (**Supplementary Figure 4D**), a marker of short-lived highly suppressive T_{reg} cells (67).

Taken together, these data indicate that in both hot and cold TMEs, high levels of PD-1 expression were associated with reduced T_{reg} cell activation levels, suggesting that T_{reg} TILs are susceptible to a form of immune exhaustion. Thus, all the while increasing anti-tumor responses, anti-PD-1 and anti-CTLA-4 promote the expansion of highly activated $Helios^+$ T_{reg} cells, in mice

with a cold TME, both locally and systematically, which contributes to acquired resistance to checkpoint blockade.

Discussion

The degree of pre-existing inflammation in the melanoma TME is one of the best predictors of response to ICI (68) and is tightly linked to tumor-intrinsic immunogenicity (69). Despite T_{reg} cells dominantly preventing tumor regression in poorly immunogenic melanoma models (70), little is known about the differences in T_{reg} cell infiltration and functional fate between hot and cold TMEs. Since T_{reg} cells express checkpoint molecules, and response to ICI is often associated with the onset of irAEs (71), a prevalent hypothesis states that ICIs dysregulate the suppressive function of T_{reg} cells in TMEs (72, 73). However, ICI-induced T_{reg} cell activation in cold TMEs could constitute a resistance mechanism to immunotherapy (74). To better understand this dichotomy, we characterized T_{reg} cell phenotype in relation to the immune landscape in two novel, preclinical models of melanoma that recapitulate hallmark genetic alterations of human melanoma but differ in their levels of immunogenicity (31).

In this study, we established Helios expression as a feature of the population of melanoma-infiltrating T_{reg} cells displaying high activity and proliferative capacity in both cold and hot murine models of melanoma. Helios^{+} T_{reg} cells preferentially expressed PD-1 in circulation, and their proliferation and activation levels were increased both locally and systemically upon PD-1 blockade despite a delay in tumor growth. While addition of anti-CTLA-4 to the treatment regimen increased anti-tumor responses, it further increased the proliferation of Helios^{+} T_{reg} cells in the TME. Finally, harnessing the potent anti-tumor responses and inter-individual variety in YUMMER1.7 tumor growth (31), we show that tumor growth is associated with increased expression levels of PD-1 by T_{reg} cells, which dampens T_{reg} cell activation and leads to reduced survival upon *ex vivo* restimulation.

The T_{reg}:T_{eff} balance between PD-1$^+$ TILs has been identified as a determinant of the outcome of tumor immunotherapy (22), yet little is known about the factors that dictate this balance. In line with this observation, T_{reg} cells expressed PD-1 in higher proportion than their CD8$^+$ TIL counterparts in the ICI-resistant D4M.3A tumors, which have a low tumor mutational burden (69, 75), whereas we observed the opposite in YUMMER1.7 melanomas, which we and others have shown responds successfully to ICIs (31, 76). PD-1 expression is induced by TCR activation, and its level of expression is proportional to TCR affinity (77). The low frequency of PD-1$^+$ CD8$^+$ TILs in the D4M.3A model suggests that a large proportion of CD8$^+$ TILs are not tumor-antigen-specific (78, 79), but rather bystander cells (80) in line with the limited number of melanocyte-lineage antigens available for T cell recognition in this model (69). Furthermore, in the poorly immunogenic B16 melanomas, immunotherapy fails to broaden their TCR repertoire (81). In contrast, T_{reg} TILs expressed PD-1 in higher frequency and level of expression than T_{eff} TILs, suggesting they harbor a higher degree of tumor-specificity. Indeed, the major melanoma-associated antigens (Tyr, Mart-1, Pmel) are self-antigens towards which the T_{reg} TCR repertoire is skewed (82). Further investigation is warranted to assess the diversity and tumor-specificity of the T_{reg} TCR repertoire in these models. However, the TCR repertoire of patient melanoma-infiltrating T_{reg} cells does not overlap with the repertoire of T_{conv} TILs and is highly tumor-specific with reactivity against both tumor autologous antigens and neoepitopes (83). Thus, using ontogenically close melanoma models that share the same oncogenic mutations (18, 31), we show that the profile of PD-1 expression by TILs is influenced by the abundance of neoepitopes.

While their high levels of PD-1 expression suggests that T_{reg} TILs are susceptible to a form of PD-L1-mediated inhibition, little is known about T_{reg} cell exhaustion. Circulating memory T_{reg} cells naturally share many hallmarks of exhausted cells, namely the co-expression of inhibitory

checkpoint molecules (84), an inability to proliferate (85) and secrete pro-inflammatory cytokines (86), and a metabolic shift towards fatty acid oxidation (87), yet they are not impaired in their suppressive effector functions (88). In both models, high levels of PD-1 expression, were associated with a loss of expression of markers associated with stably suppressive T_{reg} cells (CTLA-4, TIGIT). While paucity of TILs prevented us from assessing T_{reg} cell function in D4M.3A tumors, thanks to the high number of infiltrating T_{reg} cells found in YUMMER1.7 tumors, we were able to show that PD-1 signaling dampens T_{reg} cell activation levels, and that akin to their $CD8^+$ counterparts, T_{reg} TILs display reduced proliferation and survival at tumor endpoint, demonstrating that T_{reg} TILs at end-point suffer from a shortened life-span. In line with these observations and the lower frequency of T_{reg} TILs in D4M.3A, high levels of PD-1 expression contribute to the contraction of the T_{reg} cell pool during chronic infections (23).

While the hallmarks of successful response to ICIs are well established for T_{eff} cells, their functional consequences on T_{reg} cells remain ill-defined. In an adoptive transfer model where only T_{reg} cells express PD-1, anti-PD-1 accelerates tumor growth (28), demonstrating that T_{reg} cells respond to PD-1 blockade. We show that anti-PD-1 decreases the surface expression levels of PD-1 by both systemic and tumoral T_{reg} cells, in line with our previous report in B16 tumors (89), highlighting how ICIs may impact peripheral tolerance by targeting T_{reg} cells outside of the tumor. While these elements suggest that increased T_{reg} cell activation and proliferation promotes acquired resistance to ICI, it was correlated with a moderate systemic increase in IFNγ production, albeit insufficient to trigger irAEs in this short time span, suggesting a potential for dysregulation of T_{reg} cells. Indeed, PD-1 blockade induced the expansion of $CD25^{low}$ and $CXCR3^+$ T_{reg} cells, phenotypes observed in autoimmune patients (90, 91), and reminiscent of the IFNγ response signature identified in the T_{reg} cells of patients who develop irAEs (92).

Importantly, these cells expressed Helios, which plays a crucial role in maintaining the stability of the T_{reg} cell phenotype in TMEs, preventing their expression of IFNγ-associated genes (21, 93), promoting their cycling and survival through STAT5 signaling (94), and is required for T_{reg} cells to control T_h1 responses (95). Nonetheless, we and others have shown that Helios$^+$ T_{reg} cells harbor distinct TCR repertoires, transcriptional profiles and are more susceptible to T_h1-polarizing and inflammatory signals than their circulating Helios$^-$ counterparts (24, 63). Thus, given the low expression of Helios by T_{conv} and CD8$^+$ TILs, downregulation of Helios expression represents an attractive therapeutic option to specifically target the functional stability and survival of T_{reg} cells that are prone to the acquisition of inflammatory characteristics. Furthermore, as combination ICI did not induce ADCC-mediated T_{reg} TIL depletion in D4M.3A tumors, contrary to models that respond fully (8, 96), we suggest that certain mechanisms of actions of ICIs are dependent on the degree of inflammation in the TME (10, 97). Taken together, our results identify Helios expression as a defining feature of the T_{reg} cells that infiltrate tumors and respond to ICIs, and suggest Helios plays a key role in maintaining the functional stability of ICI-reactivated T_{reg} cells upon acquired resistance to checkpoint blockade.

Figures

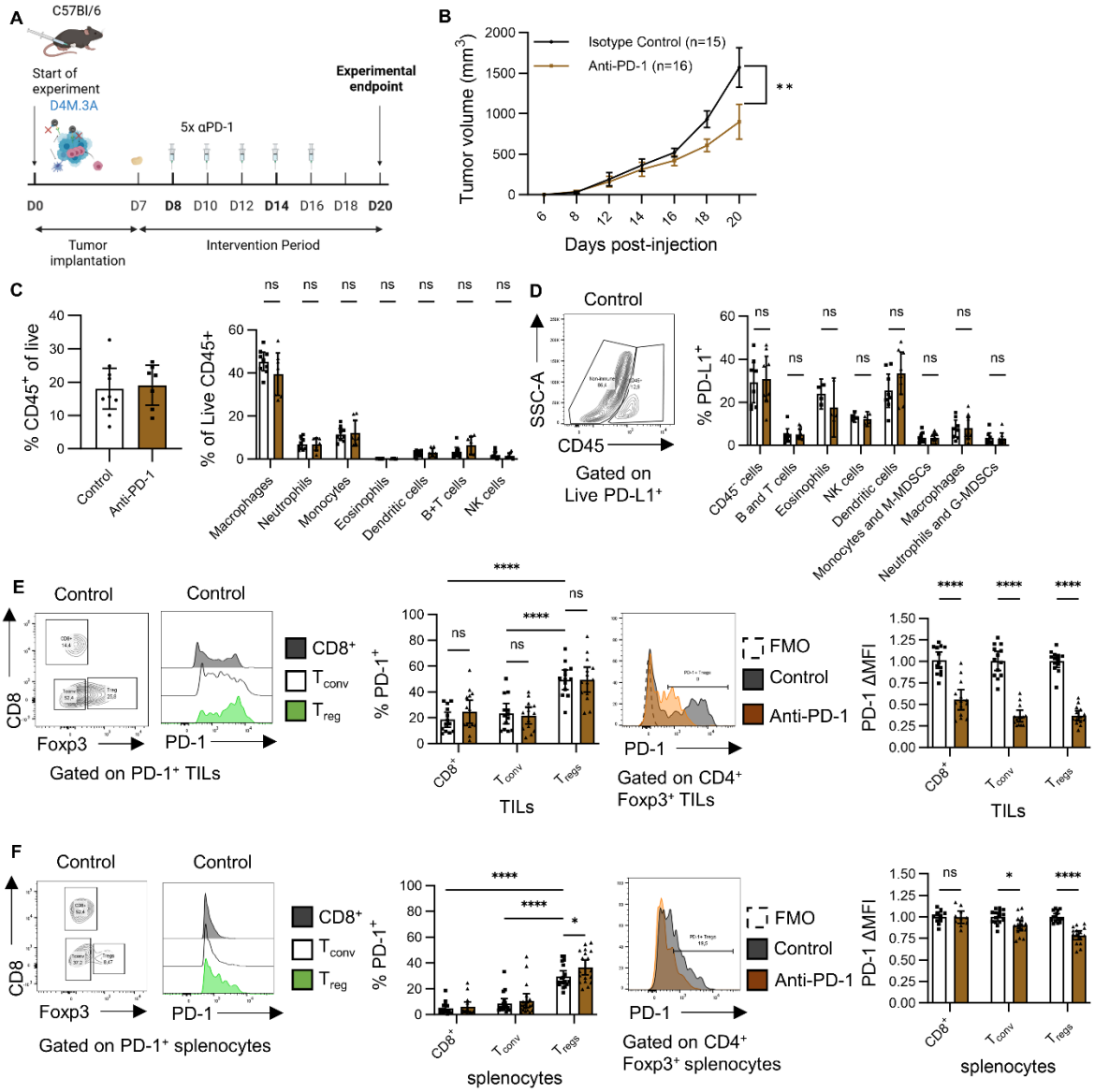

Figure 1. T_{reg} cells respond to PD-1 blockade.

A. Schematic of the experimental design. 8–12-week-old, C57Bl/6 mice were inoculated with $1x10^5$ D4M.3A cells in 50% Matrigel and were sacrificed as soon as the first mouse in the experiment reached humane endpoint (tumor volume>1500mm^3). At Day 8, mice were randomly assigned to a treatment group and received 5 injections of 250µg of anti-PD-1 (clone RMP 1-14, BioXcell) (n=16) or isotype control (n=15). Data collated from N=5 independent experiments.

B. Tumor volumes were measured three times per week using an electronic calliper. Data represented as mean and 95% CI. Tumor volumes were compared at each time point using a Two-Way ANOVA with Sidak's correction.

C. Flow cytometry analysis of proportions of $CD45^+$, $CD11b^+$ $F4/80^+$ macrophages, $CD11b^+$ $Ly6G^+$ neutrophils, $CD11b^+$ $Ly6C^+$ monocytes, $CD11b^+$ Siglec-F^+ eosinophils, $CD11c^+$ dendritic cells, $CD3/CD19^+$ B and T cells and $CD11b^-$ $CD49b^+$ NK cells in endpoint tumors.

D. Flow cytometry analysis of PD-L1 expression by immune cell subsets.

E. Flow cytometry analysis of PD-1 expression by $CD8^+$ (black) $CD4^+$ $Foxp3^-$ T_{conv} (white) and $CD4^+$ $Foxp3^+$ T_{reg} (green) TILs. For representative flow plots, all mice from a treatment group were pooled, data shown from one of N=5 independent repeat experiments.

F. Flow cytometry analysis of PD-1 expression by $CD8^+$ $CD4^+$ $Foxp3^-$ T_{conv} and $CD4^+$ $Foxp3^+$ T_{reg} splenocytes. Representative flow plots from 1 out of n=15 control mice. All flow cytometry frequencies were compared using Sidak's multiple comparisons test. Fold PD-1MFI changes were calculated by dividing each MFI by the average in the isotype control group for their respective experiment. Fold MFI changes were compared using a Two-Way ANOVA with Tukey's correction for multiple comparisons.

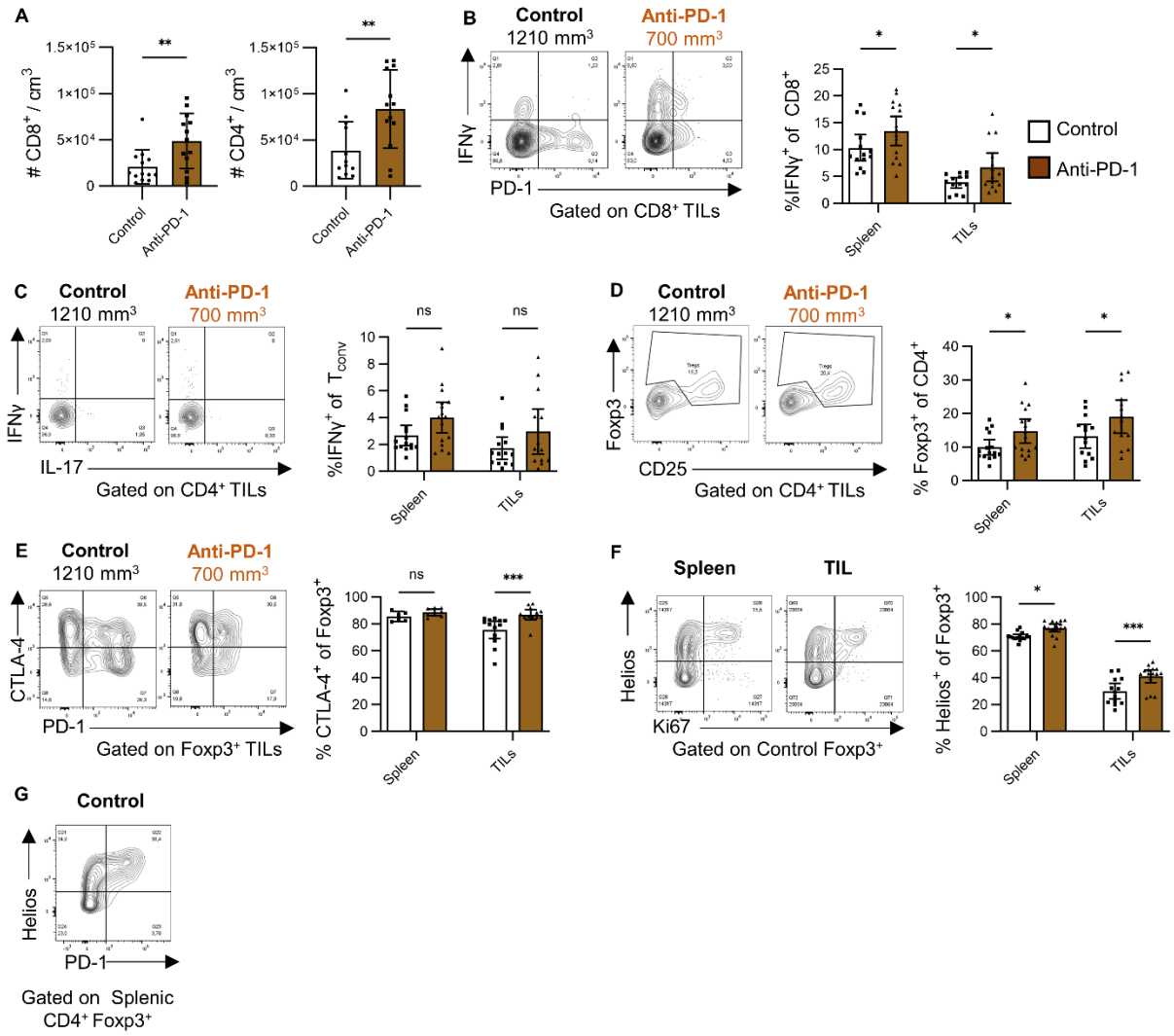

Figure 2. Increased IFNγ production upon PD-1 blockade is associated with an accumulation of highly-activated Helios$^+$ T_{reg} cells.

A. Flow cytometry analysis of CD8 and CD4 density within tumors. Number of live lymphoid-sized cells were counted post tumor digestion using a hemocytometer. CD8 and CD4 cell densities were calculated by multiplying raw counts by their respective frequency amongst live lymphoid-sized cells and dividing by the tumor volume. Means were compared using an unpaired Student's t-test.

B-C. Representative flow plots and flow cytometry analysis of IFNγ, PD-1 and IL-17 expression

by $CD8^+$ and CD4+ T_{conv} splenocytes and TILs. Single cell suspensions were stimulated in the presence of PMA, Ionomycin and GolgiStop for 3h then stained for flow cytometry analysis.

D. Representative flow plots and flow cytometry analysis of Foxp3 and CD25 expression by $CD4^+$ TILs and splenocytes.

E-F. Representative flow plots and flow cytometry analysis of CTLA-4, PD-1, Helios and Ki67 expression by T_{reg} TILs and splenocytes.

G. Representative flow plots and flow cytometry analysis of Helios and PD-1. All data represented as mean +/- 95% CI where each dot represents one mouse.

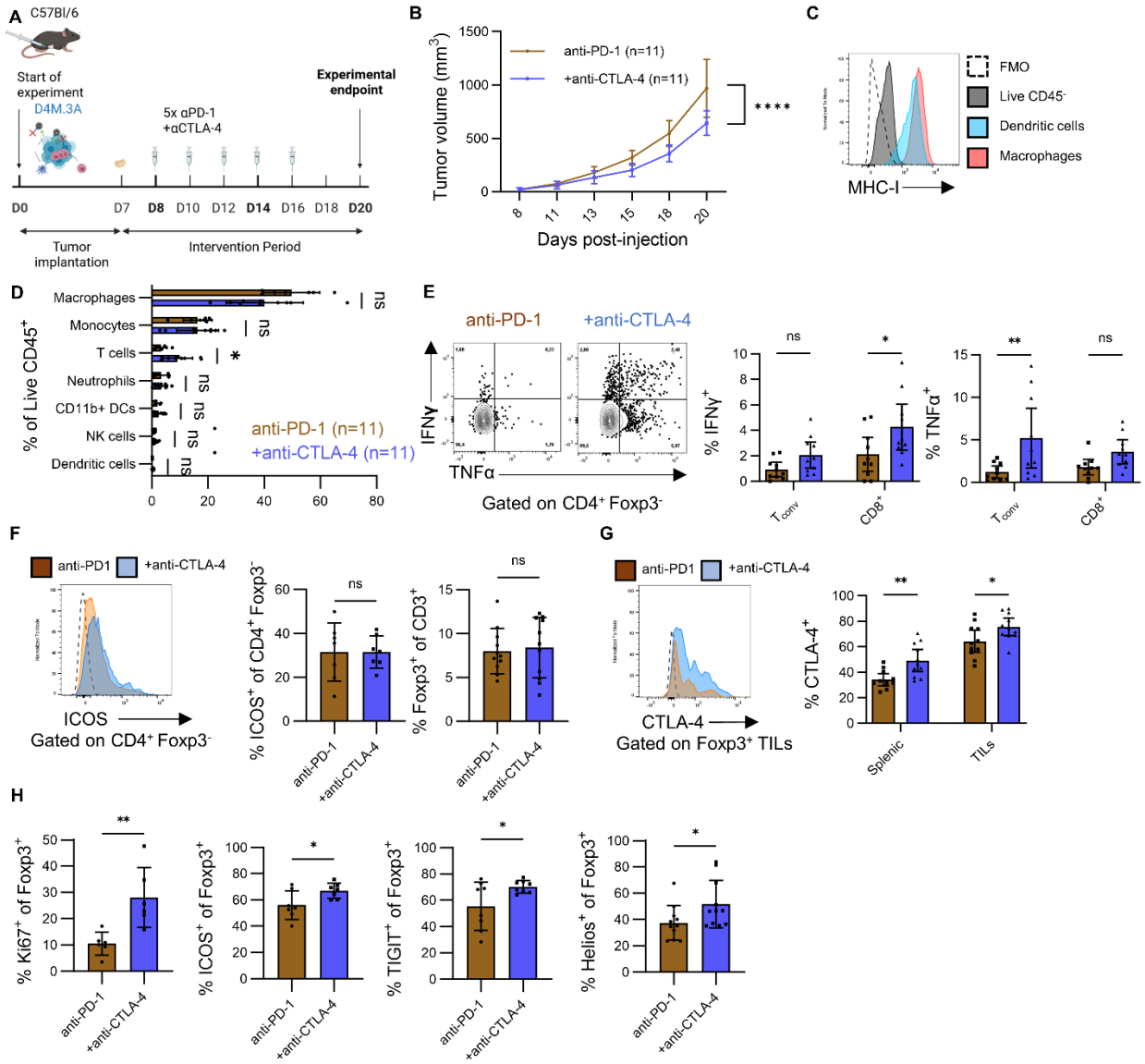

Figure 3. Combination of anti-PD-1 and anti-CTLA-4 increases anti-tumor responses and T_{reg} cell activation.

A. Schematic of the experimental design. 8–12-week-old, C57Bl/6 or Foxp3^{RFP} reporter mice were inoculated with 1x10^5 D4M.3A cells in 50% Matrigel and were sacrificed as soon as the first mouse in the experiment reached humane endpoint (tumor volume>1500mm^3). At Day 8, mice were randomly assigned to a treatment group and received 5 injections of 250µg of anti-PD-1 (clone

RMP 1-14) (n=11) or anti-PD-1 and anti-CTLA-4 (clone 9H10) (n=11). Data collated from N=3 independent experiments.

B. Tumor volumes were measured thrice weekly using an electronic calliper. Data represented as mean and 95% confidence interval in anti-PD-1 (amber) and combination ICI (blue) treated mice. Tumor volumes were compared using a Two-Way ANOVA with Sidak's correction.

C. Representative flow plots of MHC-I expression by non-immune $CD45^-$ cells (black), $CD11b^-$ $CD11c^+$ conventional dendritic cells (blue) and $CD11b^+$ $F4/80^+$ macrophages (red).

D. Flow cytometry analysis of the frequency of $CD11b^+$ $F4/80^+$ macrophages, $CD11b^+$ $Ly6C^+$ monocytes, $CD3^+$ T cells, $CD11b^+$ $Ly6G^+$ neutrophils, $CD11b^+$ $CD11c^+$ $CD11b^+$ dendritic cells, $CD11b^-$ $CD49b^+$ NK cells and $CD11b^-$ $CD11c^+$ conventional dendritic cells amongst tumor-infiltrating $CD45^+$ cells. Means compared using Sidak's multiple comparisons test.

E. Representative flow plots and flow cytometry analysis of IFNγ and TNFα production by T_{conv} and $CD8^+$ T cells. Single cell suspensions were stimulated in the presence of PMA, Ionomycin and GolgiStop® for 3h then stained for flow cytometry analysis. Means were compared using a two-way ANOVA with Holm-Sidak's correction for multiple comparisons.

F. Representative flow plots and flow cytometry analysis of ICOS and Foxp3 expression by $CD4^+$ TILs. Means were compared using unpaired Student's t-tests.

G. Representative flow plots and flow cytometry analysis of CTLA-4 expression by T_{reg} splenocytes and TILs. Means were compared using a two-way ANOVA with Holm-Sidak's correction for multiple comparisons.

H. Flow cytometry analysis of Ki67, ICOS, TIGIT and Helios expression by T_{reg} TILs. Means were compared using unpaired Student's t-tests.

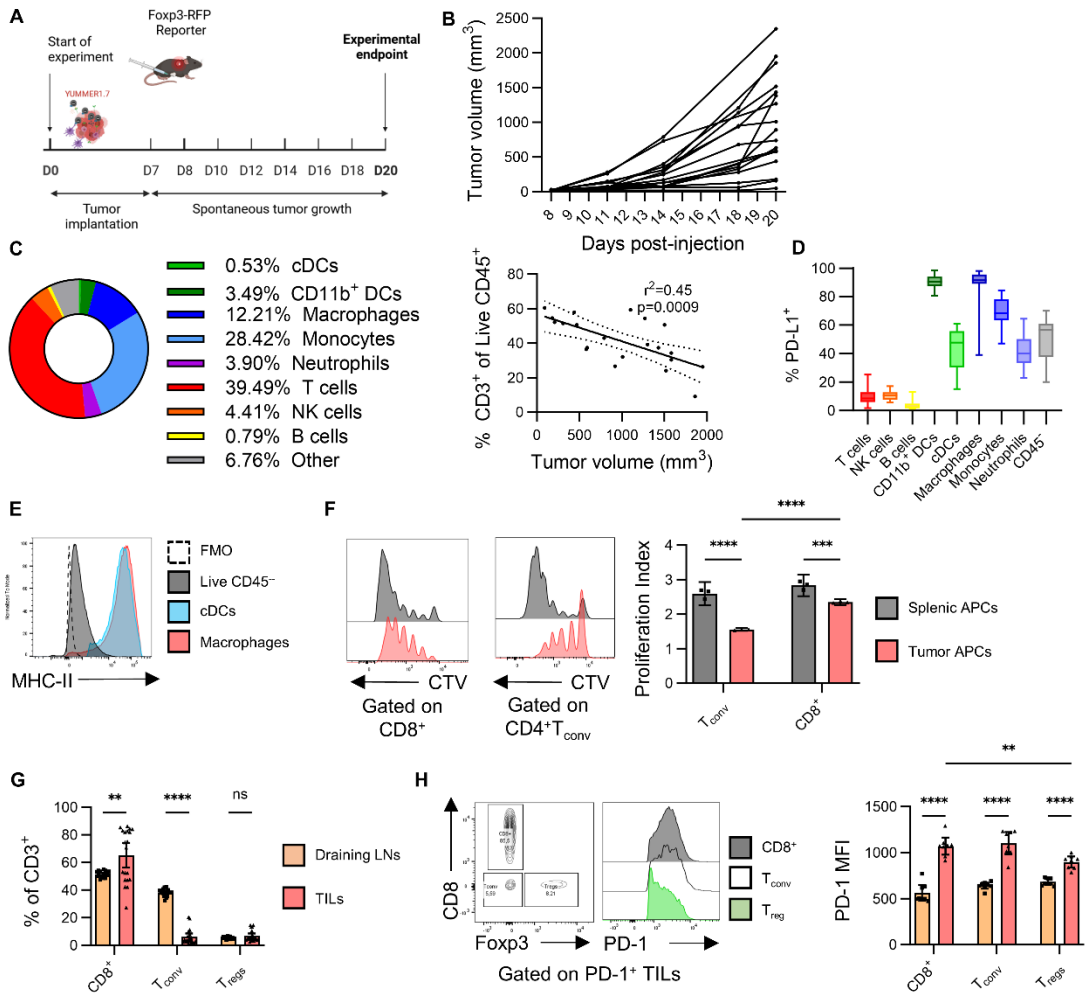

Figure 4. YUMMER1.7 tumors display inter-individual variability in tumor growth and a T-cell rich tumor microenvironment.

A. Schematic of the experimental design. 8–12-week-old, Foxp3^{RFP} reporter mice were inoculated with 2.5x10^5 YUMMER1.7 cells in 50% Matrigel and were sacrificed as soon as the first mouse in the experiment reached humane endpoint (tumor volume>1500mm^3) (n=21, N=4).

B. Tumor volumes were measured thrice weekly using an electronic calliper, data shown as individual growth curve for each mouse.

C. Flow cytometry analysis of proportions of CD11b$^-$CD11c$^+$ MHC-II$^+$ dendritic cells (green), CD11b$^+$ CD11c$^+$ MHC-II$^+$ CD11b$^+$ dendritic cells (dark green), CD11b$^+$ F4/80$^+$ macrophages (dark

blue), $CD11b^+$ $F4/80^-$ $Ly6C^+$ monocytes (blue), $CD11b^+$ $Ly6G^+$ neutrophils (purple), $CD3^+$ T cells (red), $CD11b^-$ $CD49b^+$ NK cells (orange), $CD19^+$ B cells (yellow), and other cells (grey). Data represented as parts of whole. All data points were pooled to calculate a linear correlation. The slope's deviation from zero was evaluated using Fisher's test.

D. Flow cytometry analysis of PD-L1 expression by immune cell subsets.

E. Representative flow plots of MHC-II expression by CD45- cells (black), conventional DCs (blue) and macrophages (red) in a tumor reaching humane endpoint ($1500mm^3$).

F. Live $CD45^+$ $MHC\text{-}II^+$ antigen-presenting cells were sorted and pooled from the spleens or tumors of n=2 YUMMER1.7-bearing mice at tumor endpoint. Splenic or tumoral APCs ($1x10^5$) were co-cultured with either $CD8^+$ or $CD4^+$ RFP^- T_{conv} CTV-labelled splenocytes ($5x10^5$) in the presence of soluble anti-CD3 (0.5µg/ml) for 72h. Proliferation was measured by representative flow plots of $CD8^+$ and T_{conv} CTV dilution when co-cultured with splenic (black) or tumor (red) APCs and quantified by proliferation index (total number of divisions/number of cells at the start of culture). Means were compared by two-way ANOVA. Data shown from 1 of N=3 independent repeats.

G. Flow cytometry analysis of CD8, T_{conv} and T_{reg} cell frequencies in tumor-draining (axillary and inguinal) lymph nodes and TILs. Means were compared using Tukey's multiple comparisons test.

H. Flow cytometry analysis of PD-1 expression by $CD8^+$, T_{conv} and T_{reg} TILs. Representative flow plots from a tumor reaching humane endpoint ($1500mm^3$). MFIs from one representative repeat out of 4 independent experiments were compared using Tukey's multiple comparisons test.

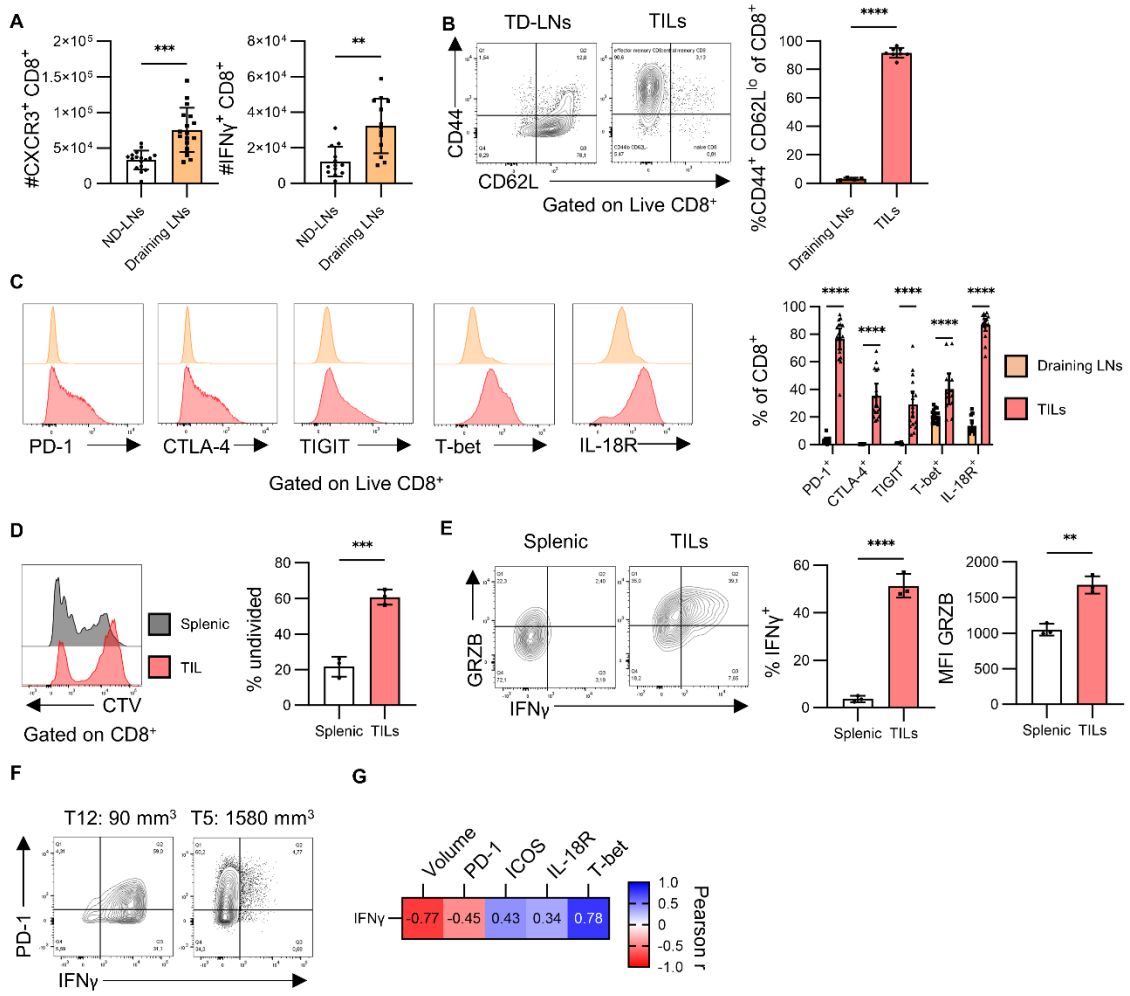

Figure 5. CD8$^+$ TILs are antigen-experienced and display a dysfunctional phenotype at tumor endpoint.

A. Flow cytometry analysis of CXCR3 and IFNγ expression by CD8$^+$ T cells in tumor draining (inguinal and axillary) right lymph nodes and their non-draining (contralateral) counterparts. Number of live lymphoid-sized cells were counted using a hemocytometer. CXCR3$^+$ and IFNγ$^+$ cell numbers were calculated by multiplying raw counts by their respective frequency amongst live lymphoid-sized. Means were compared using a paired Student's t-test (n=21, N=4).

B. Flow cytometry analysis of CD44 and CD62L expression by CD8$^+$ T cells. Representative flow plots from a mouse bearing a tumor at human endpoint volume (>1500mm^3). Means were compared using a paired Student's t-test.

C. Flow cytometry analysis of PD-1, CTLA-4, TIGIT, T-bet and IL-18R expression by $CD8^+$ T cells. All representative flow plots from tumor-draining lymph nodes (orange) and TILs (pink) from a mouse bearing a tumor at human endpoint volume (>1500mm^3). Means were compared using a two-way ANOVA with Holm-Sidak's correction for multiple comparisons.

D-E. Splenic and TIL $CD8^+$ T cells were isolated by FACS from a YUMMER1.7-bearing mouse at tumor endpoint, CTV-labelled, and co-cultured ($5x10^4$) with mitomycin C-inactivated accessory cells ($1x10^5$) in the presence of soluble anti-CD3 (0.5µg/ml) and recombinant human IL-2 (100U/ml) for 72h. After 69 hours of culture, cells were stimulated with PMA, Ionomycin and GolgiStop for 3h then stained for flow cytometry analysis. Undivided cells were defined as dead $CD8^+$ CTV^{High} cells. Representative flow plots of CTV dilution, IFNγ and GRZB expression. Means were compared using unpaired Student's t-tests.

F. Representative flow plots of IFNγ and PD-1 expression by $CD8^+$ TILs at experimental endpoint. Single cell suspensions were stimulated with PMA, Ionomycin and GolgiStop for 3h then stained for flow cytometry analysis.

G. PD-1 MFIs were normalized to their respective average PD-1 MFI for each experiment. Pearson r-correlates were computed for each pair of variables and represented as a heatmap.

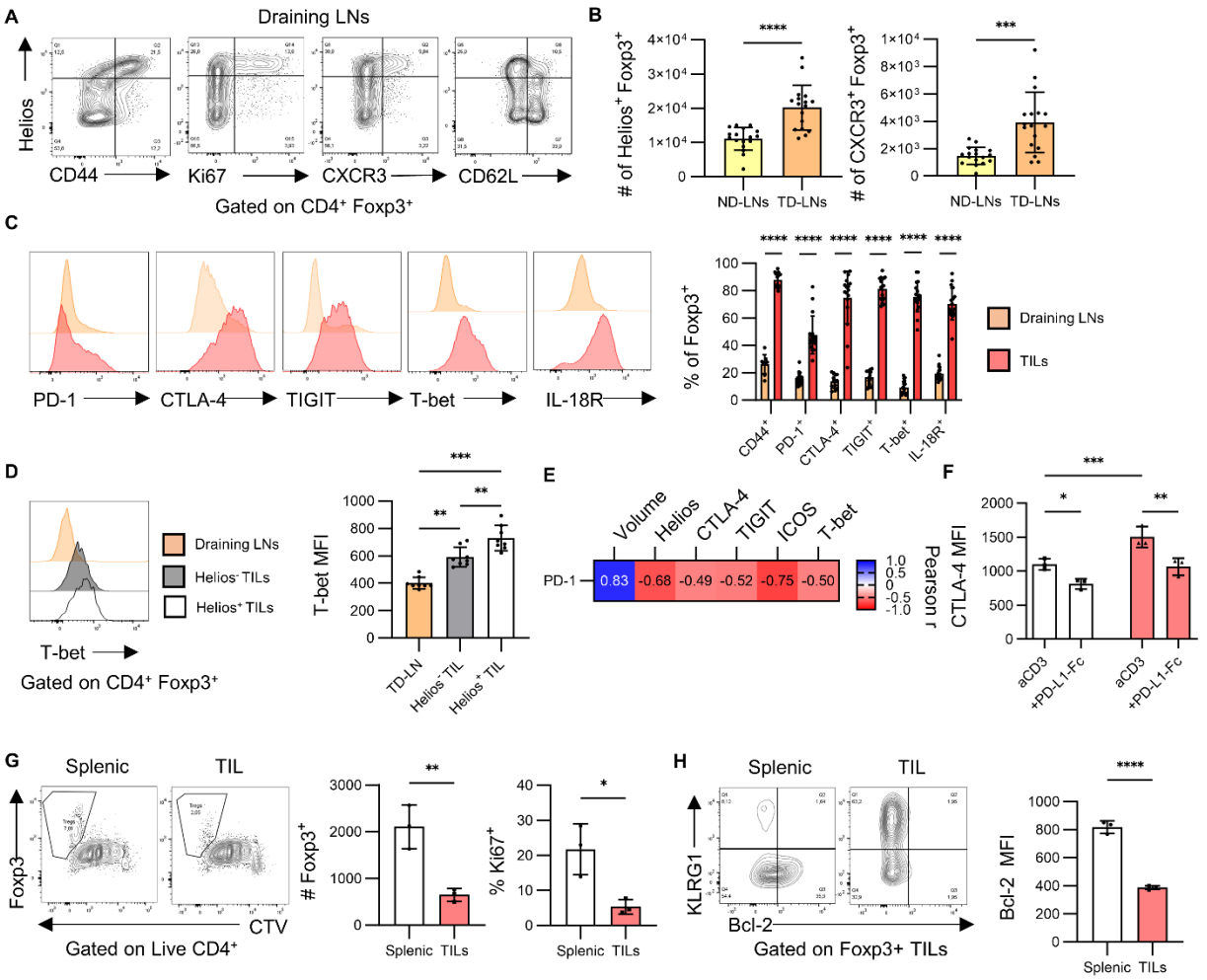

Figure 6. Highly activated Helios$^+$ T$_{reg}$ TILs display signs of immune exhaustion at tumor endpoint.

A. Representative flow plots of CD44, Ki67, CXCR3 and CD62L expression in relation to Helios by T$_{reg}$ cells in tumor-draining (inguinal and axillary) right lymph nodes.

B. Number of live lymphoid-sized cells were counted using a hemocytometer. CXCR3$^+$ and Helios$^+$ cell numbers were calculated by multiplying raw counts by their respective frequency amongst live lymphoid-sized. Means were compared using a paired Student's t-test (n=21, N=4).

C. Flow cytometry analysis of PD-1, CTLA-4, TIGIT, T-bet and IL-18R expression by Foxp3$^+$ T$_{reg}$ cells. All representative flow plots from tumor-draining lymph nodes (orange) and TILs (pink)

from a mouse bearing a tumor at human endpoint volume (>1500mm^3). Means were compared using a two-way ANOVA with Holm-Sidak's correction for multiple comparisons.

D-F. Splenic and TIL RFP$^+$ T_{reg} cells were isolated by FACS from a YUMMER1.7-bearing mouse at tumor endpoint, and co-cultured with CTV-labelled, splenic RFP$^-$ T_{conv} cells in wells previously coated with anti-CD3 (3µg/ml), anti-CD28 (2µg/ml), +/- PD-L1-Fc (5µg/ml). Flow cytometry analysis of Foxp3, Ki67, KLRG1, Bcl-2 and CTLA-4 expression by T_{reg} cells. Means were compared using unpaired Student's t-tests. Data shown from one experiment representative of N=2 repeats.

G-H. PD-1 MFIs were normalized to their respective average PD-1 MFI for each experiment. Pearson r-correlates were computed for each pair of variables and represented as a heatmap.

I. Flow cytometry analysis of T-bet by Helios$^+$ and Helios$^-$ T_{reg} cells. Data shown from one representative experiment out of N=4 independent repeats. Means were compared using a repeated-measures one-way ANOVA.

J. Representative flow plots and flow cytometry analysis of IFNγ production by T_{reg} cells. Single cell suspensions were stimulated with PMA, Ionomycin and GolgiStop for 3h then stained for flow cytometry analysis. All data points were pooled to calculate a linear correlation. The slope's deviation from zero was evaluated using Fisher's test.

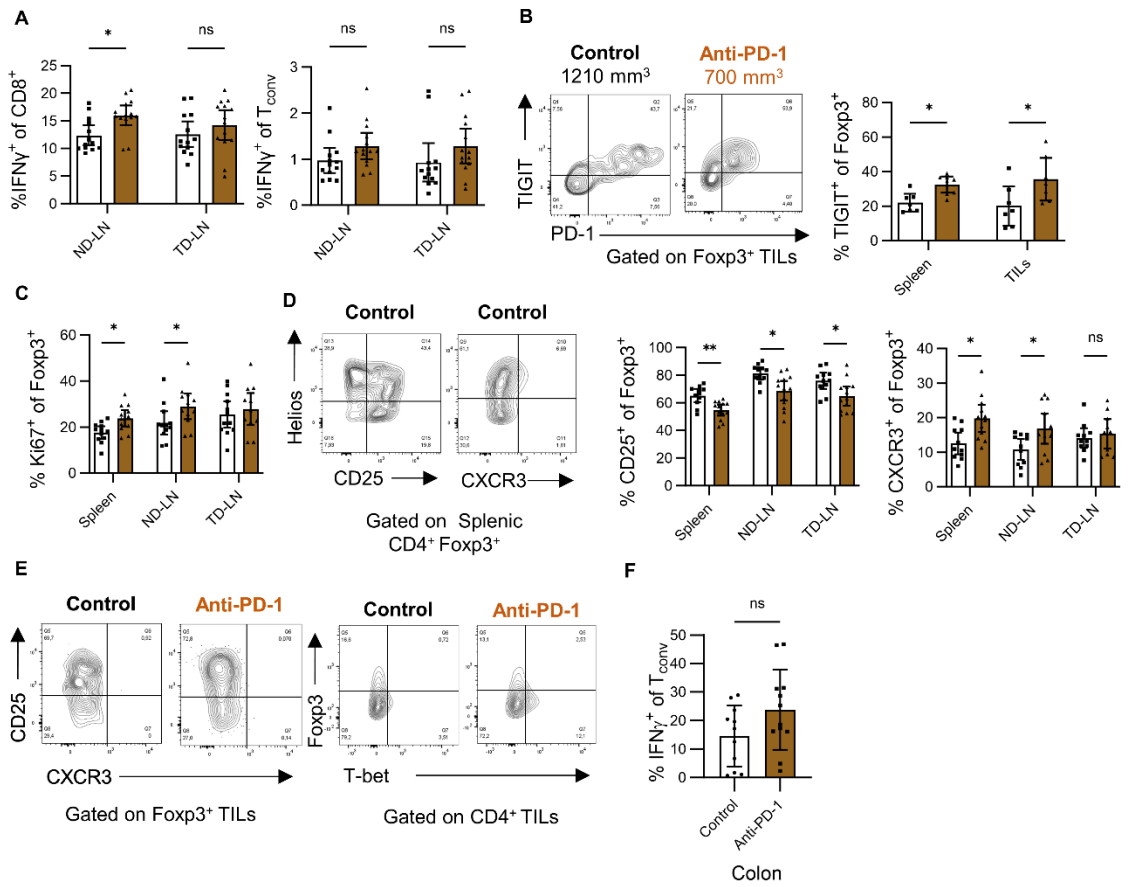

Supplementary Figure 1

A. Flow cytometry analysis of IFNγ expression by $CD8^+$ and $CD4^+$ T cells in tumor-draining (inguinal right) lymph nodes and non-draining (contralateral) lymph nodes.

B-C. Representative flow plots and flow cytometry analysis of TIGIT and Ki67 expression by T_{reg} cells. Means were compared using a two-way ANOVA with Holm-Sidak's correction for multiple comparisons.

D. Representative flow plots and flow cytometry analysis of Helios, CXCR3 and CD25 expression by circulating T_{reg} cells. Means were compared using a Two-Way ANOVA with Holm-Sidak's correction for multiple comparisons.

E. Representative flow plots of CD25, CXCR3 and T-bet expression by T_{reg} TILs. F. Flow cytometry analysis of IFNγ expression by colonic $CD4^+$ T_{conv} cells. Single cell suspensions were

obtained after digestion in collagenase IV for 1h and stimulated with PMA, Ionomycin and GolgiStop for 3h then stained for flow cytometry analysis. Means compared with an unpaired Student's t-test. Each dot represents one mouse, all data represented as mean +/- 95% CI.

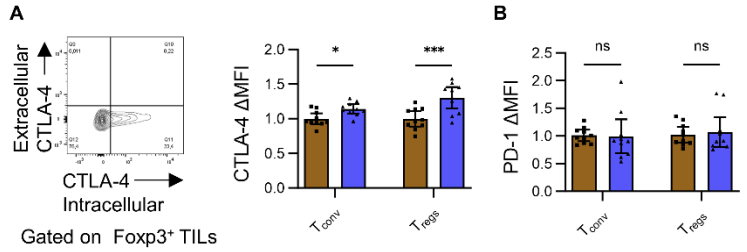

Supplementary Figure 2

A. Representative flow plots of CTLA-4 expression by T_{reg} TILs and flow cytometry analysis of intracellular CTLA-4 expression by Tconv and T_{reg} TILs. Fold CTLA-4 MFI changes were calculated by dividing each CTLA-4 MFI by the average in the anti-PD-1 group for their respective experiment. Fold MFI changes were compared using a Two-Way ANOVA with Tukey's correction for multiple comparisons.

B. Fold PD-1 MFI changes were calculated by dividing each MFI by the average in both groups for their respective experiment. Fold MFI changes were compared using a Two-Way ANOVA with Tukey's correction for multiple comparisons.

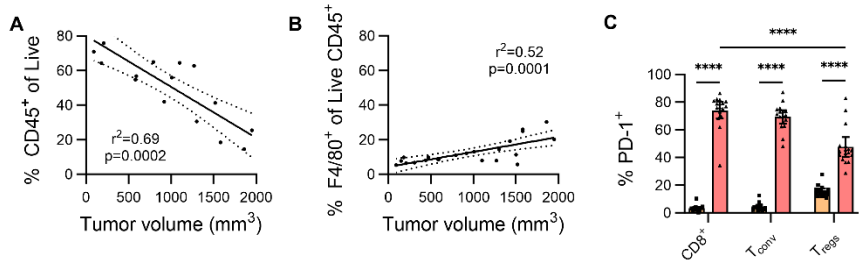

Supplementary Figure 3

A-B. Flow cytometry analysis of CD45 and F4/80 expression by tumor-infiltrating cells. All data points were pooled to calculate a linear correlation. The slope's deviation from zero was evaluated using Fisher's test.

C. Flow cytometry analysis of PD-1 expression by $CD8^+$, T_{conv} and T_{reg} cells. Means were compared using Tukey's multiple comparisons test.

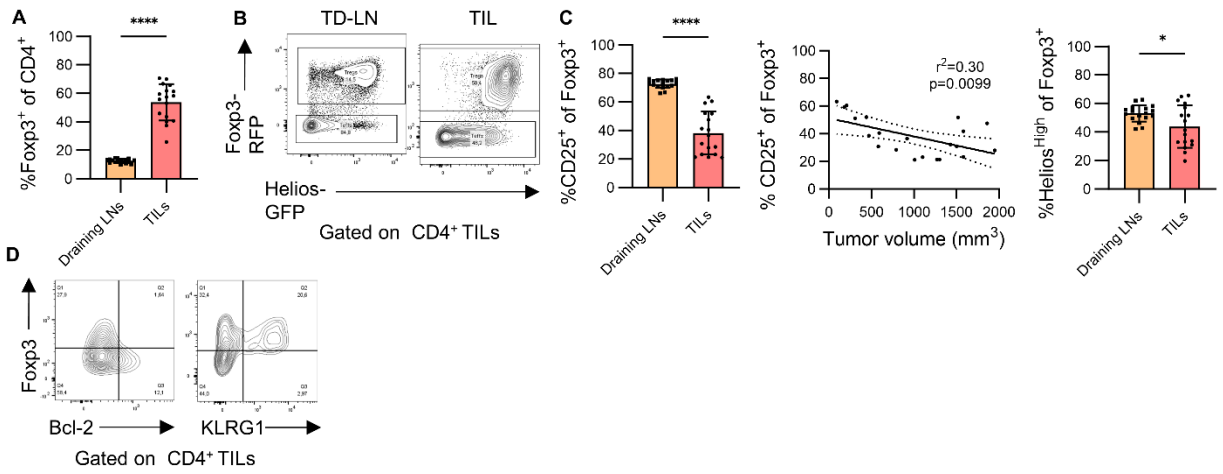

Supplementary Figure 4

A. Foxp3^{RFP} Helios^{GFP} dual reporter mice were inoculated with 2.5x10^5 YUMMER1.7 cells as previously described (N=2, n=10). For analysis of reporter protein expression, single cell suspensions were stained for extracellular markers and acquired live on the same day. Flow cytometry analysis of Foxp3 and Helios reporter protein expression.

B. Flow cytometry analysis of Foxp3 expression by CD4$^+$ T cells.

C. Flow cytometry analysis of Helios and CD25 expression by T_{reg} cells. Means were compared using a paired Student's t-test. All data points were pooled to calculate a linear correlation. The slope's deviation from zero was evaluated using Fisher's test.

D. Representative flow plots of Bcl-2 and KLRG1 expression by CD4$^+$ TILs.

References

1. Wolchok JD, et al. Long-Term Outcomes With Nivolumab Plus Ipilimumab or Nivolumab Alone Versus Ipilimumab in Patients With Advanced Melanoma. *JCO*. 2022;40(2):127–137.

2. Robert C, et al. Seven-Year Follow-Up of the Phase III KEYNOTE-006 Study: Pembrolizumab Versus Ipilimumab in Advanced Melanoma. *JCO*. 2023;41(24):3998–4003.

3. Seymour L, et al. iRECIST: guidelines for response criteria for use in trials testing immunotherapeutics. *Lancet Oncol*. 2017;18(3):e143–e152.

4. Gibney GT, Weiner LM, Atkins MB. Predictive biomarkers for checkpoint inhibitor-based immunotherapy. *Lancet Oncol*. 2016;17(12):e542–e551.

5. Kümpers C, et al. Immune Cell Infiltration of the Primary Tumor, Not PD-L1 Status, Is Associated With Improved Response to Checkpoint Inhibition in Metastatic Melanoma. *Front Med (Lausanne)*. 2019;6:27.

6. Wang J, et al. Eliciting T cell immunity against poorly immunogenic tumors by immunization with dendritic cell-tumor fusion vaccines. *J Immunol*. 1998;161(10):5516–24.

7. Zhou Q, et al. Blockade of Programmed Death-1 Pathway Rescues the Effector Function of Tumor-Infiltrating T Cells and Enhances the Antitumor Efficacy of Lentivector Immunization. *J Immunol*. 2010;185(9):5082–5092.

8. Curran MA, et al. PD-1 and CTLA-4 combination blockade expands infiltrating T cells and reduces regulatory T and myeloid cells within B16 melanoma tumors. *PNAS*. 2010;107(9):4275–4280.

9. Li B, et al. Anti-programmed death-1 synergizes with granulocyte macrophage colony-stimulating factor--secreting tumor cell immunotherapy providing therapeutic benefit to mice with established tumors. *Clin Cancer Res*. 2009;15(5):1623–1634.

10. Simpson TR, et al. Fc-dependent depletion of tumor-infiltrating regulatory T cells co-defines the efficacy of anti–CTLA-4 therapy against melanoma. *Journal of Experimental Medicine*. 2013;210(9):1695–1710.

11. Kim JW, Eder JP. Prospects for targeting PD-1 and PD-L1 in various tumor types. *Oncology (Williston Park, NY)*. 2014;28 Suppl 3:15–28.

12. Schadendorf D, et al. Melanoma. *Nat Rev Dis Primers*. 2015;1(1):1–20.

13. Hodis E, et al. A Landscape of Driver Mutations in Melanoma. *Cell*. 2012;150(2):251–263.

14. Dankort D, et al. Braf(V600E) cooperates with Pten loss to induce metastatic melanoma. *Nat Genet*. 2009;41(5):544–52.

15. Sumimoto H, et al. The BRAF-MAPK signaling pathway is essential for cancer-immune evasion in human melanoma cells. *J Exp Med*. 2006;203(7):1651–1656.

16. Peng W, et al. Loss of PTEN Promotes Resistance to T Cell–Mediated Immunotherapy. *Cancer Discov*. 2016;6(2):202–216.

17. DeNardo DG, Ruffell B. Macrophages as regulators of tumour immunity and immunotherapy. *Nat Rev Immunol*. 2019;19(6):369–382.

18. Jenkins MH, et al. Multiple murine BRafV600E melanoma cell lines with sensitivity to PLX4032. *Pigment Cell Melanoma Res*. 2014;27(3):495–501.

19. Bonaventura P, et al. Cold Tumors: A Therapeutic Challenge for Immunotherapy. *Front Immunol*. 2019;10. https://doi.org/10.3389/fimmu.2019.00168

20. Jones E, et al. Depletion of CD25+ regulatory cells results in suppression of melanoma growth and induction of autoreactivity in mice. *Cancer Immun*. 2002;2:1.

21. Nakagawa H, et al. Instability of Helios-deficient Tregs is associated with conversion to a T-effector phenotype and enhanced antitumor immunity. *PNAS*. 2016;113(22):6248–6253.

22. Kumagai S, et al. The PD-1 expression balance between effector and regulatory T cells predicts the clinical efficacy of PD-1 blockade therapies. *Nature Immunology*. 2020;21(11):1346–1358.

23. Perry JA, et al. PD-L1–PD-1 interactions limit effector regulatory T cell populations at homeostasis and during infection. *Nat Immunol*. 2022;1–14.

24. Thornton AM, et al. Helios+ and Helios− Treg subpopulations are phenotypically and functionally distinct and express dissimilar TCR repertoires. *European Journal of Immunology*. 2019;49(3):398–412.

25. Lowther DE, et al. PD-1 marks dysfunctional regulatory T cells in malignant gliomas. *JCI Insight*. 2019;1(5). https://doi.org/10.1172/jci.insight.85935

26. Guram K, et al. A Threshold Model for T-Cell Activation in the Era of Checkpoint Blockade Immunotherapy. *Front Immunol*. 2019;10. https://doi.org/10.3389/fimmu.2019.00491

27. Alissafi T, et al. Balancing cancer immunotherapy and immune-related adverse events: The emerging role of regulatory T cells. *J Autoimmun*. 2019;102310.

28. Kamada T, et al. PD-1+ regulatory T cells amplified by PD-1 blockade promote hyperprogression of cancer. *PNAS*. 2019;116(20):9999–10008.

29. Tan CL, et al. PD-1 restraint of regulatory T cell suppressive activity is critical for immune tolerance. *Journal of Experimental Medicine*. 2020;218(e20182232). https://doi.org/10.1084/jem.20182232

30. Sharma P, et al. Primary, Adaptive and Acquired Resistance to Cancer Immunotherapy. *Cell*. 2017;168(4):707–723.

31. Wang J, et al. UV-induced somatic mutations elicit a functional T cell response in the YUMMER1.7 Mouse Melanoma Model. *Pigment Cell Melanoma Res*. 2017;30(4):428–435.

32. Galon J, Bruni D. Approaches to treat immune hot, altered and cold tumours with combination immunotherapies. *Nature Reviews Drug Discovery*. 2019;18(3):197–218.

33. Galon J, et al. Type, Density, and Location of Immune Cells Within Human Colorectal Tumors Predict Clinical Outcome. *Science*. 2006;313(5795):1960–1964.

34. Gato-Cañas M, et al. PDL1 Signals through Conserved Sequence Motifs to Overcome Interferon-Mediated Cytotoxicity. *Cell Rep*. 2017;20(8):1818–1829.

35. Oestreich KJ, et al. NFATc1 regulates PD-1 expression upon T cell activation. *J Immunol*. 2008;181(7):4832–4839.

36. Jin Y, et al. Different syngeneic tumors show distinctive intrinsic tumor-immunity and mechanisms of actions (MOA) of anti-PD-1 treatment. *Sci Rep*. 2022;12(1):3278.

37. Nagasaki J, et al. PD-1 blockade therapy promotes infiltration of tumor-attacking exhausted T cell clonotypes. *Cell Reports*. 2022;38(5):110331.

38. Im SJ, et al. Defining CD8+ T cells that provide the proliferative burst after PD-1 therapy. *Nature*. 2016;537(7620):417–421.

39. Flores-Borja F, et al. Defects in CTLA-4 are associated with abnormal regulatory T cell function in rheumatoid arthritis. *Proc Natl Acad Sci USA*. 2008;105(49):19396–19401.

40. Joller N, et al. Treg cells expressing the coinhibitory molecule TIGIT selectively inhibit proinflammatory Th1 and Th17 cell responses. *Immunity*. 2014;40(4):569–581.

41. Takatori H, et al. Helios Enhances Treg Cell Function in Cooperation With FoxP3. *Arthritis Rheumatol*. 2015;67(6):1491–1502.

42. Tang Q, et al. Central Role of Defective Interleukin-2 Production in the Triggering of Islet Autoimmune Destruction. *Immunity*. 2008;28(5):687–697.

43. Kornete M, et al. Th1-Like ICOS+ Foxp3+ Treg Cells Preferentially Express CXCR3 and Home to β-Islets during Pre-Diabetes in BDC2.5 NOD Mice. *PLOS ONE*. 2015;10(5):e0126311.

44. Santegoets SJ, et al. Tbet-positive regulatory T cells accumulate in oropharyngeal cancers with ongoing tumor-specific type 1 T cell responses. *Journal for ImmunoTherapy of Cancer*. 2019;7(1):14.

45. Gunawan F, George E, Roberts A. Combination immune checkpoint inhibitor therapy nivolumab and ipilimumab associated with multiple endocrinopathies. *Endocrinology, Diabetes & Metabolism Case Reports*. 2018;2018(1). https://doi.org/10.1530/EDM-17-0146

46. Yu J, et al. Loss of MHC-I antigen presentation correlated with immune checkpoint blockade tolerance in MAPK inhibitor-resistant melanoma. *Frontiers in Pharmacology*. 2022;13.https://www.frontiersin.org/articles/10.3389/fphar.2022.928226. . Accessed July 11, 2023

47. Cornel AM, Mimpen IL, Nierkens S. MHC Class I Downregulation in Cancer: Underlying Mechanisms and Potential Targets for Cancer Immunotherapy. *Cancers (Basel)*. 2020;12(7):1760.

48. Wei SC, et al. Distinct Cellular Mechanisms Underlie Anti-CTLA-4 and Anti-PD-1 Checkpoint Blockade. *Cell*. 2017;170(6):1120-1133.e17.

49. Peggs KS, et al. Blockade of CTLA-4 on both effector and regulatory T cell compartments contributes to the antitumor activity of anti–CTLA-4 antibodies. *Journal of Experimental Medicine*. 2009;206(8):1717–1725.

50. Kavanagh B, et al. CTLA4 blockade expands FoxP3+ regulatory and activated effector CD4+ T cells in a dose-dependent fashion. *Blood*. 2008;112(4):1175–1183.

51. Chung B, et al. Interferon-gamma induces PD-L1 expression in macrophages and neutrophils. *Journal of the American College of Surgeons*. 2011;213(3):S63.

52. Muraoka D, et al. Antigen delivery targeted to tumor-associated macrophages overcomes tumor immune resistance. *J Clin Invest*. 2019;129(3):1278–1294.

53. Kuo PT, et al. The Role of CXCR3 and Its Chemokine Ligands in Skin Disease and Cancer. *Front Med*. 2018;5. https://doi.org/10.3389/fmed.2018.00271

54. Blank CU, et al. Defining 'T cell exhaustion.' *Nature Reviews Immunology*. 2019;19(11):665–674.

55. Kao C, et al. T-bet represses expression of PD-1 and sustains virus-specific CD8 T cell responses during chronic infection. *Nat Immunol*. 2011;12(7):663–671.

56. Zhu Y, et al. T-bet and Eomesodermin Are Required for T Cell-Mediated Antitumor Immune Responses. *The Journal of Immunology*. 2010;185(6):3174–3183.

57. Iwai Y, et al. An IFN-γ-IL-18 Signaling Loop Accelerates Memory CD8+ T Cell Proliferation. *PLOS ONE*. 2008;3(6):e2404.

58. Philip M, et al. Chromatin states define tumour-specific T cell dysfunction and reprogramming. *Nature*. 2017;545(7655):452–456.

59. Akimova T, et al. Helios Expression Is a Marker of T Cell Activation and Proliferation. *PLOS ONE*. 2011;6(8):e24226.

60. Iida T, et al. Regulation of cell surface expression of CTLA-4 by secretion of CTLA-4-containing lysosomes upon activation of CD4+ T cells. *J Immunol*. 2000;165(9):5062–5068.

61. Chen F, et al. TIGIT enhances CD4+ regulatory T-cell response and mediates immune suppression in a murine ovarian cancer model. *Cancer Medicine*. 2020;9(10):3584–3591.

62. Koch MA, et al. T-bet+ Treg Cells Undergo Abortive Th1 Cell Differentiation due to Impaired Expression of IL-12 Receptor β2. *Immunity*. 2012;37(3):501–510.

63. Alvarez F, et al. IL-18 is required for the TH1-adaptation of TREG cells and the selective suppression of TH17 responses in acute and chronic infections. *Mucosal Immunol*. 2023;S1933-0219(23)00035–1.

64. Joller N, et al. Treg cells expressing the coinhibitory molecule TIGIT selectively inhibit proinflammatory Th1 and Th17 cell responses. *Immunity*. 2014;40(4):569–81.

65. Vocanson M, et al. Inducible costimulator (ICOS) is a marker for highly suppressive antigen-specific T cells sharing features of TH17/TH1 and regulatory T cells. *J Allergy Clin Immunol*. 2010;126(2):280–289, 289.e1–7.

66. Murase K, et al. Low-Dose IL-2 Induces Bcl2 Expression and Resistance To Apoptosis In CD4 Regulatory T Cells. *Blood*. 2013;122(21):3475.

67. Kornete M, et al. KLRG1 expression identifies short-lived Foxp3+ Treg effector cells with functional plasticity in islets of NOD mice. *Autoimmunity*. 2017;50(6):354–362.

68. Nebhan CA, Johnson DB. Predictive biomarkers of response to immune checkpoint inhibitors in melanoma. *Expert Rev Anticancer Ther*. 2020;20(2):137–145.

69. Lo JA, et al. Epitope spreading toward wild-type melanocyte-lineage antigens rescues suboptimal immune checkpoint blockade responses. *Science Translational Medicine*. 2021;13(581):eabd8636.

70. Onda M, Kobayashi K, Pastan I. Depletion of regulatory T cells in tumors with an anti-CD25 immunotoxin induces CD8 T cell-mediated systemic antitumor immunity. *PNAS*. 2019;116(10):4575–4582.

71. Michot JM, et al. Immune-related adverse events with immune checkpoint blockade: a comprehensive review. *Eur J Cancer*. 2016;54:139–148.

72. Attias M, Al-Aubodah T, Piccirillo CA. Mechanisms of human FoxP3 $^{+}$ T $_{reg}$ cell development and function in health and disease. *Clin Exp Immunol*. 2019;cei.13290.

73. Dyck L, et al. Anti-PD-1 inhibits Foxp3+ Treg cell conversion and unleashes intratumoural effector T cells thereby enhancing the efficacy of a cancer vaccine in a mouse model. *Cancer immunology, immunotherapy: CII*. 2016;65(12):1491–1498.

74. Principe DR, et al. Regulatory T-Cells as an Emerging Barrier to Immune Checkpoint Inhibition in Lung Cancer. *Front Oncol*. 2021;11:684098.

75. Moreno BH, et al. Response to Programmed Cell Death-1 Blockade in a Murine Melanoma Syngeneic Model Requires Costimulation, CD4, and CD8 T Cells. *Cancer Immunol Res*. 2016;4(10):845–857.

76. Mehdi A, et al. S-adenosylmethionine blocks tumorigenesis and with immune checkpoint inhibitor enhances anti-cancer efficacy against BRAF mutant and wildtype melanomas. *Neoplasia*. 2023;36:100874.

77. Riley JL. PD-1 signaling in primary T cells. *Immunol Rev*. 2009;229(1):114–125.

78. Gros A, et al. PD-1 identifies the patient-specific CD8+ tumor-reactive repertoire infiltrating human tumors. *J Clin Invest*. 2014;124(5):2246–2259.

79. Schietinger A, et al. Tumor-Specific T Cell Dysfunction Is a Dynamic Antigen-Driven Differentiation Program Initiated Early during Tumorigenesis. *Immunity*. 2016;45(2):389–401.

80. Simoni Y, et al. Bystander CD8+ T cells are abundant and phenotypically distinct in human tumour infiltrates. *Nature*. 2018;557(7706):575–579.

81. Kuehm LM, et al. Checkpoint blockade immunotherapy enhances the frequency and effector function of murine tumor-infiltrating T cells but does not alter TCRβ diversity. *Cancer Immunol Immunother*. 2019;68(7):1095–1106.

82. Sakaguchi S, et al. Immunologic self-tolerance maintained by activated T cells expressing IL-2 receptor alpha-chains (CD25). Breakdown of a single mechanism of self-tolerance causes various autoimmune diseases. *The Journal of Immunology*. 1995;155(3):1151.

83. Ahmadzadeh M, et al. Tumor-infiltrating human CD4+ regulatory T cells display a distinct TCR repertoire and exhibit tumor and neoantigen reactivity. *Sci Immunol*. 2019;4(31). https://doi.org/10.1126/sciimmunol.aao4310

84. Nirschl CJ, Drake CG. Molecular Pathways: Co-Expression of Immune Checkpoint Molecules: Signaling Pathways and Implications for Cancer Immunotherapy. *Clin Cancer Res*. 2013;19(18):4917–4924.

85. Silva Morales M, Mueller D. Anergy into T regulatory cells: an integration of metabolic cues and epigenetic changes at the Foxp3 conserved non-coding sequence 2. *F1000Res*. 2018;7:F1000 Faculty Rev-1938.

86. Bettelli E, Dastrange M, Oukka M. Foxp3 interacts with nuclear factor of activated T cells and NF-kappa B to repress cytokine gene expression and effector functions of T helper cells. *Proc Natl Acad Sci U S A*. 2005;102(14):5138–5143.

87. Cluxton D, et al. Differential Regulation of Human Treg and Th17 Cells by Fatty Acid Synthesis and Glycolysis. *Frontiers in Immunology*. 2019;10.https://www.frontiersin.org/articles/10.3389/fimmu.2019.00115. . Accessed August 29, 2023

88. Gratz IK, Campbell DJ. Organ-Specific and Memory Treg Cells: Specificity, Development, Function, and Maintenance. *Front Immunol*. 2014;5. https://doi.org/10.3389/fimmu.2014.00333

89. Mehdi A, et al. Enhanced Anticancer Effect of a Combination of S-adenosylmethionine (SAM) and Immune Checkpoint Inhibitor (ICPi) in a Syngeneic Mouse Model of Advanced Melanoma. *Front Oncol*. 2020;10:1361.

90. Ferreira RC, et al. Cells with Treg-specific FOXP3 demethylation but low CD25 are prevalent in autoimmunity. *Journal of Autoimmunity*. 2017;84:75–86.

91. Zhang R, et al. Th1-Like Treg Cells Are Increased But Deficient in Function in Rheumatoid Arthritis. *Frontiers in Immunology*. 2022;13.https://www.frontiersin.org/articles/10.3389/fimmu.2022.863753. . Accessed August 30, 2023

92. Grigoriou M, et al. Regulatory T-cell Transcriptomic Reprogramming Characterizes Adverse Events by Checkpoint Inhibitors in Solid Tumors. *Cancer Immunology Research*. 2021;9(7):726–734.

93. Yates K, et al. Comparative transcriptome analysis reveals distinct genetic modules associated with Helios expression in intratumoral regulatory T cells. *PNAS*. 2018;115(9):2162–2167.

94. Kim H-J, et al. Stable inhibitory activity of regulatory T cells requires the transcription factor Helios. *Science*. 2015;350(6258):334–339.

95. Sebastian M, et al. Helios Controls a Limited Subset of Regulatory T Cell Functions. *The Journal of Immunology*. 2016;196(1):144–155.

96. Arce Vargas F, et al. Fc Effector Function Contributes to the Activity of Human Anti-CTLA-4 Antibodies. *Cancer Cell*. 2018;33(4):649-663.e4.

97. Bulliard Y, et al. Activating Fc γ receptors contribute to the antitumor activities of immunoregulatory receptor-targeting antibodies. *Journal of Experimental Medicine*. 2013;210(9):1685–1693.

Chapter 3 – Anti-PD-1 promotes a T_h1-like functional adaptation of melanoma-infiltrating regulatory T cells to alleviate immunosuppression locally.

Bridging statement for Chapter 3

In chapter 2, we described the phenotypes of melanoma-infiltrating T_{reg} cells in both cold and hot tumor microenvironments. Specifically, we identified a conserved population of T_{reg} cells expressing high levels of Helios which displayed a highly activated phenotype with preferential expression of PD-1 and proliferative capacity. In D4M.3A-bearing mice, anti-PD-1 induced an expansion and activation of Helios$^+$ T_{reg} cells, associated with an increase in IFNγ production by CD8$^+$ T cells. As these tumors displayed acquired resistance to ICIs, and T_{reg} TILs displayed phenotypic signs suggestive of immune exhaustion at tumor endpoint, we concluded that ICI-induced T_{reg} cell activation contributes to treatment resistance. However, this raises the question of reconciling this mechanism of action with the onset of tumor regression in high responder patients. We hypothesized that anti-PD-1 might dysregulate the suppressive function of Helios$^+$ T_{reg} cells through the Foxp3-destabilizing effect of Akt. Thus, in chapter 3, we assessed T_{reg} cell functional dynamics in response to PD-1 blockade in the YUMMER1.7 model which displayed a bimodal outcome with High and Low Responder tumors. Specifically, we deepen our functional characterization of the two phenotypes of YUMMER1.7-infiltrating T_{reg} cells identified in chapter 2, asking if exhausted-like T_{reg} cells are impaired in their suppressive function and are T_h1-adapted T_{reg} cells specialized in controlling IFNγ production? We show that a successful response to anti-PD-1 is associated with polyfunctional CD8$^+$ TILs evading *in situ* the potent suppressive function of T_{reg} TILs, which progressively acquire T_h1-like characteristics and expand in response to anti-PD-1.

Anti-PD-1 promotes a T_h1-like functional adaptation of melanoma-infiltrating regulatory T cells to alleviate immunosuppression locally.

Mikhaël Attias[1,2,3], Fernando Alvarez[1,2,3], Tho-Alfakar Al-Aubodah[1,2,3], Roman Istomine[1,2,3], Paige McCallum[4,5], Fan Huang[4,5], Abrahim Sleiman[1,2,3], Tamiko Nishimura[6], Constantin Polychronakos[7,8], Sonia V. Del Rincon[4,5], Yasser Riazalhosseini[6,8], Ciriaco A. Piccirillo[1,2,3,4]

Affiliations:

[1]Department of Microbiology and Immunology, McGill University, Montréal, Québec, Canada

[2]Program of Infectious Diseases and Immunity in Global Health, Centre for Translation Biology (CTB), The Research Institute of the McGill University Health Centre (RI-MUHC), Montréal, Québec, Canada

[3]Centre of Excellence in Translational Immunology (CETI), McGill University, Montréal, Québec, Canada

[4]Division of Experimental Medicine, McGill University, Montréal, Québec, Canada

[5]Segal Cancer Centre, Lady Davis Institute and Jewish General Hospital, McGill University, Montréal, Québec, Canada

[6] Victor Philip Dahdaleh Institute of Genomic Medicine at McGill University, Montréal, Québec, Canada

[7]Division of Pediatrics, McGill University, Montréal, Québec, Canada

[8]Department of Human Genetics, McGill University, Montréal, Québec, Canada

* Correspondence should be addressed to:

Dr. C.A. Piccirillo
Research Institute of McGill University Health Centre (MUHC)
Centre for Translational Biology, Bloc E, Room E-M2.3248
1001 Boul. Décarie, Montréal, Québec, H4A
ciro.piccirillo@mcgill.ca
Tel: 514-934-1934 ext. 76143

Keywords: Foxp3+ Treg cells, anti-PD-1, immuno-oncology, checkpoint inhibitors, melanoma, treatment biomarkers, spatial proteomic profiling.

Manuscript submitted to JCI Insight

Abstract

PD-1 blockade enhances the effector functions of melanoma-infiltrating $CD8^+$ T cells, leading to durable tumor remissions. However, 55% of melanoma patients do not respond to treatment. As $Foxp3^+$ regulatory T (T_{reg}) cells play an important role in tumor-induced immunosuppression and express PD-1, we hypothesized that anti-PD-1 also increases the effector functions of melanoma-infiltrating T_{reg} cells, which could be detrimental to treatment efficacy. Here, we used a highly immunogenic melanoma model to study the functional dynamics of T_{reg} cells following anti-PD-1 treatment. We show that the potent $CD8^+$ T cell responses characteristic of high responder tumors paradoxically correlate with the presence of highly-activated, Helios-expressing T_{reg} cells. In both high and low responder tumors, T_{reg} cells co-localize with $CD8^+$ cells, and display potent suppressive capacity *in vitro*. Using spatial proteomics, we demonstrate that T_{reg} cells display an increased activity of PI3K/Akt signaling in regions of high responder tumors with an elevated CD8:T_{reg} ratio. Further characterization revealed that melanoma-infiltrating T_{reg} cells progressively acquire T-bet and IFNγ expression, exclusively in high responders, and induction of this T_h1-like phenotype *in vitro* led to $CD8^+$ evasion from T_{reg} suppression. Taken together, these data suggest a mechanism through which anti-PD-1 relieves T_{reg} cell suppression in tumor microenvironments.

Introduction

Immune checkpoint inhibitors targeting PD-1 (nivolumab, pembrolizumab) are at the forefront of therapeutic guidelines for the treatment of many solid tumors but are associated with highly variable outcomes. Melanoma is the solid tumor type where nivolumab achieves the highest overall response rate, 45% (1, 2). While responses are durable and can persist after treatment interruption, most patients do not achieve a significant reduction in tumor burden and paradoxically, about 10% of patients have increased rates of tumor growth following treatment initiation (3). The degree of pre-existing inflammation within the tumor was found to be a strong predictive biomarker of response to treatment (4). As such, a pro-inflammatory or "hot" tumor microenvironment (TMEs) with abundant lymphocyte infiltration in the tumor's core and/or presence of tertiary lymphoid structures (5, 6) is predictive of strong response, whereas non-responsive tumors are deemed "cold" with sparse lymphocyte infiltration confined to the tumor margins. To increase the success rate of checkpoint inhibition, a deeper understanding of the mechanisms that govern the inflammatory status of the TME is required.

To dampen local inflammation and evade immune responses, tumors are adept at hijacking the suppressive mechanisms of Foxp3$^+$ regulatory T (T_{reg}) (7–10), a specialized subset of CD4$^+$ T cells which suppress autoreactive effector T (T_{eff}) cell functions to maintain peripheral tolerance but simultaneously inhibit anti-tumor activity. Through preferential recruitment (11) and a well-adapted metabolic profile (12, 13), T_{reg} cells accumulate within TMEs, leading to worse prognosis, metastatic potential, and resistance to treatment (11, 14). T_{reg} cell depletion leads to complete tumor clearance in immunologically cold, preclinical melanoma models, indicating that tumor-infiltrating (TIL) T_{reg} cells play a dominant role in tumor-induced immunosuppression (15).

It is well established that anti-PD-1 increases the proliferation and function of $CD8^+$ TILs in high responder patients through restoration of Akt signaling (16–18). However, little is known about the consequences of anti-PD-1 on the functional fate of T_{reg} cells systemically and in TMEs. Outside of tumor environments, deletion of PD-1 has been shown to enhance T_{reg} cell proliferation (19), activation and homing (20). Anti-PD-1 increases the proliferation of T_{reg} TILs in hyper-progressor gastric cancer patients (19), suggesting that PD-1^+ T_{reg} TILs diminish the efficacy of PD-1 blockade. However, this effect is not observed in responding patients for whom increased CD8:T_{reg} ratios have been proposed as a biomarker of successful response to treatment (21, 22). Furthermore, conditional deficiency of PD-1 expression in T_{reg} cells in a model of lung cancer also leads to a loss of lineage stability of T_{reg} TILs (23), suggesting that PD-1 blockade has the paradoxical potential to promote T_{reg} cell activation at the expense of stable Foxp3 expression. As such, it remains to be determined if anti-PD-1 impacts T_{reg} cell activation, proliferation, and suppressive function differently in responder and non-responder TMEs.

Recent evidence points to a key role of the zinc-finger transcription factor Helios in safeguarding T_{reg} cell function, fitness, and stability in TMEs. Functionally, Helios stabilizes the canonical T_{reg} cell transcriptional program by reinforcing *IL-2Rα* expression (24) and promotes the cycling and survival of activated T_{reg} cells by preserving Bcl-2 expression (25). The conditional deletion of Helios ($Helios^{-/-}$) in $Foxp3^+$ cells was sufficient to render the poorly immunogenic B16 melanoma hot, in turn, delaying tumor growth (26). In the absence of Helios, T_{reg} cell accumulation was reduced amongst TILs, and $Helios^{-/-}$ T_{reg} TILs displayed a more unstable T_{reg} cell phenotype as indicated by reduced Foxp3 and CD25 expression, secretion of otherwise-repressed inflammatory cytokines such as IFNγ (26) and expression of genes associated with T_h1 and T_h2 differentiation (27). As a Helios binding site is present in the *PDCD1* promoter (28), Helios-

expressing T_{reg} cells could preferentially respond to anti-PD-1. However, the functional consequences of anti-PD-1 on Helios$^+$ T_{reg} cells remain ill-defined. As high levels of Akt signaling drives IFNγ secretion in T_{reg} cells (29), a phenotype also associated with enhanced anti-tumor immunity in mice with Nrp-1 deficient T_{reg} cells (30), we hypothesized that anti-PD-1 preferentially increases Helios$^+$ TIL-T_{reg} cell activation but promotes their acquisition of inflammatory characteristics (29) in hot TMEs, thereby increasing anti-tumor responses.

To study the dynamics of T_{reg} cell function and fate throughout tumor development and anti-PD-1 monotherapy in both high (HR) and low (LR) responder TMEs, we used a pre-clinical mouse model of highly immunogenic melanoma that recapitulates the variability associated with response to anti-PD-1 in the clinic (31). We identify three novel hallmarks of T_{reg} cells in successful response to anti-PD-1: (*i*) increased activation and proliferation of the Helios-expressing T_{reg} cell subset, (*ii*) high PI3K/Akt activity in tumor regions with a high CD8:T_{reg} ratio, and (*iii*) the acquisition of T_h1-like characteristics, namely T-bet and IFNγ expression. Taken together, these data suggest a mechanism through which PD-1 blockade increases T_{reg} cell activation and proliferation but relieves their suppression locally in hot tumors.

Results

Helios$^+$ Foxp3$^+$ T_{reg} cells accumulate in melanoma tumors throughout successful response to anti-PD-1 monotherapy.

While the role of T_{reg} cells in promoting tumor growth is well established, their function and fate during PD-1 blockade remain ill-defined. Thus, we investigated the dynamics of T_{reg} cell infiltration in hot or cold TMEs throughout tumor development in the YUMMER1.7 murine melanoma model, which has variable outcomes in response to checkpoint blockade (31). Male Foxp3-IRES-mRFP (Foxp3^{RFP}) reporter mice were injected s.c. with YUMMER1.7 cells ($2.5x10^5$) and received treatment with either anti-PD-1 or PBS control once tumors reached palpability, at day 8. Mice were sacrificed when control tumors reached humane endpoint, on day 20 (N=10) (**Figure 1A**). As some anti-PD-1 treated mice did not experience a delay in tumor growth **(Figure 1B)**, we identified LR (tumor weight>300 mg) and HR mice (tumor weight <300mg), based on the bimodal distribution of tumor weights in the anti-PD-1 group (**Supplementary Figure 1A**). The success rate of anti-PD-1 was 52% (24 of 46 mice), like previous descriptions (31, 32). Notably, after treatment discontinuation, HR tumor volume remained below $300mm^3$ (N=3), indicative of a durable response (**Supplementary Figure 1B**).

To determine the immune cell populations that associate with response to anti-PD-1, we correlated tumor weight with the immune composition of the TME at endpoint (**Figure 1C**). As expected, tumor weight was positively correlated with a "cold" immune environment, abundantly infiltrated by CD11b$^+$ F480$^+$ macrophages (r=0.6), whereas HR tumors displayed a "hot" phenotype with high frequencies of CD8$^+$ (r=-0.6) and CD4$^+$ T cells (r=-0.5). There was no significant difference in immune composition between control and LR tumors (**Supplementary Figure 1C-E**).

To determine the dynamics of T cell responses, we sacrificed tumor-bearing mice at earlier timepoints: pre-treatment on day 7 (N=3), or halfway through endpoint, at day 14 (N=2), and assessed the immune composition of TILs. In control tumors, $CD8^+$ T cells gradually accumulated and represented up to 80% of all T cells at tumor endpoint. While anti-PD-1 did not increase the proportion of $CD8^+$ T cells amongst T cells, the density of $CD8^+$ TILs increased with time during a successful response (**Figure 1D**). Notably, T_{reg} cell density was increased 10-fold between pre-treatment and HR tumors, but not in control and LR tumors (**Figure 1E**). As such, CD8:T_{reg} cell ratios in TMEs did not correlate with tumor weight (**Supplementary Figure 1F)**. In contrast, HR $CD8^+$ TILs displayed lower levels of PD-1 and Tim-3 expression (**Supplementary Figure 1G)** and were polyfunctional ($IFN\gamma^+$ $TNF\alpha^+$, **Figure 1F**), a major hallmark of response to anti-PD-1, despite the increasing frequency of T_{reg} cells.

Since Helios expression is associated with stable, potent T_{reg} cell suppressive function (24) and promotes T_{reg} cell cycling and survival in TMEs (26), we investigated its expression in $CD4^+$ TILs. Strikingly, the frequency of $Helios^{High}$ T_{reg} cells within $CD4^+$ T cells increased throughout successful response to anti-PD-1 and was significantly increased compared to LR and PBS tumors (**Figure 1G**). As such, one of the strongest indicators of the presence of polyfunctional $CD8^+$ TILs at endpoint was the frequency of $Helios^{High}$ T_{reg} cells (r^2=0.50, $p<0.0001$, **Figure 1H**). Taken together, these data indicate that successful response to anti-PD-1 promotes the simultaneous accumulation of polyfunctional $CD8^+$ T cells and $Helios^{High}$ T_{reg} TILs.

PD-1 upregulation alters the phenotype of melanoma-infiltrating T_{reg} cells at tumor endpoint.

To better characterize the functional consequences of PD-1 blockade on $Helios^{High}$ T_{reg} cells, we first investigated their fate during spontaneous tumor growth. To this end, we

characterized T_{reg} cell phenotype in tumors and draining lymph-node of PBS-treated mice. While most T_{reg} TILs expressed high levels of Helios at day 7, the proportion of Helios^{High} cells contracted by day 20, in favor of Helios^{low} T_{reg} TILs that expressed higher levels of PD-1 (**Figure 2A**). As Helios promotes T_{reg} cell expression of CD25 and proliferation (24), we observed a corresponding decrease in the proportion of CD25^{High} and mitotically active (Ki67^{+}) T_{reg} cells through time (**Supplementary Figure 2A and B**), which was not observed in the tumor-draining lymph nodes. Furthermore, at all timepoints, cycling cells were exclusively found in the Helios^{High} compartment, indicating that Helios^{low} cells do not emerge through cellular expansion (**Supplementary Figure 2B**). As the highest levels of PD-1 expression are reached upon chronic antigenic stimulation (33), and PD-1^{+} Helios^{low} cells were not observed at day 7 (**Figure 2A**), we hypothesized that Helios^{low} cells originate from Helios^{High} T_{reg} TILs undergoing chronic activation in the TME. In lymphoid tissues, PD-1 expression was restricted to the Helios^{High} compartment at all timepoints (**Supplementary Figure 2C**), and the proportion of PD-1^{+} T_{reg} TILs increased through time (**Supplementary Figure 2D**). Furthermore, high levels of PD-1 expression at endpoint were associated with reduced Foxp3, Helios and CD25 expression levels (**Figure 2B**), a phenotype associated with an absence of IL-2 production by CD4^{+} T_{conv} cells at endpoint (**Supplementary Figure 2E**). Taken together these data indicate that T_{reg} cells display reduced fitness at tumor endpoint.

To test if PD-1 signaling could directly lead to a reduction in the expression of T_{reg} cell canonical markers, we turned to an *in vitro* T cell activation model. Using Helios^{GFP}-Foxp3^{RFP} dual reporter mice, we cultured purified splenic and TIL Helios^{High} Foxp3^{+} (GFP^{High}/RFP^{+}) cells isolated from untreated mice at tumor endpoint, in the presence or absence of PD-L1-Fc (5µg/ml) (**Figure 2C**). At the end of our culture, the expression of Helios and CD25 was decreased in splenic

T_{reg} cells activated with PD-L1-Fc and further reduced in T_{reg} TILs (**Figure 2D**, N=3), suggesting a direct link between PD-1 signalling and the altered phenotype of T_{reg} TILs. Furthermore, T_{reg} TILs expressed significantly lower levels of Foxp3 and Bcl-2, suggesting reduced STAT5 signaling and increased susceptibility to apoptosis (**Supplementary Figure 2F**).

Expression of high levels of PD-1 renders $CD8^+$ TILs dysfunctional (34) and loss of Foxp3 expression is often associated with reduced suppressive potency (35). To determine if T_{reg} TILs maintain their suppressive function at tumor endpoints, we isolated splenic and TIL RFP^+ T_{reg} cells from untreated, tumor-bearing $Foxp3^{RFP}$ mice and co-cultured them at various ratios with splenic, CTV-labelled, $CD4^+$ RFP^- T responder (T_{resp}) cells ($5x10^4$) (**Figure 2E**). T_{reg} TILs displayed more potent suppressive activity than their splenic counterparts, as measured by the reduction of T_{resp} division index, despite fewer T_{reg} TILs at the end the assay (**Figure 2F**). Indeed, as observed *ex vivo*, T_{reg} TILs had low expression of CD25 and Ki67 (**Supplementary Figure 2G**) but expressed higher levels of ICOS, GRZB and IL-10 than their splenic counterparts (**Supplementary Figure 2H**), indicating their highly differentiated state with enhanced suppressive mechanisms. Taken together, despite reduced fitness at endpoint, T_{reg} TILs display enhanced suppressive function and contribute to the maintenance of an immunosuppressed tumor environment.

PD-1 blockade promotes the activation and proliferation of highly suppressive Helios-expressing T_{reg} cells.

Given that successful response to PD-1 blockade was associated with an increased frequency of $Helios^{High}$ T_{reg} cells in $CD4^+$ TILs, and that PD-1^+ T_{reg} cells expressed Helios before treatment initiation (**Figure 2A)**, we hypothesized that these cells might preferentially respond to anti-PD-1. At day 7, $Helios^{High}$ T_{reg} cells displayed greater expression of checkpoint molecules associated with highly-suppressive T_{reg} cells (CTLA-4 (36), TIGIT (37), ICOS (38)), compared to

their Helios^{low} counterparts (**Figure 3A)**, and T_{reg} TILs expressed higher levels of checkpoint molecules compared to their lymph node counterparts (**Figure 3A**), suggesting ongoing local TCR activation (38). At day 14, there was no reduction in tumor weight, and we did not identify any difference in immune phenotype between PBS and anti-PD-1 mice (**Supplementary Figure 3A**). Nonetheless, we observed systemic effects of anti-PD-1 on T_{reg} cell phenotype as shown by the increased frequency of splenic PD-1^{+} and proliferating (Ki67^{+}) T_{reg} cells, in contrast to other T_{eff} cells (**Figure 3B**). Furthermore, the proportion of T_{reg} cells, and specifically the Helios^{High} subset, within the T cell compartment was increased and expressed checkpoint molecules such as ICOS in higher levels and proportion (**Figure 3C**) in the spleen. Thus, anti-PD-1 increases the activation and proliferation of Helios^{High} T_{reg} cells in circulation as early as six days following treatment onset.

To assess the consequences of anti-PD-1 treatment on T_{reg} TILs, we assessed their expression of T_{reg} cell activation markers (CTLA-4, TIGIT and ICOS) relative to their cycling status (Ki67) at endpoint. Frequencies of cells expressing Helios were elevated in T_{reg} cells from HR tumors than those from PBS and LR tumors (**Figure 3D**). Accordingly, HR T_{reg} TILs were also more proliferative as shown by the percentage of Ki-67^{+} cells, and expressed higher levels of CTLA-4, TIGIT, and ICOS (**Figure 3D**) suggesting that successful response to PD-1 blockade increases the proliferation and activation of Helios^{High} T_{reg} TILs, all-the-while enabling strong anti-tumor responses.

Indeed, high expression of checkpoint molecules such as CTLA-4 and ICOS, while associated with highly suppressive T_{reg} cells (36–38), strongly correlated with the frequency of IFNγ^{+} CD8^{+} T cells (**Supplementary Figure 3B**). Thus, we assessed the suppressive potency of T_{reg} TILs from either HR or LR tumors (**Figure 3E**). While HR T_{reg} TILs failed to curtail anti-

tumor responses *in vivo*, they nonetheless displayed the most potent suppressive capacity, with up to 80% suppression at a 1:4 T_{reg}:T_{resp} ratio, compared to LR T_{reg} TILs (50%) and splenic T_{reg} cells (40%) (**Figure 3F**). Nonetheless, HR and LR T_{reg} cells displayed similar suppressive potency on a per cell basis (**Supplementary Figure 3C**). Indeed, HR T_{reg} cells displayed increased expression of fitness markers (Foxp3, CD25, Ki67) and ICOS compared to their LR counterparts (**Supplementary Figure 3D**). Taken together, these data indicate that HR T_{reg} cells are not intrinsically impaired in their suppressive capacity and suggests that conditions within the HR TME allow for $CD8^+$ TIL evasion from suppression.

T_{reg} cells preferentially co-localize with $CD8^+$ T cells in tumor microenvironments.

We then asked whether differential localization of T_{reg} cells relative to $CD8^+$ TILs in hot and cold TMEs results in local T_{reg}/CD8 imbalances and consequential T_{eff} evasion from suppression in highly inflamed areas of the TME. To this end, we performed immunofluorescence analysis of FFPE tumor sections collected from PBS (n=6), LR (n=4) and HR (n=6) mice. There were no differences in terms of T_{reg} and $CD8^+$ T cell infiltration between PBS and LR tumors. TILs were mostly restricted to peritumoral regions, whereas HR tumors presented with abundant infiltration in the tumor core (**Figure 4A**). Furthermore, we observed a 2-fold increase in $CD8^+$ T cell density in HR tumors compared to LR and PBS (**Figure 4B)**. Similarly, T_{reg} cell density was also increased 3-fold in HR tumors compared to LR and PBS (**Figure 4C**).

Melanoma invasiveness is associated with a process of de-differentiation through which the expression of Mart-1 and other melanoma antigens, and the resulting immunogenicity, is reduced (39). Thus, to determine if tumor immunogenicity alters the pattern of lymphocyte infiltration, we analyzed the distribution of Mart-1 expression in our tumors. Mart-1 expression was mostly restricted to the tumor periphery in cold tumors (**Figure 4D, left panel**), whereas Mart-

1^{High} melanocytes were found in the core of HR tumors (**Figure 4D, right panel**). Furthermore, the proportion of Mart-1^{High} tumor cells within the whole tissue was increased in HR tumors (**Figure 4E**), confirming their higher immunogenicity. We hypothesized that $CD8^+$ TILs are recruited to immunogenic and differentiated Mart-1-expressing melanoma cells to exert their anti-tumor activity. Therefore, we overlayed the annotated regions of Mart-1 expression with heatmaps of CD8 density (**Figure 4D**). In all 3 groups, $CD8^+$ T cell density was increased in Mart-1^{High} tumor regions compared to the rest of the tissue (**Figure 4F**). Taken together, these data suggest that expression of tumor-antigens shapes the localization of $CD8^+$ TILs within the tumor bed.

Next, we assessed the localization of RFP^+ T_{reg} cells relative to $CD8^+$ TILs. To this end, we identified the localization of the five hotspots of maximal Foxp3 density within each tumor. In PBS and LR tumors, T_{reg} cell density was maximal in peritumoral areas (**Figure 4G, left and central panel**). In HR tumors, T_{reg} cells also co-localized with $CD8^+$ TILs and were present in abundance within the tumor's core (**Figure 4G, right panel**). As such, $CD8^+$ T cell density was increased in T_{reg} cell dense areas compared to the whole tissue average (**Figure 4H**). Nonetheless, we identified regions in HR tumors where despite significant T_{reg} cell infiltration, the local CD8:T_{reg} ratio was very high (**Figure 4D and G, white arrow**), suggesting localized evasion from suppression. Taken together, these data indicate that tumor immunogenicity shapes the lymphocyte infiltration pattern and that T_{reg} cells co-localize with $CD8^+$ T cells in both hot and cold TMEs.

Spatial proteomic profiling reveals increased PI3K/Akt activity in both $CD8^+$ and T_{reg} cells located in T_{reg} sparse regions of high responder tumors.

To determine if T_{reg} cell phenotype is impacted by localization within the TME of LR and HR tumors, we performed spatial proteomic profiling using GeoMx® DSP (Nanostring). We selected 15 regions of interest (ROIs) based on low and high T_{reg} cell density in LR (n=1) and HR

(n=3) tumors (**Figure 5A**). Within the LR tumor, T_{reg} sparse areas (<300 T_{reg}/mm^2) had reduced $CD8^+$ T cell density (<1500 $CD8^+/mm^2$) compared to T_{reg} dense areas (**Figure 5B**), indicative of immunologically cold regions. However, in HR tumors, there was no difference in $CD8^+$ T cell density (>1500 $CD8/mm^2$) between T_{reg} sparse and dense areas indicating that the local T_{reg} cell density was not associated with the level of $CD8^+$ T cell infiltration (**Figure 5C**). Within each ROI, $CD8^+$, T_{reg} cells, and Mart-1^+ tumor cell masks, were applied based on fluorescent antibody expression to segment each cell population in their respective areas of interest (AOIs). Each AOI was then profiled for the expression of 53 proteins by next-generation sequencing of photocleavable barcodes (**Supplementary Table 1**). Unsupervised hierarchical clustering and principal component analysis revealed that areas of interest clustered according to cell type and ROI type (**Supplementary Figure 4A**) and appropriate levels of CD45, CD8 and Foxp3 expression within each AOI (**Supplementary Figure 4B**).

To confirm the increased levels of $CD8^+$ and T_{reg} cell activation observed *ex vivo* in HR tumors, we pooled ROIs based on tumor type. We observed a significant increase in CD28 and ICOS expression in $CD8^+$ segments from HR tumors (fold change >1.65, false discovery rate= 5%), indicating increased co-stimulatory capacity in these regions (**Figure 5D**). Furthermore, in both $CD8^+$ and T_{reg} cell segments, there was higher expression of PLCG1, an enzyme that mobilizes intracellular Ca^{2+} upon TCR engagement (40), in HR ROIs, denoting higher TCR-induced activation (**Figure 5E**). Thus, a reduction in TCR signal strength and co-stimulatory signals is a major feature underlying the differences between hot and cold TMEs.

To assess T_{reg} cell-mediated suppression *in situ* in HR tumors, we compared the functional status of neighbouring $CD8^+$ T cells in T_{reg} rich and sparse ROIs. In T_{reg} sparse regions, $CD8^+$ T cells had increased expression of ICOS and phosphorylation of mediators of the PI3K/Akt pathway

(pAkt1, pPras40, pS6), indicating highly functional cells (fold change>1.65, FDR=10%) (**Figure 5F**), and denoting enhanced pharmacological efficacy of the anti-PD-1 antibody in these regions. Furthermore, these cells displayed increased expression of p21 and BCLXL, suggesting reduced susceptibility to apoptosis compared to $CD8^+$ T cells in T_{reg} dense regions. Next, we asked if differences in signaling characteristics in T_{reg} TILs could underlie the local evasion from suppression. In T_{reg} sparse regions, T_{reg} cells also displayed increased PI3K/Akt activity (pAkt1, pGSK3a and b, pPras40 and pS6) and expression of CD44 compared to T_{reg} dense ROIs (fold-change>1,65, FDR=10%, **Figure 5G**), suggesting anti-PD-1 also increases TCR signal strength in these T_{reg} cells. Furthermore, we observed increased expression of BatF3, which has been shown to antagonize Foxp3 expression (41). Taken together, these data indicate that successful response to PD-1 blockade is associated with increased activation of the PI3K/Akt signaling pathway in both $CD8^+$ and T_{reg} cells in the most inflamed regions of the tumor, a condition permissive to $CD8^+$ T cell evasion from T_{reg} cell suppression.

Successful response to anti-PD-1 is associated with a T_h1-like functional adaptation by T_{reg} cells.

Since increased *in situ* $CD8^+$ T cell activation was associated with phosphorylation of Akt in T_{reg} cells, which has been shown to promote their acquisition of the transcription factor T-bet (29), we asked if increased Akt signaling could modulate T_{reg} cell functional adaptation in hot TMEs. Functional adaptation is a process that leads to the upregulation of transcription factors from T helper lineages and is linked to increased T_{reg} cell functionality through enhanced homing and local proliferation (42), but also acquisition of inflammatory, effector functions (43). Thus, we assessed the expression of T-bet and IFNγ by tumor-infiltrating T_{reg} cells through time. Before the initiation of treatment, T-bet expression was mostly restricted to $Foxp3^-$ T_{conv} cells and seldom

expressed in T_{reg} cells (**Figure 6A**). In contrast, 30% of early infiltrating T_{reg} cells co-expressed Gata-3 and the IL-33 receptor ST2, indicative of a T_h2-bias which is often associated with tissue-resident T_{reg} cells (44) (**Supplementary Figure 5A**). However, these cells did not express PD-1, suggesting that they are likely not readily targeted by the treatment (**Supplementary Figure 5B**). However, throughout a successful response to PD-1 blockade, we observed an increased influx of T-bet$^+$ T_{reg} TILs in the tumor, but not in its draining lymph node (**Figure 6A and 6B**). Furthermore, T-bet expression increased by ~15% (MFI) in T_{reg} TILs from HR tumors compared to both LR and control tumors (**Figure 6B**), mostly in Helios^{High} T_{reg} cells (**Supplementary Figure 5C)** and these T-bet levels were sufficient to induce IFNγ production by T_{reg} cells in HR tumors (**Figure 6C**), indicating a dysregulation of the T_{reg} cell canonical transcription program (45). High levels of Akt signaling have been shown to promote the T_h1 adaptation of T_{reg} cells and indeed, upregulation of these markers was inversely correlated with PD-1 expression (**Figure 6D**), suggesting that IFNγ$^+$ T_{reg} cells are likely found in the T_{reg} sparse regions of the TME.

We and others have shown that IL-12 is the predominant inducer of T-bet in T cells and promotes the local T_h1 differentiation of T_{reg} cells (46). Given the potent *ex vivo* CD8$^+$ T cell responses in the presence of T-bet$^+$ T_{reg} cells and the suppressive potency of HR T_{reg} TILs *in vitro*, we asked if the T_h1-like phenotype was stable outside of the TME and how it relates to suppressive function. Thus, we assessed the impact of IL-12 signaling on T_{reg} cell phenotype and function *in vitro* (**Figure 6E**). Interestingly, HR T_{reg} TILs lost their T_h1 phenotype when cultured in control media alone and produced IFNγ only when exposed to IL-12 (**Figure 6F**). Furthermore, IL-12 induced significant IFNγ production by LR T_{reg} TILs, suggesting that all tumor-infiltrating T_{reg} cells are sensitive to this inflammatory signal. Moreover, consistent with a previous report (47), IL-12 promoted T_{resp} cell evasion from suppression and IFNγ production (**Figure 6G**). Taken

together, these data indicate that T_{reg} TILs exposed to local IL-12 undergo a T_h1-adaptation during a successful response to anti-PD-1, hindering their capacity to suppress *in situ*. Collectively, these results show that PD-1 targeting antibodies increase T_{reg} cell activation and proliferation and provide a novel mechanism through which PD-1 blockade and local inflammatory signals modulate $Helios^{High}$ T_{reg} cell suppression.

Discussion

Anti-PD-1 ICIs were designed to counteract the exhaustion of $CD8^+$ TILs by antagonizing PD-1 signaling (48), thus promoting their proliferation, cytokine production and ensuing anti-tumor functions. However, in tumors and at steady state, T_{reg} cells express PD-1, and the use of ICIs is often associated with the onset of irAEs (49), indicating a breach in peripheral tolerance. Thus, it has long been hypothesized that ICIs target T_{reg} cells and compromise their functional stability (50). The role of T_{reg} cells in tumor-induced immunosuppression is well established, yet little is known about the consequences of PD-1 expression, and its ligation by ICI, on their functional fate. To answer this, we exploited the bimodal response to anti-PD-1 in the highly immunogenic melanoma tumor YUMMER1.7 (31, 32) to assess the functional dynamics and fate of T_{reg} cells in LR and HR TMEs.

In this study, we established increased T_{reg} cell activation and functional adaptation as novel hallmark features of successful response to PD-1 blockade. First, we identified Helios-expressing cells as the main subset of T_{reg} cells expressing PD-1 and infiltrating tumors. In PBS control tumors, we established that chronic PD-1 signaling alters the fitness of terminally-differentiated and potently suppressive T_{reg} cells, localized in peripheral, immunogenic regions of the tumor. In lymphoid organs, treatment with anti-PD-1 increased the activation and proliferation of $Helios^{High}$ T_{reg} cells, but not T_{eff} cells, highlighting systemic effects of ICIs on non-TILs. In HR tumors, we show that highly-activated $Helios^{High}$ T_{reg} accumulate and transiently acquire T_h1-like characteristics, a process driven by Akt signaling (29), which alleviates their suppressive potency in hot TMEs. Finally, through spatial proteomics, we identified elevated phosphorylation of Akt as a feature of the T_{reg} cells present in regions of highest $CD8^+$ T cell activation, suggesting that IFNγ-producing T_{reg} cells fail to suppress *in situ*.

Collectively, these results provide new insights regarding the synergy between PD-1 signalling and T_{reg} cell function to render immunogenic tumors cold. We established that, akin to terminally-exhausted $CD8^+$ T cells, T_{reg} TILs display a phenotype consistent with dampened activation, proliferation, and survival in endpoint tumors, in line with observations that PD-1 restricts T_{reg} cell activation and proliferation in murine models of T_{reg}-specific, conditional PD-1 deletion (19, 20). In contrast to dysfunctional $CD8^+$ TILs, this phenotype was associated with potent T_{reg} cell suppressive effector functions, consistent with other reports (13, 51, 52). The reduced expression of Helios and CD25 was suggestive of low IL-2 signaling, which may occur because of gradual loss of IL-2 secretion by TILs. Indeed, IL-2 overrides PD-1 inhibition through STAT5 (53) and downregulates PD-1 expression in chronic settings (54). Our results are consistent with a model where T_{reg} cell suppression and PD-1 inhibition concur to dampen IL-2 production and suppress $CD4^+$ T cell help, in turn, triggering gradual $CD8^+$ T cell dysfunction in immunogenic tumors (55). Furthermore, their distribution in peripheral regions of the tumor suggests that T_{reg} cells suppress $CD8^+$ TILs upon tumor entry, at a site of local inflammation rather than through enforcing immunosuppression in cold areas, from which they are absent.

Our observation that PD-1 blockade increases T_{reg} cell activation systemically is in line with what is seen using PD-L1 blockade in treatment-resistant models (56). Furthermore, T_{reg} cells express lower levels of PD-1 than T_{eff} cells in this model, suggesting that in LR and colder tumors, anti-PD-1 could successfully reactivate T_{reg} and not terminally-exhausted $CD8^+$ cells. Indeed, in other cancers, the pre-treatment, baseline CD8:T_{reg} ratio amongst PD-1^+ cells determines clinical outcome (57), and anti-PD-1-induced T_{reg} cell proliferation has been linked with disease hyper-progression (19). While these elements position T_{reg} cell activation as an acquired mechanism of resistance to treatment, our discovery that highly-activated T_{reg} cells produce IFNγ and fail to

suppress $CD8^+$ responses *in situ,* reconciles T_{reg} cell hyper-activation with potent anti-tumor responses. HR T_{reg} TILs displayed reduced levels of PD-1 expression, as well as strong levels of phosphorylated Akt locally. Indeed, anti-PD-1 was shown to increase Akt signaling in T_{reg} cells (57), which triggers glycolysis, in turn dampening their suppressive function temporarily (58) while promoting their proliferation and CTLA-4 expression (59). Furthermore, these results are in line with the increased efficacy of anti-PD-1 and induction of IFNγ-secreting T_{reg} cells in mice treated with a small molecule activator of Akt (60). However, to our knowledge, this is the first demonstration of anti-PD-1 monotherapy inducing IFNγ secretion by T_{reg} cells, a phenotype associated with clinical outcome.

The induction of T-bet expression is dependent on Akt (29) and promotes the proliferation and survival of tissue-localized T_{reg} cells during T_h1 responses (61), consistent with increased T_{reg} cell proliferation and fitness in HR tumors compared to controls. T_h1-adapted T_{reg} cells specialize in controlling type 1 inflammation (62) by colocalizing with TILs (63, 64) through the chemoattraction of $CXCR3^+$ T_{reg} cells towards CCL9-producing DCs and inhibition of neighbouring $CD8^+$ T cell reactivation (65). In contrast, IFNγ secretion has also been associated with dysregulated T_{reg} cell function in melanoma (26, 30). Interestingly, while $IFN\gamma^+$ T_{reg} TILs expressed high levels of T-bet, there was no correlation between IFNγ and CXCR3 expression, suggesting $IFN\gamma^+$ and $CXCR3^+$ T_{reg} cells might represent two different populations of T_h1-like T_{reg} cells with different suppressive capacity and tissue localization. Given the paucity of TILs in preclinical melanoma models (66, 67), the suppressive function of T_{reg} TILs is often assessed using indirect *in vivo* readouts such as $CD8:T_{reg}$ ratios and IFNγ secretion. In this study, we show that while $T\text{-}bet^+$ T_{reg} TILs fail to control IFNγ production *in vivo*, they remain potent suppressors of T_h1 differentiation *in vitro*. Our results suggest that the capacity to respond to persistent intra-

tumoral IL-12 is a key factor in the initiation of the T_h1-like differentiation of Helios$^+$ rather than Helios$^-$ T_{reg} cells (46). Furthermore, the fact that a higher proportion of LR T_{reg} TILs than splenocytes produce IFNγ in response to IL-12 alludes to the fact that while Helios$^+$ T_{reg} cells are more prone to acquire these T_h1-like characteristics (27), not all of them can respond to IL-12.

Taken together, our results identify the acquisition of T_h1-like characteristics by highly-activated Helios$^+$ T_{reg} cells as a novel hallmark of response to treatment. Determining the effects of PD-1 blockade on T_{reg} cells is key to dissecting the role of T_{reg} cells in supporting immune exhaustion and treatment failure and provide translational therapeutic avenues such as increasing tumor antigenicity (32), targeting TCR signal strength (60) and T_h1-differentiation pathways (46) to synergize with anti-PD-1 and increase response rates.

Material and Methods

Mice

C57Bl/6.Foxp3$^{IRES\text{-}mRFP}$ reporter knock-in (Foxp3^{RFP}) mice were provided by Jonathan Spicer. C57Bl/6.Foxp3$^{IRES\text{-}mRFP}$.Helios$^{IRES\text{-}GFP}$ dual reporter knock-in (Foxp3^{RFP}-Helios^{GFP}) mice were provided by Ethan Shevach. Wild Type C57Bl/6 mice were purchased from Charles River Laboratories. All mice used were males and 8 to 14 weeks of age, the examiner was blinded to group repartition until the end of the analysis.

Tumor cell lines

The YUMMER1.7 cell line was generated by Wang and colleagues by irradiating Braf^{V600E} PTEN$^{-/-}$ Cdkn2a$^{-/-}$ cells and expanding a single clone bearing additional somatic mutations (31). YUMMER1.7 cells were kindly provided by Marcus Bosenberg (Yale University) and cultured in advanced DMEM/F12 supplemented with 10%FBS (Wisent), 1% Penicillin/Streptomycin (Wisent) and 1% MEM Non-essential Amino Acids (Wisent). Tumor cells were tested for mycoplasma and viral contamination by the McGill Comparative Medicine Animal Resources Centre. Cells were expanded in 225 cm^2 tissue culture flasks and $5x10^6$ cells/ml were frozen down and stored in 10% DMSO/FBS in liquid nitrogen. Prior to injection, cells were thawed and passaged twice at 37°C in humidified air with 5% CO_2 and washed twice in cold PBS before preparation of the inoculum.

In vivo tumor studies

YUMMER1.7 cells were resuspended in PBS and then mixed in Corning® Matrigel Basement Membrane HC at a 1:1 PBS to Matrigel ratio. YUMMER1.7 cells ($2.5x10^5$) were injected subcutaneously in the right flank of male mice, under anesthesia. Mice were monitored thrice weekly. Tumor volumes were measured using an electronic calliper and calculated as: length

x width^2 x 0.5. Experimental endpoint was defined either as a pre-determined timepoint (day 7, day 14) or as soon as one mouse reached humane endpoint (tumor volume > 1500mm^3). At necropsy, tumors were harvested, and their weights and volumes were measured post-mortem. Once every tumor had reached palpability (day 8), mice were randomly attributed to a treatment group. They received 5 doses of either 250µg of anti-PD-1 (clone RMP1-14, BioXcell) or PBS, intraperitoneally, thrice weekly. At the predetermined experimental endpoint, all mice were sacrificed, and we harvested tumors, tumor-draining axillary and inguinal lymph nodes, non-tumor draining contralateral lymph nodes, and spleen. All mice were cohoused from birth and the success rate of anti-PD-1 did not vary significantly across experiments.

Isolation of tumor-infiltrating lymphocytes

After CO_2 euthanasia, Tumors were collected in serum-free Hank's Balanced Salt Solution (Wisent), then minced manually in 1mm^3 pieces using razor blades. Tumors were then digested in the presence of collagenase IV (1mg/ml, Gibco) and DNAse I (0.005µM, Sigma-Aldrich) at 37°C for 1 hour. Cells were then pushed through a 21G needle and washed in cold complete RPMI 1640 with 5% FBS. Red blood cells were lysed by incubating the cells for 30 seconds with ACK buffer, washed, resuspended in complete RPMI1640, and filtered twice through a 70µm mesh.

Purification of T cell subsets

Prior to FACS-sorting splenocytes and TILs, CD4$^+$ and CD8$^+$ T cells were purified using CD4/CD8 TIL Microbeads (Miltenyi) and an autoMACS (Miltenyi). T_{reg} cells were sorted as CD4$^+$ RFP$^+$, Helios^{High} T_{reg} cells were sorted as CD4$^+$ RFP$^+$ GFP^{Hi}, T_{conv} cell were sorted as either CD4$^+$ RFP$^-$ or CD8$^+$ RFP$^-$ cells (purity>99%) using a FACSAria™ (BD Biosciences).

***In vitro* activation with PD-L1-Fc**

FACS-sorted Helios^{High} T_{reg} cells isolated from either the spleen or endpoint tumors. CD4^{+} RFP^{-} GFP^{-} splenic T_{conv} cells were labelled with CellTrace™ Violet (Thermofisher). T_{conv} cells ($5x10^4$) and Helios^{High} T_{reg} cells ($2.5x10^4$) in RPMI 1640 (Wisent) supplemented with 10%FBS were placed in 96-well flat-bottomed (0.2ml) plates previously coated with αCD3 (3µg/ml), αCD28 (1µg/ml) +/- PD-L1-Fc (5µg/ml, R&D systems). Cells were then incubated for 72 hours at 37°C, then washed and stained for flow cytometry analysis.

***In vitro* suppression assays**

CD4^{+} RFP^{+} T_{reg} cells were sorted from the splenocytes or endpoint tumors of either untreated mice, or high or low responders to anti-PD-1. Depending on the experiment, T_{resp} cells were either CD4^{+} RFP^{-} or CD8^{+} RFP^{-} splenocytes. Antigen-presenting cells were purified from the negative fraction of the CD4/CD8 MACS and mitomycin-C inactivated for 1 hour at 37°C. T_{reg} cells were co-cultured with T_{resp} cells ($5x10^4$) at various ratios (0:1, 1:2, 1:4, 1:8, 1:16), and antigen-presenting cells ($1x10^5$) in RPMI 1640 (Wisent) supplemented with 10%FBS in the presence of soluble αCD3 (0.5µg/mL) for 72 hours at 37°C. For T_h1 polarization assays, cells were incubated in the presence of IL-12 (10ng/ml, R&D Systems) at the start of the culture. After 69h, cells were additionally stimulated with PMA, Ionomycin, and Golgi Stop at manufacturer-recommended concentrations for 3h for assessment of cytokine production.

Flow cytometry analysis

After lymphocyte isolation, the cells were washed in PBS and stained with antiCD16/CD32 (clone 2.4G2, BD) and fixable viability dye eFluor780 or 506 (Thermofisher). Following a wash, cells were marked with extracellular markers. For analysis of Foxp3-reporter protein expression, cells were acquired live within one hour of extracellular staining. For analysis of other transcription

factors, cytokine secretion and intracellular markers, cells were fixed and permeabilized with the Foxp3 Transcription Staining Buffer Set (eBioscience™) and then stained for intracellular markers). Samples were acquired on the same day of the intracellular staining using a BD Fortessa LSR-X20 and analyzed using FlowJo v10 (TreeStar and BD). The following anti-mouse antibodies were used: CD45.2 (clone 104), CD19 (clone 1D3), CD11c (clone HL3), I-A[b] (clone AF6-120.1), CD86 (clone GL1), Ly6C (clone AL21), PD-L1 (clone MIH5), CD3 (clone 17A2), CD8a (clone 53-6.7), CD8b (clone H35-17.2), PD-1 (clone J43), Ki67 (clone B56), KLRG1 (clone 2F1), TCF-1 (clone S33-966), Gata-3 (clone L50-823), IFNγ (clone XMG1.2), IL-2 (clone JES6-5H4), TNFα (clone MP6-XT22), RORγt (clone Q31-378) from BD; CD4 (clone RM4-5), CTLA-4 (clone UC-4B9), Helios (clone 22F6), Bcl-2 (clone BCL/10C4), GRZB (clone Q16A02), Ly6G (clone 1A8) from Biolegend; Foxp3 (clone FJK-16S), ICOS (clone C396.4A), T-bet (clone 4B10), TIGIT (clone GIGD7), CD25 (clone PC61.5), Tim-3 (clone RMT3-23), ST2 (clone RMST2-2), IL-17A (clone ebio17B7), IL-10 (clone JES5-16E3), F4/80 (clone BM8), CD11b (clone M1/70) from eBioscience.

Histological assessment

For histological assessment, we repeated the same tumor injection and treatment protocol. At tumor endpoint (day 19), mice were sacrificed and identified as HR (n=6), LR (n=4) and PBS (n=6). Tumors were resected and cut in half. Half of the tumor was fixed in 10% Formalin for 72h then washed and permeabilized in 70% ethanol overnight before being paraffin embedded according to standard pathology procedures. The other halves were processed as described previously for confirmatory flow cytometry analysis. The tissues were sectioned at 5 μm thickness and mounted on Superfrost Plus Slides (Fisherbrand).

For immunofluorescence studies, slides were baked at 60°C for 30 minutes, then deparaffinized and rehydrated using xylene and 100%EtOH. Slides were incubated for 20 minutes with 1X Tris-EDTA for antigen retrieval. Tissue sections were blocked with a 3% BSA/PBS solution for 1 hour, followed by primary antibody incubation overnight in a cold room. The antibodies used were αCD8-AF647 (clone EPR21769, Abcam), polyclonal αRFP-CF594 (Biotium), αCD4-eFl660 (clone 4SM95, Thermofisher) or αMart-1-AF532 (clone A103, Novus Biologicals) at 1:100 dilution, then counterstained with DAPI. After 3 washes with 1x TBS-T, 24x50mm coverslips (VWR) were mounted and cells were stored in the dark at 4°C. Images were acquired using a Zeiss LSM780 Laser Scanning Confocal Microscope and analyzed by QuPath.

For GeoMx Digital Spatial Profiling, tissue sections were baked at 60°C for 45 minutes, deparaffinized with CitriSolv (Decon Labs) and rehydrated. Antigen retrieval was achieved by incubating slides with 1X Citrate Buffer (pH 6.0) in a pressure cooker at 121°C and 1.0 bar for 15 minutes. Tissue sections were blocked with manufacture-recommended Buffer W for 1 hour at room temperature in a closed humidity chamber. Slides were then incubated overnight with 3 morphology markers, and 6 commercially available panels of antibodies coupled to photocleavable oligos (Supplementary Table 3). αMart-1-AF532 (clone A103, Novus Biologicals) was used to detect differentiated melanoma cells, αCD8-AF647 (clone EPR21769, Abcam) to detect $CD8^+$ T cells and polyclonal αRFP-CF594 (Biotium) to detect T_{reg} cells. Cells were then post-fixed with 4% paraformaldehyde at room temperature for 30 minutes in closed humidity chamber and counter-stained with SYTO 13 Green Fluorescent Nucleic Acid Stain (Thermofisher) for 15 minutes. In all tumors, ROIs were selected based on sparse or dense RFP^+ T_{reg} cell density. Each ROI type was identified in 3 replicate HR tumors and 1 LR tumor. In total, 15 ROIs of a maximal surface area of 350 000 μm^2 were selected. Within each ROI, tumor cells, $CD8^+$ T cells and T_{reg}

cells were segmented into Areas of Interest (AOIs) using adapted fluorescence intensity thresholds to generate object masks. Each segment was then individually exposed to UV light using digital micromirror devices to release the oligonucleotide tags. Tags were collected in liquid phase and placed in a 96well-plate. A library was generated from each well with Illumina unique dual index primers for paired-end next-generation sequencing, allowing for quantitative measurement of protein expression within each AOI. Each segment passed sequencing QC, however one T_{reg} AOI was removed from the analysis for an insufficient Foxp3 count (<20, manufacturer-recommended threshold). Counts were scaled to the number of nuclei within each ROI to enable comparisons on a per cell basis. Multiple normalization strategies were then evaluated. The selected method was to normalize each count to the geometric mean of the pair of housekeeping controls with maximal consistency (Histone H3 and GAPDH) in its respective AOI.

Statistical analysis

Unless otherwise stated, all data is depicted as mean +/- 95%CI. For tumor growth curves, multiple comparisons were made using a mixed-effects analysis with a Geiser-Greenhouse correction for sphericity and a Sidak correction for multiple comparisons. Tumor weights at endpoint were compared using a two-tailed unpaired t-test with Welch's correction. The normality of tumor weights in each group was determined with a Shapiro-Wilk test. Given the bimodal distribution of tumor volumes in the anti-PD-1 group, mice were categorized as HR or LR based on a cut-off volume of 300mg. Tumor weights were then compared using a Brown-Forsythe and Welch ANOVA test with a Dunnett T3 correction for multiple comparisons.

For flow cytometry data, the normality of each data set's distribution was determined with a Shapiro-Wilk test. Homoscedasticity was tested using Fisher's test. If both conditions were met, when applicable, proportions and MFIs were compared using ordinary One-Way ANOVA with a

correction to account for multiple comparisons. If the normality condition was not met, a non-parametric Mann-Whitney test was used. For PD-1 MFI comparisons, data was normalized to the average expression of PD-1 within the T cell compartment within each experiment. For other MFI comparisons, data was normalized to the average expression within its T cell subset within each experiment. Correlation matrixes were generated by computing Pearson r-correlates with tumor weight at endpoint for each variable and represented as a heatmap. For linear correlation analyses, all data points were pooled to calculate linear correlations. The slope's deviation from zero was evaluated using Fisher's test. All statistical analysis was conducted using GraphPad Prism v9.5.

For *in vitro* experiments, all conditions were realized in triplicates (n=3) and each experiment was repeated 3 times (N=3). Data is shown from N of 1 representative repeat.

For differential protein expression, normalized counts were compared using a linear mixed model with Benjamini-Hochberg adjustment for multiple comparisons, accounting for the individual tumors from which AOIs were repeatedly sampled.

Study approval

All mice were housed and bred in specific pathogen-free conditions in the same facility and used according to the regulations of the Canadian Council of Animal Care Guidelines and Animal Care and Use Committees at McGill University.

Data availability

Numerical data values presented in the graphs are uploaded as supplementary material. Raw CZI files generated by confocal microscopy and FCS files generated by flow cytometry are available upon request from the corresponding author.

Figures

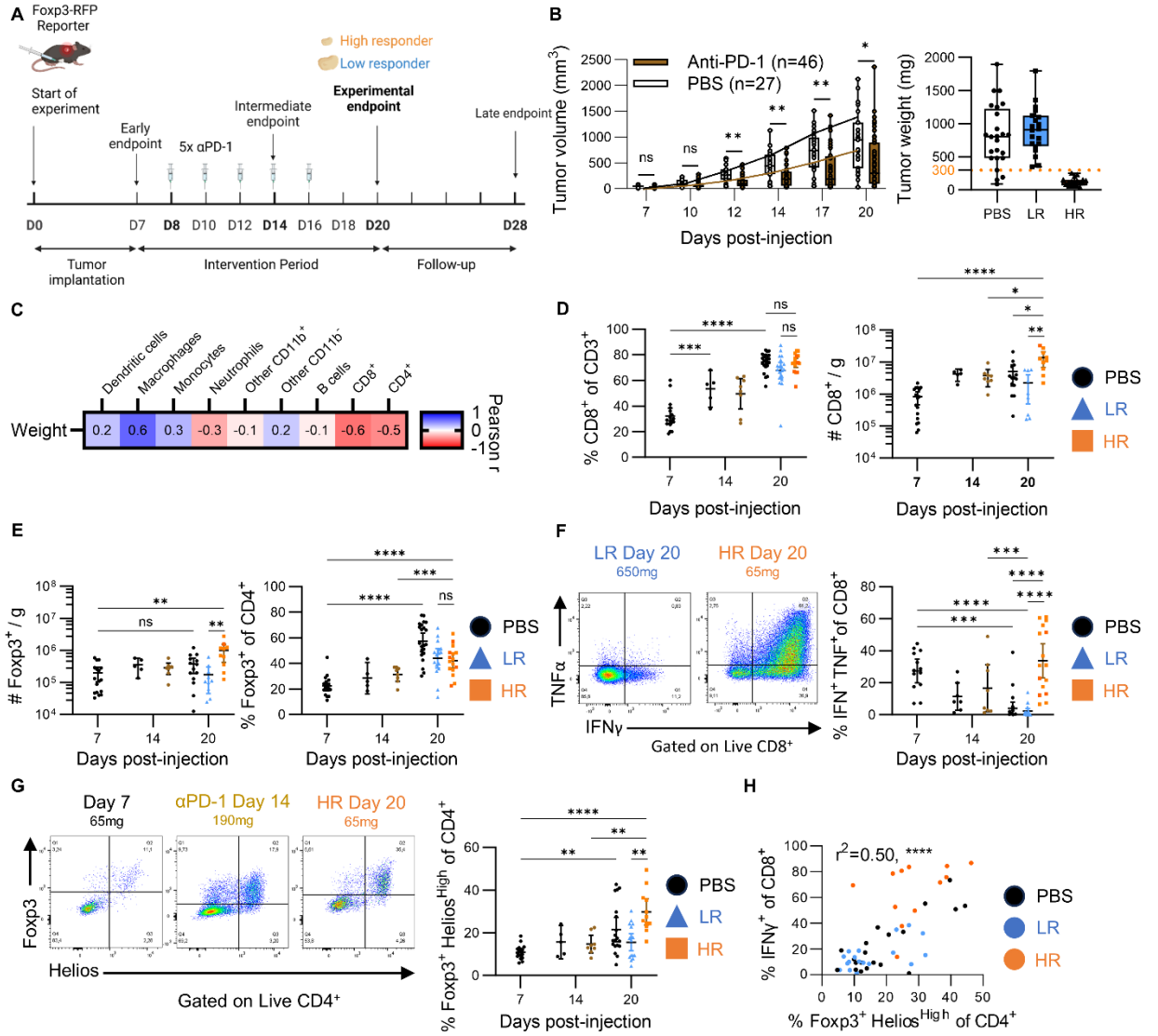

Figure 1. Helios⁺ Foxp3⁺ T_{reg} cells accumulate in melanoma tumors throughout successful response to anti-PD-1 monotherapy.

A. Schematic of the experimental design. At Day 8, mice were randomly assigned to a treatment group and received 5 injections of 250µg of anti-PD-1 (clone RMP 1-14, BioXcell) (n=46) or PBS (n=27) every 48 hours.
B. Tumor growth curves shown as boxplots from minimum to maximum (N=10). Each dot represents one mouse. Tumor volumes were fitted with a mixed-effects model and compared using Sidak's multiple comparisons test. Mice sacked on day 20 for flow cytometry analysis were categorized as HR (n=18) or LR (n=20) based on a cut-off weight of 300mg.
C. Frequency of Dendritic cells (CD11c⁺ MHC-II⁺), Macrophages (CD11b⁺ F4/80⁺), Monocytes (CD11b⁺ Ly6C⁺ F480⁻), Neutrophils (CD11b⁺ Ly6G⁺), B cells (CD19⁺), CD8⁺ and CD4⁺ cells amongst live CD45⁺ cells were measured at endpoint. Pearson r-correlates were computed for each pair of variables and represented as a heatmap.

D. In subsequent experiments, mice were sacrificed either pre-treatment, at Day 7 (N=3, n=18) or on Day 14 (N=2, n= 15), before HR and LR can be discriminated. Flow cytometry analysis of CD8 expression.
E. Flow cytometry analysis of Foxp3-RFP expression.
F. Flow cytometry analysis and representative flow plots of IFN and TNF expression by $CD8^+$ cells. Single cell suspensions were stimulated in the presence of PMA, Ionomycin and GolgiStop for 3h.
G. Flow cytometry analysis of Foxp3 and Helios expression. Representative flow plots from independent experiments acquired on different days. All flow cytometry results shown as mean and 95% CI, compared using a Two-Way ANOVA with Tukey's correction for multiple comparisons (****$p<0.0001$, ***$p<0.001$, **$p<0.01$, *$p<0.05$).
H. Day 20 data points were pooled to calculate a linear correlation and color-coded to identify treatment groups. The slope's deviation from zero was evaluated using Fisher's test.

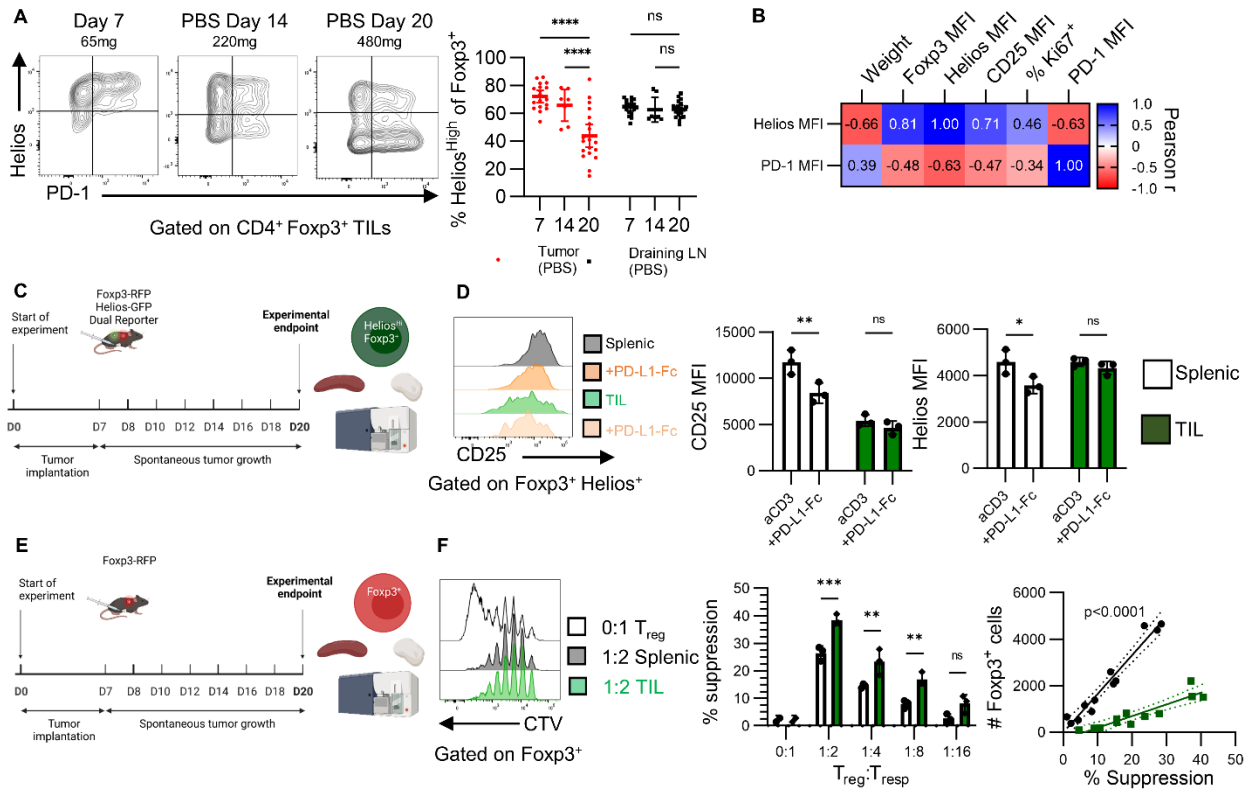

Figure 2. PD-1 signalling alters the phenotype of melanoma-infiltrating T_{reg} cells at tumor endpoint.

A. Representative flow plots of Helios and PD-1 expression by PBS control TIL-T_{reg} at day 7 (n=18, N=3), day 14 (n=7, N=2), and day 20 (n=24, N=10). Mean and 95% CI, every dot represents one mouse.

B. MFIs of Foxp3, Helios, CD25 and PD-1 expression by endpoint T_{reg} TILs were normalized to their respective average in each experiment. Pearson r-correlates were computed for each pair of variables and represented as a heatmap.

C. Helios^{GFP}-Foxp3^{RFP} mice were injected with YUMMER1.7 cells ($2.5x10^5$) and received no treatment until humane endpoint. Splenic and TIL Helios-GFP^{High} T_{reg} cells were sorted and pooled from n=2 mice and restimulated *in vitro* with plate-bound anti-CD3 (3µg/ml), anti-CD28 (2µg/ml), with or without PD-L1-Fc (5µg/ml) and splenic T_{conv} cells ($5x10^4$) for 72h (N=2).

D. Representative flow plots of CD25 expression by Helios$^+$ T_{reg} cells isolated from the spleen (black, orange) or the tumor (green and light orange) and restimulated with or without PD-L1-Fc. MFIs were compared using a Two-Way ANOVA with Sidak's correction for multiple comparisons.

E. Foxp3^{RFP} mice were injected with YUMMER1.7 cells ($2.5x10^5$) and received no treatment until humane endpoint. Splenic and TIL Foxp3-RFP$^+$ cells were sorted and pooled from n=2 mice, then co-cultured with CTV-labelled splenic CD4$^+$ RFP$^-$ T_{resp} cells ($5x10^4$), mitomycin-C inactivated feeders ($1x10^5$) and soluble anti-CD3 (0.5 µg/ml) for 72h (N=3).

F. Flow cytometry analysis of T_{resp} cell proliferation (CTV dilution analysis), when cultured with no T_{reg} cells (white), 1:2 splenic T_{reg} cells (black) or 1:2 T_{reg} TILs (green). % suppression was calculated by comparing division indexes using 0:1 as a baseline for the absence of suppression. Means were compared using a Two-Way ANOVA with Sidak's correction. Slopes were compared using Fisher's test (****p<0.0001, ***p<0.001, **p<0.01, *p<0.05).

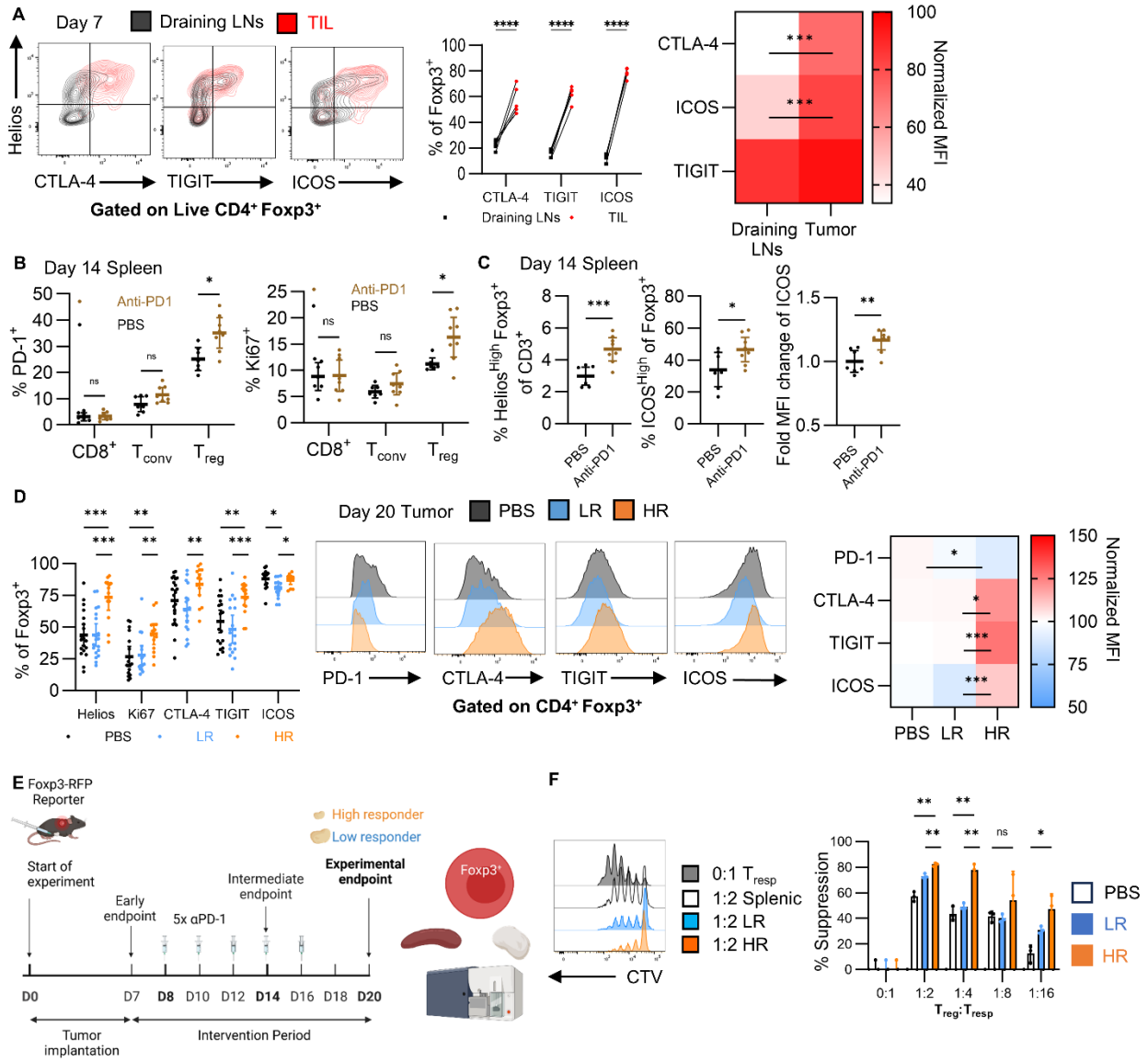

Figure 3. PD-1 blockade promotes the activation and proliferation of highly suppressive Helios-expressing T_{reg} cells.

Mice were injected with $2.5x10^5$ YUMMER1.7 cells and received up to 5 doses of anti-PD-1, as previously described.

A. Representative flow plots and analysis of CTLA-4, TIGIT and ICOS expression by T_{reg} cells in the tumor-draining lymph nodes and the tumor at day 7 (N=3). Proportions and MFIs from 1 representative experiment (n=5) were compared using a paired Two-way ANOVA with Sidak's correction and MFIs are represented as a heatmap (****p<0.0001, ***p<0.001, **p<0.01, *p<0.05).

B-C. Flow cytometry analysis of Ki67, PD-1, Helios and ICOS expression by splenic cells at day 14 in PBS control (n=7) or anti-PD-1 treated mice (n=8) (N=2). Means were compared using either a Two-Way ANOVA with Sidak's correction or Student's t-test. Fold MFI increase was calculated using the average MFI intensity in the control group for each experiment as baseline.

D. Representative flow cytometry plots and analysis of Helios, Ki67, ICOS, CTLA-4, TIGIT and PD-1 expression by T_{reg} TILs from PBS (n=24), LR (n=20) and HR (n=18) tumors at endpoint (N=10). MFIs were normalized to the average expression in the control group within each experiment and represented as a heatmap. Means were compared using Two-Way ANOVA with Sidak's correction. Frequency of $Helios^{High}$ T_{reg} cells in the PBS group is also shown in Figure 2A. **E.** Splenic and TIL-T_{reg} cells were sorted from 2 HR and 2 LR mice, and then co-cultured as previously described (N=3). **F.** Flow cytometry analysis of CTV expression by T_{resp} cells in each condition. % suppression was calculated by comparing division indexes using 0:1 as a baseline for the absence of suppression. Means were compared using a Two-Way ANOVA with Sidak's correction. Dot plots show mean and 95%CI.

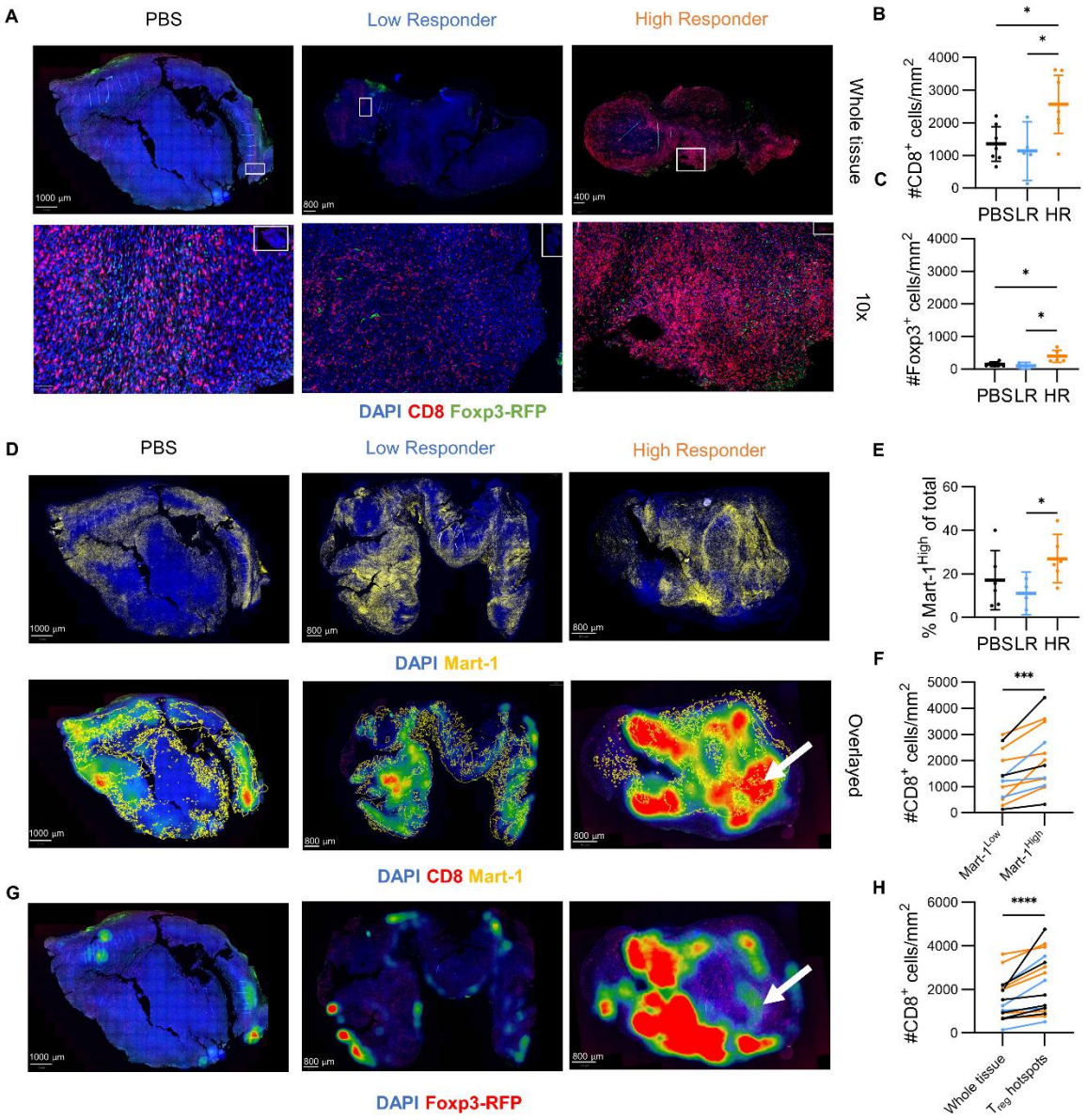

Figure 4. T_{reg} cells preferentially colocalize with $CD8^+$ T cells in tumor microenvironments.

A-C. At tumor endpoint, mice were sacked, and PBS Control (n=6), HR (n=6) and LR (n=4) tumors were resected and processed into formalin-fixed paraffin embedded blocks (N=2). Slides were deparaffinized and stained for assessment of CD8, Foxp3-RFP and Mart-1 expression. Whole tissue and 10x magnification views of representative tumors from each group. Tissue area, CD8 and Foxp3 counts were obtained from QuPath analysis of fluorescence intensity. Means were compared using a One-Way ANOVA with Tukey's correction for multiple comparisons (****p<0.0001, ***p<0.001, **p<0.01, *p<0.05).

D-E. Mart-1 was stained on independent slides of adjacent tissue sections. Regions of high Mart-1 expression were annotated and superimposed to the CD8 scan to assess co-localization. CD8 density represented as a heatmap overlayed with Mart-1 regions. CD8 densities were measured in and out of Mart-1 annotated regions and compared using Wilcoxon's matched-pairs signed rank test.

F. Hotspots of maximal Foxp3 density were localized using QuPath and represented as heatmaps. **G.** T_{reg} cells are localized in zones of high $CD8^+$ density in tumor microenvironments. $CD8^+$ density was summed within the 5 major hotspots of Foxp3 density within each tumor and compared to the whole tissue CD8 density using Wilcoxon's matched-pairs signed rank test.

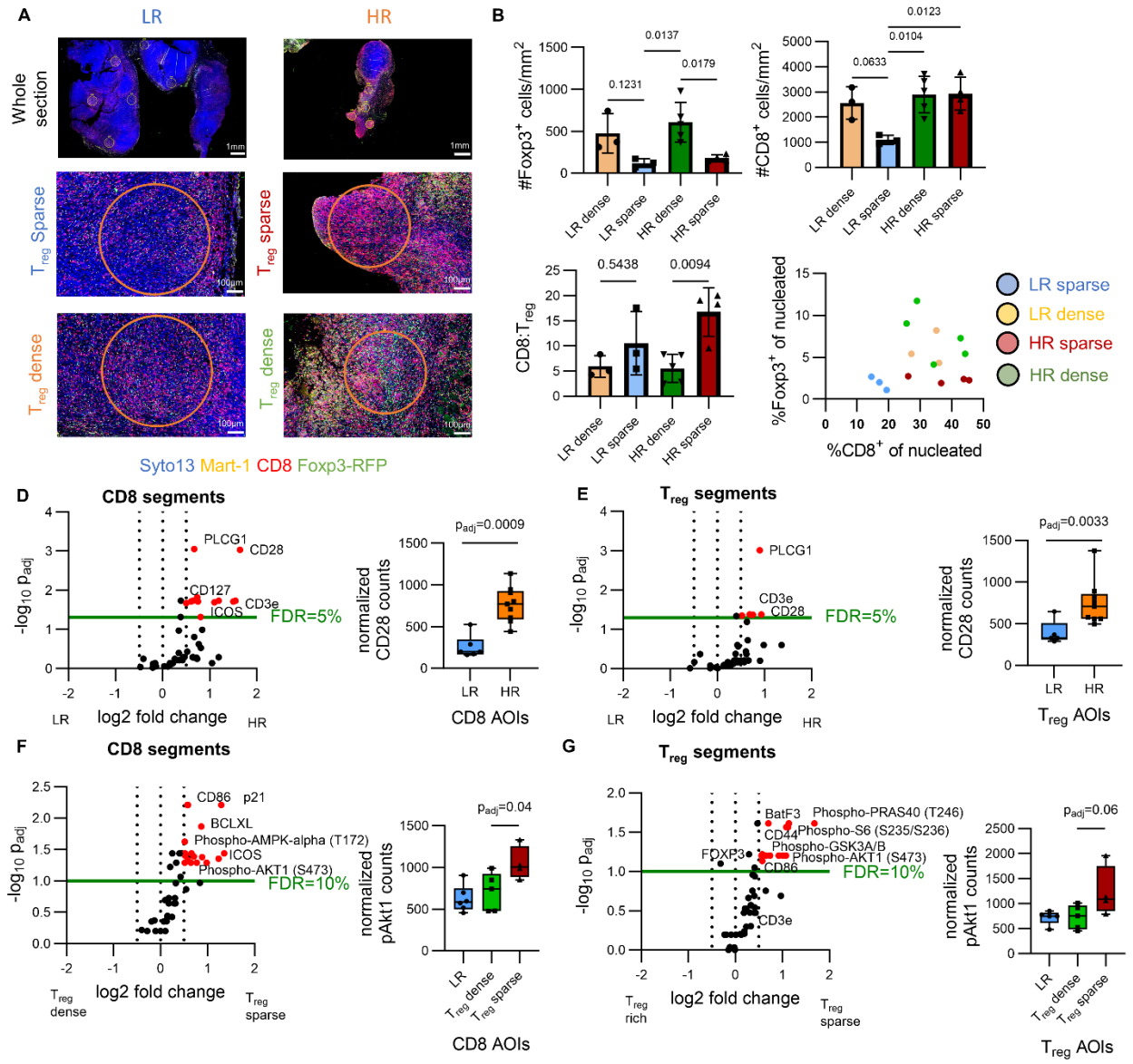

Figure 5. Spatial proteomic profiling reveals increased PI3K/Akt activity in both CD8$^+$ and T_{reg} cells located in T_{reg} sparse regions of high responder tumors.

A. Merged immunofluorescence of LR (n=1) and HR (n=3) samples (scale bars, 1mm for whole section, 100µm for ROIs; Syto13: blue, Mart-1: yellow, CD8: red, Foxp3-RFP: green). ROIs selected for profiling (n=15) are delimited by orange circles and all spanned 0.34mm^2 in the LR tumor and 0.19mm^2 in the HR tumors. Samples and ROIs were chosen as representative of the patterns observed by immunofluorescence in n=4 LR and n=6 HR samples.

B-C. CD8 and Foxp3 counts were obtained from the immunofluorescence staining and divided by the surface area of each ROI. The proportion of CD8 and T_{reg} cells were derived, plotted, and colored by ROI type. Means were compared using One-Way ANOVA with Tukey's correction for multiple comparisons.

D-G. Differential protein expression between ROIs from LR and HR Tumors. Colored genes have a fold-change expression greater than 1.65 and a BH adjusted p-value < 0.10 by testing with a

linear mixed model for multiple comparisons accounting for the individual tumors from which ROIs are repeatedly sampled. CD28 counts in HR (n=9) and LR (n=6) AOIs in CD8 and Foxp3 segments. One LR T_{reg} segment was removed from the analysis due to insufficient Foxp3 counts. Boxplots presented as min to max. phosphoAkt1 counts in LR (n=6), T_{reg} dense (n=5) and T_{reg} sparse (n=4) AOIs in CD8 and Foxp3 segments. Cell counts were scaled to nuclei count in each segment to allow for comparison on a per cell basis. Scaled counts were subsequently normalized to the geometric mean of the pair of housekeeper proteins with the maximal consistency (GAPDH and Histone H3).

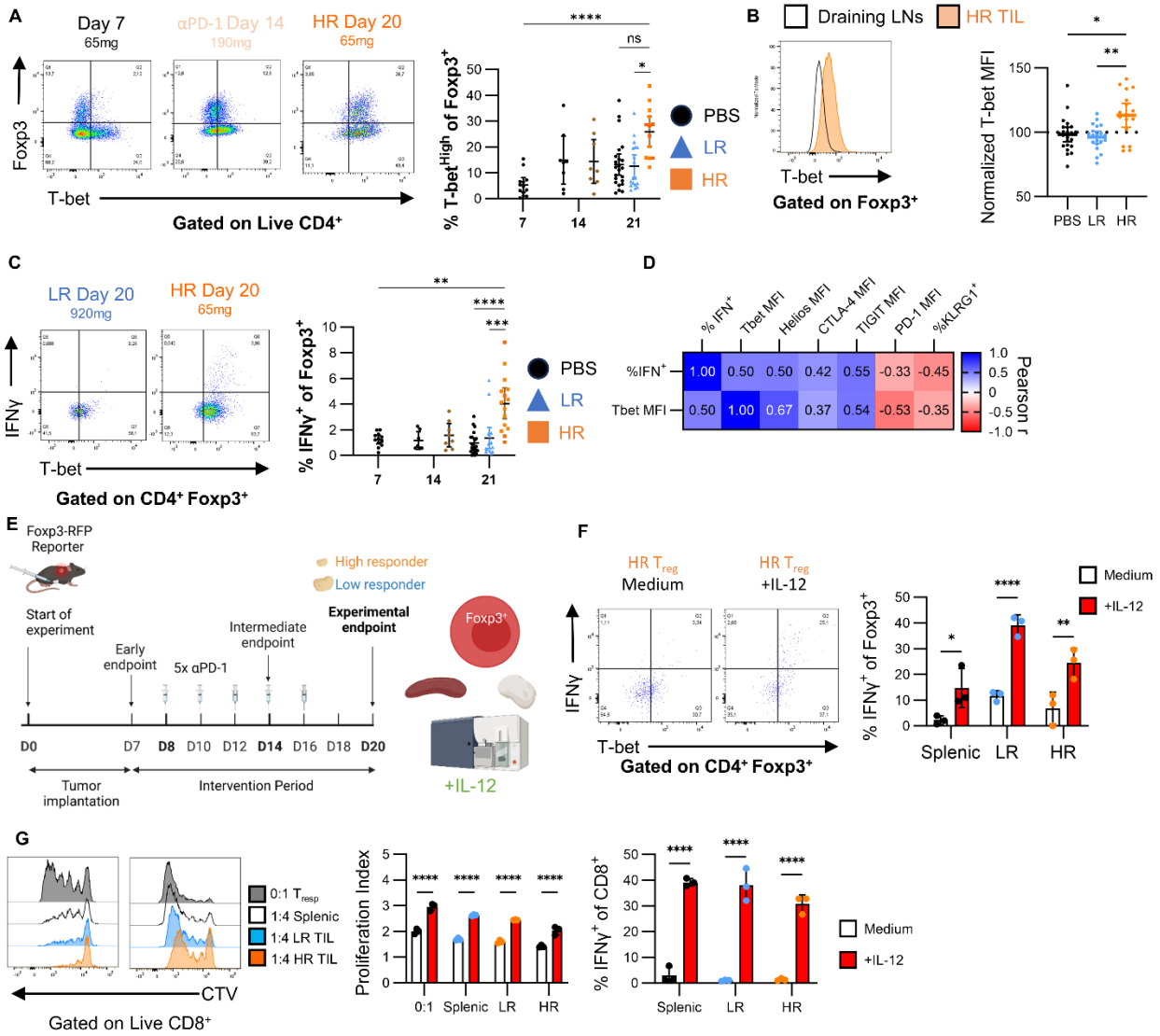

Figure 6. Successful response to anti-PD-1 is associated with a T_h1-like functional adaptation by T_{reg} cells.

A. Representative flow cytometry plots and analysis of T-bet expression by $CD4^+$ T cells on day 7 (N=3), day 14 (N=2) or day 20 (N=10). Means were compared by pairs using a Two-Way ANOVA with Sidak's correction for multiple comparisons (****p<0.0001, ***p<0.001, **p<0.01, *p<0.05) and represented with their 95% confidence interval.
B. Representative flow plots of T-bet expression by T_{reg} cells from an HR tumor and its draining lymph node. Flow cytometry analysis of T-bet mean fluorescence intensity in T_{reg} TILs. MFIs were normalized to the average expression in the control group within each experiment and compared using a One-Way ANOVA with Tukey's correction.
C. Flow cytometry analysis of IFNγ expression by T_{reg} TILs. Single cell suspensions were incubated for 3 hours in the presence of PMA, Ionomycin and GolgiStop.
D. Measurements were pooled from all 3 groups at endpoint and Pearson r-correlates were computed for each pair of variables and represented as a heatmap.

E. Splenic and TIL-T_{reg} cells were sorted from 2 HR and 2 LR mice and cultured at a 1:4 ratio with $CD8^+$ cells, accessory cells and soluble anti-CD3, in the presence or absence of 10ng/ml of IL-12 then re-stimulated in the presence of PMA, Ionomycin and GolgiStop at the end of the 72-hour culture (N=2)
F. Flow cytometry analysis of IFNγ and T-bet expression by HR T_{reg} cells after in vitro restimulation.
G. Flow cytometry analysis of $CD8^+$ T_{resp} cell proliferation (measured by CTV expression and quantified by proliferation index), and IFNγ production. Means were compared using a Two-Way ANOVA with Sidak's correction. Data shown from one representative experiment from N=2 independent repeats.

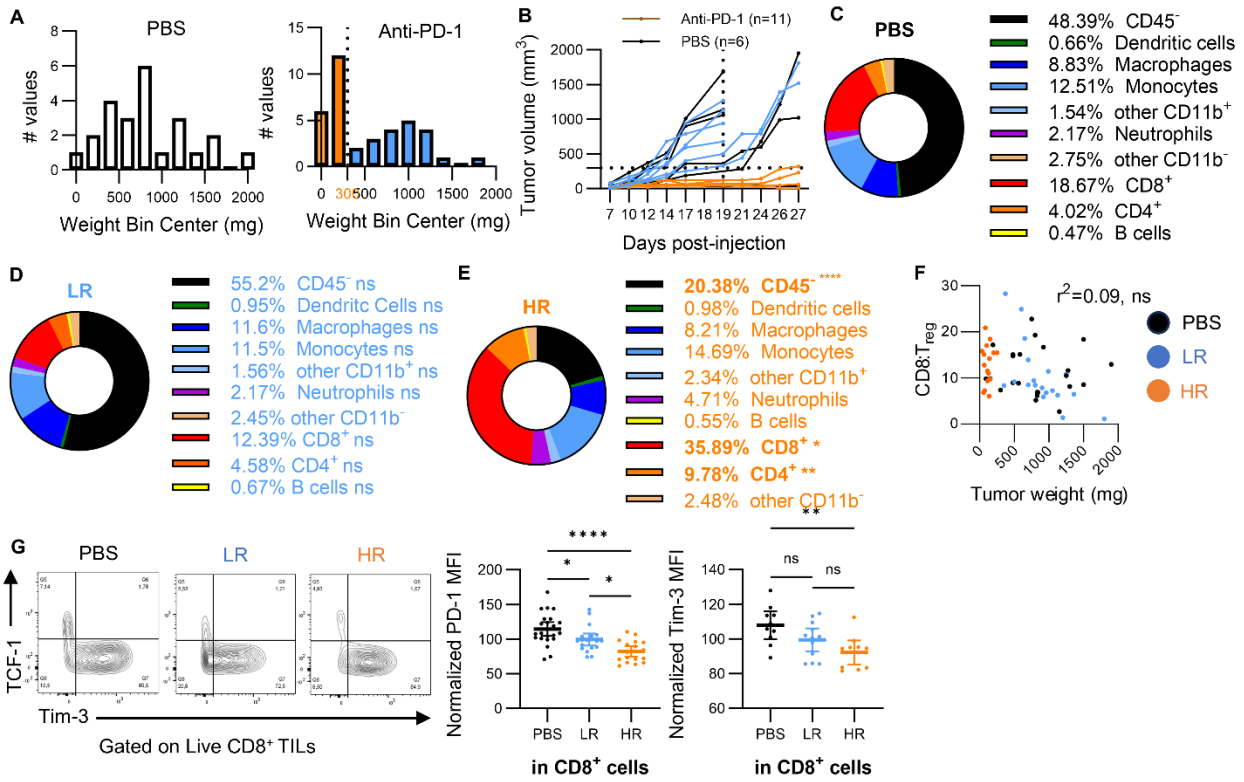

Supplementary Figure 1

A. Distribution of tumor weights at tumor endpoint in the PBS control and the anti-PD-1 group. Normality of distributions was tested using a Shapiro-Wilk Test.
B. Tumor growth curves shown as a line graph, each line represents one mouse. Mice were treated as described in Figure 1 (N=3). At day 17, treatment was stopped. At day 19, tumors >500mm^3 were sacrificed and tumor growth was monitored in the remaining mice. Remaining mice were sacrificed when the first tumor reached experimental endpoint, on day 28. Anti-PD-1 treated mice with a volume <300mm^3 at endpoint are colored in orange, and those with a volume >300mm^3 are colored in blue.
C-E. Flow cytometry analysis of the proportions of CD45$^-$ (black), CD11c$^+$ MHC-II$^+$ Dendritic cells (green), CD11b+ F4/80$^+$ Macrophages (dark blue), CD11b$^+$ F4/80$^-$ Ly6C$^+$ Monocytes (blue), CD11b$^+$ Ly6G$^+$ Neutrophils (purple), other CD11b$^+$ (light blue), CD8$^+$ (red), CD4$^+$ (orange), CD19$^+$ B cells (yellow), and other CD11b$^-$ (light orange). Data represented as parts of whole. All means were compared using One-Way ANOVA with Welch's correction.
F. CD8:T$_{reg}$ ratios were measured by flow cytometry. All data points were pooled to calculate a linear correlation. The slope's deviation from zero was evaluated using Fisher's test.
G. Flow cytometry analysis and representative flow plots of TCF-1, Tim-3, and PD-1 expression by CD8$^+$ cells. Mean and 95%CI, every dot represents one mouse. MFIs of Tim-3 and PD-1 expression by endpoint T$_{reg}$ TILs were normalized to their respective average in each experiment and compared using a One-Way ANOVA with Tukey's correction.

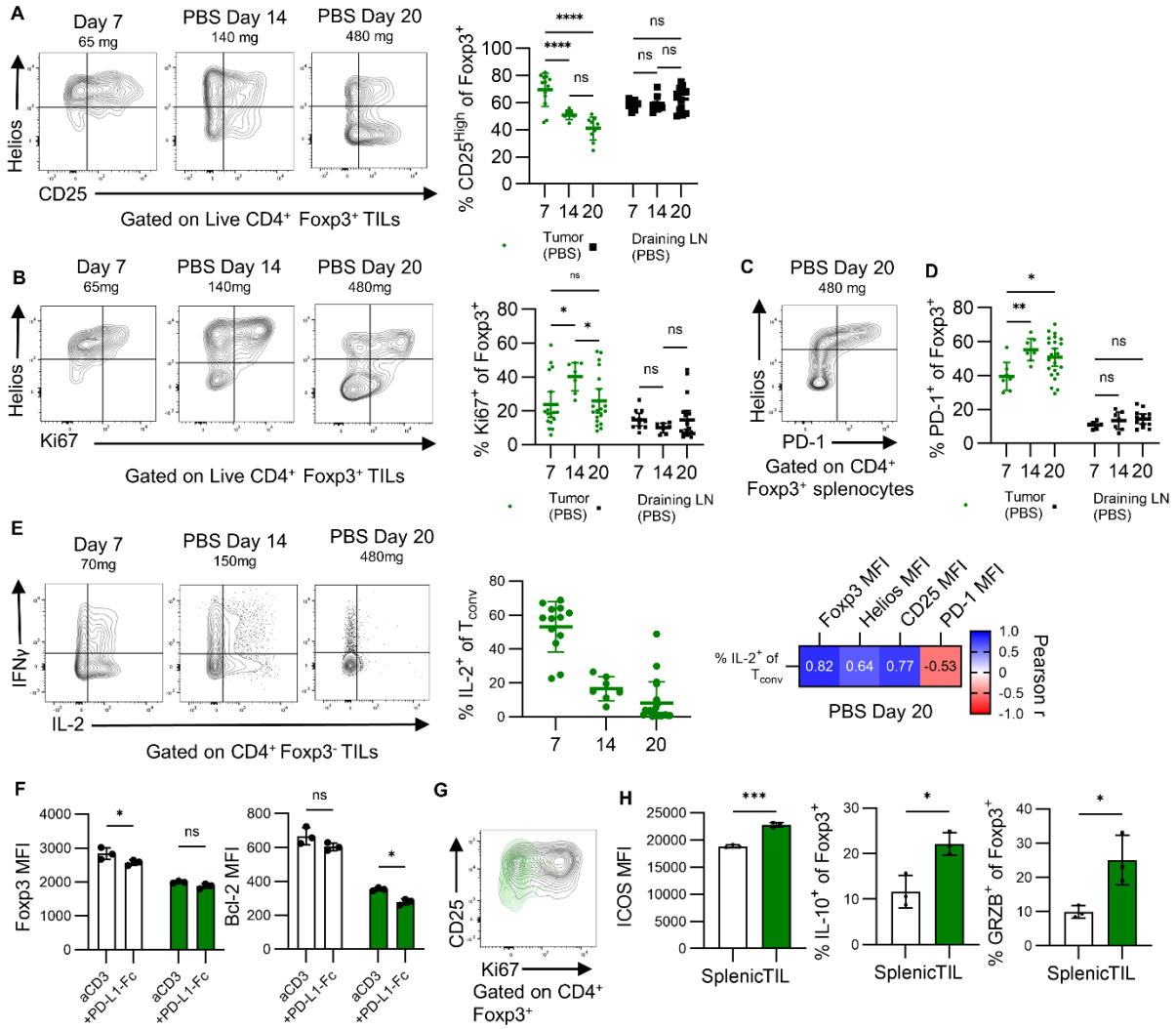

Supplementary Figure 2

A-B, D. Representative flow plots of Helios, CD25, Ki67 and PD-1 expression by PBS control tumor-draining lymph node-dwelling and TIL-T_{reg} at day 7 (n=18, N=3), day 14 (n=7, N=2), and day 20 (n=24, N=10). Mean and 95% CI, every dot represents one mouse.
C. Representative flow plots of Helios and PD-1 expression by T_{reg} splenocytes in PBS control mouse at day 20 (n=24, N=10).
E. Representative flow plots and analysis of IL-2 expression by CD4+ Foxp3- Tconv cells in the control group. Single cell suspensions were stimulated in the presence of PMA, Ionomycin and GolgiStop for 3h. Data represented as mean and 95%CI, means were compared using a One-Way ANOVA with Tukey's correction. At endpoint, Pearson r-correlates were computed for each pair of variables and represented as a heatmap.
F. Flow cytometry analysis of Foxp3 and Bcl-2 expression by Helios$^+$ T_{reg} splenocytes (white) or TILs (green) co-cultured with or without PD-L1-Fc (5µg/ml). MFIs were compared using a Two-Way ANOVA with Sidak's correction for multiple comparisons. Data representative of N=3 repeats.
G. Representative flow plots of CD25 and Ki67 expression by RFP+ T_{reg} splenocytes (black) and TILs (green) after 72h of culture. Data representative of N=3 repeats.

H. Flow cytometry analysis of ICOS, IL-10 and GRZB expression by T_{reg} cells. Data shown as mean and standard deviation and compared using Student's t-test. Data representative of N=3 repeats.

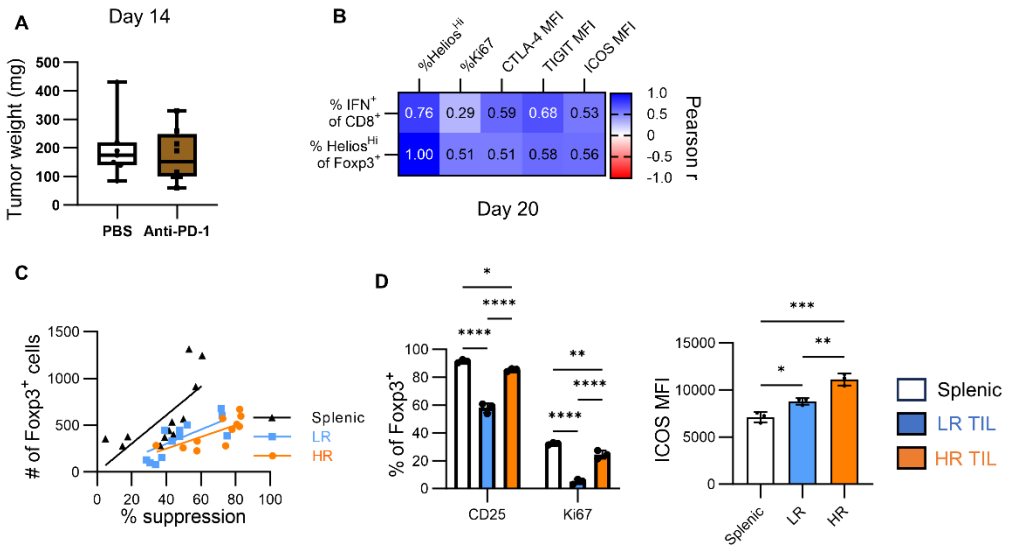

Supplementary Figure 3

A. Mice were injected with 2.5x10^5 YUMMER1.7 cells, received 3 doses of either anti-PD-1 (n=8) or PBS control (n=7) and were sacked on day 14. Tumor weights at day 14, boxplots are shown as min to max, each points represents one mouse, compiled from N=2.
B. Flow cytometry analysis of IFNγ production by CD8$^+$ TILs and Helios, Ki67, CTLA-4, TIGIT and ICOS expression by T_{reg} TILs at day 20. MFIs were normalized to the average MFI intensity in the control group for each experiment as baseline. Pearson r-correlates were computed for each pair of variables and represented as a heatmap.
C. Flow cytometry analysis of % suppression and number of live Foxp3+ cells. Data points from all T_{reg}:T_{resp} ratios were pooled. Data representative from N=3 repeats.
D. Flow cytometry analysis of CD25, Ki67 and ICOS expression at a 1:4 T_{reg}:T_{resp} ratio. Data shown as mean +/- SD. Frequencies were compared using a Two-Way ANOVA with Sidak's correction. MFIs were compared using a One Way ANOVA with Welch's correction. Data representative from N=3 repeats.

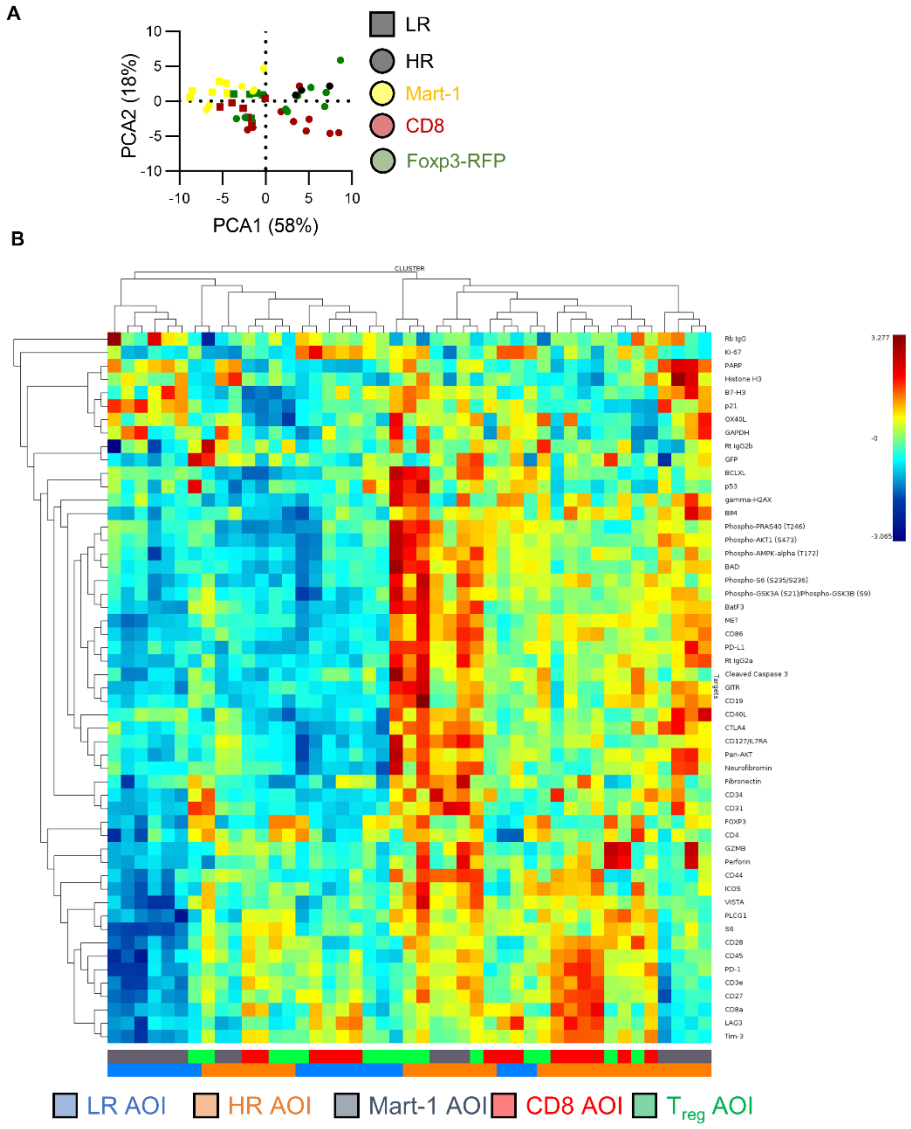

Supplementary Figure 4

A. Principal components were determined using GeoMX DSP Control Center. AOIs are coded by cell type: Mart-1 AOIs (yellow), CD8 AOIs (red), T_{reg} AOIs (green) and tumor type: LR AOIs (square) and HR AOIs (circles).
B. Cluster Heatmap plot of each segment-target with color representing the counts' Z-scores. Target counts were normalized according to housekeeper protein expression (GAPDH and Histone H3). AOI types are colored by type: LR AOIs (blue), HR AOIs (orange), Mart-1 AOIs (grey), CD8 AOIs (red) T_{reg} AOIs (green).

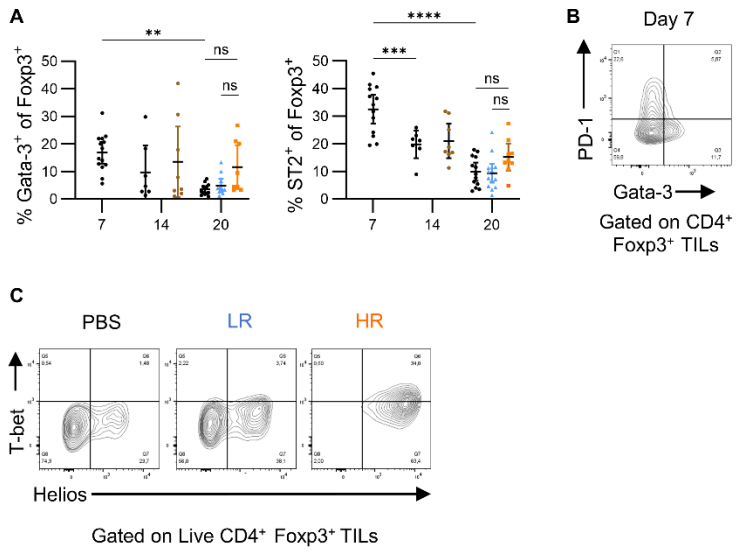

Supplementary Figure 6

A. Flow cytometry analysis of ST2 and Gata-3 expression by T_{reg} TILs at day 7 (N=3), day 14 (N=2) and Day 20 (N=10). Data shown as mean +/- 95%CI. Means were compared using a two-way ANOVA with Sidak's correction.
B. Representative flow plot of PD-1 and Gata-3 expression by T_{reg} TILs at day 7 (N=3, n=18).
C. Representative flow plots of Helios and T-bet expression by T_{reg} TILs at endpoint (N=10).

Supplementary Table 1 List of antibody targets for GeoMX Digital Spatial Profiling

PANEL NAME	Targets
Core	Rb IgG, Ms IgG1, Ms IgG2a, Histone H3, S6, GAPDH, CD45, Ki-67, GFP, CD31
Immune Cell Typing	BatF3, CD19, CD28, CD34, CD3e, CD4, CD8e, Fibronectin, FOXP3, GZMB
IO Drug Target	B7-H3, CTLA4, GITR, LAG3, OX40L, Tim-3, VISTA
Immune Activation Status	CD127, CD27, CD40L, CD44, CD86, ICOS, PD-1, PD-L1
Cell Death	BAD, BCLXL, BIM, PARP, Cleaved Caspase 3, gamma-H2AX, Neurofibromin, p21, p53, Perforin
P13K/AKT Signaling	MET, Pan-AKT, Phophso-AKT1 (S473), Phospho-AMPK-alpha (T172), Phsopho-GSK3A (S21)/Phospho-GSK3B (S9), Phospho-PRAS40 (T246), Phospho-S6 (S235/S236), PLCG1

References

1. Kim JW, Eder JP. Prospects for targeting PD-1 and PD-L1 in various tumor types. *Oncology (Williston Park, NY)*. 2014;28 Suppl 3:15–28.

2. Wolchok JD, et al. CheckMate 067: 6.5-year outcomes in patients (pts) with advanced melanoma. *JCO*. 2021;39(15_suppl):9506–9506.

3. Champiat S, et al. Hyperprogressive Disease Is a New Pattern of Progression in Cancer Patients Treated by Anti-PD-1/PD-L1. *Clin Cancer Res*. 2017;23(8):1920–1928.

4. Gajewski TF, et al. Cancer Immunotherapy Targets Based on Understanding the T Cell-Inflamed Versus Non-T Cell-Inflamed Tumor Microenvironment. In: Kalinski P, ed. *Tumor Immune Microenvironment in Cancer Progression and Cancer Therapy*. Cham: Springer International Publishing; 2017:19–31

5. Binnewies M, et al. Understanding the tumor immune microenvironment (TIME) for effective therapy. *Nat Med*. 2018;24(5):541–550.

6. Galon J, Bruni D. Approaches to treat immune hot, altered and cold tumours with combination immunotherapies. *Nature Reviews Drug Discovery*. 2019;18(3):197–218.

7. Strauss L, et al. A unique subset of CD4+CD25highFoxp3+ T cells secreting interleukin-10 and transforming growth factor-beta1 mediates suppression in the tumor microenvironment. *Clin Cancer Res*. 2007;13(15 Pt 1):4345–54.

8. Cederbom L, Hall H, Ivars F. CD4+CD25+ regulatory T cells down-regulate co-stimulatory molecules on antigen-presenting cells. *Eur J Immunol*. 2000;30(6):1538–43.

9. Cao X, et al. Granzyme B and perforin are important for regulatory T cell-mediated suppression of tumor clearance. *Immunity*. 2007;27(4):635–46.

10. Pandiyan P, et al. CD4+CD25+Foxp3+ regulatory T cells induce cytokine deprivation-mediated apoptosis of effector CD4+ T cells. *Nat Immunol*. 2007;8(12):1353–62.

11. Curiel TJ, et al. Specific recruitment of regulatory T cells in ovarian carcinoma fosters immune privilege and predicts reduced survival. *Nature Medicine*. 2004;10(9):942–949.

12. Fallarino F, et al. Modulation of tryptophan catabolism by regulatory T cells. *Nat Immunol*. 2003;4(12):1206–12.

13. Miska J, et al. HIF-1α Is a Metabolic Switch between Glycolytic-Driven Migration and Oxidative Phosphorylation-Driven Immunosuppression of Tregs in Glioblastoma. *Cell Reports*. 2019;27(1):226-237.e4.

14. Saleh R, Elkord E. Treg-mediated acquired resistance to immune checkpoint inhibitors. *Cancer Letters*. 2019;457:168–179.

15. Jones E, et al. Depletion of CD25+ regulatory cells results in suppression of melanoma growth and induction of autoreactivity in mice. *Cancer Immun*. 2002;2:1.

16. Aranda F, et al. Adjuvant combination and antigen targeting as a strategy to induce polyfunctional and high-avidity T-cell responses against poorly immunogenic tumors. *Cancer Res*. 2011;71(9):3214–3224.

17. Wang C, et al. In vitro characterization of the anti-PD-1 antibody nivolumab, BMS-936558, and in vivo toxicology in non-human primates. *Cancer Immunol Res*. 2014;2(9):846–56.

18. Kamphorst AO, et al. Rescue of exhausted CD8 T cells by PD-1–targeted therapies is CD28-dependent. *Science*. 2017;355(6332):1423–1427.

19. Kamada T, et al. PD-1+ regulatory T cells amplified by PD-1 blockade promote hyperprogression of cancer. *PNAS*. 2019;116(20):9999–10008.

20. Tan CL, et al. PD-1 restraint of regulatory T cell suppressive activity is critical for immune tolerance. *Journal of Experimental Medicine*. 2020;218(e20182232). https://doi.org/10.1084/jem.20182232

21. Curran MA, et al. PD-1 and CTLA-4 combination blockade expands infiltrating T cells and reduces regulatory T and myeloid cells within B16 melanoma tumors. *PNAS*. 2010;107(9):4275–4280.

22. Goda N, et al. The ratio of CD8 + lymphocytes to tumor-infiltrating suppressive FOXP3 + effector regulatory T cells is associated with treatment response in invasive breast cancer. *Discov Onc*. 2022;13(1):27.

23. Kim MJ, et al. Deletion of PD-1 destabilizes the lineage identity and metabolic fitness of tumor-infiltrating regulatory T cells. *Nat Immunol*. 2023;24(1):148–161.

24. Kim H-J, et al. Stable inhibitory activity of regulatory T cells requires the transcription factor Helios. *Science*. 2015;350(6258):334–339.

25. Baine I, et al. Helios induces epigenetic silencing of IL2 gene expression in regulatory T cells. *J Immunol*. 2013;190(3):1008–1016.

26. Nakagawa H, et al. Instability of Helios-deficient Tregs is associated with conversion to a T-effector phenotype and enhanced antitumor immunity. *PNAS*. 2016;113(22):6248–6253.

27. Yates K, et al. Comparative transcriptome analysis reveals distinct genetic modules associated with Helios expression in intratumoral regulatory T cells. *PNAS*. 2018;115(9):2162–2167.

28. Fishilevich S, et al. GeneHancer: genome-wide integration of enhancers and target genes in GeneCards. *Database*. 2017;2017:bax028.

29. Kitz A, et al. AKT isoforms modulate Th1-like Treg generation and function in human autoimmune disease. *EMBO reports*. 2016;17(8):1169–1183.

30. Overacre-Delgoffe AE, et al. Interferon-γ Drives Treg Fragility to Promote Anti-tumor Immunity. *Cell*. 2017;169(6):1130-1141.e11.

31. Wang J, et al. UV-induced somatic mutations elicit a functional T cell response in the YUMMER1.7 Mouse Melanoma Model. *Pigment Cell Melanoma Res*. 2017;30(4):428–435.

32. Mehdi A, et al. S-adenosylmethionine blocks tumorigenesis and with immune checkpoint inhibitor enhances anti-cancer efficacy against BRAF mutant and wildtype melanomas. *Neoplasia*. 2023;36:100874.

33. Staron MM, et al. The transcription factor FoxO1 sustains expression of the inhibitory receptor PD-1 and survival of antiviral CD8+ T cells during chronic infection. *Immunity*. 2014;41(5):802–814.

34. Wherry EJ, Kurachi M. Molecular and cellular insights into T cell exhaustion. *Nat Rev Immunol*. 2015;15(8):486–499.

35. Hoffmann P, et al. Loss of FOXP3 expression in natural human CD4+CD25+ regulatory T cells upon repetitive in vitro stimulation. *European Journal of Immunology*. 2009;39(4):1088–1097.

36. Tekguc M, et al. Treg-expressed CTLA-4 depletes CD80/CD86 by trogocytosis, releasing free PD-L1 on antigen-presenting cells. *Proc Natl Acad Sci U S A*. 2021;118(30):e2023739118.

37. Joller N, et al. Treg cells expressing the coinhibitory molecule TIGIT selectively inhibit proinflammatory Th1 and Th17 cell responses. *Immunity*. 2014;40(4):569–581.

38. Kornete M, Sgouroudis E, Piccirillo CA. ICOS-dependent homeostasis and function of Foxp3+ regulatory T cells in islets of nonobese diabetic mice. *J Immunol*. 2012;188(3):1064–74.

39. Huang F, et al. Inhibiting the MNK1/2-eIF4E axis impairs melanoma phenotype switching and potentiates antitumor immune responses. *J Clin Invest*131(8):e140752.

40. Braiman A, et al. Recruitment and activation of PLCγ1 in T cells: a new insight into old domains. *EMBO J*. 2006;25(4):774–784.

41. Zhang X, et al. OX40 Costimulation Inhibits Foxp3 Expression and Treg Induction via BATF3-Dependent and Independent Mechanisms. *Cell Rep*. 2018;24(3):607–618.

42. Kornete M, et al. Th1-Like ICOS+ Foxp3+ Treg Cells Preferentially Express CXCR3 and Home to β-Islets during Pre-Diabetes in BDC2.5 NOD Mice. *PLOS ONE*. 2015;10(5):e0126311.

43. Alvarez F, et al. Mechanisms of TREG cell adaptation to inflammation. *Journal of Leukocyte Biology*. 2020;108(2):559–571.

44. Miragaia RJ, et al. Single-Cell Transcriptomics of Regulatory T Cells Reveals Trajectories of Tissue Adaptation. *Immunity*. 2019;50(2):493-504.e7.

45. Bettelli E, Dastrange M, Oukka M. Foxp3 interacts with nuclear factor of activated T cells and NF-kappa B to repress cytokine gene expression and effector functions of T helper cells. *Proc Natl Acad Sci U S A*. 2005;102(14):5138–5143.

46. Alvarez F, et al. IL-18 is required for the TH1-adaptation of TREG cells and the selective suppression of TH17 responses in acute and chronic infections. *Mucosal Immunol*. 2023;S1933-0219(23)00035–1.

47. Zhao J, Zhao J, Perlman S. Differential Effects of IL-12 on Tregs and Non-Treg T Cells: Roles of IFN-γ, IL-2 and IL-2R. *PLOS ONE*. 2012;7(9):e46241.

48. Dahan R, et al. FcγRs Modulate the Anti-tumor Activity of Antibodies Targeting the PD-1/PD-L1 Axis. *Cancer Cell*. 2015;28(3):285–295.

49. Weber JS, et al. Safety Profile of Nivolumab Monotherapy: A Pooled Analysis of Patients With Advanced Melanoma. *J Clin Oncol*. 2017;35(7):785–792.

50. Nair VS, Elkord E. Immune checkpoint inhibitors in cancer therapy: a focus on T-regulatory cells. *Immunology & Cell Biology*. 2018;96(1):21–33.

51. Angelin A, et al. Foxp3 Reprograms T Cell Metabolism to Function in Low-Glucose, High-Lactate Environments. *Cell Metab*. 2017;25(6):1282-1293.e7.

52. Maj T, et al. Oxidative stress controls regulatory T cell apoptosis and suppressor activity and PD-L1-blockade resistance in tumor. *Nat Immunol*. 2017;18(12):1332–1341.

53. Carter LL, et al. PD-1:PD-L inhibitory pathway affects both CD4+ and CD8+ T cells and is overcome by IL-2. *European Journal of Immunology*. 2002;32(3):634–643.

54. West EE, et al. PD-L1 blockade synergizes with IL-2 therapy in reinvigorating exhausted T cells. *J Clin Invest*. 2013;123(6):2604–2615.

55. Ahrends T, et al. CD4+ T Cell Help Confers a Cytotoxic T Cell Effector Program Including Coinhibitory Receptor Downregulation and Increased Tissue Invasiveness. *Immunity*. 2017;47(5):848-861.e5.

56. van Gulijk M, et al. PD-L1 checkpoint blockade promotes regulatory T cell activity that underlies therapy resistance. *Science Immunology*. 2023;8(83):eabn6173.

57. Kumagai S, et al. The PD-1 expression balance between effector and regulatory T cells predicts the clinical efficacy of PD-1 blockade therapies. *Nature Immunology*. 2020;21(11):1346–1358.

58. Gerriets VA, et al. Foxp3 and Toll-like receptor signaling balance Treg cell anabolic metabolism for suppression. *Nat Immunol*. 2016;17(12):1459–1466.

59. Tanimine N, et al. Differential effects of 2-deoxy-D-glucose on in vitro expanded human regulatory T cell subsets. *PLOS ONE*. 2019;14(6):e0217761.

60. Santinon F, et al. Direct AKT activation in tumor-infiltrating lymphocytes markedly increases interferon-γ (IFN-γ) for the regression of tumors resistant to PD-1 checkpoint blockade. *Sci Rep*. 2022;12(1):18509.

61. Koch MA, et al. The transcription factor T-bet controls regulatory T cell homeostasis and function during type 1 inflammation. *Nat Immunol*. 2009;10(6):595–602.

62. Koch MA, et al. T-bet+ Treg Cells Undergo Abortive Th1 Cell Differentiation due to Impaired Expression of IL-12 Receptor β2. *Immunity*. 2012;37(3):501–510.

63. Redjimi N, et al. CXCR3+ T regulatory cells selectively accumulate in human ovarian carcinomas to limit type I immunity. *Cancer Res*. 2012;72(17):4351–4360.

64. Santegoets SJ, et al. Tbet-positive regulatory T cells accumulate in oropharyngeal cancers with ongoing tumor-specific type 1 T cell responses. *Journal for ImmunoTherapy of Cancer*. 2019;7(1):14.

65. Moreno Ayala MA, et al. CXCR3 expression in regulatory T cells drives interactions with type I dendritic cells in tumors to restrict CD8+ T cell antitumor immunity. *Immunity*. [published online ahead of print: June 30, 2023]; https://doi.org/10.1016/j.immuni.2023.06.003

66. Wang J, et al. Eliciting T cell immunity against poorly immunogenic tumors by immunization with dendritic cell-tumor fusion vaccines. *J Immunol*. 1998;161(10):5516–24.

67. Meeth K, et al. The YUMM lines: a series of congenic mouse melanoma cell lines with defined genetic alterations. *Pigment Cell & Melanoma Research*. 2016;29(5):590–597.

Chapter 4 – T cell responses to IL-18 promote the establishment of an inflamed melanoma environment and are required for successful response to anti-PD-1.

Bridging statement for Chapter 4

In chapter 3, we identified the acquisition of T_h1-like characteristics by T_{reg} cells as a hallmark of successful response to PD-1. Despite IFNγ production suggesting a dysregulation of T_{reg} cell stability, T_{reg} TILs from high responders displayed potent suppressive capacity, pointing to the existence of factors released within the TME that modulate evasion from suppression without directly compromising T_{reg} cell suppressive capacity. While IL-12 is known to induce the differentiation of T-bet$^+$ T_{reg} cells, little is known about the factors that promote the maintenance of this population. Indeed, the acquisition of this phenotype was transient, as T_h1-like characteristics were lost upon *in vitro* restimulation. Furthermore, while IFNγ production by T_{reg} cells was restricted to HR TMEs, T-bet was expressed, albeit to reduced levels by T_{reg} cells in tumors that achieved immune evasion, suggesting the need for additional signals to further amplify their T_h1-differentation. In chapter 2, we identified that upregulation of T-bet was associated with expression of the IL-18R in both CD8$^+$ and T_{reg} TILs. Given the role of IL-18 in promoting the expansion and effector functions of T_h1 and effector CD8$^+$ T cells, and our lab's report that IL-18 alters the T_{reg}:T_{eff} balance during lung infections, we reasoned that TIL responses to IL-18 could mediate the evasion from suppression observed in HR TMEs and induce the expression of IFNγ by T_{reg} TILs. In chapter 4, using mice with T-cell deletion of IL-18R1, we identify IL-18 as a key player in the establishment of a hot TME and a determinant factor in the control of the T_h1:T_{reg} balance and subsequent response to checkpoint blockade.

T cell responses to IL-18 promote the establishment of an inflamed melanoma environment and are required for successful response to anti-PD-1.

Authors: Mikhaël Attias[1,2,3], Fernando Alvarez[1,2,3], Tho-Alfakar Al-Aubodah[1,2,3], Constantin Polychronakos[4,5], Ciriaco A. Piccirillo[1,2,3]

Affiliations:

[1]Department of Microbiology and Immunology, McGill University, Montreal, Quebec, Canada

[2]Program of Infectious Diseases and Immunity in Global Health, Centre for Translation Biology (CTB), The Research Institute of the McGill University Health Centre (RI-MUHC), Montreal, Quebec, Canada

[3]Centre of Excellence in Translational Immunology (CETI), McGill University, Montreal, Quebec, Canada

[4]Division of Pediatrics, McGill University, Montreal, Quebec, Canada

[5]Department of Human Genetics, McGill University, Montreal, Quebec, Canada

* Correspondence should be addressed to:

Dr. C.A. Piccirillo

Research Institute of McGill University Health Centre (MUHC)

Centre for Translational Biology, Bloc E, Room E-M2.3248

1001 Boul. Décarie, Montréal, Québec, H4A 3J1

ciro.piccirillo@mcgill.ca

Tel: 514-934-1934 ext. 76143

Keywords: Foxp3+ Treg cells, IL-18, anti-PD-1, immuno-oncology, melanoma

Manuscript in submission

Abstract

IFNγ-producing $CD8^+$ and $CD4^+$ T cells are the most potent effectors of anti-tumor responses, and their presence in the tumor core is a major predictive biomarker of response to cancer immunotherapy. However, their effector functions are potently suppressed locally by tumor-infiltrating $Foxp3^+$ Regulatory T (T_{reg}) cells. To devise adjuvant strategies that improve treatment efficacy, a better understanding of the factors that govern the abundance of lymphocyte infiltration and the evolution of their cytokine-secreting capacity through time is warranted. IL-18, a member of the IL-1 family of alarmins, is abundantly secreted by tumor cells and promotes the expansion and survival of effector T cells (T_{eff}) over T_{reg} cells in viral diseases. Yet, its role in governing the functional fate of melanoma-infiltrating T cells remains ill-defined. To study the role of IL-18 signaling on shaping the inflammatory phenotype of melanoma, we studied spontaneous tumor growth and response to anti-PD-1 in a murine model with a T cell-specific deletion of IL18R1. The inability of T cells to sense local IL-18 lead to the accumulation of T_{reg} over $IFN\gamma^+$ T_h1 cells, $CD8^+$ T cell exhaustion and accelerated tumor growth. Upon treatment with anti-PD-1, IL18R1-deficient T_{reg} cells failed to acquire T_h1-like characteristics, and clinical response to treatment was abrogated. Taken together, these data suggest that IL-18 plays a crucial role in mediating the balance between T_h1 and T_{reg} cells in tumor microenvironments (TME) and provides further rationale for targeting IL-18 signaling to enhance the efficacy of anti-PD-1 therapy.

Introduction

A tumor's immune phenotype is one of the main determinants of the success of immune checkpoint inhibition (ICI) therapy (1). In the "cold" tumors associated with resistance to treatment, T cells are excluded to the margins and display impaired function (2). At the opposite end of this spectrum, "hot" tumors are characterised by an abundant infiltration of tumor antigen-specific $CD4^+$ T_h1 and $CD8^+$ T cells in the tumor core (3), allowing for the blockade of checkpoint signals to readily support their activation. However, because of the interplay between tumor-infiltrating immune populations, local metabolic conditions, and immunomodulatory molecules produced in the tumor microenvironment (TME) (4), "hot" tumors ultimately become immunosuppressed. As such, a better understanding of the pathways that regulate inflammation within the tumor is paramount to pave the way to novel adjuvant strategies that synergize with the use of ICI (5).

Strong type 1 adaptive immune responses are key to the establishment of a "hot" TME (6). This process is orchestrated by IL-12-producing antigen presenting cells (APCs) that promote the differentiation of tumor-specific $CD4^+$ T_h1 cells (7, 8), which, in turn, support $CD8^+$ tumor-infiltrating lymphocytes (TILs), by enhancing their survival and effector functions (9). While polyfunctional $CD8^+$ TILs are the most potent effectors of anti-tumor immunity (10), they induce the expression of PD-L1 by tumor and antigen-presenting cells (11), which in turn inhibits their effector functions and leads to their apoptosis (12), gradually dampening inflammation in the TME. In addition, regulatory T cells (T_{reg}) play a dominant role in keeping tumors cold through direct suppression of TILs (13), reducing the co-stimulatory properties of dendritic cells (14), and producing anti-inflammatory cytokines that further inhibit T cell function (15). While treatment

with ICIs increases inflammation in TMEs by preventing T cell exhaustion, it also increases T_{reg} cell activation, which can limit their efficacy (16, 17).

Importantly, we and others have shown that T_{reg} TILs adapt to a given TME by differentiating into T_h-like subsets that respond differentially to inflammatory signals (18–22). During a successful response to anti-PD-1, T_{reg} TILs acquire T_h1-like characteristics, which leads to local alleviation from T_{reg} cell suppression (Attias *et al*., under review). However, as PD-1 blockade is not sufficient to induce this phenotype in colder tumors or outside the TME, further investigation is warranted on the local conditions that induce the T_h1-adaptation of T_{reg} TILs. We have previously shown that T_h1-adapted T_{reg} cells preferentially respond to IL-18, a member of the IL-1 family of alarmins and important potentiator of type 1 responses (23), during Influenza A Virus infection (24). In this setting, T_{reg} cell responses to IL-18 were required for the specialized suppression of T_h17 cells and favored the expansion of T_h1 cells over T_{reg} cells, which increased immunopathology in the lung and delayed return to homeostasis (24). However, in the context of an ongoing anti-tumor response, promoting T_h1 cell accumulation contributes to the establishment of a more inflamed TME and increases responsiveness to treatment with anti-PD-1 (25), leading us to hypothesize that IL-18 is a key factor involved in the establishment of strong type 1 responses and the T_h1-adaptation of T_{reg} cells that govern a tumor's responsiveness to anti-PD-1.

While there are many reports on the beneficial role of IL-18 in anti-melanoma responses, its direct effect in governing T cell responses remains ill-defined. IL-18 is abundantly produced by tumor cells and APCs in melanoma (26) and synergizes with IL-12 to promote the proliferation, and survival of T_{eff} cells (23, 27). As such, administration of IL-18 was shown to have anti-melanoma effects by activating $CD4^+$ T and NK cell responses (28), inhibiting angiogenesis through an IFNγ-dependent mechanism (29) and reducing metastasis formation (30). Furthermore,

administration of recombinant IL-18 was shown to potentiate the efficacy of ICIs in a preclinical model of metastatic melanoma (31). On the other hand, tumors counter this effect by producing its decoy receptor, IL-18BP, limiting the anti-tumor effects of IL-18 (32). Furthermore, depending on the administration scheme, exogenous IL-18 can promote immune evasion (33, 34). Indeed, IL-18 signaling promotes PD-1 expression in NK cells (34) and contributes to $CD8^+$ T cell exhaustion (35), which in turn induces the loss of IL18R expression (36). Thus, a better understanding of the ways in which IL-18 governs the fate of T_{eff} and T_{reg} TILs and controls the T_{reg}:T_{eff} balance in the context of anti-tumor responses is warranted.

To dissect the role of IL-18 signaling on T cell function and fate in hot TMEs, we studied the consequences of a T cell-specific conditional deletion of IL18R1 expression on tumor growth and responsiveness to anti-PD-1 in the highly immunogenic YUMMER1.7 model of murine melanoma (37). In the absence of IL18R1 expression by T cells, the composition of the TME was remodeled towards a colder phenotype with reduced co-stimulatory capacity of dendritic cells, reduced T cell infiltration and preferential accumulation of T_{reg} cells over T_h1 cells, leading, in turn, to accelerated tumor growth. Upon treatment with anti-PD-1, T_{reg} TILs failed to acquire T_h1-like characteristics, and $CD8^+$ cells displayed a dysfunctional phenotype in the absence of IL18R1 expression by T cells, abrogating clinical response. Collectively, these results position IL-18 signaling as a crucial factor mediating T_h1 evasion from T_{reg} cell suppression in tumor microenvironments.

Material and Methods

Mice

C57Bl/6.Foxp3$^{IRES\text{-}mRFP}$ reporter knock-in (Foxp3^{RFP}) mice were provided by Jonathan Spicer. C57Bl/6.CD4-Cre$^{+/-}$ IL18R1$^{fl/fl}$ mice were provided by Dr. Giorgio Trinchieri (NIH, Bethesda, MA), and were bred to generate CD4-Cre$^{-/-}$ IL18R1$^{fl/fl}$ (CD4^{WT}) mice and further crossed for two generations to obtain CD4-Cre$^{+/+}$ IL18R1$^{fl/fl}$ (CD4$^{\Delta IL18R1}$) mice, to obtain high numbers of age and sex-matched groups. All mice used were males and 8 to 14 weeks of age, the examiner was blinded to group repartition until the end of the analysis.

Tumor cell lines

The YUMMER1.7 cell line was generated by Wang and colleagues by irradiating Braf^{V600E} PTEN$^{-/-}$ Cdkn2a$^{-/-}$ cells and expanding a single clone bearing additional somatic mutations (37). YUMMER1.7 cells were kindly provided by Marcus Bosenberg (Yale University) and cultured in advanced DMEM/F12 supplemented with 10%FBS (Wisent), 1% Penicillin/Streptomycin (Wisent) and 1% MEM Non-essential Amino Acids (Wisent). Tumor cells were tested for mycoplasma and viral contamination by the McGill Comparative Medicine Animal Resources Centre. Cells were expanded in 225 cm^2 tissue culture flasks and 5x10^6 cells/ml were frozen down and stored in 10% DMSO/FBS in liquid nitrogen. Prior to injection, cells were thawed and passaged twice at 37°C in humidified air with 5% CO_2 and washed twice in cold PBS before preparation of the inoculum.

In vivo tumor studies

YUMMER1.7 cells were resuspended in PBS and then mixed in Corning® Matrigel Basement Membrane HC at a 1:1 PBS to Matrigel ratio. YUMMER1.7 cells (2.5x10^5) were injected subcutaneously in the right flank of male mice, under anesthesia. Mice were monitored

thrice weekly. Tumor volumes were measured using an electronic calliper and calculated as: length x width^2 x 0.5. Experimental endpoint was defined as soon as one mouse reached humane endpoint (tumor volume > 1500mm^3). At necropsy, tumors were harvested, and their weights and volumes were measured post-mortem. For experiments with administration of anti-PD-1, mice received 5 doses of either 250µg of anti-PD1 (clone RMP1-14, BioXcell) or PBS, intraperitoneally, thrice weekly, starting on day 8. At the predetermined experimental endpoint, all mice were sacrificed, and we harvested tumors, tumor-draining axillary and inguinal lymph nodes, and non-tumor draining contralateral lymph nodes.

Isolation of tumor-infiltrating lymphocytes

After CO_2 euthanasia, tumors were collected in serum-free Hank's Balanced Salt Solution (Wisent), then minced manually in <1mm^3 pieces using razor blades. Tumors were then digested in the presence of collagenase IV (1mg/ml, Gibco) and DNAse I (0.005µM, Sigma-Aldrich) at 37°C for 1 hour. Cells were then pushed through a 21G needle and washed in cold complete RPMI 1640 with 5% FBS. Red blood cells were lysed by incubating the cells for 30 seconds with ACK buffer, washed, resuspended in complete RPMI1640, and filtered twice through a 70µm mesh.

Purification of T cell subsets

Prior to FACS-sorting splenocytes and TILs, CD4$^+$ and CD8$^+$ T cells were purified using CD4/CD8 TIL Microbeads (Miltenyi) and an autoMACS (Miltenyi). T_{reg} cells were sorted as CD4$^+$ RFP$^+$, T_{resp} cells were sorted as either CD4$^+$ RFP$^-$ or CD8$^+$ RFP$^-$ cells (purity>99%) using a FACSAria™ (BD Biosciences).

***In vitro* T cell assays**

CD4$^+$ RFP$^+$ T_{reg} cells were sorted from the splenocytes or endpoint tumors of untreated mice. Depending on the experiment, T_{resp} cells were either CD4$^+$ RFP$^-$ or CD8$^+$ RFP$^-$ splenocytes.

Antigen-presenting cells were purified from the negative fraction of the CD4/CD8 MACS and mitomycin-C inactivated for 1 hour at 37°C. T_{resp} cells ($5x10^4$) were cultured alone or co-cultured with splenic or TIL T_{reg} cells at a 4:1 ratio, and antigen-presenting cells ($1x10^5$) in RPMI 1640 (Wisent) supplemented with 10%FBS in the presence of soluble αCD3 (0.5µg/mL) for 72 hours at 37°C, in 96-well flat bottom plates (0.2ml). Cells were incubated in the presence of IL-12 (10ng/ml, R&D Systems) and/or IL-18 (10ng/ml, R&D Systems) at the start of the culture. After 69h, cells were additionally stimulated with PMA, Ionomycin, and Golgi Stop at manufacturer-recommended concentrations for 3h for assessment of cytokine production.

Flow cytometry analysis

After lymphocyte isolation, the cells were washed in PBS and stained with anti-CD16/CD32 (clone 2.4G2, BD) and fixable viability dye eFluor780 or 506 (Thermofisher). Following a wash, cells were marked with extracellular markers. For analysis of other transcription factors, cytokine secretion and intracellular markers, cells were fixed and permeabilized with the Foxp3 Transcription Staining Buffer Set (eBioscience™) and then stained for intracellular markers). Samples were acquired on the same day of the intracellular staining using a BD Fortessa LSR-X20 and analyzed using FlowJo v10 (TreeStar and BD). The following anti-mouse antibodies were used: CD45.2 (clone 104), CD19 (clone 1D3), CD11c (clone HL3), I-A[b] (clone AF6-120.1), CD86 (clone GL1), Ly6C (clone AL21), PD-L1 (clone MIH5), CD3 (clone 17A2), CD8a (clone 53-6.7), CD8b (clone H35-17.2), PD-1 (clone J43), Ki67 (clone B56), KLRG1 (clone 2F1), TCF-1 (clone S33-966), Gata-3 (clone L50-823), IFNγ (clone XMG1.2), IL-2 (clone JES6-5H4), TNFα (clone MP6-XT22), RORγt (clone Q31-378) from BD; CD4 (clone RM4-5), CTLA-4 (clone UC-4B9), Helios (clone 22F6), Bcl-2 (clone BCL/10C4), GRZB (clone Q16A02), Ly6G (clone 1A8) from Biolegend; Foxp3 (clone FJK-16S), ICOS (clone C396.4A), T-bet (clone 4B10), TIGIT

(clone GIGD7), CD25 (clone PC61.5), Tim-3 (clone RMT3-23), ST2 (clone RMST2-2), IL-17A (clone ebio17B7), IL-10 (clone JES5-16E3), F4/80 (clone BM8), CD11b (clone M1/70) from eBioscience.

Statistical analysis

Unless otherwise stated, all data is depicted as mean +/- SD. For tumor growth curves, multiple comparisons were made using a mixed-effects analysis with a Geiser-Greenhouse correction for sphericity and a Sidak correction for multiple comparisons. Tumor weights at endpoint were compared using a two-tailed unpaired t-test with Welch's correction. The normality of tumor weights in each group was determined with a Shapiro-Wilk test. Given the bimodal distribution of tumor volumes in the anti-PD-1-treated mice, they were categorized as HR or LR based on a cut-off volume of 300mg. Tumor weights were then compared using a Brown-Forsythe and Welch ANOVA test with a Dunnett T3 correction for multiple comparisons.

For flow cytometry data, the normality of each data set's distribution was determined with a Shapiro-Wilk test. Homoscedasticity was tested using Fisher's test. If both conditions were met, when applicable, proportions and MFIs were compared using ordinary One-Way ANOVA with a correction to account for multiple comparisons. If the normality condition was not met, a non-parametric Mann-Whitney test was used. For experiments without treatment, MFI fold changes were calculated by dividing each MFI measurement by the average MFI in the $CD4^{WT}$ group for a given experiment. For experiments with anti-PD-1, all samples were stained with the exact same antibody panels and lots and acquired on an LSR-Fortessa x20 using the same application settings. Voltage settings were calibrated using Sphero® Rainbow Calibration Particles (8 peaks), 3.0 - 3.4 µm (BD). Correlation matrixes were generated by computing Pearson r-correlates with tumor weight at endpoint for each variable and represented as a heatmap. For linear correlation analyses,

all data points were pooled to calculate linear correlations. The slope's deviation from zero was evaluated using Fisher's test. All statistical analysis was conducted using GraphPad Prism v10.1.

For *in vitro* experiments, all conditions were realized in triplicates (n=3) and each experiment was repeated twice (N=2). Data is shown from N of 1 representative repeat.

Study approval

All mice were housed and bred in specific pathogen-free conditions in the same facility and used according to the regulations of the Canadian Council of Animal Care Guidelines and Animal Care and Use Committees at McGill University.

Data availability

Numerical data values presented in the graphs are uploaded as supplementary material. FCS files generated by flow cytometry are available upon request from the corresponding author.

Results

IL-18 signaling in T cells delays tumor growth and contributes to the establishment of a hot tumor microenvironment.

While IL-18 was shown to promote anti-melanoma responses by enhancing the expansion and survival of $CD8^+$ and T_h1 cells (28, 38), it can also induce immune evasion by promoting the development of myeloid-derived suppressor cells (39, 40) and inducing $CD8^+$ TIL exhaustion (35). To determine the impact of endogenous IL-18 signaling in T cells on melanoma growth and the functional fate of TILs, we used the highly immunogenic YUMMER1.7 murine melanoma model (37) and a constitutive, T cell-specific deletion of IL-18R1, which targets both $CD4^+$ and $CD8^+$ T cells during the double positive stage of thymic selection. Male CD4-$Cre^{+/+}$ IL-$18R1^{fl/fl}$ ($CD4^{\Delta IL18R1}$, n=9) and CD4-$Cre^{-/-}$ IL-$18R1^{fl/fl}$ ($CD4^{WT}$, n=7) were injected s.c. with YUMMER1.7 cells ($2.5x10^5$) and sacrificed as soon as one tumor reached humane endpoint (volume>$1500mm^3$, **Figure 1A**). $CD8^+$, $CD4^+$ $Foxp3^-$ T_{conv} and $CD4^+$ T_{reg} TILs expressed the IL-18R in higher proportions than their draining lymph node-resident counterparts in the $CD4^{\Delta WT}$ group, and the increase was most pronounced in T_{conv} cells (mean= 3.35 vs 78.24, **Supplementary Figure 1A**). Furthermore, abrogation of the IL-18R1 was fully penetrant in both draining lymph nodes and TILs in the $CD4^{\Delta IL18R1}$ group (frequency <1%, **Supplementary Figure 1A**). Absence of IL18R1 in T cells accelerated tumor growth, with humane endpoint reached on day 17 (N=2). At endpoint, there was a 3-fold increase in tumor volume, and a 4-fold increase in tumor weight in the $CD4^{\Delta IL18R1}$ group (**Figure 1B**).

Next, we asked if a T cell-specific deletion of IL18R promotes the establishment of a "cold" TME. To this end, we determined the immune composition of the TME at endpoint in both groups. Absence of IL-18 signaling reduced the overall immune infiltration, as evidenced by the reduced

proportion of $CD45^+$ hematopoietic cells, and specifically a reduction in $CD4^+$ and $CD8^+$ T cell infiltration (**Figure 1C**). As a result, while $CD8^+$ T cells were the most abundant in the $CD4^{WT}$ group, $CD11b^+$ $F4/80^{High}$ macrophages and $CD11b^+$ $Ly6C^+$ monocytes were predominant in tumors from $CD4^{\Delta IL18R1}$ mice, (**Figure 1D**), feature that is characteristic of a poorly inflamed TME (41). Indeed, while tumor-infiltrating macrophages from WT mice displayed an M1-phenotype, associated with pro-inflammatory functions and tumor-antigen presentation in the TME (42) their level of MHC-II expression was reduced in the $CD4^{\Delta IL18R1}$ group (**supplementary Figure 1B**). In addition, dendritic cells displayed a more tolerogenic phenotype, evidenced by reduced expression of MHC-II and CD86 in the $CD4^{\Delta IL18R1}$ group (**Figure 1E**). Taken together, these data show that T cells require IL-18 to promote the establishment of a hot TME and enhance the co-stimulatory properties of local antigen-presenting cells.

Functional T_h1 cells accumulate in the tumor microenvironment in response to IL-18.

IL-18 promotes the expansion and survival of IFNγ-secreting T_h1 and $CD8^+$ T cells (23), key effectors of anti-tumor immunity, but IFNγ signaling induces PD-L1 expression which in turn promotes the gradual exhaustion of these cells throughout tumor progression (11). To better discern the functional impact of IL-18 on TILs, we next assessed how the T cell-specific abrogation of IL18R1 expression affects the balance between T cell subsets in the TME. In this model, $CD8^+$ T cells dominated the T cell compartment, and their proportion was unchanged, suggesting IL-18 does not promote their accumulation over other T cell subsets. **(Figure 2A)**. However, the proportion of T_{conv} cells was halved from 10 to 5% of total T cells in $CD4^{\Delta IL18R1}$ tumors and there was a converse trend towards increased T_{reg} cell frequency ($p=0.1$) compared to WT (**Figure 2A**).

$CD4^+$ T_h1 cell differentiation is required to produce IFNγ and to support the cytotoxic activity of $CD8^+$ TILs (43). T_h1 cell function is dependent on the expression of the master

transcription factor T-bet (44) and inhibited by Foxp3$^+$ T_{reg} cells (45). To assess how IL-18 signaling impacts the functional balance between T_h1 and T_{reg} cells, we investigated T-bet expression in T_{conv} TILs in relation to T_{reg} cell frequency. While Foxp3$^-$ T-bet$^+$ T_h1 cells were more abundant than Foxp3$^+$ T_{reg} cells in CD4^{WT} TILs (T_h1:T_{reg} ratio =2), the inverse was observed in CD4$^{\Delta IL18R1}$ TILs (T_h1:T_{reg} ratio = 0.3). Accordingly, the frequency of differentiated T-bet$^+$ TILs was reduced 3-fold within the T_{conv} compartment of CD4$^{\Delta IL18R1}$ mice relative to CD4^{WT} mice, which correlated strongly with increased tumor weight (r^2=0.44, $p<0.01$). Furthermore, a lack of IL-18 signaling led to a 20% reduction in T-bet MFI intensity within T_h1 cells (**Figure 2B**). Accordingly, we observed both a reduced frequency of IFNγ$^+$ T_{conv} TILs and lower amounts of IFNγ on a per-cell basis (MFI) (**Figure 2C**). Interestingly, IL-2 secretion, was almost fully abrogated (frequency <2% of T_{conv} cells) in CD4$^{\Delta IL18R1}$ TILs (**Figure 2C**), suggesting reduced T cell activity. Indeed, the loss of T_h1 cell function was associated with a 30% increase in PD-1 MFI in CD4$^{\Delta IL18R1}$ T_{conv} cells, compared to their WT counterparts, indicative of an exhausted phenotype (**Supplementary Figure 2A**). Furthermore, there was no sign of immune deviation towards a T_h2 or a T_h17 phenotype, as evidenced by the absence of Gata-3, or RORγT, and IL-17A expression, respectively (**Supplementary Figure 2B**). Taken together, these data indicate that IL-18 modulates the T_{eff}:T_{reg} balance by promoting the accumulation of cytokine-secreting T_h1 cells over T_{reg} cells, demonstrating its key role in the establishment of "hot" TMEs.

IL-18 impairs T_{reg} cell-mediated suppression of IFNγ production *in vitro*.

While IL-18 is not required for the differentiation of T_h1 cells, it synergizes with IL-12 to promote their expansion (46). However, the impact of IL-18 on the suppressive function of T_{reg} TILs remains unknown. Since we observed decreased proportions of T_h1 TILs compared to T_{reg} in CD4$^{\Delta IL18R1}$ mice, we hypothesized that IL-18 decreases the potency of T_{reg} TILs to suppress T_h1

cell function and expansion. To test this hypothesis, we inoculated male Foxp3-IRES-mRFP ($Foxp3^{RFP}$) reporter mice with YUMMER1.7 cells ($2.5x10^5$) s.c. and isolated splenic and TIL RFP^+ T_{reg} cells when tumors reached humane endpoint to assess their suppressive function in the presence the presence or absence of IL-18 (**Figure 3A)**. While IL-18 increased responder $CD4^+$ RFP^- T cell (T_{resp}) proliferation, quantified by division index, T_{reg} TILs were more potent suppressors of T_{resp} cells, regardless of the presence of IL-18 (30% for TILs versus 20% for splenic T_{reg}) (**Figure 3B**). Interestingly, IL-18 improved the capacity of T_{resp} cells to produce IFNγ in the presence of splenic T_{reg} cells, but not with T_{reg} TILs (**Figure 3B**), suggesting that T_{reg} TILs are more potent suppressors of T_h1 cell function. Overall, these results suggest IL-18 promotes T_h1 cell expansion and function rather than cause a direct impairment of T_{reg} cell-mediated suppression.

However, IL-18 was insufficient to induce a complete T_h1 differentiation, with less than 10% of T_{resp} cells producing IFNγ in our assay, in line with previous reports (27). Therefore, to assess the capacity of T_{reg} TILs to suppress the T_h1 polarization of T_{conv} cells, we cultured these cells in the presence of saturating concentrations of recombinant mouse IL-12 (10 ng/ml), the main initiator of T_h1-differentiation (47). While IL-12 reduced the suppression provided by splenic T_{reg} cells, the suppression of proliferation of T_{resp} cells cultured in the presence of T_{reg} TILs remained stable even in the presence of IL-18 (**Figure 3C**). On the other hand, while T_{reg} TILs displayed superior potency in inhibiting the production of IFNγ by T_{resp} cells compared to their splenic counterparts in the presence of IL-12 alone, addition of IL-18 facilitated the complete evasion of $IFN\gamma^+$ T_{resp} cells, which maintained levels of IFNγ (MFI) equivalent to that of cells cultured in the absence of T_{reg} cells (**Figure 3D**). Thus, a synergy between IL-12 and IL-18 is required for T_h1 cells to fully evade T_{reg} TIL-mediated suppression.

T cell responses to IL-18 promote T-bet expression by melanoma-infiltrating T_{reg} cells.

Cumulating evidence links the acquisition of T_h1-like characteristics by T_{reg} cells with increased anti-tumor immunity (48–50), while deviation to a T_h2-like phenotype promotes immune evasion (51, 52). Yet, little is known on the role of IL-18 in this adaptation. Given the decreased accumulation of T_h1 cells in $CD4^{\Delta IL18R1}$ TILs and the fact that IL-18 impairs T_{reg}-cell control of IFNγ production *in vitro*, we next asked how IL-18 signaling impacts the phenotype of T_{reg} TILs. To this end, we assessed the expression of markers associated with T_{reg} cell fitness in the TME (Helios, CD25, PD-1) and tissue-adaptation (T-bet, Gata-3). The proportion of T_{reg} cells amongst total $CD4^+$ T cells was increased in in $CD4^{\Delta IL18R1}$ TILs compared to WT. However, these cells had reduced expression of Helios and CD25, by both frequency and MFI (**Figure 4A**), which correlated strongly with the abrogation of IL-2 production by T_{conv} TILs (r^2=0.51, **Supplementary Figure 3A**). Furthermore, $CD4^{\Delta IL18R1}$ T_{reg} TILs had a 20% increase in PD-1 MFI compared to WT T_{reg} TILs (**Figure 4B**). Conversely, they displayed a reduction in levels of CTLA-4 expression (25% reduction in MFI versus WT) (**Figure 4C**), in line with decreased expression of CD86 on dendritic cells (**Figure 1E**). Thus, despite accumulating readily over T_{conv} cells, $CD4^{\Delta IL18R1}$ T_{reg} cells display signs of reduced fitness.

Recently, we identified the acquisition of T_h1-like characteristics by T_{reg} TILs as a condition permissive to TIL evasion from suppression (Attias *et al.,* manuscript submitted). Therefore, we asked if IL-18 impacts the tissue adaptation of T_{reg} cells. The frequency of T-bet$^+$ T_{reg} cells was reduced in $CD4^{\Delta IL18R1}$ T_{reg} TILs, as was T-bet MFI compared to WT counterparts (**Figure 4D**). This was not compensated by a deviation towards a T_h2-like phenotype, as there also was a decrease in the proportion of Gata-3 and ST2-expressing T_{reg} TILs (**Supplementary Figure 3B**).

Next, we asked if recombinant IL-18 was sufficient to modulate the expression of T-bet and IFNγ by T_{reg} cells. To this end, we cultured T_{reg} TILs in the presence of IL-18, as described in Figure 3. While IL-18 alone had no effect on T-bet and IFNγ expression of splenic T_{reg} cells, it induced a two-fold increase in the frequency of T-bet$^+$ T_{reg} TILs and a four-fold increase in IFNγ$^+$ T_{reg} TILs, suggesting that TILs are more responsive to IL-18 (**Figure 4E**). Furthermore, this effect was amplified by the addition of IL-12, upon which 80% of T_{reg} cells secreted IFNγ, conditions upon which T_{reg} cells did not reduce IFNγ production by T_{resp} cells (**Figure 3D**). Taken together, these data show that while T_{reg} TILs are potent suppressors of T_h1 responses, IL-18 can promote their acquisition of T_h1-like characteristics, which, in turn, alleviates their capacity to suppress IFNγ production by T_h1 cells.

IL-18 promotes the expansion and effector functions of CD8$^+$ TILs.

As deletion of IL18R1 accelerated tumor growth, and CD8$^+$ T cells are the main effectors of anti-tumor immunity, we next asked how IL-18 impacts the function of CD8$^+$ TILs. To this end, we assessed the expression of pro-inflammatory cytokines (IFNγ, TNFα), and markers of cytotoxic activity (CD107a, GRZB) and functional status (PD-1, T-bet) at tumor endpoint. CD4$^{\Delta IL18R1}$ CD8$^+$ TILs displayed a dysfunctional phenotype, with a reduced proportion of IFNγ$^+$ cells, a 30% reduction in IFNγ MFI compared to their WT counterparts, and abrogated production of TNFα (frequency <2% of CD8$^+$ TILs, **Figure 5A**). Furthermore, these cells had no surface expression of CD107a, indicating an absence of capacity to degranulate (53), which was corroborated by a trend of increased accumulation of GRZB (**Figure 5B**). In line with this reduced functionality, ΔIL18R1 CD8$^+$ TILs displayed a 25% reduction in T-bet MFI and a converse 40% increase in PD-1 MFI (**Supplementary Figure 4A**) compared to their WT counterparts, indicative of a terminally exhausted phenotype.

Next, we asked if IL-18 could restore the effector functions of exhausted $CD8^+$ TILs. To this end, we purified $CD8^+$ TILs and splenocytes isolated from YUMMER1.7-bearing $Foxp3^{RFP}$ mice at tumor endpoint, and cultured them with accessory cells ($1x10^5$), in the presence or absence of recombinant murine IL-18 (10ng/ml). In line with previous reports (27), IL-18 increased the proliferation of IFNγ-secreting cells (**Figure 5C**). In addition, while $CD8^+$ TILs reactivated poorly upon *in vitro* restimulation, IL-18 increased their proliferation and restored their capacity to secrete IFNγ (**Figure 5C**). To assess if IL-18 influenced the evasion of $CD8^+$ cells from T_{reg} cell-mediated suppression, we then co-cultured $CD8^+$ splenocytes ($5x10^4$) with splenic or TIL-T_{reg} cells ($1.25x10^4$), with or without recombinant murine IL-18 (10ng/ml). Contrary to what we observed with $CD4^+$ T_{conv} cells, addition of IL-18 impaired T_{reg} cell suppression of $CD8^+$ T cell proliferation, and IFNγ-production, and further addition of IL-12 completely abrogated it (**Figure 5D**). Taken together, these data indicate that IL-18 promotes the effector functions of $CD8^+$ TILs and their evasion from T_{reg} cell suppression.

Successful response to anti-PD-1 is dependent on IL-18 signaling in T cells.

Given that abrogation of IL-18R expression promoted the establishment of a cold TME and altered the T_h1:T_{reg} balance in tumors, we then asked if T cell responsiveness to IL-18 was required for a successful response to anti-PD-1. To this end, we injected $CD4^{\Delta IL18R1}$ (n=8) and $CD4^{WT}$(n=9) mice with YUMMER1.7 cells ($2.5x10^5$) s.c. and treated them with anti-PD-1, starting on day 8 (N=2). All mice were sacrificed as soon as one tumor reached humane endpoint (volume>$1500mm^3$, **Figure 6A**). There was a significant acceleration of tumor growth in the $CD4^{\Delta IL18R1}$ group, as evidenced by the 10-fold increase in tumor volume compared to the WT group (**Figure 6B**). In line with previous reports (54), there was a bimodal distribution of tumor weights at endpoint, thus we used the same 300mg cut-off as established in our previous work to

assess treatment success. In the $CD4^{WT}$ group, the success rate was 7 out of 9 mice, whereas in the $CD4^{\Delta IL18R1}$ group, response to anti-PD-1 was abrogated in 7 out of 8 mice (odds ratio=24.5, **Figure 6C**). Since absence of IL-18R1 expression in T cells abrogated the response to anti-PD-1, we next asked if adjuvant treatment with IL-18 could potentiate the efficacy of anti-PD-1 in our model. To this end, we administered 5 daily doses of 0.2μg of recombinant mouse IL-18, starting at day 8 (34, 55) to mice treated with anti-PD-1 thrice weekly. However, in line with previous reports (32), exogenous IL-18 did not increase the previously observed 50% success rate of anti-PD-1 in YUMMER1.7 tumors (2 out of 5 mice, p=0.83) (**Supplementary Figure 5A)**.

In line with the failed response to anti-PD-1, tumors in the $CD4^{\Delta IL18R1}$ group displayed a "colder" immune phenotype with reduced $CD8^+$ and $CD4^+$ TIL frequencies compared to WT tumors (**Supplementary Figure 5B**), and a predominance of macrophages with reduced MHC-II and PD-L1 expression (**Supplementary Figure 5C-D**). Furthermore, while $CD4^{WT}$ TILs displayed polyfunctional ($IFN\gamma^+$ $TNF\alpha^+$) $CD8^+$ TILs, $CD8^+$ TILs from $CD4^{\Delta IL18R1}$ mice had a dysfunctional phenotype, evidenced by the absence of $TNF\alpha^+$ and $CD107a^+$ cells, the reduced MFI of IFNγ (**Figure 6D**), and the increased levels of PD-1 expression (**Supplementary Figure 5E**) compared to their WT counterparts. In parallel, cytokine-secretion capacity was also impaired in the $CD4^+$ T_{conv} compartment of $CD4^{\Delta IL18R1}$ TILs (**Figure 6E**), correlating strongly with increased tumor weight (r=-0.75) and reduced expression of MHC-II by dendritic cells (r=0.92) (**Supplementary Figure 5F**). In the $CD4^{\Delta IL18R1}$ group, T_{reg} cells outnumbered T_h1 cells, in stark contrast with the $CD4^{WT}$ group (mean T_h1:T_{reg}= 0.4 vs 4.44, **Figure 6E**). Taken together, these data indicate that the direct effect of IL-18 on T cells plays a crucial role in the success of anti-PD-1 therapy.

IL-18 is required for the acquisition of a T_h1-like phenotype by T_{reg} cells in response to anti-PD-1.

While anti-PD-1 increases T_{reg} cell activation, evasion from suppression is not observed in poorly responsive TMEs (Attias *et al.*, manuscript submitted). Thus, we asked if T cell responses to IL-18 were required for the induction of permissive IFNγ$^+$ T_{reg} cells in response to anti-PD-1. Tumors in the WT group displayed an abundance of Helios$^+$ T_{reg} cells with high levels of CD25 and CTLA-4 expression (MFI), but these markers were significantly reduced in their CD4$^{\Delta IL18R1}$ counterparts (**Figure 7A**). Furthermore, the proportion and level of expression of T-bet was reduced in T_{reg} TILs from the CD4$^{\Delta IL18R1}$ group (**Figure 7B**). Correspondingly, while IFNγ$^+$ and TNFα$^+$ T_{reg} cells were readily observed in the CD4^{WT} group, their frequency was reduced in the CD4$^{\Delta IL18R1}$ group, as was their level of expression of IFNγ and TNFα (MFI) (**Figure 7C**).

Given the potent T_h1 responses observed *in vivo*, we then asked if T_{reg} cells isolated from tumors that responded to PD-1 blockade were capable of suppressing IFNγ production when re-stimulated outside of the TME. To this end, we purified T_{reg} TILs and splenocytes isolated from anti-PD-1 treated Low Responder and High Responder YUMMER1.7-bearing Foxp3^{RFP} mice at tumor endpoint, and cultured them with splenic CD4$^+$ T_{resp} cells, accessory cells ($1x10^5$), and recombinant murine IL-12 (10ng/ml). T_{reg} cells isolated from tumors successfully responding to PD-1 blockade displayed the most potent capacity to suppress IFNγ production and T-bet upregulation (**Figure 7D**), suggesting that an additional factor is required to enable T_{eff} evasion from their suppression *in vivo*. Taken together, these data indicate that IL-18 plays a crucial role in the establishment of a hot tumor microenvironment and the control of the T_{reg}:T_{eff} balance within tumors. In turn, this promotes the T_h1-adaptation of T_{reg} cells and alleviates their suppression of IFNγ production, thus enabling a successful response to anti-PD-1.

Discussion

The degree of inflammation in the TME is the result of the recruitment of TILs and the competitive balance between the anti-tumor effector and regulatory cells, and the respective cytokines they release in the local environment (3, 57), and is one of the main determinants of the success of tumor immunotherapy (58). Amongst the abundant factors involved in modulating immune responses, IL-18 contributes to anti-tumor immunity by inducing IFNγ production in $CD8^+$ and $CD4^+$ T_{eff} cells (27) but was also shown to contribute to T cell exhaustion (34). As such, its role in determining the functional fate of TILs and promoting a successful response to anti-PD-1 blockade remains to be determined. Here, we dissected the role of IL-18 on the growth and immune phenotype of the highly immunogenic YUMMER1.7 murine melanoma (37) in mice with a T cell-specific conditional deletion of the IL18R1 ($CD4^{\Delta IL18R1}$). We uncovered that preventing IL-18 signaling in T cells not only limits TIL accumulation, but also alters the phenotype of tumor-associated macrophages and dendritic cells towards a more tolerogenic profile, positioning IL-18 as a key determinant of "hot" versus "cold" melanoma phenotype.

Collectively these results provide new insights on how IL-18 shapes the T_{reg}:T_{eff} balance in TMEs to promote a stronger anti-tumor T_h1 response. While $CD4^+$ and $CD8^+$ T cell frequencies were reduced in $CD4^{\Delta IL18R1}$ mice, we did not observe a difference in the proportion of cycling ($Ki67^+$) $CD4^+$ and $CD8^+$ TILs, suggesting that dysfunctional TIL subsets can proliferate in the TME. However, although IL-18 favors T_h1 over T_{reg} cells in the TME, it is not required for the T_h1-differentiation of $CD4^+$ TILs. Indeed, while the STAT4-dependent IL-12 signal is key to the acquisition of the T_h1 master transcription factor T-bet (59), IL-18 increases their production of IFNy and their survival (46), thus preferentially promoting the expansion of $IFN\gamma^+$ T_h1 and $CD8^+$ T cells. Similarly, IL-12 is the main driver of the T_h1-like adaptation of T_{reg} cells (60) and induces

their expression of IL18R1 in the process (24). T-bet expression promotes the proliferation of tissue-infiltrating T_{reg} cells during type 1 immune responses (61) and allows them to suppress TILs by enabling their co-localization through CXCR3 expression (19, 62). In line with these observations, we demonstrate that, in the absence of IL-18 signaling, T_{reg} TILs are potent suppressors of T_h1-polarization and IFNγ production. However, while IL-18R is not required for the acquisition of T-bet by T_{reg} TILs, it potentiates its expression to levels that allow for IFNγ production *in vitro*, and in response to anti-PD-1 *in vivo*, leading T_{eff} cells to evade T_{reg} cell suppression in both experimental conditions, a mechanism conserved in Influenza A Virus infection (24). Thus, while IL-18 promotes the evasion of IFNγ$^+$ T_{eff} cells from T_{reg} cell-mediated suppression, further investigation is warranted regarding the role of IL-18 on T_{reg} cell functional fate specifically. Indeed, while IFNγ production by T_{reg} TILs is associated with increased anti-tumor responses (37, 38, Attias et al. manuscript submitted), it remains to be determined if it compromises T_{reg} cell suppressive function (49).

Our finding that T cell response to IL-18 shifts the immune phenotype in the TME and is required for a successful response to PD-1 blockade has important therapeutic and translational implications. The scarcity of functional TILs prior to treatment is one of the principal mechanisms of primary resistance to treatment with ICIs (63). Thus, increasing the level of inflammation in the tumor to promote a “hot” immune phenotype represents an attractive target for the development of adjuvant treatment strategies (6, 64). Here, we show that IL-18 not only increases TIL accumulation, but in doing so, reinforces the M1-polarization of tumor-associated macrophages and the expression of co-stimulatory molecules by dendritic cells, presumably through reinforcing IFNγ signaling locally (65). Indeed, IL-18 has been shown to potentiate the efficacy of ICIs in various preclinical models (31). Here, we observed that PD-1 expression levels were reduced in

IL-18R-expressing T_{conv}, T_{reg} and $CD8^+$ TILs, in line with the increased local availability of IL-2 (66) and the role of functional T_h1 cells in preventing terminal-exhaustion (9). However, these results contrast with a report, using a model of adoptive $CD8^+$ T cells transfer, stating that IL-18 promotes PD-1 expression on T cells and their subsequent exhaustion (35). While our model encompasses the entire T cell compartment, this report focused on monoclonal $CD8^+$ T cells whose function is partially directed by local T_h1 and T_{reg} cell responses. Indeed, in the absence of sufficient T_h1 cytokines, IL-18 has pro-tumorigenic effects by notably inducing NK cell exhaustion (34), promoting the differentiation of myeloid-derived suppressor cells in the bone marrow (39, 40), and facilitating metastatic dissemination of melanoma by modulating their expression of adhesion molecules (67). Furthermore, IFNγ promotes the release of its decoy receptor IL-18BP (68), which constitutes an inhibitory feedback loop on IL-18 signaling. As such, IL-18 has failed to provide significant clinical benefits in clinical trials (69). In line with previous findings (32), we did not observe any potentiation of the efficacy of anti-PD-1 by IL-18 in our model. This could be due to pharmacokinetic considerations, as some of the pro and anti-tumor effects of IL-18 can be attributed to the dosing and administration scheme (34, 39). Finally, elevated serum levels of IL-18 are associated with worse prognosis (70) and poor response to ICI (71), highlighting that the systemic impacts of IL-18, distally from the TME, might impair the efficacy of IL-18 therapy. Thus, further investigation into the kinetics of IL-18 secretion is warranted to better understand the temporal role of IL-18 in promoting T_h1 responses in the tumor and guide the development of therapeutic strategies. Development of a decoy-resistant variant of IL-18 has shown promising results in potentiating the efficacy of anti-PD-1 in various preclinical models (32). Furthermore, strategies to target IL-18 delivery specifically towards TILs could be envisaged to limit systemic toxicities and enhance the specificity of IL-18 towards T cells.

Taken together, we show that IL-18 plays a critical role in governing the T_{eff}:T_{reg} balance, promoting the expansion of functional T_h1 cells in TMEs and their evasion from T_{reg} cell suppressive function. Furthermore, IL-18 promotes IFNγ secretion by T_{reg} TILs, a phenotype associated with successful response to PD-1 blockade. Thus, therapeutic strategies targeting IL-18 signaling and T_{reg} cell adaptation provides an interesting therapeutic avenue to increase response rates to anti-PD-1.

Figures

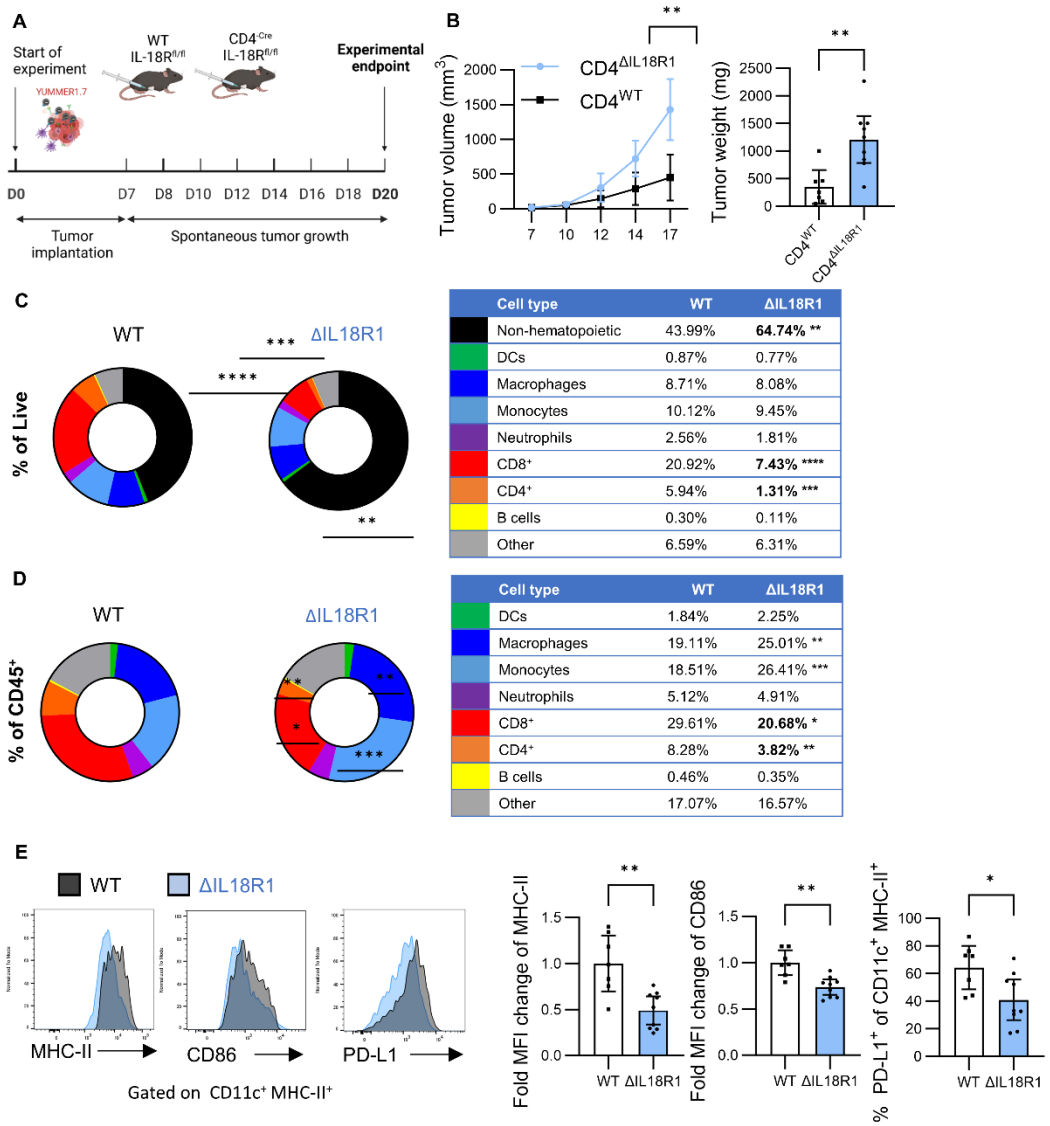

Cell type	WT	ΔIL18R1
Non-hematopoietic	43.99%	**64.74%** **
DCs	0.87%	0.77%
Macrophages	8.71%	8.08%
Monocytes	10.12%	9.45%
Neutrophils	2.56%	1.81%
CD8+	20.92%	**7.43%** ****
CD4+	5.94%	**1.31%** ***
B cells	0.30%	0.11%
Other	6.59%	6.31%

Cell type	WT	ΔIL18R1
DCs	1.84%	2.25%
Macrophages	19.11%	25.01% **
Monocytes	18.51%	26.41% ***
Neutrophils	5.12%	4.91%
CD8+	29.61%	**20.68%** *
CD4+	8.28%	**3.82%** **
B cells	0.46%	0.35%
Other	17.07%	16.57%

Figure 1. IL-18 signaling in T cells delays tumor growth and contributes to the establishment of a hot tumor microenvironment.

A. Schematic of the experimental design. 8–12-week-old, age-matched CD4-Cre IL-18R1$^{fl/fl}$ (CD4$^{\Delta IL18R1}$, n=9) and IL-18R1$^{fl/fl}$ (CD4^{WT}, n=7) mice were inoculated with 2.5x10^5 YUMMER1.7 cells in 50% Matrigel and were sacrificed as soon as the first mouse in the experiment reached humane endpoint (tumor volume>1500mm^3). Data collated from N=2 independent experiments.

B. Tumor growth curves and tumor weight at endpoint. Tumor volumes were measured thrice weekly using an electronic calliper. Data resented as mean and 95% confidence interval. Tumor volumes were compared using a Two-Way ANOVA with Sidak's correction. Tumor weights were compared using Welch's t-test.

C-D. Flow cytometry analysis of proportions of $CD45^-$ (black), $CD11c^+$ $MHC\text{-}II^+$ dendritic cells (green), $CD11b^+$ $F4/80^+$ Macrophages (dark blue), $CD11b^+$ $F4/80^-$ $Ly6C^+$ Monocytes (blue), $CD11b^+$ $Ly6G^+$ Neutrophils (purple), $CD8^+$ (red), $CD4^+$ (orange), $CD19^+$ B cells (yellow), and other cells (grey) of live (C) or live $CD45^+$ (D) cells. Data represented as parts of whole. All means were compared using One-Way ANOVA with Welch's correction.

E. Representative flow plots of MHC-II, CD86 and PD-L1 expression by $CD11c^+$ $MHC\text{-}II^+$ dendritic cells from $CD4^{WT}$ (black) and $CD4^{\Delta IL\text{-}18R1}$ (blue) TILs.

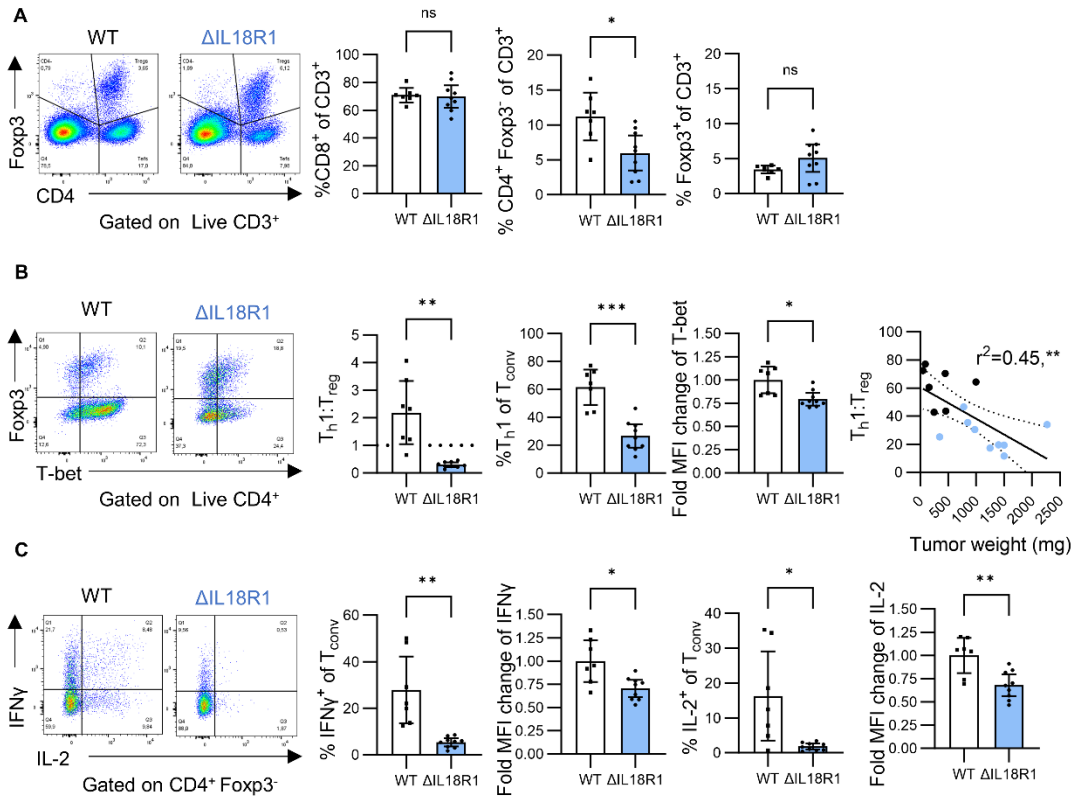

Figure 2. Functional T_h1 cells accumulate in the TME in response to IL-18.

A. Flow cytometry analysis of CD8, CD4 and Foxp3 expression by $CD3^+$ TILs. Data represented as representative flow plots and mean and 95% CI. Means were compared using Welch's t-test.

B. Flow cytometry analysis of Foxp3 and T-bet expression by $CD4^+$ TILs. Data represented as representative flow plots and mean and 95% CI. T_h1:T_{reg} ratios were calculated by dividing the proportion of $CD4^+$ T-bet$^+$ T_h1 cells by the proportion of $CD4^+$ $Foxp3^+$ T_{reg} cells. Fold MFI changes were calculated by dividing each individual measurement by the average MFI in the $CD4^{WT}$ group for its respective experiment. Means were compared using Welch's t-test. All data points were pooled to calculate a linear correlation, $CD4^{WT}$ points are colored in black and $CD4^{\Delta IL\text{-}18R1}$ are in light blue. The slope's deviation from zero was evaluated using Fisher's test.

C. Flow cytometry analysis and representative flow plots of IFN and IL-2 expression by $CD4^+$ $Foxp3^-$ TILs. Single cell suspensions were stimulated in the presence of PMA, Ionomycin and

GolgiStop® for 3h then stained for flow cytometry analysis. Means were compared using Welch's t-test. Data represented as representative flow plots and means with 95%CI.

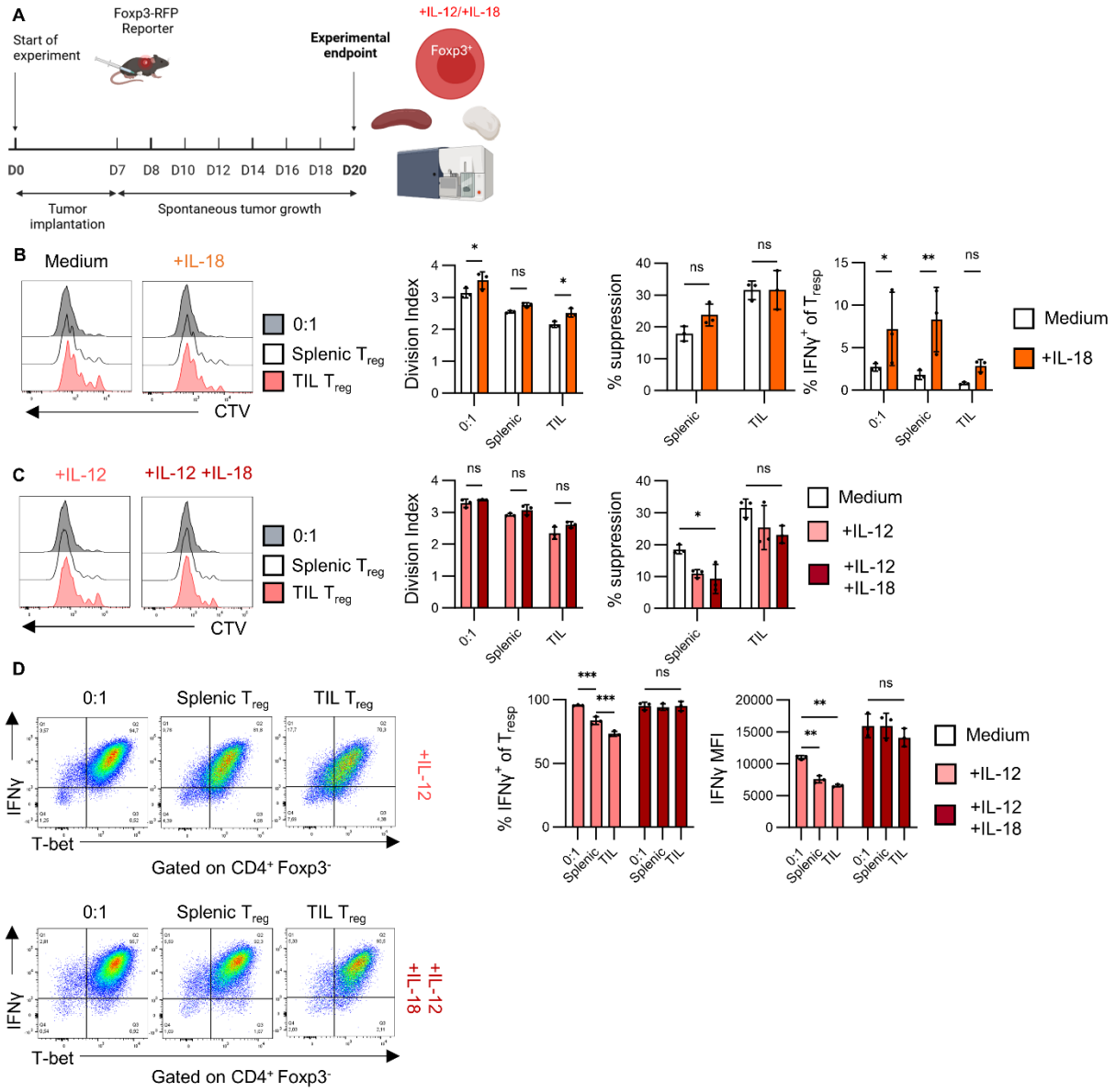

Figure 3. IL-18 impairs T_{reg} cell-mediated suppression of IFNγ production *in vitro*.

A. Schematic of the experimental workflow. 8–12-week-old Foxp3$^{-mIRES-RFP}$ reporter mice were inoculated with 2.5x10^5 YUMMER1.7 cells in 50% Matrigel and were sacrificed as soon as the first mouse in the experiment reached humane endpoint (tumor volume>1500mm^3). TILs and splenocytes were pooled from n=2 mice bearing endpoint tumors (N=2).

B-C. CTV-labelled $CD4^+$ Foxp3-RFP^- T_{resp} cells ($5x10^4$) were co-cultured with either splenic or TIL $CD4^+$ Foxp3-RFP^+ T_{reg} cells ($1.25x10^4$) in the presence of mitomycin-C inactivated accessory cells ($1x10^5$), soluble anti-CD3 (0.5µg/ml), with or without recombinant murine IL-12 (10ng/ml) and/or IL-18 (10ng/ml) for 72h. After 69h, cells were additionally stimulated with PMA, Ionomycin, and Golgi Stop for assessment of cytokine production. % suppression measurements were derived from the division indexes for their respective culture conditions.

D. Flow cytometry analysis of IFNγ and T-bet expression by T_{resp} cells. Data shown as representative flow plots and mean +/-95%CI and compared using a Two-Way ANOVA with Tukey's correction. Data shown from one representative experiment of N=2 independent repeats.

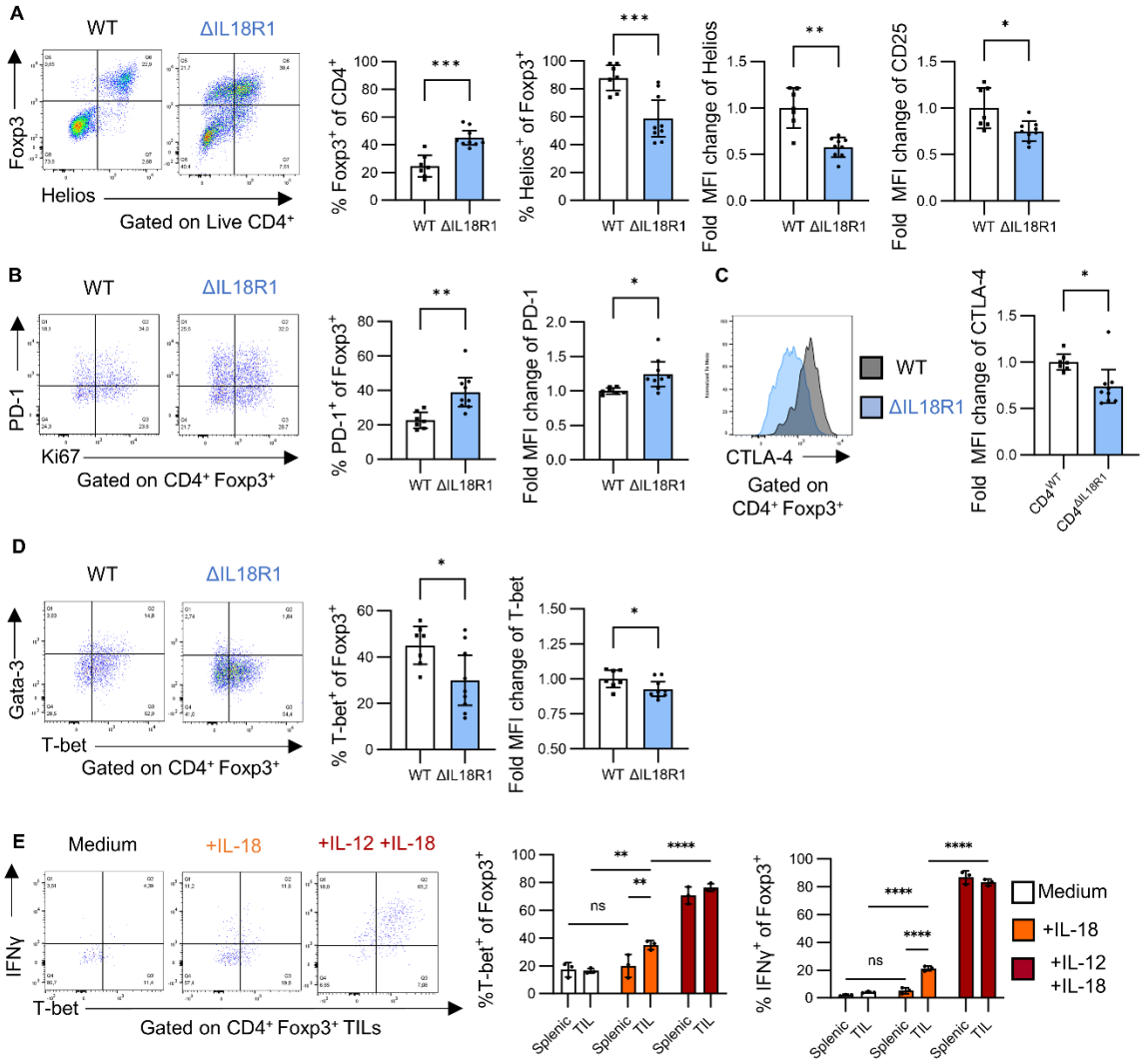

Figure 4. T cell responses to IL-18 promote T-bet expression by melanoma-infiltrating T_{reg} cells.

A. Flow cytometry analysis of Foxp3 and Helios expression by $CD4^+$ TILs. Data represented as representative flow plots and mean and 95% CI. Means were compared using Welch's t-test.

B. Flow cytometry analysis of PD-1 and Ki67 expression by $CD4^+$ $Foxp3^+$ TILs. Fold changes were calculated by dividing each data point by the average in the WT group for the respective experiment. Data represented as representative flow plots and mean and 95% CI. Means were compared using Welch's t-test. **C.** Flow cytometry analysis of CTLA-4 expression by $CD4^+$ $Foxp3^+$

TILs. Data represented as representative flow plots from $CD4^{WT}$ (black) and $CD4^{\Delta IL\text{-}18R1}$ (light blue) and mean and 95% CI. Means were compared using Welch's t-test.

D. Flow cytometry analysis of T-bet and Gata-3 expression by $CD4^{+}$ $Foxp3^{+}$ TILs. Data represented as representative flow plots and mean and 95% CI. Means were compared using Welch's t-test.

E. Foxp3-RFP^{+} T_{reg} cells were isolated and pooled from n=2 YUMMER1.7-bearing mice and co-cultured as previously described in Figure 3. Flow cytometry analysis of IFNγ and T-bet expression by T_{reg} cells. Data shown as representative flow plots and mean with 95%CI and compared using a Two-Way ANOVA with Tukey's correction. Data shown from one representative experiment of N=2 independent repeats.

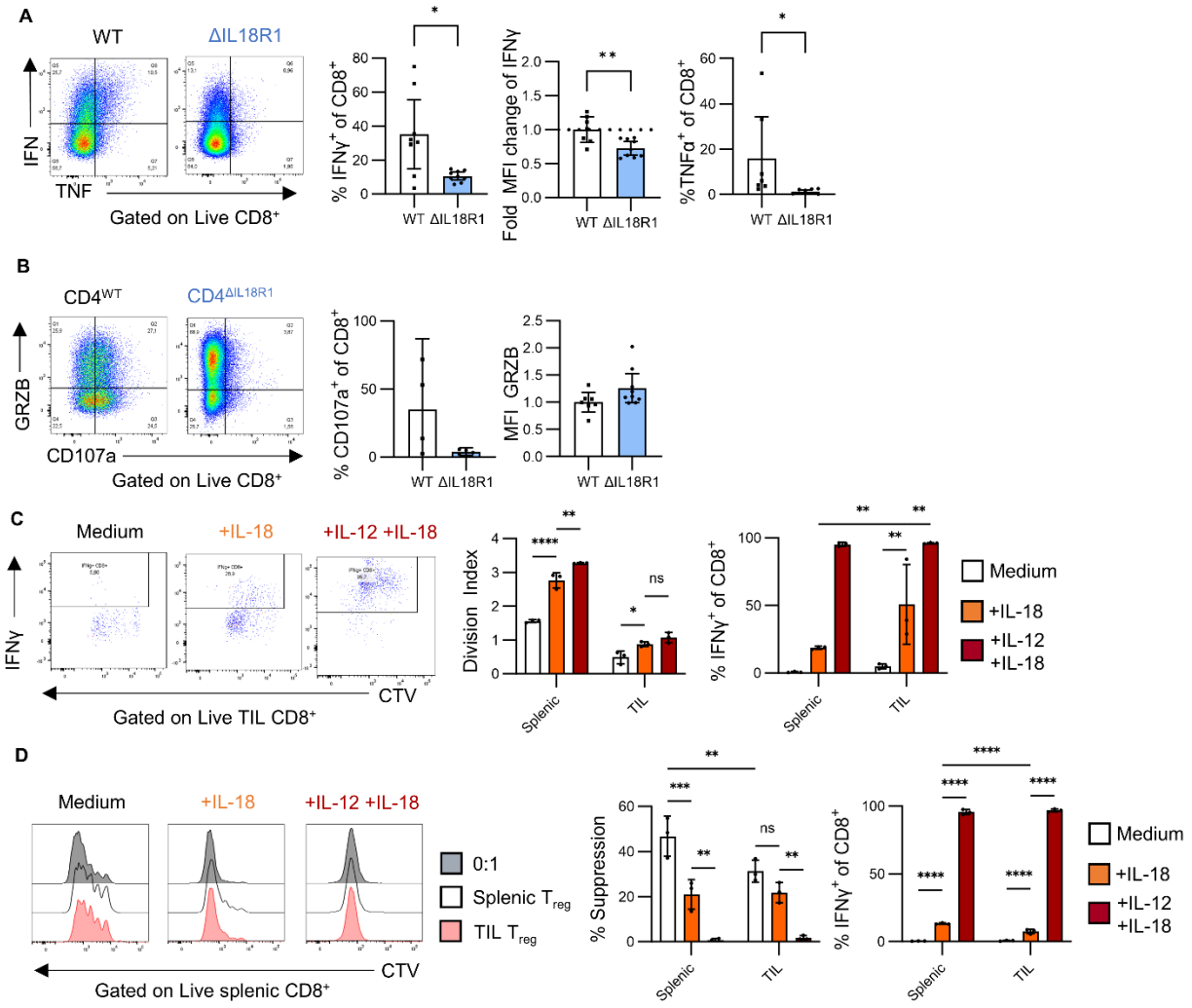

Figure 5. IL-18 promotes the expansion and effector functions of CD8$^+$ TILs.

A-B. Flow cytometry analysis and representative flow plots of IFNγ, TNFα, CD107a and GRZB expression by CD8$^+$ TILs. Single cell suspensions were stimulated in the presence of PMA, Ionomycin and GolgiStop for 3h then stained for flow cytometry analysis Fold MFI changes were calculated by dividing each individual measurement by the average MFI in the CD4^{WT} group for its respective experiment. Means were compared using Welch's t-test. Data represented as representative flow plots and means with 95%CI.

C. $CD8^+$ TILs were isolated and pooled from n=2 YUMMER1.7-bearing mice. $CD8^+$ TILs were CTV-labelled and cultured ($5x10^4$) with or without recombinant murine IL-18 (10ng/ml) and IL-12 (10ng/ml) in the presence of accessory cells ($1x10^5$) and anti-CD3 (0.5µg/ml) for 72h. After 69h, cells were additionally stimulated with PMA, Ionomycin, and Golgi Stop for assessment of cytokine production. Flow cytometry analysis of CTV and IFNγ expression by $CD8^+$ TILs. Flow cytometry data shown as representative flow plots and mean with 95%CI and compared using a Two-Way ANOVA with Tukey's correction. Data shown from one representative experiment of N=2 independent repeats.

D. $CD8^+$ splenocytes and $CD4^+$ Foxp3-RFP^+ T_{reg} cells were isolated and pooled from n=2 YUMMER1.7-bearing mice. $CD8^+$ T_{resp} cells ($5x10^4$) were co-cultured with splenic or TIL T_{reg} cells ($1.25x10^4$) with or without recombinant murine IL-18 (10ng/ml) and IL-12 (10ng/ml) in the presence of accessory cells ($1x10^5$) and anti-CD3 (0.5µg/ml) for 72h. After 69h, cells were additionally stimulated with PMA, Ionomycin, and Golgi Stop for assessment of cytokine production. Flow cytometry analysis of CTV and IFNγ expression. Flow cytometry data shown as representative flow plots and mean with 95%CI and compared using a Two-Way ANOVA with Tukey's correction. Data shown from one representative experiment of N=2 independent repeats.

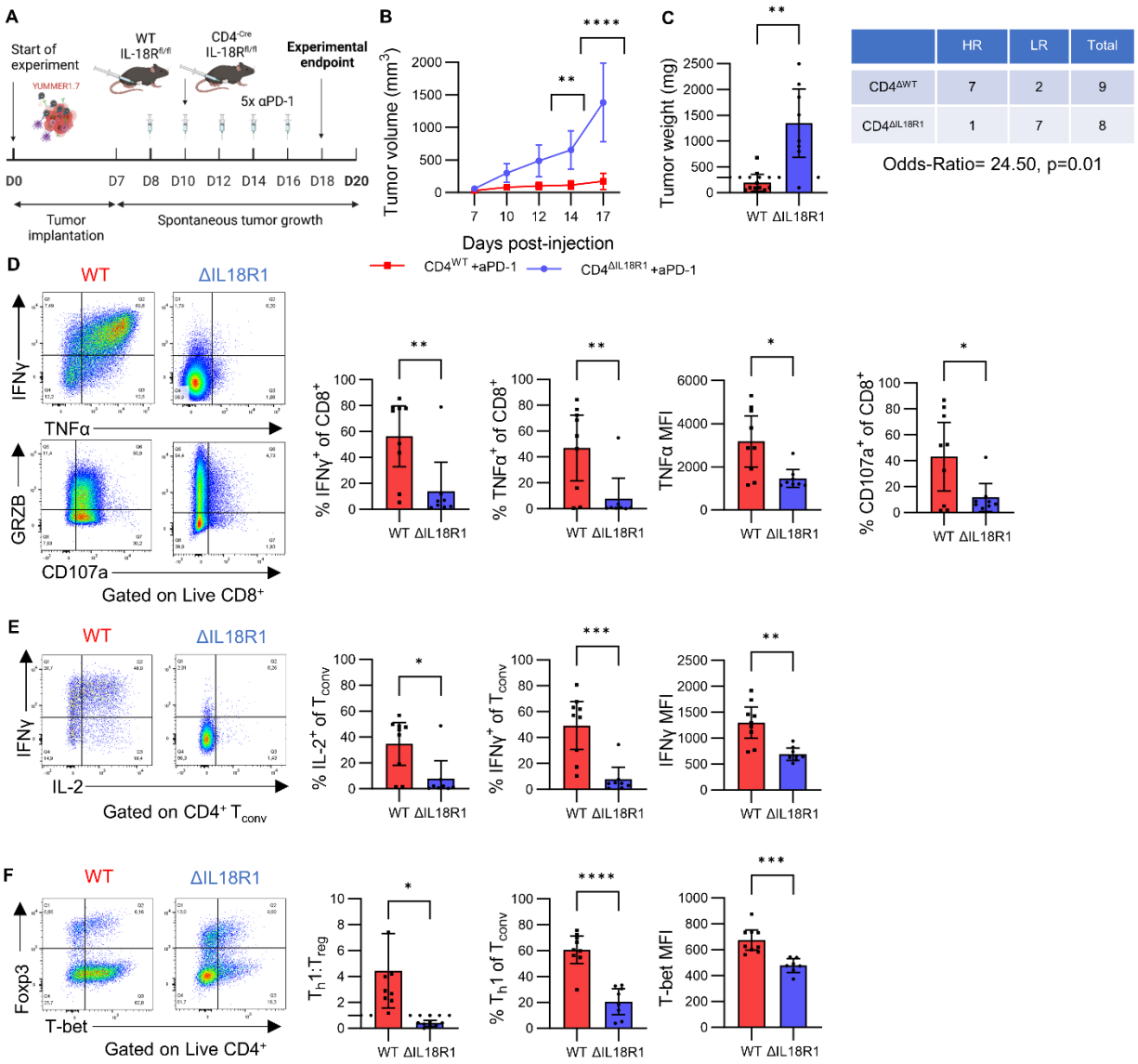

	HR	LR	Total
CD4ΔWT	7	2	9
CD4ΔIL18R1	1	7	8

Figure 6. Successful response to anti-PD-1 is dependent on IL-18 signaling in T cells.

A. Schematic of the experimental design. 8–12-week-old, age-matched $CD4^{WT}$ (n=9) and $CD4^{\Delta IL18R1}$ (n=8) mice were inoculated with $2.5x10^5$ YUMMER1.7 cells in 50% Matrigel. On day 8, treatment with 250µg of anti-PD-1 (clone RMP1-14) was initiated for each mouse. Mice were sacrificed as soon as the first mouse in the experiment reached humane endpoint (tumor volume>1500mm^3). Data collated from N=2 independent experiments.

B. Tumor volumes were measured thrice weekly using an electronic calliper. Data resented as mean and 95% CI and compared using a Two-Way ANOVA with Sidak's correction.

C. Tumor weights were measured post-necropsy and represented as mean and 95% CI. As we determined previously that treatment with anti-PD-1 results in a bimodal outcome, with Low Responders being phenotypically not distinguishable from PBS controls, we forewent the control group and compared the ratio of High Responders in each group using Fisher's test.

D. Flow cytometry analysis and representative flow plots of IFNγ, TNFα, CD107a and GRZB expression by $CD8^+$ TILs. Single cell suspensions were stimulated in the presence of PMA, Ionomycin and GolgiStop for 3h then stained for flow cytometry analysis. Means were compared using Welch's t-test. Data represented as representative flow plots and means with 95%CI.

E. Flow cytometry analysis and representative flow plots of IFN and IL-2 expression by $CD4^+$ $Foxp3^-$ TILs. Single cell suspensions were stimulated in the presence of PMA, Ionomycin and GolgiStop for 3h then stained for flow cytometry analysis. Means were compared using Welch's t-test. Data represented as representative flow plots and means with 95%CI.

F. Flow cytometry analysis of Foxp3 and T-bet expression by $CD4^+$ TILs. Data represented as representative flow plots and mean and 95% CI. Means were compared using Welch's t-test. For MFI comparisons, all samples were stained with the exact same antibody panels and lots and acquired using the same application settings following voltage calibration.

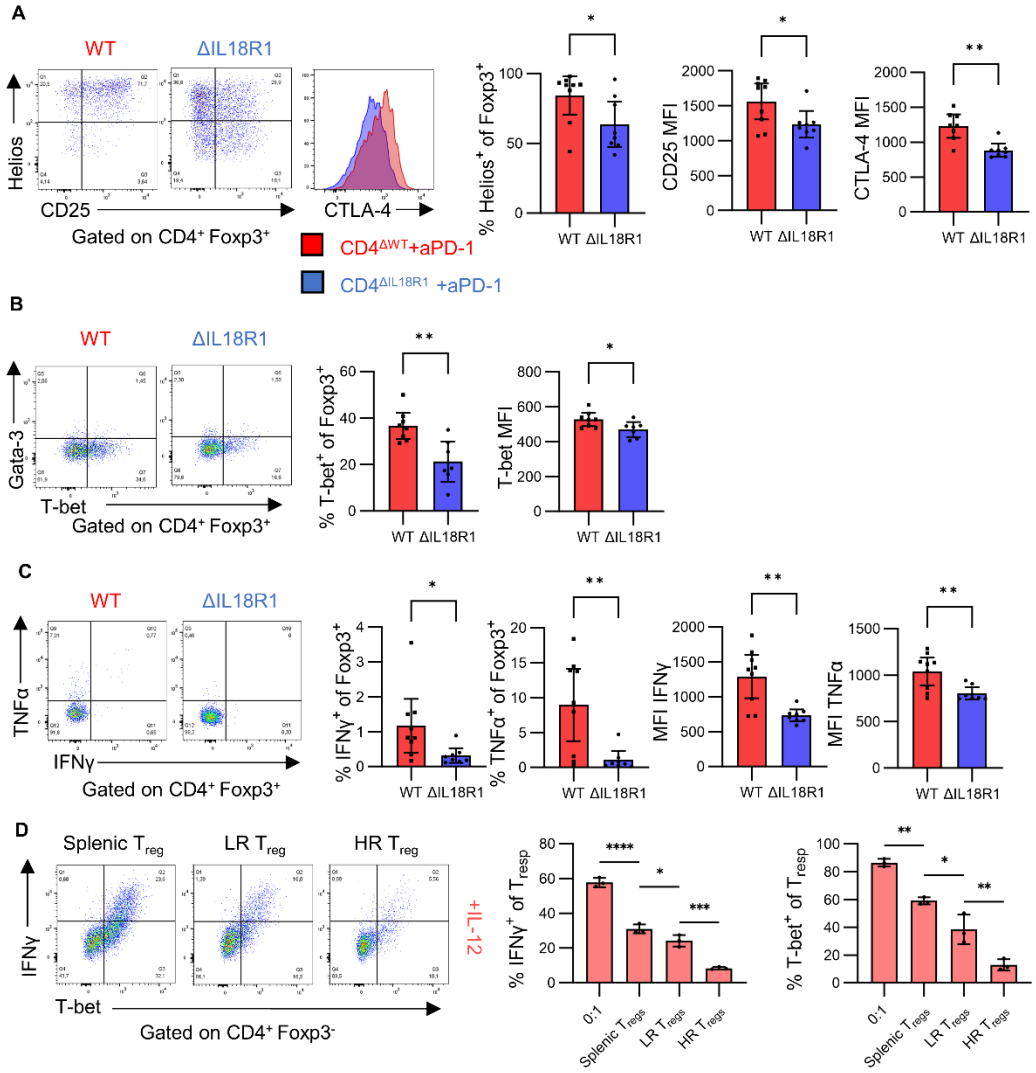

Figure 7. IL-18 is required for the acquisition of a T_h1-like phenotype by T_{reg} cells in response to anti-PD-1.

A. Flow cytometry analysis of Helios, CD25, and CTLA-4 expression by $CD4^+$ $Foxp3^+$TILs. Data represented as representative flow plots and mean and 95% CI. Means were compared using Welch's t-test.

B. Flow cytometry analysis of T-bet expression by $CD4^+$ $Foxp3^+$TILs. Data represented as representative flow plots and mean and 95% CI. Means were compared using Welch's t-test.

C. Flow cytometry analysis of T-bet, IL-10, IL-2 and TNFα production by $CD4^+$ $Foxp3^+$ TILs. Single cell suspensions were stimulated in the presence of PMA, Ionomycin and GolgiStop for 3h then stained for flow cytometry analysis. Means were compared using Welch's t-test. Data represented as representative flow plots and means with 95%CI. For MFI comparisons, all samples were stained with the exact same antibody panels and lots and acquired using the same application settings following voltage calibration.

D. $CD4^+$ Foxp3-RFP^+ T_{reg} TILs and splenocytes were isolated and pooled from n=2 YUMMER1.7-bearing High Responder (tumor weight<300mg) and n=2 Low Responder (tumor weight>300mg) to anti-PD-1 mice. $CD4^+$ Foxp3-RFP^- T_{resp} cells ($5x10^4$) were co-cultured with splenic or TIL T_{reg} cells ($1.25x10^4$) with or without recombinant murine IL-12 (10ng/ml) in the presence of accessory cells ($1x10^5$) and anti-CD3 (0.5µg/ml) for 72h. After 69h, cells were additionally stimulated with PMA, Ionomycin, and Golgi Stop for assessment of cytokine production. Flow cytometry analysis of CTV and IFNγ expression by T_{resp} cells. Flow cytometry data shown as representative flow plots and mean with 95%CI and compared using a Two-Way ANOVA with Tukey's correction. Data shown from one representative experiment of N=2 independent repeats.

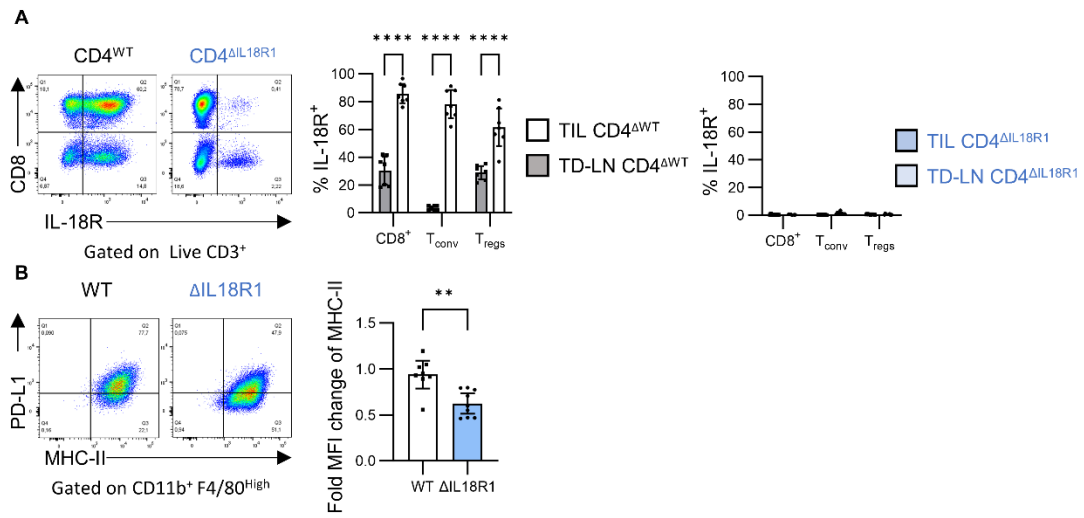

Supplementary Figure 1.

A. Flow cytometry analysis of IL-18R1 expression by TILs and T cells from the tumor-draining lymph nodes. Data represented as representative flow plots and mean and 95% CI. Means were compared using Sidak's multiple comparisons test.

B. Flow cytometry analysis of PD-L1 and MHC-II by CD11b^{+} F4/80^{High} tumor-associated macrophages. Data represented as representative flow plots and mean and 95% CI. Means were compared using Welch's t-test.

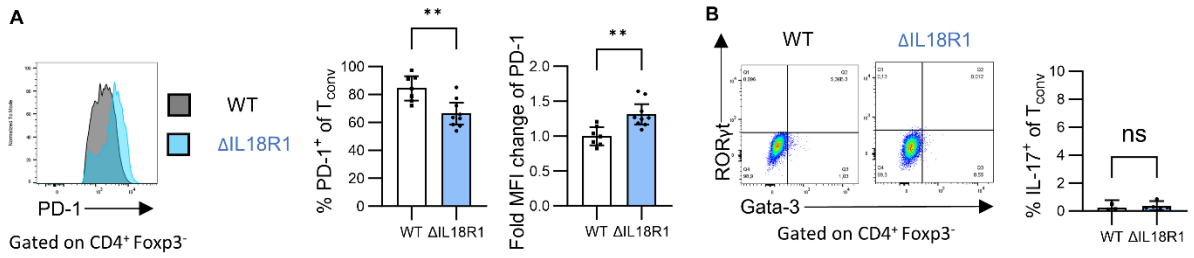

Supplementary Figure 2.

A. Flow cytometry analysis of PD-1 expression by $CD4^+$ $Foxp3^+$ TILs. Data represented as representative flow plots and mean and 95% CI. Means were compared using Welch's t-test. Fold MFI changes in PD-1 expression were calculated by dividing each measurement by the average PD-1 MFI in the WT group for a given experiment.

B. Flow cytometry analysis of RORγt, Gata-3 and IL-17 by $CD4^+$ $Foxp3^-$ TILs. Data represented as representative flow plots and mean and 95% CI. Means were compared using Welch's t-test.

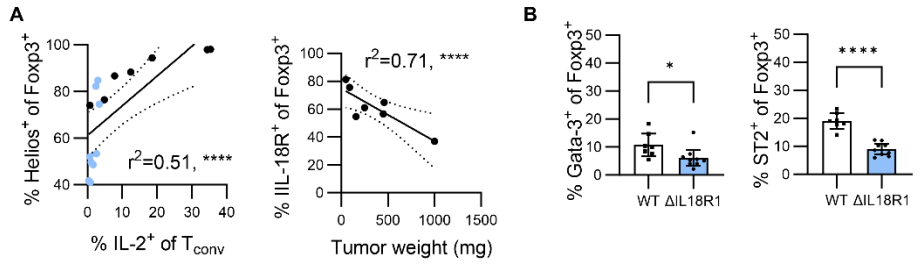

Supplementary Figure 3.

A. Flow cytometry analysis of Helios, IL-2 and IL-18R expression. All data points were pooled to calculate a linear correlation, $CD4^{WT}$ points are colored in black and $CD4^{\Delta IL\text{-}18R1}$ are in light blue. The slope's deviation from zero was evaluated using Fisher's test.

B. Flow cytometry analysis of Gata-3 and ST2 expression by $CD4^{+}$ $Foxp3^{+}$ TILs. Data represented as mean and 95% CI. Means were compared using Welch's t-test.

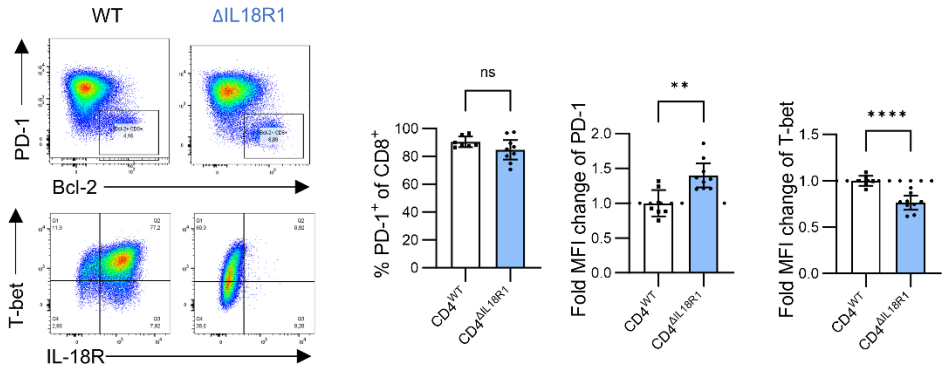

Supplementary Figure 4.

Flow cytometry analysis of PD-1, T-bet and IL-18R1 expression by $CD8^+$ TILs. Data shown as representative flow plots and mean with 95% CI. Fold MFI changes in PD-1 expression were calculated by dividing each measurement by the average PD-1 MFI in the WT group for a given experiment. Means were compared using Welch's t-test.

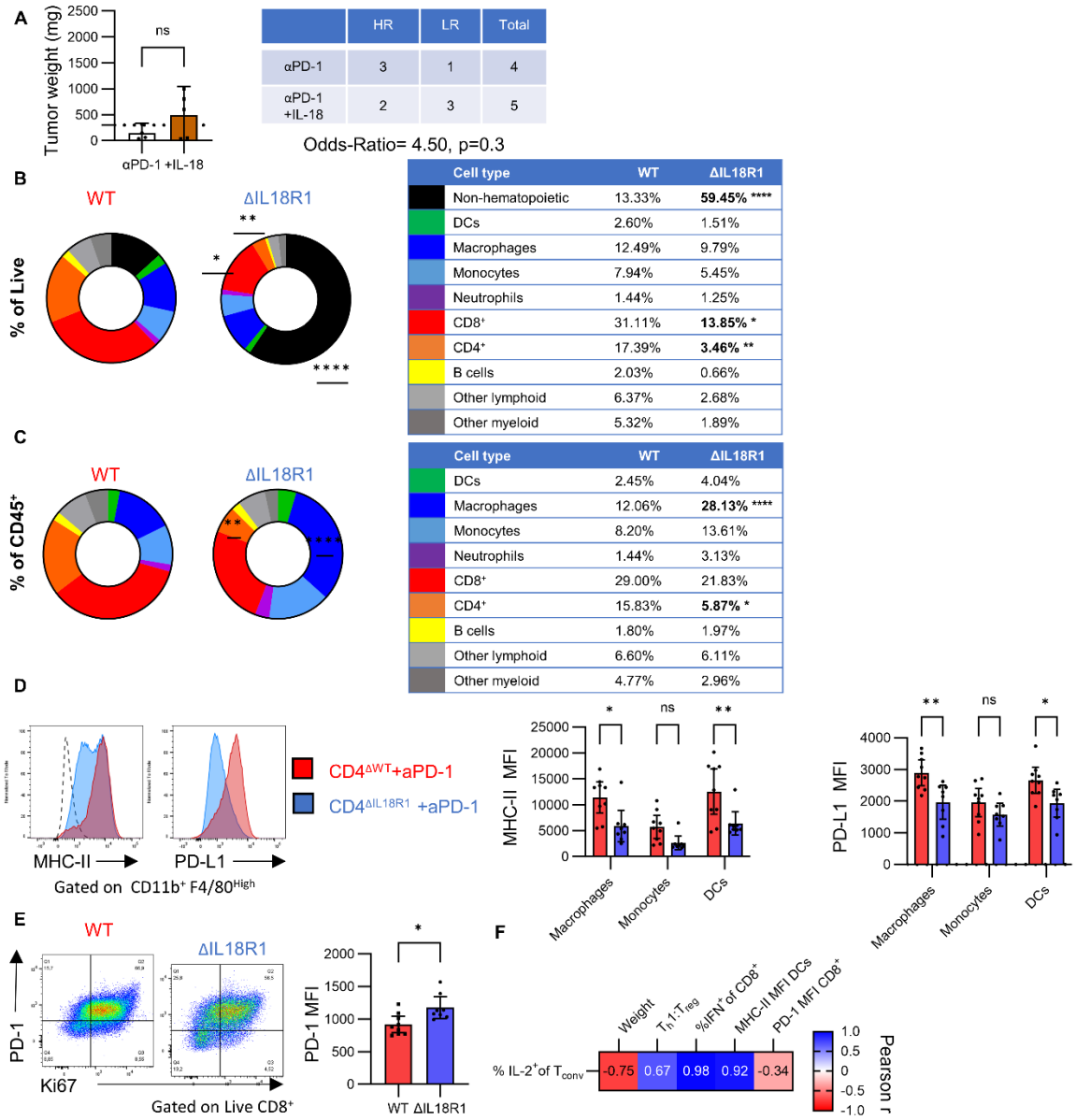

Supplementary Figure 5.

A. Male Foxp3^{RFP} reporter mice were inoculated with 2.5x10^5 YUMMER1.7 cells in 50% Matrigel and received 5 doses of 250µg of anti-PD-1, starting on day 8 post tumor-inoculation. Starting on day 8, we also administered 5 daily doses of 0.2µg of recombinant mouse IL-18 (n=5) or PBS (n=4). Mice were sacrificed as soon as the first mouse in the experiment reached humane endpoint (tumor volume>1500mm^3). Tumor weights were measured post-necropsy and represented as mean and 95% CI. As we determined previously that treatment with anti-PD-1

results in a bimodal outcome, with Low Responders being phenotypically not distinguishable from PBS controls, we forewent the control group and compared the ratio of High Responders in each group using Fisher's test.

B-C. Flow cytometry analysis of proportions of $CD45^-$ (black), $CD11c^+$ $MHC\text{-}II^+$ dendritic cells (green), $CD11b^+$ $F4/80^+$ Macrophages (dark blue), $CD11b^+$ $F4/80^-$ $Ly6C^+$ Monocytes (blue), $CD11b^+$ $Ly6G^+$ Neutrophils (purple), $CD8^+$ (red), $CD4^+$ (orange), $CD19^+$ B cells (yellow), other lymphoid cells (grey) and other myeloid cells (dark grey) of live (C) or live CD45+ (D) cells. Data represented as parts of whole. All means were compared using One-Way ANOVA with Welch's correction.

D. Flow cytometry analysis of MHC-II and PD-L1 expression by tumor-associated macrophages, monocytes, and dendritic cells. Data shown as representative flow plots and mean with 95% CI. For MFI comparisons, all samples were stained with the exact same antibody panels and lots and acquired using the same application settings following voltage calibration. Means were compared using Sidak's multiple comparisons test.

E. Flow cytometry analysis of PD-1 expression by $CD8^+$ TILs. Data shown as representative flow plots and mean with 95% CI. Means were compared using Welch's t-test.

F. Frequency of IL-2^+ T_{conv},IFNγ^+ $CD8^+$, T_h1:T_{reg} ratio ($CD4^+$ $Foxp3^-$ T-bet^+/ $CD4^+$ $Foxp3^+$), MHCII-MFI in DCs and PD-1 MFI in $CD8^+$ T cells were measured at endpoint. Pearson r-correlates were computed for each pair of variables and represented as a heatmap.

References

1. Gajewski TF, et al. Cancer Immunotherapy Targets Based on Understanding the T Cell-Inflamed Versus Non-T Cell-Inflamed Tumor Microenvironment. In: Kalinski P, ed. *Tumor Immune Microenvironment in Cancer Progression and Cancer Therapy*. Cham: Springer International Publishing; 2017:19–31

2. Bonaventura P, et al. Cold Tumors: A Therapeutic Challenge for Immunotherapy. *Front Immunol*. 2019;10. https://doi.org/10.3389/fimmu.2019.00168

3. Binnewies M, et al. Understanding the tumor immune microenvironment (TIME) for effective therapy. *Nat Med*. 2018;24(5):541–550.

4. Lo JA. Regulation of the Inflamed Tumor Phenotype in Melanoma Immunotherapy:157.

5. Wang M, et al. Therapeutic strategies to remodel immunologically cold tumors. *Clinical & Translational Immunology*. 2020;9(12):e1226.

6. Liu Y-T, Sun Z-J. Turning cold tumors into hot tumors by improving T-cell infiltration. *Theranostics*. 2021;11(11):5365–5386.

7. Giermasz AS, et al. Type-1 polarized dendritic cells primed for high IL-12 production show enhanced activity as cancer vaccines. *Cancer Immunol Immunother*. 2009;58(8):1329–1336.

8. Mirlekar B, Pylayeva-Gupta Y. IL-12 Family Cytokines in Cancer and Immunotherapy. *Cancers*. 2021;13(2):167.

9. Ahrends T, et al. CD4+ T Cell Help Confers a Cytotoxic T Cell Effector Program Including Coinhibitory Receptor Downregulation and Increased Tissue Invasiveness. *Immunity*. 2017;47(5):848-861.e5.

10. Wimmers F, et al. Long-lasting multifunctional CD8+ T cell responses in end-stage melanoma patients can be induced by dendritic cell vaccination. *OncoImmunology*. 2016;5(1):e1067745.

11. Garcia-Diaz A, et al. Interferon Receptor Signaling Pathways Regulating PD-L1 and PD-L2 Expression. *Cell Rep*. 2017;19(6):1189–1201.

12. Wherry EJ, Kurachi M. Molecular and cellular insights into T cell exhaustion. *Nat Rev Immunol*. 2015;15(8):486–499.

13. Cao X, et al. Granzyme B and perforin are important for regulatory T cell-mediated suppression of tumor clearance. *Immunity*. 2007;27(4):635–46.

14. Tekguc M, et al. Treg-expressed CTLA-4 depletes CD80/CD86 by trogocytosis, releasing free PD-L1 on antigen-presenting cells. *Proc Natl Acad Sci U S A*. 2021;118(30):e2023739118.

15. Strauss L, et al. A unique subset of CD4+CD25highFoxp3+ T cells secreting interleukin-10 and transforming growth factor-beta1 mediates suppression in the tumor microenvironment. *Clin Cancer Res*. 2007;13(15 Pt 1):4345–54.

16. van Gulijk M, et al. PD-L1 checkpoint blockade promotes regulatory T cell activity that underlies therapy resistance. *Science Immunology*. 2023;8(83):eabn6173.

17. Kamada T, et al. PD-1+ regulatory T cells amplified by PD-1 blockade promote hyperprogression of cancer. *PNAS*. 2019;116(20):9999–10008.

18. Sugiyama D, et al. Anti-CCR4 mAb selectively depletes effector-type FoxP3+CD4+ regulatory T cells, evoking antitumor immune responses in humans. *PNAS*. 2013;110(44):17945–17950.

19. Redjimi N, et al. CXCR3+ T regulatory cells selectively accumulate in human ovarian carcinomas to limit type I immunity. *Cancer Res*. 2012;72(17):4351–4360.

20. Halvorsen EC, et al. IL-33 increases ST2+ Tregs and promotes metastatic tumour growth in the lungs in an amphiregulin-dependent manner. *Oncoimmunology*. 2018;8(2):e1527497.

21. Mair F, et al. Extricating human tumour immune alterations from tissue inflammation. *Nature*. 2022;605(7911):728–735.

22. Liu J, et al. Tumor-Associated Macrophages Recruit CCR6+ Regulatory T Cells and Promote the Development of Colorectal Cancer via Enhancing CCL20 Production in Mice. *PLOS ONE*. 2011;6(4):e19495.

23. Kohno K, et al. IFN-gamma-inducing factor (IGIF) is a costimulatory factor on the activation of Th1 but not Th2 cells and exerts its effect independently of IL-12. *J Immunol*. 1997;158(4):1541–1550.

24. Alvarez F, et al. IL-18 is required for the TH1-adaptation of TREG cells and the selective suppression of TH17 responses in acute and chronic infections. *Mucosal Immunol*. 2023;S1933-0219(23)00035–1.

25. Zuazo M, et al. Functional systemic CD4 immunity is required for clinical responses to PD-L1/PD-1 blockade therapy. *EMBO Molecular Medicine*. 2019;11(7):e10293.

26. Park H, et al. Enhanced IL-18 expression in common skin tumors. *Immunology Letters*. 2001;79(3):215–219.

27. Ahn HJ, et al. A mechanism underlying synergy between IL-12 and IFN-gamma-inducing factor in enhanced production of IFN-gamma. *The Journal of Immunology*. 1997;159(5):2125–2131.

28. Osaki T, et al. IFN-γ-Inducing Factor/IL-18 Administration Mediates IFN-γ- and IL-12-Independent Antitumor Effects1. *The Journal of Immunology*. 1998;160(4):1742–1749.

29. Coughlin CM, et al. Interleukin-12 and interleukin-18 synergistically induce murine tumor regression which involves inhibition of angiogenesis. *J Clin Invest*. 1998;101(6):1441–1452.

30. Cho D, et al. Endogenous Interleukin-18 Modulates Immune Escape of Murine Melanoma Cells by Regulating the Expression of Fas Ligand and Reactive Oxygen Intermediates. *Cancer Res*. 2000;60(10):2703–2709.

31. Ma Z, et al. Augmentation of Immune Checkpoint Cancer Immunotherapy with IL18. *Clinical Cancer Research*. 2016;22(12):2969–2980.

32. Zhou T, et al. IL-18BP is a secreted immune checkpoint and barrier to IL-18 immunotherapy. *Nature*. 2020;583(7817):609–614.

33. Fabbi M, Carbotti G, Ferrini S. Context-dependent role of IL-18 in cancer biology and counter-regulation by IL-18BP. *J Leukoc Biol*. 2015;97(4):665–675.

34. Terme M, et al. IL-18 Induces PD-1–Dependent Immunosuppression in Cancer. *Cancer Research*. 2011;71(16):5393–5399.

35. Lutz V, et al. IL18 Receptor Signaling Regulates Tumor-Reactive CD8+ T-cell Exhaustion via Activation of the IL2/STAT5/mTOR Pathway in a Pancreatic Cancer Model. *Cancer Immunology Research*. 2023;11(4):421–434.

36. Ingram JT, Yi JS, Zajac AJ. Exhausted CD8 T cells downregulate the IL-18 receptor and become unresponsive to inflammatory cytokines and bacterial co-infections. *PLoS Pathog*. 2011;7(9):e1002273.

37. Wang J, et al. UV-induced somatic mutations elicit a functional T cell response in the YUMMER1.7 Mouse Melanoma Model. *Pigment Cell Melanoma Res*. 2017;30(4):428–435.

38. Li W, et al. Protection of CD8+ T cells from activation-induced cell death by IL-18. *J Leukoc Biol*. 2007;82(1):142–151.

39. Nakamura K, et al. Dysregulated IL-18 Is a Key Driver of Immunosuppression and a Possible Therapeutic Target in the Multiple Myeloma Microenvironment. *Cancer Cell*. 2018;33(4):634-648.e5.

40. Lim HX, et al. IL-18 Enhances Immunosuppressive Responses by Promoting Differentiation into Monocytic Myeloid-Derived Suppressor Cells. *The Journal of Immunology*. 2014;193(11):5453–5460.

41. Qiu Y, et al. Next frontier in tumor immunotherapy: macrophage-mediated immune evasion. *Biomarker Research*. 2021;9(1):72.

42. Muraoka D, et al. Antigen delivery targeted to tumor-associated macrophages overcomes tumor immune resistance. *J Clin Invest*. 2019;129(3):1278–1294.

43. Zaidi MR. The Interferon-Gamma Paradox in Cancer. *J Interferon Cytokine Res*. 2019;39(1):30–38.

44. Kanhere A, et al. T-bet and GATA3 orchestrate Th1 and Th2 differentiation through lineage-specific targeting of distal regulatory elements. *Nat Commun*. 2012;3(1):1268.

45. Shen E, et al. The suppressive effect of CD25+Treg cells on Th1 differentiation requires cell-cell contact partially via TGF-β production. *Cell Biol Int*. 2011;35(7):705–712.

46. Robinson D, et al. IGIF does not drive Th1 development but synergizes with IL-12 for interferon-gamma production and activates IRAK and NFkappaB. *Immunity*. 1997;7(4):571–581.

47. Interleukin 12 signaling in T helper type 1 (Th1) cells involves tyrosine phosphorylation of signal transducer and activator of transcription (Stat)3 and Stat4. *J Exp Med*. 1995;181(5):1755–1762.

48. Santegoets SJ, et al. Tbet-positive regulatory T cells accumulate in oropharyngeal cancers with ongoing tumor-specific type 1 T cell responses. *Journal for ImmunoTherapy of Cancer*. 2019;7(1):14.

49. Overacre-Delgoffe AE, et al. Interferon-γ Drives Treg Fragility to Promote Anti-tumor Immunity. *Cell*. 2017;169(6):1130-1141.e11.

50. Nakagawa H, et al. Instability of Helios-deficient Tregs is associated with conversion to a T-effector phenotype and enhanced antitumor immunity. *PNAS*. 2016;113(22):6248–6253.

51. Hatzioannou A, et al. An intrinsic role of IL-33 in Treg cell-mediated tumor immunoevasion. *Nat Immunol*. 2020;21(1):75–85.

52. Curiel TJ, et al. Specific recruitment of regulatory T cells in ovarian carcinoma fosters immune privilege and predicts reduced survival. *Nature Medicine*. 2004;10(9):942–949.

53. Betts MR, et al. Sensitive and viable identification of antigen-specific CD8+ T cells by a flow cytometric assay for degranulation. *J Immunol Methods*. 2003;281(1–2):65–78.

54. Mehdi A, et al. S-adenosylmethionine blocks tumorigenesis and with immune checkpoint inhibitor enhances anti-cancer efficacy against BRAF mutant and wildtype melanomas. *Neoplasia*. 2023;36:100874.

55. Smyth MJ, et al. NKG2D Recognition and Perforin Effector Function Mediate Effective Cytokine Immunotherapy of Cancer. *Journal of Experimental Medicine*. 2004;200(10):1325–1335.

56. Wang S, et al. Intratumoral injection of a CpG oligonucleotide reverts resistance to PD-1 blockade by expanding multifunctional CD8+ T cells. *Proceedings of the National Academy of Sciences*. 2016;113(46):E7240–E7249.

57. Attias M, Al-Aubodah T, Piccirillo CA. Mechanisms of human FoxP3 $^{+}$ T $_{reg}$ cell development and function in health and disease. *Clin Exp Immunol*. 2019;cei.13290.

58. Galon J, Bruni D. Approaches to treat immune hot, altered and cold tumours with combination immunotherapies. *Nature Reviews Drug Discovery*. 2019;18(3):197–218.

59. Thieu VT, et al. Stat4 is required for T-bet to promote IL-12-dependent Th1 fate determination. *Immunity*. 2008;29(5):679–690.

60. Koch MA, et al. T-bet+ Treg Cells Undergo Abortive Th1 Cell Differentiation due to Impaired Expression of IL-12 Receptor β2. *Immunity*. 2012;37(3):501–510.

61. Koch MA, et al. The transcription factor T-bet controls regulatory T cell homeostasis and function during type 1 inflammation. *Nat Immunol*. 2009;10(6):595–602.

62. Moreno Ayala MA, et al. CXCR3 expression in regulatory T cells drives interactions with type I dendritic cells in tumors to restrict CD8+ T cell antitumor immunity. *Immunity*. [published online ahead of print: June 30, 2023]; https://doi.org/10.1016/j.immuni.2023.06.003

63. Shergold AL, Millar R, Nibbs RJB. Understanding and overcoming the resistance of cancer to PD-1/PD-L1 blockade. *Pharmacological Research*. 2019;145:104258.

64. Barrueto L, et al. Resistance to Checkpoint Inhibition in Cancer Immunotherapy. *Transl Oncol*. 2020;13(3). https://doi.org/10.1016/j.tranon.2019.12.010

65. Castro F, et al. Interferon-Gamma at the Crossroads of Tumor Immune Surveillance or Evasion. *Front Immunol*. 2018;9. https://doi.org/10.3389/fimmu.2018.00847

66. West EE, et al. PD-L1 blockade synergizes with IL-2 therapy in reinvigorating exhausted T cells. *J Clin Invest*. 2013;123(6):2604–2615.

67. Vidal-Vanaclocha F, et al. IL-18 regulates IL-1beta-dependent hepatic melanoma metastasis via vascular cell adhesion molecule-1. *Proc Natl Acad Sci U S A*. 2000;97(2):734–739.

68. Paulukat J, et al. Expression and release of IL-18 binding protein in response to IFN-gamma. *J Immunol*. 2001;167(12):7038–7043.

69. Tarhini AA, et al. Phase III Study of Adjuvant Ipilimumab (3 or 10 mg/kg) Versus High-Dose Interferon Alfa-2b for Resected High-Risk Melanoma: North American Intergroup E1609. *JCO*. 2020;38(6):567–575.

70. Dinarello CA. The paradox of pro-inflammatory cytokines in cancer. *Cancer Metastasis Rev*. 2006;25(3):307–313.

71. Wang Y, et al. Plasma cytokines interleukin-18 and C-X-C motif chemokine ligand 10 are indicative of the anti-programmed cell death protein-1 treatment response in lung cancer patients. *Ann Transl Med*. 2021;9(1):33.

Chapter 5 – General Discussion and Conclusions

1. Recapitulation of major findings

The role of Foxp3$^+$ Regulatory T cells in peripheral tolerance and tumor immunity has been the focus of extensive research since their discovery in 1995 (71). Indeed, systemic depletion of T_{reg} cells, through targeting their high surface expression of CD25, leads to tumor clearance in poorly immunogenic murine models, at the cost of systemic autoimmunity (110). As such, immunotherapies aimed at depleting T_{reg} cells and presenting a satisfactory safety, efficacy and quality profile remain to be successfully developed and receive marketing authorisation. On the other hand, immune checkpoint inhibitors, a pharmacological class targeting co-inhibitory ligands and receptors highly expressed by TILs, has provided significant clinical benefits to advanced melanoma patients, inducing durable remissions in the absence of further treatment (239) and considerably increasing the median overall survival from 6-12 months until the 2010s (4) to 72 months for patients receiving a combination of ipilimumab and nivolumab (240). While ICIs were designed to primarily target exhausted TILs, it is apparent that they also target T_{reg} cells (176). Given the variable outcomes of tumor immunotherapy (177), and the differential responsivity of various subsets of PD-1$^+$ CD8$^+$ TILs to PD-1 signaling and its blockade (190, 243), it was important to characterize the functional consequences of PD-1 signaling and anti-PD-1 administration on T_{reg} cells in the contexts of both successful and failed response to ICI.

While reliable and clinically-applicable predictive biomarkers remain to be validated, the consensus determinant of successful response to ICIs is the degree of pre-existing inflammation in the TME, which is dictated by the abundance and tissue distribution of lymphocyte infiltrates (44). While abundant T_{reg} cell infiltration is associated with poor prognosis and resistance to treatment in most solid tumors (244), little is known regarding the difference between T_{reg} cell infiltration and PD-1 expression patterns in “cold” and “hot” TMEs. To address this, in Chapter 2, we

characterized anti-melanoma T cell responses in a novel melanoma model, driven by genetic alterations to Braf and PTEN, but displaying low tumor mutational burden (23). In cold D4M.3A melanomas, we established that T cells expressed PD-1 in higher proportions and MFIs than their T_{eff} counterparts, an observation we reproduced in poorly immunogenic B16 melanomas (245). Furthermore, treatment with anti-PD-1 resulted in a downregulation of PD-1 expression by T_{reg} cells and a systemic expansion of Helios$^+$ T_{reg} cells, a subset which displayed preferential expression of PD-1 as well of other checkpoint molecules associated with enhanced suppressive capacity (95, 246, 247), in line with the emerging hypothesis that ICI-induced T_{reg} cell proliferation is a mechanism of acquired resistance to treatment (176, 209, 248).

To investigate if PD-1 blockade dysregulates the suppressive function of highly-activated Helios$^+$ T_{reg} cells, in chapter 3, we studied their functional dynamics in a model that yields high responders to anti-PD-1 monotherapy (25). We established three novel hallmarks of successful response to anti-PD-1: (*i*) expansion of highly activated Helios$^+$ T_{reg} cells, (*ii*) high levels of Akt signaling, which drive T-bet expression in T_{reg} cells (249), in the tumor regions where CD8$^+$ TILs evade T_{reg} cell suppression, and (*iii*) secretion of IFNγ by T_h1-like T_{reg} TILs. On the other hand, LR T_{reg} cells eventually succumbed to the same exhausted-like phenotype as control T_{reg} TILs.

As IFNγ$^+$ T_{reg} TILs were observed at day 14, but not at endpoint in low responder tumors, in chapter 4, we asked what factors maintain this population. Our attention was drawn to IL-18, which is a known potentiator of IFNγ production in T_{eff} cells, whose receptor was highly expressed in TILs. We demonstrate that IL-18 is sufficient to induce IFNγ production by T_{reg} TILs *in vitro*. Furthermore, using a T cell-specific deletion of IL18R1, we show that the acquisition of inflammatory characteristics by T_h1-like T_{reg} TILs in response to PD-1 blockade is dependent on IL-18. Furthermore, IL-18 promotes the accumulation of T_h1 cells over T_{reg} TILs, thereby

promoting the establishment of a hot TME that is required for successful response to anti-PD-1. Collectively, these data demonstrate that while anti-PD-1 targets T_{reg} cells both locally and systemically, its efficacy in inducing T_{eff} cell evasion from T_{reg} cell suppression depends on the presence of inflammatory factors within the TME to unleash anti-tumor immunity (**Figure 7**).

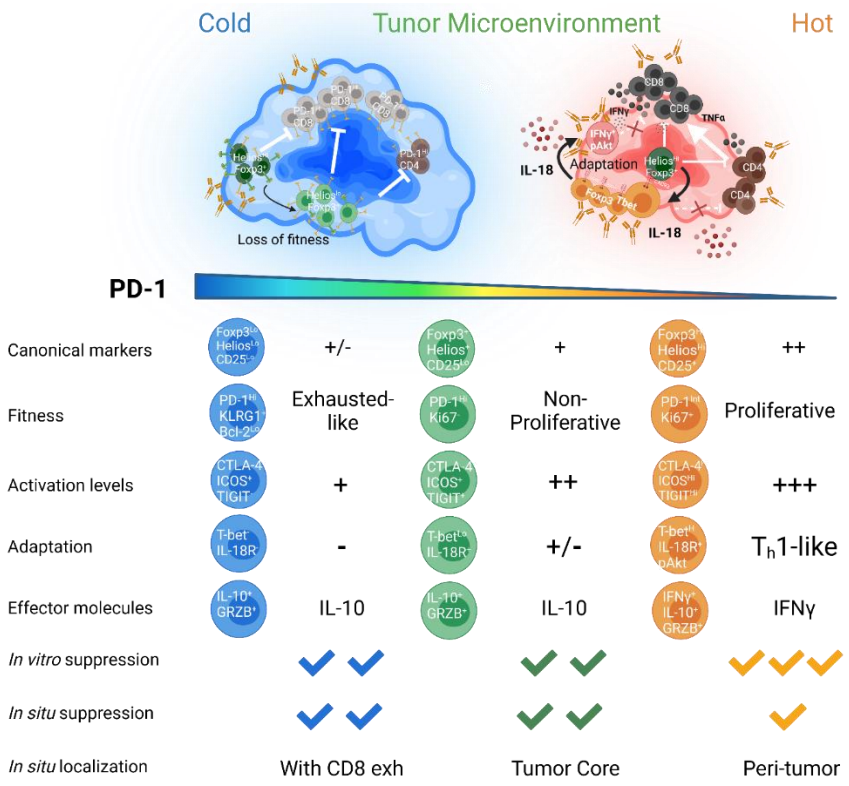

Figure 7. Graphical summary of the role of PD-1 signaling gradients on dictating the functional adaptation of melanoma-infiltrating T_{reg} cells.

Adapted from Attias et, JCI Insight, 2023 (manuscript submitted). In hot TMEs, at low levels of PD-1 signaling, T_{reg} TILs are highly-activated and proliferative. Expression of T-bet enables them to co-localize with T_{eff} cells and suppress IFNγ production by TILs. However, in response to local IL-18, T_{reg} cells secrete IFNγ as T_{eff} cells evade their suppression. Upon chronic signaling through PD-1, T_{reg} TILs progressively lose the expression of Foxp3, CD25 and Helios and adopt a short-lived, exhausted-like phenotype, despite retaining suppressive potency.

2. Roles of PD-1 signaling throughout T_{reg} cell homeostasis

PD-1 signaling determines T cell fate during thymic selection (250, 251), T cell activation (252), differentiation (253), memory formation (254) and apoptosis of tissue-resident cells (255). Yet, the function of PD-1 signaling in T_{reg} cells is not well understood. Indeed, T_{reg}-specific models of PD-1 deletion were not developed until 2020 (223), after the start of this project, are not commercially available, and have yet to be investigated in the context of anti-melanoma responses. While early reports established the role of PD-1 signaling on curtailing T_{reg} cell activation in proliferation (176, 223), numerous knowledge gaps remain to be addressed.

2.1. Does PD-L1 promote pT_{reg} cell induction in TMEs?

While PD-1 does not impact the thymic development of tT_{reg} cells, it regulates pT_{reg} development (222). Indeed, PD-L1 and PD-L2 synergize with TGFβ by antagonizing Akt signaling to promote the induction of Foxp3 expression in naïve T_{conv} cells (103, 256). Furthermore, acute activation of human memory T cells in the presence of PD-L1 promotes a transient upregulation of Foxp3 expression, in the absence of the T_{reg}-polarizing cytokines TGFβ and IL-2 (257).

As absence of Helios expression was proposed as a marker of pT_{reg} cells, we originally hypothesized that $Helios^{low}$ T_{reg} TILs were locally induced. However, Helios is not a reliable marker of T_{reg} cell ontogeny (258), as we show in Chapter 3 that PD-1 signaling modulates its expression levels. Furthermore, using adoptive transfer models, we found little evidence of pT_{reg} induction in both D4M.3A and YUMMER1.7 models (data not shown), in line with the absence of Foxp3-induction by OT-II specific TILs in B16-OVA melanomas (85). Thus, while PD-1 regulates pT_{reg} development, the relevance of this mechanism in the context of anti-tumor immunity remains to be determined.

2.2. Does chronic PD-1 signaling trigger T_{reg} cell exhaustion?

Little is known regarding the role of PD-1 signaling on T_{reg} cells during situations of chronic activation. Indeed, in our hands, anergic T_{reg} cells failed to expand using *in vitro* models of chronic activation of T_{eff} cells, which rely on sequential activations with anti-CD3 (259, 260). Furthermore, *in vitro* T_{reg} cell monocultures require high concentrations of exogenous IL-2, which overrides PD-1 signaling and T cell exhaustion (233). Recently, Perry et al showed that a T_{reg}-specific deletion of PD-1 reduces the ratio of pathogen-specific T_{eff} cell to T_{reg} cells during Toxoplasma gondii infection, indicating that PD-1 signaling plays a role in the contraction of T_{reg} cells during chronic infections. In line with this observation, we observed smaller T_{reg} TIL frequencies in D4M.3A tumors, where T_{reg} cell expressed the highest level of PD-1, than in YUMMER1.7 TMEs. Furthermore, through *in vitro* studies, we show in Chapter 3 that PD-1 signaling reduces the expression of Foxp3, Helios and CD25, which play a crucial role in T_{reg} cell fitness and survival (114, 261, 262). Future experiments will be aimed at assessing STAT5 signaling in T_{reg} TILs and upon PD-1 signaling, but *ex vivo* PD-L1 blockade was shown to increase STAT5 phosphorylation in patients with Hepatitis C Virus Infection (263). While these elements suggest that, in chronic contexts, PD-L1 mediated inhibition of STAT5 signalling reduces T_{reg} cell survival, it was nonetheless shown to protect T_{reg} cells from activation induced cell death during low-dose IL-2 therapy (264).

The differentiation pathways that induce $CD8^+$ T cell exhaustion or dysfunction in chronic inflammatory contexts have been recently characterized (63, 65). As steady-state T_{reg} cells share multiple features of exhausted T_{eff} cells, namely expression of multiple inhibitory checkpoint molecules, absence of production of inflammatory cytokines, reduced proliferation, and high rates of fatty acid oxidation; the concept of T_{reg} cell exhaustion has not been defined in the literature. In

chapter 2, we show that T_{reg} TILs express higher levels of PD-1 than their dysfunctional T_{eff} counterparts in a poorly immunogenic model of melanoma, suggesting that T_{reg} cells undergo chronic activation in the TME. In line with these findings, PD-1^{High} T_{reg} cells display short telomeres and transcriptional signatures of exhaustion in malignant gliomas (265). In chapter 3, we identify that akin to terminally-exhausted $CD8^+$ TILs, a subset of T_{reg} TILs express Tim-3 but not Tcf-1, a transcription factor whose deletion reduces T_{reg} cell survival (266), yet increases their suppression of $CD8^+$ T cell cytotoxicity (267). Nonetheless, it remains to be determined if the acquisition of this terminally-exhausted-like T_{reg} cell phenotype is also driven by expression of the transcription factor Tox (63) and how much their transcriptional signature is shared with dysfunctional $CD8^+$ TILs. Furthermore, the consequences of this form of exhaustion on T_{reg} cell suppressive capacity remain to be determined.

2.3. Does PD-1 signaling inhibit T_{reg} cell suppressive function?

To tackle this question, in Chapters 3 and 4, we took advantage of the high level of TIL infiltration in YUMMMER1.7 tumors to sort out Foxp3-RFP^+ T_{reg} TILs and cultured these cells in a variety of conditions to test multiple aspects of their fitness, activation levels, responsiveness to inflammatory signals, and suppressive capacity. In line with numerous reports (99, 248, 268), we show that T_{reg} TILs display potent suppressive function, with an enhanced expression of multiple T_{reg} cell suppressive mechanisms (CTLA-4, GRZB, IL-10). These results suggest that contrary to $CD8^+$ TILs, the induction of an "exhausted" phenotype does not render T_{reg} cells dysfunctional. However, T_{reg} TILs are heterogeneous in their levels of PD-1 expression, and T_{reg} TIL reactivation was significantly reduced compared to splenic T_{reg} cells, which introduces a survival bias. As such, the increased suppressive potency at the populational level could be driven by the expansion of PD-1^{low} cells with no contribution from the most exhausted cells. Nonetheless, release of adenosine

by apoptotic T_{reg} cells has been proposed as a suppressive mechanism of T_{reg} TILs (99). In addition, it remains to be determined if this reduced survival is caused by the death of exhausted cells. Indeed, we also identified a subset of KLRG1^{+} T_{reg} TILs, a marker of terminally-differentiated, short-lived effector T_{reg} cells whose expression is dependent on multiple rounds of IL-2 induced proliferation (269, 270). Thus, further investigation, using single-cell transcriptomic analysis, should be aimed at characterizing the heterogeneity of T_{reg} cell populations in TMEs and their developmental pathways.

Finally, the unavailability of PD-1 deficient mice prevents us from directly testing the role of PD-1 signaling on T_{reg} cell suppressive function. Using PD-1^{KO} T_{reg} cells isolated respectively from CD4^{Cre} PD-1$^{fl/fl}$ Foxp3$^{-ires-DTR-GFP}$ mice and Foxp3^{Cre} PD-1$^{fl/fl}$ mice, Kamada et al and Tan et al, found a modest increase in the *in vitro* suppressive potency PD-1$^{-/-}$ T_{reg} cells (176, 223). However, we argue that this effect is caused by the increased frequency of highly-activated effector T_{reg} cells in the spleens of these mice, rather than a direct consequence of PD-1 signaling, as there is no source of PD-L1 signaling provided during *in vitro* suppression assays. Unfortunately, the use of PD-L1-Fc requires plate-bound activation conditions with high concentrations of anti-CD28 which override T_{reg} cell suppression (271). However, this limitation could be addressed using tumoral APCs, which express PD-L1 and inhibit T cell proliferation, as shown in Chapter 2.

2.4. Does PD-1 prevent T_{reg} cell reprogramming in TMEs?

In highly inflammatory contexts, we and others have shown that T_{reg} cells can lose Foxp3 expression and become potently inflammatory *ex*Foxp3 cells (128, 129). Fate mapping experiments using Foxp3$^{GFP-Cre}$-Rosa26^{RFP} reporter mice showed that PD-1$^{-/-}$ mice have an increased frequency of Foxp3-GFP^{-} Rosa-RFP^{+} *ex*Foxp3 cells in circulation (230). However, Rubtsov *et al*., generated a different, tamoxifen-inducible fate-mapping system, and dispute the

prevalence of (RFP$^+$ GFP$^-$) *ex*Foxp3 cells (272). Recently, Kim et al combined the tamoxifen-inducible fate-mapping system to a conditional deletion of PD-1 expression in Foxp3$^+$ T_{reg} cells to study the role of PD-1 in *ex*Foxp3 generation during anti-tumor responses. They found that conditional deletion of PD-1 in T_{reg} cells delays the growth of TC-1 lung cancer and increased the frequency of *ex*Foxp3 cells amongst cells with a history of Foxp3 expression (RFP$^+$) (225). However, these results have important caveats: (*i*) notably the authors observed a reduction in T_{reg} cell proliferation, activation levels, suppressive capacity, and survival upon PD-1 deletion, in complete contrast with reports by Tan et al, in both constitutive and tamoxifen-inducible models. This could be explained by unproper controlling for the effects of tamoxifen, which is highly toxic to T cells, especially during phases of clonal expansion, reducing the proliferative rate of surviving cells (273, 274). (*ii*) Using the same tamoxifen-inducible fate-mapping mice, we observed spontaneous regression of YUMMER1.7 tumors (data not shown), even in the absence of tamoxifen administration. Indeed, integration of large cassettes in Foxp3 3'UTR regions has the potential to alter Foxp3 stability. For example, a Foxp3-GFP^{-KI} model impairs the interaction between Foxp3 and histone acetyltransferase Tip60 leading to accelerated onset of T1D in NOD mice (275), and was sufficient to render D4M.3A melanomas hot and fully responsive to PD-1 blockade in our hands (data not shown). Thus, we could not assess ourselves the generation of *ex*Foxp3 cells in TMEs and their biological significance remains highly controversial.

3. Impact of PD-1 blockade on T_{reg} cell functional fate.

Despite retrospective data spanning almost 10 years since its first marketing authorization, the impact of PD-1 blockade on T_{reg} cell functional fate is still debated. Indeed, in conventional T cell assays, T_{resp} cells are mostly naïve and do not express PD-1, and the antibodies used to FACS-sort PD-1^+ cells have antagonistic pharmacological activity. As such, nivolumab has little effect on T cell proliferation and effector functions *in vitro* (228). Furthermore, anti-PD-1 fails to reinvigorate terminally exhausted cells (189) and as such, we found little effect of anti-PD-1 on IFNγ production upon *in vitro* restimulation of $CD8^+$ TILs (data not shown).

3.1. What is the mechanism of action of anti-PD-1 on T_{reg} cells?

3.1.1. Cell-intrinsic mechanism

In chapters 2 and 3, we identified that PD-1 blockade induces a reduction in PD-1 expression levels by TILs, as well as by splenic T_{reg} cells. This observation is in line with the fact that the reported mechanism of action of anti-PD-1 mAbs is pharmacological inhibition of PD-1, and not dependent on Fc-effector functions (202). These results suggest that anti-PD-1 can induce PD-1 endocytosis, but the precise mechanism of PD-1 downmodulation remains to be determined, as we were not able to observe this effect upon *in vitro* activation where PD-1 expression is transient. Indeed, several transcription factors, cytokines, and metabolic factors could further modulate PD-1 expression in response to anti-PD-1 (232, 233, 276). As such, in chapter 3, we observed a steeper reduction in PD-1 expression in High Responder TILs compared to Low Responders. Nonetheless, this observation provides a novel pharmacodynamic readout of anti-PD-1 activity.

The systemic impact of checkpoint blockade on T_{reg} cell phenotype is in line with pharmacokinetic studies that show that anti-PD-1 antibodies distribute in the spleen and lymph nodes and remains stable in circulation seven days after injection (277, 278). Furthermore, the

increased expansion of activated effector T_{reg} cells was observed in models of PD-1 deletion (223) and upon treatment with anti-PD-L1 in the peripheral blood of lung cancer patients (248).

To identify the cell-intrinsic effect of anti-PD-1 on T_{reg} cells, Kamada et al devised an adoptive transfer system in which lymphodepleted tumor-bearing mice are reconstituted with PD-1^{KO} T_{eff} cells and PD-1^{WT} T_{reg} cells. In their model, only T_{reg} cells can bind the mAb, and administration of anti-PD-1 accelerated tumor growth, suggesting that this expansion of highly-activated T_{reg} cells is detrimental to treatment efficacy. Taken together with our observations in chapter 2, these results suggest that increased T_{reg} cell activation acts as a mechanism of secondary resistance to treatment in non-responder patients.

3.1.2. Environment-dependent effects

In chapter 3, our spatial proteomics data, which identifies increased phosphorylation of multiple effectors of the Akt signaling pathway in regions with a high CD8:T_{reg}, ratio, suggests that IFNγ production by T_{reg} TILs happens in the zones where the pharmacological inhibition of PD-1 signaling is most efficacious (**Figure 8**). Nonetheless, while anti-PD-1 was required to maintain a population of IFNγ^+ T_{reg} cells at endpoint, this effect was not observed in low responder tumors or outside the TME, suggesting that environmental conditions play a role in mediating this effect. As such, T_{reg} cells from high responders were highly suppressive once removed from the TME, and the expansion of Helios$^+$ T_{reg} cells was a conserved mechanism of action in high responder mice, indicating that the ICI-induced evasion from local suppression in hot TMEs is mediated via cell-extrinsic mechanisms. Indeed, in chapter 4, we show that T cell responsiveness to IL-18 is required to achieve this effect, revealing a synergy between PD-1 blockade and inflammatory cues to promote the T_h1-adaptation of T_{reg} cells.

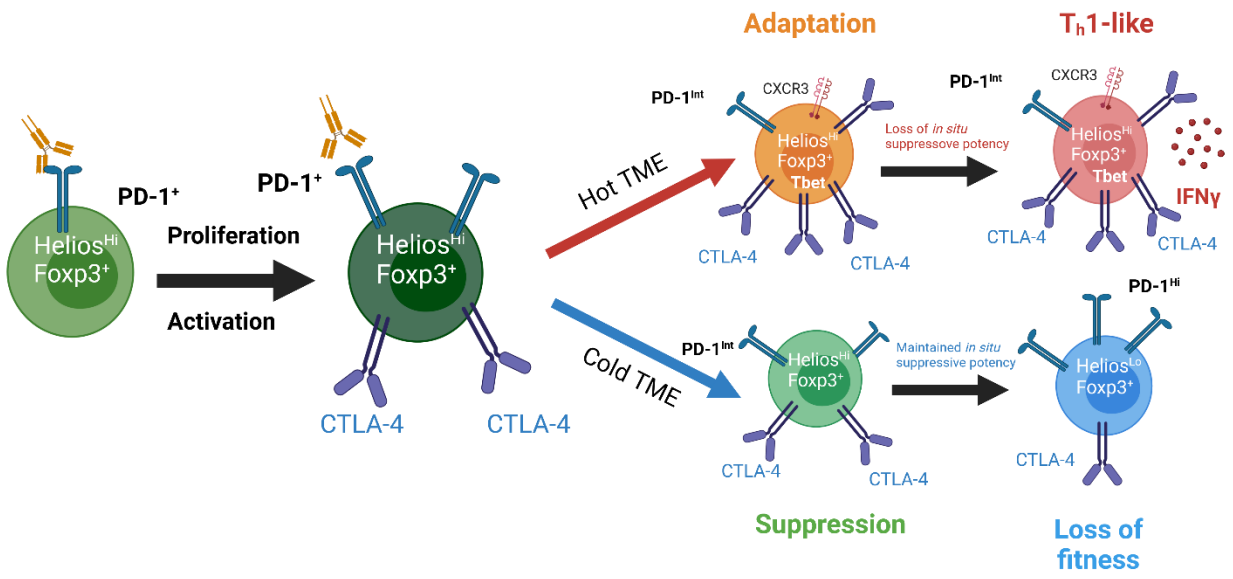

Figure 8. Proposed model for the systemic and local effect of anti-PD-1 on T_{reg} cells.

In circulation and lymphoid organs, anti-PD-1 selectively targets Helios$^+$ T_{reg} cells. In both tumor models, treatment with anti-PD-1 resulted in a downregulation of PD-1 expression and an expansion of highly-activated T_{reg} cells. In hot TMEs, Helios$^+$ T_{reg} cells acquire T_h1-like characteristics which enable them to potently suppress IFNγ production. In high responders, a subset of these cells secretes IFNγ while T_{eff} cells evade suppression. In cold TMEs, ICI-reactivated T_{reg} cells contribute to acquired resistance before adopting an exhausted phenotype themselves. Created with Biorender.com®.

3.1.3. Is the T_h1-adaptation of T_{reg} cells detrimental to tumor growth?

Through characterizing T_{reg} cell phenotypes at multiple time points through anti-tumor responses, we show that the abundance of T_h1-like T_{reg} cells is higher in high responders than at day 14, suggesting that this population enables the maintenance of abundant IFNγ production in the TME. Nonetheless, these cells display potent suppressive capacity, in line with the hypothesis that these cells are specialized in suppressing type 1 responses (125). Indeed, we show that the

acquisition of these inflammatory characteristics is transient, thus, T_{reg} cells could downregulate T-bet expression in cold TMEs, subsequently to a successful inhibition of the $CD8^+$ T cell response. As such, further characterization of the heterogeneity of these T_{reg} cell subsets is warranted to evaluate their degree of transcriptional overlap with *bona fide* T_h1 cells, their developmental relationship with exhausted-like T_{reg} cells and their TCR repertoire. Given the association between TCR signal strength, Akt signaling and the generation of T_h1-like T_{reg} cells (237), we reason that clonotypes with the highest affinity for tumor self-antigens are the most prone towards T_h1-adaptation. Furthermore, we hypothesize that PD-1 blockade promotes the oligoclonal expansion of these cells rather than increasing T_{reg} cell repertoire diversity.

While we took advantage of the natural inter-individual variability in tumor growth rate to associate the T_h1-adaptation of T_{reg} cells with enhanced anti-tumor responses and show that response to treatment persists for 10 days post-treatment interruption, this correlation is not predictive of treatment outcome. However, tumors injected bilaterally in one mouse show synchronous growth (279) and respond symmetrically to checkpoint blockade, indicating that the variability in response is a mouse-centric phenomenon (280). Therefore, to characterize the fate of T_h1- adapted T_{reg} cells, we propose a bilateral tumor injection approach where one tumor can be surgically resected and immunophenotyped while the second one can be used for survival analysis. Indeed, this paired approach would allow us to identify predictive biomarkers of response to treatment. Furthermore, mechanistic approaches such as T_{reg}-specific deletions of T-bet, CXCR3, IL-18R1 and IFNγ are warranted to elucidate the role of these individual T_h1-like features on T_{reg} cell migration, proliferation, specialized suppression of T_h1 cells, functional stability, and survival in TMEs.

3.2. Can PD-1 blockade promote the adaptation of T_{reg} cells towards other helper subsets?

PD-L1 is thought to mainly suppress T_h1 cells and T_h1-like T_{reg} cell generation (281). As such, Gata-3$^+$ T_{reg} cells did not express PD-1 in YUMMER1.7 tumors, and RORγt$^+$ T_{reg} cells were not readily detected, suggesting that these T_{reg} cell subsets are not cellular targets of anti-PD-1. As T_h2-adpated T_{reg} cells play a strong pro-tumorigenic role in melanoma (102, 144), anti-PD-1 could promote anti-tumor responses by favoring the T_h1-adaptation of T_{reg} cells, in a process akin to immune deviation. In both our tumor models, we did not find evidence of ongoing T_h2 or T_h17 responses at any stage of tumor growth, although mixed tumor-specific responses are often seen in melanoma lesions (282–284). Furthermore, these results raise the question of whether PD-1 blockade can promote the development of T_h2 and T_h17 responses in other cancer types, such as colon cancer, where these specialized responses are more prevalent and contribute to anti-tumor immunity (285, 286), or even distally from the primary tumor lesion.

As evidenced by the limited B cell infiltration and the absence of naïve TILs, our models did not induce the formation of tertiary lymphoid structures, a feature that improves the response rate to ICIs in melanoma (49). Notably, PD-1 expression is a defining feature of T_{fh} and T_{fr} cells, suggesting that these subsets are also targets of anti-PD-1. Indeed, through mining of publicly-available single-cell transcriptomic datasets, Eschweiler et al found that a subset of tumor-infiltrating T_{reg} cells express high levels of Bcl-6, Tcf-1, PD-1 and ICOS, features of T_{fr} cells, and expands following PD-1 blockade, limiting its anti-tumor efficacy in preclinical models (287). However, it remains to be determined if these tumor-infiltrating cells were truly specialized in inhibiting germinal center reactions or if this phenotype was a T_{reg} equivalent of progenitor-exhausted CD8$^+$ TILs. Notably, the Helios^{High} CD25$^-$ T_{reg} subset that expands in spleens and lymph nodes upon PD-1 blockade is also reminiscent of the phenotype of T_{fr} cells (288). A systemic

impairment of T_{fr} cells could favor the production of auto-antibodies, a feature found in close to 50% of patients with irAEs (289).

3.3. Which therapeutic approaches could target adapted T_{reg} cell subsets?

Our results suggest that the acquisition of T_h1-like characteristics by T_{reg} cells in response to PD-1 blockade renders them more permissive to sustained IFNγ production by TILs without triggering systemic autoimmunity. As such, promoting the T_h1-adaptation of T_{reg} TILs appears as a more relevant therapeutic strategy than depletion of this subset. This body of work provides a strong rationale for developing several translational approaches to adjuvant ICIs by modulating T_{reg} cell functional adaptation through: (*i*) dysregulating their lineage stability by impairing Helios signaling (112), or increasing Akt signaling (290), (*ii)* synergizing with PD-1 blockade to reduce PD-1 expression with small molecules inhibitors (291), (*iii*) promoting T_h1 cell accumulation by maximizing local IL-18 availability (292), (*iv*) reducing local T_{reg} cell fitness with CD25-antagonizing IL-2 muteins (293), and (*v)* alter the CD8:T_{reg} ratio within tumor-specific TILs by increasing the release of neoepitopes using epigenetic modifiers (294).

In contrast, the recruitment of T_h2-like T_{reg} cells through CCR4 signaling leads to the development of a cold TME (295). In addition, CCR8, while not required for T_{reg} cell recruitment to the tumor bed (296), promotes the trafficking of clonally expanded T_{reg} cells towards M2 TAMs, contributing to the establishment of highly immunosuppressive niches within the TME (297). As such, anti-CCR8 mAbs are currently under clinical investigation for their potential to selectively target TIL T_{reg} cells and unleash $CD8^+$ T cells and anti-tumor responses (298). Alternatively, deletion of the IL-33 receptor ST2 on T_{reg} cells leads to their conversion to a T_h1-like phenotype in melanoma TMEs, all the while delaying tumor growth (145), highlighting the fact that IL-1 family alarmins can counter-regulate the tissue-adaptation of T_{reg} cells (131). Thus, therapeutic

approaches promoting an immune deviation towards T_h1-like T_{reg} cells could prove sufficient to enhance anti-tumor immunity while presenting a potentially safer risk profile than T_{reg} cell depleting strategies.

3.4. Does PD-1 blockade dysregulate T_{reg} cell function to induce irAEs?

As evidenced in chapters 2 and 3, PD-1 blockade alters T_{reg} cell phenotype systemically, highlighting the potential for T_{reg} cell dysregulation. Nonetheless, the short-time span of our experimental approach did not enable us to detect irAEs symptoms in non-predisposed mice. Indeed, the onset of irAEs is often secondary to tumor regression (185), which was not achieved in our models. Furthermore, while ICIs are indicated to neutralize metastatic lesions, our models do not spontaneously metastasize, presumably limiting the circulation of tumor-specific $CD8^+$ T cells to other tissues than the primary lesion. Alternatively, we could use tail vein injections of our melanoma models to mimic their metastasis to the lung.

Furthermore, we could adapt an existing model of immunotherapy-induced vitiligo secondary to melanoma clearance. B16 tumor clearance necessitated immunization with an altered peptide ligand and high doses IL-2 to support the activation and proliferation of adoptively transferred gp100-specific $CD8^+$ T cells. Gp100, a melanocyte antigen, is also expressed by both D4M.3A tumors and YUMMER1.7 tumors (23, 294). Given the high responsiveness of YUMMER1.7 tumors to PD- 1 blockade, we hypothesize that ICI would be sufficient to reactivate adoptively transferred Gp100-specifc cells. Alternatively, we could reduce the initial inoculum of YUMMER1.7 cells and assess tumor-rejection, vitiligo onset, and eventually characterize T_{reg} cell phenotype within the lesioned skin.

Finally, PD-1 blockade could mediate irAEs through non-tumor-specific T cells. Given the role of PD-L1 in promoting Foxp3 induction in synergy with TGFβ (103), it has long been proposed

that anti-PD-1 modulates the T_{reg}:T_{eff} balance by inhibiting pT_{reg} generation (299). *In vitro*, we saw no effect of PD-1 blockade on pT_{reg} cell induction using soluble instead of plate-bound anti-CD3 (data not shown). To assess the impact of PD-1 blockade on pT_{reg} cell induction *in vivo*, we propose to focus our efforts on the gut, where pT_{reg} cells play a crucial role in the maintenance of peripheral tolerance (81). Adoptive transfer of congenically-labelled purified $CD4^+$ Foxp3-RFP^- T_{conv} cells in lymphopenic $TCR\beta^{-/-}$ hosts results in both pT_{reg} induction and the induction of a T_h1 and T_h17-driven colitis whose development is inhibited by the co-transfer of T_{reg} cells. Using this system, we expect that immunotherapy will inhibit the induction of congenically-labelled RFP^+ pT_{reg} cells, thus facilitating the onset of colitis. This model would demonstrate the direct biological effect of PD-1 blockade on T_{reg} cell homeostasis in a known T-cell mediated autoimmune model.

4. Concluding remarks

In this work, we demonstrate that the functional consequences of PD-1 blockade on the functional fate of T_{reg} cells are dependent on the inflammatory context in the TME. Akin to $CD8^+$ T cells, the strength of PD-1 signaling differentially affects T_{reg} cell effector functions (243), and their responsiveness to PD-1 blockade (190). As such, while increased T_{reg} cell activation was observed in both high and low responders and at the systemic level upon treatment, T_{reg} cell proliferative capacity was lost at end-stages of tumor growth. Furthermore, in high responder TMEs, anti-PD-1 promotes the T_h1-adaptation of T_{reg} cells, a phenotype associated with T_{eff} cell evasion from T_{reg} cell-mediated suppression, and dependent on local IL-18 signaling. Finally, we identify expression of Helios as a defining feature of the population of T_{reg} cells that expands in response to PD-1 blockade.

The next frontier to enhance responsiveness to ICIs lies in the understanding of the mechanisms that govern the localization of T cell subsets within the tumor to propagate inflammation within immunosuppressed niches of the TME. Our results provide a framework for the assessment of T_{reg} cell suppressive activity *in situ* using spatial proteomics. Furthermore, they highlight that the pharmacological efficacy of PD-1 blockade varies regionally within the tumor microenvironment, which provides a strong rationale to clarify the intercellular communications that potentiate or inhibit PD-1 signaling within the tissue and allow for the propagation of inflammation to colder regions of the TME.

Understanding the functional consequences of PD-1 signaling and its blockade on T_{reg} cells is key to better understanding the role of T_{reg} cells in immune exhaustion as well as treatment failure, improving clinical care by predicting the variable outcomes of tumor immunotherapy, and reducing the onset of irAEs.

Bibliography

1. Lee S. Non-melanoma skin cancer statistics [Internet]. *Canadian Cancer Society*. https://cancer.ca/en/cancer-information/cancer-types/skin-non-melanoma/statistics. Accessed July 11, 2023.

2. Schadendorf D, et al. Melanoma. *Nat Rev Dis Primers*. 2015;1(1):1–20.

3. Lee S. Melanoma skin cancer statistics [Internet]. *Canadian Cancer Society*. 2022. https://cancer.ca/en/cancer-information/cancer-types/skin-melanoma/statistics. Accessed July 11, 2023.

4. Kim C, et al. Long-Term Survival in Patients with Metastatic Melanoma Treated with DTIC or Temozolomide. *Oncologist*. 2010;15(7):765–771.

5. Larkin JMG, et al. 5-year survival outcomes of the CheckMate 067 phase III trial of nivolumab plus ipilimumab (NIVO+IPI) combination therapy in advanced melanoma. *Annals of Oncology*. 2019;30:v904–v905.

6. Smalley KSM, Sondak VK. Melanoma--an unlikely poster child for personalized cancer therapy. *N Engl J Med*. 2010;363(9):876–878.

7. Preston S, Aras S, Zaidi MR. Spatiotemporal Labeling of Melanocytes in Mice. *Int J Mol Sci*. 2018;19(5):1469.

8. Vanover JC, et al. Stem cell factor rescues dark epidermal pigmentation in discreet anatomic locations in albino and fair-skinned mice. *Pigment Cell Melanoma Res*. 2009;22(6):827–838.

9. Griewank KG, et al. TERT Promoter Mutation Status as an Independent Prognostic Factor in Cutaneous Melanoma. *J Natl Cancer Inst*. 2014;106(9):dju246.

10. Alexandrov LB, et al. Signatures of mutational processes in human cancer. *Nature*. 2013;500(7463):415–421.

11. Davies H, et al. Mutations of the BRAF gene in human cancer. *Nature*. 2002;417(6892):949–954.

12. Dankort D, et al. Braf(V600E) cooperates with Pten loss to induce metastatic melanoma. *Nat Genet*. 2009;41(5):544–52.

13. Hodis E, et al. A Landscape of Driver Mutations in Melanoma. *Cell*. 2012;150(2):251–263.

14. Catalanotti F, et al. PTEN Loss-of-Function Alterations Are Associated With Intrinsic Resistance to BRAF Inhibitors in Metastatic Melanoma. *JCO Precision Oncology*. 2017;(1):1–15.

15. Damsky WE, et al. β-Catenin Signaling Controls Metastasis in Braf-Activated Pten-Deficient Melanomas. *Cancer Cell*. 2011;20(6):741–754.

16. Cancer Genome Atlas Network. Genomic Classification of Cutaneous Melanoma. *Cell*. 2015;161(7):1681–1696.

17. Robichaud N, et al. Phosphorylation of eIF4E promotes EMT and metastasis via translational control of SNAIL and MMP-3. *Oncogene*. 2015;34(16):2032–2042.

18. Huang F, et al. Inhibiting the MNK1/2-eIF4E axis impairs melanoma phenotype switching and potentiates antitumor immune responses. *J Clin Invest*. 2021;131(8):e140752.

19. Hoek KS, et al. In vivo switching of human melanoma cells between proliferative and invasive states. *Cancer Res*. 2008;68(3):650–656.

20. Boshuizen J, et al. Reversal of pre-existing NGFR-driven tumor and immune therapy resistance. *Nat Commun*. 2020;11(1):3946.

21. Wang J, et al. Eliciting T cell immunity against poorly immunogenic tumors by immunization with dendritic cell-tumor fusion vaccines. *J Immunol*. 1998;161(10):5516–24.

22. Meeth Katrina, et al. The YUMM lines: a series of congenic mouse melanoma cell lines with defined genetic alterations. *Pigment Cell & Melanoma Research*. 2016;29(5):590–597.

23. Jenkins MH, et al. Multiple murine BRafV600E melanoma cell lines with sensitivity to PLX4032. *Pigment Cell Melanoma Res*. 2014;27(3):495–501.

24. Boon T, et al. Human t cell responses against melanoma. *Annu Rev Immunol*. 2006;24(1):175–208.

25. Wang J, et al. UV-induced somatic mutations elicit a functional T cell response in the YUMMER1.7 Mouse Melanoma Model. *Pigment Cell Melanoma Res*. 2017;30(4):428–435.

26. Hanson HL, et al. Eradication of Established Tumors by CD8+ T Cell Adoptive Immunotherapy. *Immunity*. 2000;13(2):265–276.

27. Spranger S, et al. Tumor-Residing Batf3 Dendritic Cells Are Required for Effector T Cell Trafficking and Adoptive T Cell Therapy. *Cancer Cell*. 2017;31(5):711-723.e4.

28. Woo S-R, et al. STING-Dependent Cytosolic DNA Sensing Mediates Innate Immune Recognition of Immunogenic Tumors. *Immunity*. 2014;41(5):830–842.

29. Zaidi MR. The Interferon-Gamma Paradox in Cancer. *J Interferon Cytokine Res*. 2019;39(1):30–38.

30. Yu J, et al. Loss of MHC-I antigen presentation correlated with immune checkpoint blockade tolerance in MAPK inhibitor-resistant melanoma. *Frontiers in Pharmacology*. 2022;13. https://www.frontiersin.org/articles/10.3389/fphar.2022.928226. Accessed July 11, 2023.

31. Spranger S, Bao R, Gajewski TF. Melanoma-intrinsic β-catenin signalling prevents anti-tumour immunity. *Nature*. 2015;523(7559):231–235.

32. Rangel Rivera GO, et al. Fundamentals of T Cell Metabolism and Strategies to Enhance Cancer Immunotherapy. *Frontiers in Immunology*. 2021;12. https://www.frontiersin.org/articles/10.3389/fimmu.2021.645242. Accessed May 11, 2023.

33. Godin-Ethier J, et al. Indoleamine 2,3-dioxygenase expression in human cancers: clinical and immunologic perspectives. *Clin Cancer Res*. 2011;17(22):6985–91.

34. DeNardo DG, Ruffell B. Macrophages as regulators of tumour immunity and immunotherapy. *Nat Rev Immunol*. 2019;19(6):369–382.

35. Doedens AL, et al. Macrophage expression of hypoxia-inducible factor-1 alpha suppresses T-cell function and promotes tumor progression. *Cancer Res*. 2010;70(19):7465–7475.

36. Shinde-Jadhav S, et al. Role of neutrophil extracellular traps in radiation resistance of invasive bladder cancer. *Nat Commun*. 2021;12(1):2776.

37. Cools-Lartigue J, et al. Neutrophil extracellular traps sequester circulating tumor cells and promote metastasis. *J Clin Invest*. 2013;123(8):3446–3458.

38. Shen M, et al. Tumor-Associated Neutrophils as a New Prognostic Factor in Cancer: A Systematic Review and Meta-Analysis. *PLOS ONE*. 2014;9(6):e98259.

39. Gabrilovich DI, Nagaraj S. Myeloid-derived suppressor cells as regulators of the immune system. *Nat Rev Immunol*. 2009;9(3):162–174.

40. Sumimoto H, et al. The BRAF-MAPK signaling pathway is essential for cancer-immune evasion in human melanoma cells. *J Exp Med*. 2006;203(7):1651–1656.

41. Peng W, et al. Loss of PTEN Promotes Resistance to T Cell–Mediated Immunotherapy. *Cancer Discov*. 2016;6(2):202–216.

42. Peranzoni E, et al. Macrophages impede CD8 T cells from reaching tumor cells and limit the efficacy of anti–PD-1 treatment. *Proceedings of the National Academy of Sciences*. 2018;115(17):E4041–E4050.

43. Galon J, et al. Type, Density, and Location of Immune Cells Within Human Colorectal Tumors Predict Clinical Outcome. *Science*. 2006;313(5795):1960–1964.

44. Galon J, Bruni D. Approaches to treat immune hot, altered and cold tumours with combination immunotherapies. *Nature Reviews Drug Discovery*. 2019;18(3):197–218.

45. Gajewski TF, et al. Cancer Immunotherapy Targets Based on Understanding the T Cell-Inflamed Versus Non-T Cell-Inflamed Tumor Microenvironment. In: Kalinski P, ed. *Tumor Immune Microenvironment in Cancer Progression and Cancer Therapy*. Cham: Springer International Publishing; 2017:19–31.

46. Liu Y-T, Sun Z-J. Turning cold tumors into hot tumors by improving T-cell infiltration. *Theranostics*. 2021;11(11):5365–5386.

47. Binnewies M, et al. Understanding the tumor immune microenvironment (TIME) for effective therapy. *Nat Med*. 2018;24(5):541–550.

48. Jackaman C, et al. Chemotherapy broadens the range of tumor antigens seen by cytotoxic CD8(+) T cells in vivo. *Cancer Immunol Immunother*. 2012;61(12):2343–2356.

49. Cabrita R, et al. Tertiary lymphoid structures improve immunotherapy and survival in melanoma. *Nature*. 2020;577(7791):561–565.

50. Martinet L, et al. Human solid tumors contain high endothelial venules: association with T- and B-lymphocyte infiltration and favorable prognosis in breast cancer. *Cancer Res*. 2011;71(17):5678–5687.

51. Sautès-Fridman C, et al. Tertiary lymphoid structures in the era of cancer immunotherapy. *Nat Rev Cancer*. 2019;19(6):307–325.

52. Kroeger DR, Milne K, Nelson BH. Tumor-Infiltrating Plasma Cells Are Associated with Tertiary Lymphoid Structures, Cytolytic T-Cell Responses, and Superior Prognosis in Ovarian Cancer. *Clin Cancer Res*. 2016;22(12):3005–3015.

53. Muraoka D, et al. Antigen delivery targeted to tumor-associated macrophages overcomes tumor immune resistance. *J Clin Invest*. 2019;129(3):1278–1294.

54. Shin DS, et al. Primary resistance to PD-1 blockade mediated by JAK1/2 mutations. *Cancer Discov*. 2017;7(2):188–201.

55. Jacquelot N, et al. Sustained Type I interferon signaling as a mechanism of resistance to PD-1 blockade. *Cell Res*. 2019;29(10):846–861.

56. Clark NM, et al. Regulatory T Cells Support Breast Cancer Progression by Opposing IFN-γ-Dependent Functional Reprogramming of Myeloid Cells. *Cell Rep*. 2020;33(10):108482.

57. Taube JM, et al. Colocalization of Inflammatory Response with B7-H1 Expression in Human Melanocytic Lesions Supports an Adaptive Resistance Mechanism of Immune Escape. *Sci Transl Med*. 2012;4(127):127ra37.

58. Rudd CE, Taylor A, Schneider H. CD28 and CTLA-4 coreceptor expression and signal transduction. *Immunol Rev*. 2009;229(1):12–26.

59. Marasco M, et al. Molecular mechanism of SHP2 activation by PD-1 stimulation. *Sci Adv*. 2020;6(5):eaay4458.

60. Parry RV, et al. CTLA-4 and PD-1 receptors inhibit T-cell activation by distinct mechanisms. *Mol Cell Biol*. 2005;25(21):9543–53.

61. Bally APR, Austin JW, Boss JM. Genetic and Epigenetic Regulation of PD-1 Expression. *JI*. 2016;196(6):2431–2437.

62. Philip M, et al. Chromatin states define tumour-specific T cell dysfunction and reprogramming. *Nature*. 2017;545(7655):452–456.

63. Beltra J-C, et al. Developmental Relationships of Four Exhausted CD8+ T Cell Subsets Reveals Underlying Transcriptional and Epigenetic Landscape Control Mechanisms. *Immunity*. 2020;52(5):825-841.e8.

64. Miller BC, et al. Subsets of exhausted CD8+ T cells differentially mediate tumor control and respond to checkpoint blockade. *Nat Immunol*. 2019;20(3):326–336.

65. Paley MA, et al. Progenitor and terminal subsets of CD8+ T cells cooperate to contain chronic viral infection. *Science*. 2012;338(6111):1220–1225.

66. Blank CU, et al. Defining 'T cell exhaustion.' *Nature Reviews Immunology*. 2019;19(11):665–674.

67. Philip M, Schietinger A. Heterogeneity and fate choice: T cell exhaustion in cancer and chronic infections. *Curr Opin Immunol*. 2019;58:98–103.

68. Simoni Y, et al. Bystander CD8+ T cells are abundant and phenotypically distinct in human tumour infiltrates. *Nature*. 2018;557(7706):575–579.

69. Ahrends T, et al. CD4+ T Cell Help Confers a Cytotoxic T Cell Effector Program Including Coinhibitory Receptor Downregulation and Increased Tissue Invasiveness. *Immunity*. 2017;47(5):848-861.e5.

70. Sakaguchi S, et al. Regulatory T cells and immune tolerance. *Cell*. 2008;133(5):775–787.

71. Sakaguchi S, et al. Immunologic self-tolerance maintained by activated T cells expressing IL-2 receptor alpha-chains (CD25). Breakdown of a single mechanism of self-tolerance causes various autoimmune diseases. *The Journal of Immunology*. 1995;155(3):1151.

72. Komatsu N, et al. Heterogeneity of natural Foxp3+ T cells: A committed regulatory T-cell lineage and an uncommitted minor population retaining plasticity. *PNAS*. 2009;106(6):1903–1908.

73. Bennett CL, et al. The immune dysregulation, polyendocrinopathy, enteropathy, X-linked syndrome (IPEX) is caused by mutations of FOXP3. *Nature Genetics*. 2001;27:20.

74. Brunkow ME, et al. Disruption of a new forkhead/winged-helix protein, scurfin, results in the fatal lymphoproliferative disorder of the scurfy mouse. *Nature Genetics*. 2001;27:68.

75. Zorn E, et al. IL-2 regulates FOXP3 expression in human CD4+CD25+ regulatory T cells through a STAT-dependent mechanism and induces the expansion of these cells in vivo. *Blood*. 2006;108(5):1571–1579.

76. Yao Z, et al. Nonredundant roles for Stat5a/b in directly regulating Foxp3. *Blood*. 2007;109(10):4368.

77. Hsieh C-S, Lee H-M, Lio C-WJ. Selection of regulatory T cells in the thymus. *Nature Reviews Immunology*. 2012;12:157.

78. Thornton AM, et al. Expression of Helios, an Ikaros transcription factor family member, differentiates thymic-derived from peripherally induced Foxp3+ T regulatory cells. *J Immunol*. 2010;184(7):3433–41.

79. Davidson TS, et al. Cutting Edge: IL-2 is essential for TGF-beta-mediated induction of Foxp3+ T regulatory cells. *J Immunol*. 2007;178(7):4022–4026.

80. Moo-Young TA, et al. Tumor-derived TGF-β Mediates Conversion of CD4+Foxp3+ Regulatory T Cells in a Murine Model of Pancreas Cancer. *Journal of Immunotherapy*. 2009;32(1):12–21.

81. Bilate AM, Lafaille JJ. Induced CD4+Foxp3+ Regulatory T Cells in Immune Tolerance. *Annual Review of Immunology*. 2012;30(1):733–758.

82. Syed Khaja AS, et al. Preferential accumulation of regulatory T cells with highly immunosuppressive characteristics in breast tumor microenvironment. *Oncotarget*. 2017;8(20):33159–33171.

83. Syed Khaja AS, et al. Intratumoral FoxP3+Helios+ Regulatory T Cells Upregulating Immunosuppressive Molecules Are Expanded in Human Colorectal Cancer. *Front Immunol*. 2017;8:619.

84. Gottschalk RA, Corse E, Allison JP. Expression of Helios in peripherally induced Foxp3+ regulatory T cells. *J Immunol*. 2012;188(3):976–980.

85. Quatromoni JG, et al. T cell receptor transgenic lymphocytes infiltrating murine tumors are not induced to express foxp3. *J Hematol Oncol*. 2011;4:48.

86. Miragaia RJ, et al. Single-Cell Transcriptomics of Regulatory T Cells Reveals Trajectories of Tissue Adaptation. *Immunity*. 2019;50(2):493-504.e7.

87. Sainz-Perez A, et al. The T-cell Receptor Repertoire of Tumor-Infiltrating Regulatory T Lymphocytes Is Skewed Toward Public Sequences. *Cancer Res*. 2012;72(14):3557–3569.

88. Bonertz A, et al. Antigen-specific Tregs control T cell responses against a limited repertoire of tumor antigens in patients with colorectal carcinoma. *J Clin Invest*. 2009;119(11):3311–21.

89. Ahmadzadeh M, et al. Tumor-infiltrating human CD4+ regulatory T cells display a distinct TCR repertoire and exhibit tumor and neoantigen reactivity. *Sci Immunol*. 2019;4(31). https://doi.org/10.1126/sciimmunol.aao4310.

90. Fourcade J, et al. Human tumor antigen-specific helper and regulatory T cells share common epitope specificity but exhibit distinct T cell repertoire. *J Immunol*. 2010;184(12):6709–6718.

91. Cao X, et al. Granzyme B and perforin are important for regulatory T cell-mediated suppression of tumor clearance. *Immunity*. 2007;27(4):635–46.

92. Strauss L, et al. A unique subset of CD4+CD25highFoxp3+ T cells secreting interleukin-10 and transforming growth factor-beta1 mediates suppression in the tumor microenvironment. *Clin Cancer Res*. 2007;13(15 Pt 1):4345–54.

93. Mirlekar B. Tumor promoting roles of IL-10, TGF-β, IL-4, and IL-35: Its implications in cancer immunotherapy. *SAGE Open Med*. 2022;10:20503121211069012.

94. Liang B, et al. Regulatory T cells inhibit dendritic cells by lymphocyte activation gene-3 engagement of MHC class II. *J Immunol*. 2008;180(9):5916–5926.

95. Tekguc M, et al. Treg-expressed CTLA-4 depletes CD80/CD86 by trogocytosis, releasing free PD-L1 on antigen-presenting cells. *Proc Natl Acad Sci USA*. 2021;118(30):e2023739118.

96. Cederbom L, Hall H, Ivars F. CD4+CD25+ regulatory T cells down-regulate co-stimulatory molecules on antigen-presenting cells. *Eur J Immunol*. 2000;30(6):1538–43.

97. Fallarino F, et al. Modulation of tryptophan catabolism by regulatory T cells. *Nat Immunol*. 2003;4(12):1206–12.

98. Deaglio S, et al. Adenosine generation catalyzed by CD39 and CD73 expressed on regulatory T cells mediates immune suppression. *J Exp Med*. 2007;204(6):1257–1265.

99. Maj T, et al. Oxidative stress controls regulatory T cell apoptosis and suppressor activity and PD-L1-blockade resistance in tumor. *Nat Immunol*. 2017;18(12):1332–1341.

100. Bopp T, et al. Cyclic adenosine monophosphate is a key component of regulatory T cell-mediated suppression. *J Exp Med*. 2007;204(6):1303–1310.

101. Pandiyan P, et al. CD4+CD25+Foxp3+ regulatory T cells induce cytokine deprivation-mediated apoptosis of effector CD4+ T cells. *Nat Immunol*. 2007;8(12):1353–62.

102. Curiel TJ, et al. Specific recruitment of regulatory T cells in ovarian carcinoma fosters immune privilege and predicts reduced survival. *Nature Medicine*. 2004;10(9):942–949.

103. Francisco LM, et al. PD-L1 regulates the development, maintenance, and function of induced regulatory T cells. *J Exp Med*. 2009;206(13):3015–3029.

104. Ribas A, et al. Intratumoral Immune Cell Infiltrates, FoxP3, and Indoleamine 2,3-Dioxygenase in Patients with Melanoma Undergoing CTLA4 Blockade. *Clinical Cancer Research*. 2008;15(1):390–399.

105. Pacella I, et al. Fatty acid metabolism complements glycolysis in the selective regulatory T cell expansion during tumor growth. *PNAS*. 2018;115(28):E6546–E6555.

106. Miska J, et al. HIF-1α Is a Metabolic Switch between Glycolytic-Driven Migration and Oxidative Phosphorylation-Driven Immunosuppression of Tregs in Glioblastoma. *Cell Reports*. 2019;27(1):226-237.e4.

107. Fisher SA, et al. Transient Treg depletion enhances therapeutic anti-cancer vaccination. *Immun Inflamm Dis*. 2016;5(1):16–28.

108. Klages K, et al. Selective Depletion of Foxp3+ Regulatory T Cells Improves Effective Therapeutic Vaccination against Established Melanoma. *Cancer Research*. 2010;70(20):7788–7799.

109. Boissonnas A, et al. Foxp3+ T Cells Induce Perforin-Dependent Dendritic Cell Death in Tumor-Draining Lymph Nodes. *Immunity*. 2010;32(2):266–278.

110. Jones E, et al. Depletion of CD25+ regulatory cells results in suppression of melanoma growth and induction of autoreactivity in mice. *Cancer Immun*. 2002;2:1.

111. Overacre-Delgoffe AE, et al. Interferon-γ Drives Treg Fragility to Promote Anti-tumor Immunity. *Cell*. 2017;169(6):1130-1141.e11.

112. Nakagawa H, et al. Instability of Helios-deficient Tregs is associated with conversion to a T-effector phenotype and enhanced antitumor immunity. *PNAS*. 2016;113(22):6248–6253.

113. Rudra D, et al. Transcription factor Foxp3 and its protein partners form a complex regulatory network. *Nature Immunology*. 2012;13(10):1010–1019.

114. Kim H-J, et al. Stable inhibitory activity of regulatory T cells requires the transcription factor Helios. *Science*. 2015;350(6258):334–339.

115. Sebastian M, et al. Helios Controls a Limited Subset of Regulatory T Cell Functions. *The Journal of Immunology*. 2016;196(1):144–155.

116. Yates K, et al. Comparative transcriptome analysis reveals distinct genetic modules associated with Helios expression in intratumoral regulatory T cells. *PNAS*. 2018;115(9):2162–2167.

117. Hoffmann P, et al. Loss of FOXP3 expression in natural human CD4+CD25+ regulatory T cells upon repetitive in vitro stimulation. *European Journal of Immunology*. 2009;39(4):1088–1097.

118. Thornton AM, et al. Helios+ and Helios− Treg subpopulations are phenotypically and functionally distinct and express dissimilar TCR repertoires. *European Journal of Immunology*. 2019;49(3):398–412.

119. Yang YH, et al. Salt Sensing by Serum/Glucocorticoid-Regulated Kinase 1 Promotes Th17-like Inflammatory Adaptation of Foxp3+ Regulatory T Cells. *Cell Reports*. 2020;30(5):1515-1529.e4.

120. Duhen T, et al. Functionally distinct subsets of human FOXP3+ Treg cells that phenotypically mirror effector Th cells. *Blood*. 2012;119(19):4430–4440.

121. Koch MA, et al. T-bet+ Treg Cells Undergo Abortive Th1 Cell Differentiation due to Impaired Expression of IL-12 Receptor β2. *Immunity*. 2012;37(3):501–510.

122. Alvarez F, et al. Mechanisms of TREG cell adaptation to inflammation. *Journal of Leukocyte Biology*. 2020;108(2):559–571.

123. Redjimi N, et al. CXCR3+ T regulatory cells selectively accumulate in human ovarian carcinomas to limit type I immunity. *Cancer Res*. 2012;72(17):4351–4360.

124. Santegoets SJ, et al. Tbet-positive regulatory T cells accumulate in oropharyngeal cancers with ongoing tumor-specific type 1 T cell responses. *Journal for ImmunoTherapy of Cancer*. 2019;7(1):14.

125. Moreno Ayala MA, et al. CXCR3 expression in regulatory T cells drives interactions with type I dendritic cells in tumors to restrict CD8+ T cell antitumor immunity. *Immunity*. [published online ahead of print: June 30, 2023]. https://doi.org/10.1016/j.immuni.2023.06.003.

126. Zhao J, Zhao J, Perlman S. Differential Effects of IL-12 on Tregs and Non-Treg T Cells: Roles of IFN-γ, IL-2 and IL-2R. *PLOS ONE*. 2012;7(9):e46241.

127. Duarte João H, et al. Natural Treg cells spontaneously differentiate into pathogenic helper cells in lymphopenic conditions. *European Journal of Immunology*. 2009;39(4):948–955.

128. Yurchenko E, et al. Inflammation-driven reprogramming of CD4+ Foxp3+ regulatory T cells into pathogenic Th1/Th17 T effectors is abrogated by mTOR inhibition in vivo. *PLOS ONE*. 2012;7(4):e35572.

129. Sharma MD, et al. Reprogrammed Foxp3+ Regulatory T Cells Provide Essential Help to Support Cross-presentation and CD8+ T Cell Priming in Naive Mice. *Immunity*. 2010;33(6):942–954.

130. Munn DH, Mellor AL. IDO in the Tumor Microenvironment: Inflammation, Counter-Regulation, and Tolerance. *Trends Immunol*. 2016;37(3):193–207.

131. Alvarez F, et al. The alarmins IL-1 and IL-33 differentially regulate the functional specialisation of Foxp3+ regulatory T cells during mucosal inflammation. *Mucosal Immunol*. 2019;12(3):746–760.

132. Ahn HJ, et al. A mechanism underlying synergy between IL-12 and IFN-gamma-inducing factor in enhanced production of IFN-gamma. *The Journal of Immunology*. 1997;159(5):2125–2131.

133. Li W, et al. Protection of CD8+ T cells from activation-induced cell death by IL-18. *J Leukoc Biol*. 2007;82(1):142–151.

134. Halvorsen EC, et al. IL-33 increases ST2+ Tregs and promotes metastatic tumour growth in the lungs in an amphiregulin-dependent manner. *Oncoimmunology*. 2018;8(2):e1527497.

135. Alvarez F, et al. IL-18 is required for the TH1-adaptation of TREG cells and the selective suppression of TH17 responses in acute and chronic infections. *Mucosal Immunol*. 2023;S1933-0219(23)00035–1.

136. Arpaia N, et al. A Distinct Function of Regulatory T Cells in Tissue Protection. *Cell*. 2015;162(5):1078–1089.

137. Ma Z, et al. Augmentation of Immune Checkpoint Cancer Immunotherapy with IL18. *Clinical Cancer Research*. 2016;22(12):2969–2980.

138. Lutz V, et al. IL18 Receptor Signaling Regulates Tumor-Reactive CD8+ T-cell Exhaustion via Activation of the IL2/STAT5/mTOR Pathway in a Pancreatic Cancer Model. *Cancer Immunology Research*. 2023;11(4):421–434.

139. Chakraborty S, et al. Transcriptional regulation of FOXP3 requires integrated activation of both promoter and CNS regions in tumor-induced CD8+ Treg cells. *Sci Rep*. 2017;7:1628.

140. Bromley SK, Mempel TR, Luster AD. Orchestrating the orchestrators: chemokines in control of T cell traffic. *Nat Immunol*. 2008;9(9):970–980.

141. Halim L, et al. An Atlas of Human Regulatory T Helper-like Cells Reveals Features of Th2-like Tregs that Support a Tumorigenic Environment. *Cell Rep*. 2017;20(3):757–770.

142. Schiering C, et al. The alarmin IL-33 promotes regulatory T-cell function in the intestine. *Nature*. 2014;513(7519):564–568.

143. Siede J, et al. IL-33 Receptor-Expressing Regulatory T Cells Are Highly Activated, Th2 Biased and Suppress CD4 T Cell Proliferation through IL-10 and TGFβ Release. *PLoS One*. 2016;11(8):e0161507.

144. Li A, et al. IL-33 Signaling Alters Regulatory T Cell Diversity in Support of Tumor Development. *Cell Rep*. 2019;29(10):2998-3008.e8.

145. Hatzioannou A, et al. An intrinsic role of IL-33 in Treg cell-mediated tumor immunoevasion. *Nat Immunol*. 2020;21(1):75–85.

146. Lochner M, et al. In vivo equilibrium of proinflammatory IL-17+ and regulatory IL-10+ Foxp3+ RORgamma t+ T cells. *J Exp Med*. 2008;205(6):1381–1393.

147. Yang B-H, et al. Foxp3(+) T cells expressing RORγt represent a stable regulatory T-cell effector lineage with enhanced suppressive capacity during intestinal inflammation. *Mucosal Immunol*. 2016;9(2):444–457.

148. Blatner NR, et al. Expression of RORγt Marks a Pathogenic Regulatory T Cell Subset in Human Colon Cancer. *Sci Transl Med*. 2012;4(164):164ra159.

149. Chang L-Y, et al. Tumor-derived chemokine CCL5 enhances TGF-β-mediated killing of CD8(+) T cells in colon cancer by T-regulatory cells. *Cancer Res*. 2012;72(5):1092–1102.

150. Saito T, et al. Two FOXP3(+)CD4(+) T cell subpopulations distinctly control the prognosis of colorectal cancers. *Nat Med*. 2016;22(6):679–84.

151. Tosolini M, et al. Clinical impact of different classes of infiltrating T cytotoxic and helper cells (Th1, th2, treg, th17) in patients with colorectal cancer. *Cancer Res*. 2011;71(4):1263–1271.

152. Correale P, et al. Regulatory (FoxP3+) T-cell tumor infiltration is a favorable prognostic factor in advanced colon cancer patients undergoing chemo or chemoimmunotherapy. *J Immunother*. 2010;33(4):435–441.

153. Salama P, et al. Tumor-infiltrating FOXP3+ T regulatory cells show strong prognostic significance in colorectal cancer. *J Clin Oncol*. 2009;27(2):186–192.

154. Erdman SE, et al. CD4(+)CD25(+) regulatory lymphocytes require interleukin 10 to interrupt colon carcinogenesis in mice. *Cancer Res*. 2003;63(18):6042–6050.

155. Rizzo A, et al. RORγt-Expressing Tregs Drive the Growth of Colitis-Associated Colorectal Cancer by Controlling IL6 in Dendritic Cells. *Cancer Immunology Research*. 2018;6(9):1082–1092.

156. Tang A, Harding F. The challenges and molecular approaches surrounding interleukin-2-based therapeutics in cancer. *Cytokine X*. 2018;1(1):100001.

157. Kim JW, Eder JP. Prospects for targeting PD-1 and PD-L1 in various tumor types. *Oncology (Williston Park, NY)*. 2014;28 Suppl 3:15–28.

158. Luke JJ, et al. Pembrolizumab versus placebo as adjuvant therapy in completely resected stage IIB or IIC melanoma (KEYNOTE-716): a randomised, double-blind, phase 3 trial. *Lancet*. 2022;399(10336):1718–1729.

159. Long GV, et al. Adjuvant Dabrafenib plus Trametinib in Stage III BRAF-Mutated Melanoma. *N Engl J Med*. 2017;377(19):1813–1823.

160. Weber J, et al. Adjuvant Nivolumab versus Ipilimumab in Resected Stage III or IV Melanoma. *N Engl J Med*. 2017;377(19):1824–1835.

161. Tarhini AA, et al. Phase III Study of Adjuvant Ipilimumab (3 or 10 mg/kg) Versus High-Dose Interferon Alfa-2b for Resected High-Risk Melanoma: North American Intergroup E1609. *JCO*. 2020;38(6):567–575.

162. Weber JS, et al. Nivolumab versus chemotherapy in patients with advanced melanoma who progressed after anti-CTLA-4 treatment (CheckMate 037): a randomised, controlled, open-label, phase 3 trial. *Lancet Oncol*. 2015;16(4):375–84.

163. Treatment of Melanoma by Stage [Internet]. https://www.cancer.org/cancer/types/melanoma-skin-cancer/treating/by-stage.html. Accessed June 28, 2023.

164. Patel SP, et al. Neoadjuvant–Adjuvant or Adjuvant-Only Pembrolizumab in Advanced Melanoma. *New England Journal of Medicine*. 2023;388(9):813–823.

165. Lucas MW, et al. The NADINA trial: A multicenter, randomised, phase 3 trial comparing the efficacy of neoadjuvant ipilimumab plus nivolumab with standard adjuvant nivolumab in macroscopic resectable stage III melanoma. *JCO*. 2022;40(16_suppl):TPS9605–TPS9605.

166. Delgado A, Guddati AK. Clinical endpoints in oncology - a primer. *Am J Cancer Res*. 2021;11(4):1121–1131.

167. Wolchok JD, et al. CheckMate 067: 6.5-year outcomes in patients (pts) with advanced melanoma. *JCO*. 2021;39(15_suppl):9506–9506.

168. Larkin J, Hodi FS, Wolchok JD. Combined Nivolumab and Ipilimumab or Monotherapy in Untreated Melanoma. *N Engl J Med*. 2015;373(13):1270–1.

169. Nishijima TF, et al. Safety and Tolerability of PD-1/PD-L1 Inhibitors Compared with Chemotherapy in Patients with Advanced Cancer: A Meta-Analysis. *Oncologist*. 2017;22(4):470–479.

170. Burzykowski T, et al. Evaluation of tumor response, disease control, progression-free survival, and time to progression as potential surrogate end points in metastatic breast cancer. *J Clin Oncol*. 2008;26(12):1987–1992.

171. Seymour L, et al. iRECIST: guidelines for response criteria for use in trials testing immunotherapeutics. *Lancet Oncol*. 2017;18(3):e143–e152.

172. Park HJ, et al. Incidence of Pseudoprogression during Immune Checkpoint Inhibitor Therapy for Solid Tumors: A Systematic Review and Meta-Analysis. *Radiology*. 2020;297(1):87–96.

173. Borcoman E, et al. Novel patterns of response under immunotherapy. *Annals of Oncology*. 2019;30(3):385–396.

174. Champiat S, et al. Hyperprogressive Disease Is a New Pattern of Progression in Cancer Patients Treated by Anti-PD-1/PD-L1. *Clin Cancer Res*. 2017;23(8):1920–1928.

175. Kanjanapan Y, et al. Hyperprogressive disease in early-phase immunotherapy trials: Clinical predictors and association with immune-related toxicities. *Cancer*. 2019;125(8):1341–1349.

176. Kamada T, et al. PD-1+ regulatory T cells amplified by PD-1 blockade promote hyperprogression of cancer. *PNAS*. 2019;116(20):9999–10008.

177. Borcoman E, et al. Patterns of Response and Progression to Immunotherapy. *American Society of Clinical Oncology Educational Book*. 2018;(38):169–178.

178. European Medicines Agency. European Medicines Agency: EMEA/H/C/003985—Nivolumab Product information 19/06/2015 Opdivo [Internet]. *European Medicines Agency*. 2018.

179. Champiat S, et al. Management of immune checkpoint blockade dysimmune toxicities: a collaborative position paper. *Ann Oncol*. 2016;27(4):559–74.

180. Gibney GT, et al. Safety, Correlative Markers, and Clinical Results of Adjuvant Nivolumab in Combination with Vaccine in Resected High-Risk Metastatic Melanoma. *Clin Cancer Res*. 2015;21(4):712–720.

181. Wang DY, et al. Fatal Toxic Effects Associated With Immune Checkpoint Inhibitors: A Systematic Review and Meta-analysis. *JAMA Oncol*. 2018;4(12):1721–1728.

182. Lengagne R, et al. Spontaneous Vitiligo in an Animal Model for Human Melanoma: Role of Tumor-specific CD8+ T Cells. *Cancer Res*. 2004;64(4):1496–1501.

183. Nakashima C, et al. Identification of CD49a+ CD8+ resident memory T cells in vitiligo-like lesions associated with nivolumab treatment for melanoma. *J Eur Acad Dermatol Venereol*. 2020;34(2):e79–e82.

184. Nardin C, et al. Vitiligo under anti–programmed cell death-1 therapy is associated with increased survival in melanoma patients. *Journal of the American Academy of Dermatology*. 2020;82(3):770–772.

185. Weber JS, et al. Safety Profile of Nivolumab Monotherapy: A Pooled Analysis of Patients With Advanced Melanoma. *JCO*. 2016;35(7):785–792.

186. Nowicki TS, et al. Infiltration of CD8 T cells and expression of PD-1 and PD-L1 in synovial sarcoma. *Cancer Immunol Res*. 2017;5(2):118–126.

187. Kümpers C, et al. Immune Cell Infiltration of the Primary Tumor, Not PD-L1 Status, Is Associated With Improved Response to Checkpoint Inhibition in Metastatic Melanoma. *Front Med (Lausanne)*. 2019;6:27.

188. Chow MT, et al. Intratumoral Activity of the CXCR3 Chemokine System Is Required for the Efficacy of Anti-PD-1 Therapy. *Immunity*. 2019;50(6):1498-1512.e5.

189. Im SJ, et al. Defining CD8+ T cells that provide the proliferative burst after PD-1 therapy. *Nature*. 2016;537(7620):417–421.

190. Ngiow SF, et al. A Threshold Level of Intratumor CD8+ T-cell PD1 Expression Dictates Therapeutic Response to Anti-PD1. *Cancer Res*. 2015;75(18):3800–3811.

191. Kamphorst AO, et al. Rescue of exhausted CD8 T cells by PD-1–targeted therapies is CD28-dependent. *Science*. 2017;355(6332):1423–1427.

192. Aranda F, et al. Adjuvant combination and antigen targeting as a strategy to induce polyfunctional and high-avidity T-cell responses against poorly immunogenic tumors. *Cancer Res*. 2011;71(9):3214–3224.

193. Wang S, et al. Intratumoral injection of a CpG oligonucleotide reverts resistance to PD-1 blockade by expanding multifunctional CD8+ T cells. *Proceedings of the National Academy of Sciences*. 2016;113(46):E7240–E7249.

194. Wimmers F, et al. Long-lasting multifunctional CD8+ T cell responses in end-stage melanoma patients can be induced by dendritic cell vaccination. *OncoImmunology*. 2016;5(1):e1067745.

195. Curran MA, et al. PD-1 and CTLA-4 combination blockade expands infiltrating T cells and reduces regulatory T and myeloid cells within B16 melanoma tumors. *PNAS*. 2010;107(9):4275–4280.

196. Goda N, et al. The ratio of CD8 + lymphocytes to tumor-infiltrating suppressive FOXP3 + effector regulatory T cells is associated with treatment response in invasive breast cancer. *Discov Onc*. 2022;13(1):27.

197. Phillips D, et al. Immune cell topography predicts response to PD-1 blockade in cutaneous T cell lymphoma. *Nat Commun*. 2021;12(1):6726.

198. Gide TN, et al. Close proximity of immune and tumor cells underlies response to anti-PD-1 based therapies in metastatic melanoma patients. *Oncoimmunology*. 2019;9(1):1659093.

199. Chen JH, et al. Spatial analysis of human lung cancer reveals organized immune hubs enriched for stem-like CD8 T cells and associated with immunotherapy response. *bioRxiv*. 2023;2023.04.04.535379.

200. Kamphorst AO, et al. Proliferation of PD-1+ CD8 T cells in peripheral blood after PD-1-targeted therapy in lung cancer patients. *Proc Natl Acad Sci USA*. 2017;114(19):4993–4998.

201. Fessas P, et al. A molecular and preclinical comparison of the PD-1–targeted T-cell checkpoint inhibitors nivolumab and pembrolizumab. *Semin Oncol*. 2017;44(2):136–140.

202. Dahan R, et al. FcγRs Modulate the Anti-tumor Activity of Antibodies Targeting the PD-1/PD-L1 Axis. *Cancer Cell*. 2015;28(3):285–295.

203. Ingram JR, et al. Anti–CTLA-4 therapy requires an Fc domain for efficacy. *PNAS*. 2018;115(15):3912–3917.

204. Simpson TR, et al. Fc-dependent depletion of tumor-infiltrating regulatory T cells co-defines the efficacy of anti–CTLA-4 therapy against melanoma. *Journal of Experimental Medicine*. 2013;210(9):1695–1710.

205. Romano E, et al. Ipilimumab-dependent cell-mediated cytotoxicity of regulatory T cells ex vivo by nonclassical monocytes in melanoma patients. *Proc Natl Acad Sci U S A*. 2015;112(19):6140–5.

206. Arce Vargas F, et al. Fc Effector Function Contributes to the Activity of Human Anti-CTLA-4 Antibodies. *Cancer Cell*. 2018;33(4):649-663.e4.

207. Davis-Marcisak EF, et al. Transfer learning between preclinical models and human tumors identifies a conserved NK cell activation signature in anti-CTLA-4 responsive tumors. *Genome Med*. 2021;13(1):1–22.

208. Sharma A, et al. Anti-CTLA-4 Immunotherapy Does Not Deplete FOXP3+ Regulatory T Cells (Tregs) in Human Cancers. *Clin Cancer Res*. 2019;25(4):1233–1238.

209. Marangoni F, et al. Expansion of tumor-associated Treg cells upon disruption of a CTLA-4-dependent feedback loop. *Cell*. 2021;184(15):3998-4015.e19.

210. Kavanagh B, et al. CTLA4 blockade expands FoxP3+ regulatory and activated effector CD4+ T cells in a dose-dependent fashion. *Blood*. 2008;112(4):1175–1183.

211. Peggs KS, et al. Blockade of CTLA-4 on both effector and regulatory T cell compartments contributes to the antitumor activity of anti–CTLA-4 antibodies. *Journal of Experimental Medicine*. 2009;206(8):1717–1725.

212. Wei SC, et al. Distinct Cellular Mechanisms Underlie Anti-CTLA-4 and Anti-PD-1 Checkpoint Blockade. *Cell*. 2017;170(6):1120-1133.e17.

213. Gibney GT, Weiner LM, Atkins MB. Predictive biomarkers for checkpoint inhibitor-based immunotherapy. *Lancet Oncol*. 2016;17(12):e542–e551.

214. Daud AI, et al. Tumor immune profiling predicts response to anti–PD-1 therapy in human melanoma. *J Clin Invest*. 2016;126(9):3447–3452.

215. André T, et al. Pembrolizumab in Microsatellite-Instability–High Advanced Colorectal Cancer. *New England Journal of Medicine*. 2020;383(23):2207–2218.

216. Kumagai S, et al. The PD-1 expression balance between effector and regulatory T cells predicts the clinical efficacy of PD-1 blockade therapies. *Nature Immunology*. 2020;21(11):1346–1358.

217. Flores-Borja F, et al. Defects in CTLA-4 are associated with abnormal regulatory T cell function in rheumatoid arthritis. *Proc Natl Acad Sci USA*. 2008;105(49):19396–19401.

218. Kornete M, Sgouroudis E, Piccirillo CA. ICOS-dependent homeostasis and function of Foxp3+ regulatory T cells in islets of nonobese diabetic mice. *J Immunol*. 2012;188(3):1064–74.

219. Dhuban KB, et al. Coexpression of TIGIT and FCRL3 Identifies Helios+ Human Memory Regulatory T Cells. *The Journal of Immunology*. 2015;194(8):3687–3696.

220. Kornete M, et al. Th1-Like ICOS+ Foxp3+ Treg Cells Preferentially Express CXCR3 and Home to β-Islets during Pre-Diabetes in BDC2.5 NOD Mice. *PLOS ONE*. 2015;10(5):e0126311.

221. Joller N, et al. Treg cells expressing the coinhibitory molecule TIGIT selectively inhibit proinflammatory Th1 and Th17 cell responses. *Immunity*. 2014;40(4):569–581.

222. Chen Xiufen, et al. PD-1 regulates extrathymic regulatory T-cell differentiation. *European Journal of Immunology*. 2014;44(9):2603–2616.

223. Tan CL, et al. PD-1 restraint of regulatory T cell suppressive activity is critical for immune tolerance. *Journal of Experimental Medicine*. 2020;218(e20182232). https://doi.org/10.1084/jem.20182232.

224. Gianchecchi E, Fierabracci A. Inhibitory Receptors and Pathways of Lymphocytes: The Role of PD-1 in Treg Development and Their Involvement in Autoimmunity Onset and Cancer Progression. *Front Immunol*. 2018;9. https://doi.org/10.3389/fimmu.2018.02374.

225. Kim MJ, et al. Deletion of PD-1 destabilizes the lineage identity and metabolic fitness of tumor-infiltrating regulatory T cells. *Nat Immunol*. 2023;24(1):148–161.

226. Sauer S, et al. T cell receptor signaling controls Foxp3 expression via PI3K, Akt, and mTOR. *PNAS*. 2008;105(22):7797–7802.

227. Patsoukis N, et al. Selective Effects of PD-1 on Akt and Ras Pathways Regulate Molecular Components of the Cell Cycle and Inhibit T Cell Proliferation. *Sci Signal*. 2012;5(230):ra46.

228. Wang C, et al. In Vitro Characterization of the Anti-PD-1 Antibody Nivolumab, BMS-936558, and In Vivo Toxicology in Non-Human Primates. *Cancer Immunol Res*. 2014;2(9):846–856.

229. Stathopoulou C, et al. PD-1 Inhibitory Receptor Downregulates Asparaginyl Endopeptidase and Maintains Foxp3 Transcription Factor Stability in Induced Regulatory T Cells. *Immunity*. 2018;49(2):247-263.e7.

230. Zhang B, et al. Nonoverlapping roles of PD-1 and FoxP3 in maintaining immune tolerance in a novel autoimmune pancreatitis mouse model. *PNAS*. 2016;113(30):8490–8495.

231. Lal G, et al. Epigenetic regulation of Foxp3 expression in regulatory T cells by DNA methylation. *J Immunol*. 2009;182(1):259–273.

232. Kumagai S, et al. Lactic acid promotes PD-1 expression in regulatory T cells in highly glycolytic tumor microenvironments. *Cancer Cell*. 2022;40(2):201-218.e9.

233. West EE, et al. PD-L1 blockade synergizes with IL-2 therapy in reinvigorating exhausted T cells. *J Clin Invest*. 2013;123(6):2604–2615.

234. Preillon J, et al. Restoration of T-cell Effector Function, Depletion of Tregs, and Direct Killing of Tumor Cells: The Multiple Mechanisms of Action of a-TIGIT Antagonist Antibodies. *Molecular Cancer Therapeutics*. 2021;20(1):121–131.

235. Sainson RCA, et al. An Antibody Targeting ICOS Increases Intratumoral Cytotoxic to Regulatory T-cell Ratio and Induces Tumor Regression. *Cancer Immunology Research*. 2020;8(12):1568–1582.

236. Huang C-T, et al. Role of LAG-3 in regulatory T cells. *Immunity*. 2004;21(4):503–513.

237. Kirsch I, Vignali M, Robins H. T-cell receptor profiling in cancer. *Molecular Oncology*. 2015;9(10):2063–2070.

238. Lathrop SK, et al. Peripheral education of the immune system by colonic commensal microbiota. *Nature*. 2011;478(7368):250–4.

239. Spain L, Larkin J, Turajlic S. New survival standards for advanced melanoma. *Br J Cancer*. 2020;122(9):1275–1276.

240. Wolchok JD, et al. Long-Term Outcomes With Nivolumab Plus Ipilimumab or Nivolumab Alone Versus Ipilimumab in Patients With Advanced Melanoma. *JCO*. 2022;40(2):127–137.

241. Li B, et al. Anti-programmed death-1 synergizes with granulocyte macrophage colony-stimulating factor--secreting tumor cell immunotherapy providing therapeutic benefit to mice with established tumors. *Clin Cancer Res*. 2009;15(5):1623–1634.

242. Zhou Q, et al. Blockade of Programmed Death-1 Pathway Rescues the Effector Function of Tumor-Infiltrating T Cells and Enhances the Antitumor Efficacy of Lentivector Immunization. *J Immunol*. 2010;185(9):5082–5092.

243. Wei F, et al. Strength of PD-1 signaling differentially affects T-cell effector functions. *Proceedings of the National Academy of Sciences*. 2013;110(27):E2480–E2489.

244. Shang B, et al. Prognostic value of tumor-infiltrating FoxP3+ regulatory T cells in cancers: a systematic review and meta-analysis. *Sci Rep*. 2015;5(1):15179.

245. Mehdi A, et al. Enhanced Anticancer Effect of a Combination of S-adenosylmethionine (SAM) and Immune Checkpoint Inhibitor (ICPi) in a Syngeneic Mouse Model of Advanced Melanoma. *Front Oncol*. 2020;10:1361.

246. Chen F, et al. TIGIT enhances CD4+ regulatory T-cell response and mediates immune suppression in a murine ovarian cancer model. *Cancer Medicine*. 2020;9(10):3584–3591.

247. Vocanson M, et al. Inducible costimulator (ICOS) is a marker for highly suppressive antigen-specific T cells sharing features of TH17/TH1 and regulatory T cells. *J Allergy Clin Immunol*. 2010;126(2):280–289, 289.e1–7.

248. van Gulijk M, et al. PD-L1 checkpoint blockade promotes regulatory T cell activity that underlies therapy resistance. *Science Immunology*. 2023;8(83):eabn6173.

249. Kitz A, et al. AKT isoforms modulate Th1-like Treg generation and function in human autoimmune disease. *EMBO reports*. 2016;17(8):1169–1183.

250. Ishida Y, et al. Induced expression of PD-1, a novel member of the immunoglobulin gene superfamily, upon programmed cell death. *EMBO J*. 1992;11(11):3887–95.

251. Keir ME, et al. Programmed Death-1 (PD-1):PD-Ligand 1 Interactions Inhibit TCR-Mediated Positive Selection of Thymocytes. *J Immunol*. 2005;175(11):7372–7379.

252. Mizuno R, et al. PD-1 Primarily Targets TCR Signal in the Inhibition of Functional T Cell Activation. *Frontiers in Immunology*. 2019;10. https://www.frontiersin.org/articles/10.3389/fimmu.2019.00630. Accessed September 5, 2023.

253. Probst HC, et al. Resting dendritic cells induce peripheral CD8+ T cell tolerance through PD-1 and CTLA-4. *Nat Immunol*. 2005;6(3):280–286.

254. Pauken KE, et al. The PD-1 Pathway Regulates Development and Function of Memory CD8+ T Cells following Respiratory Viral Infection. *Cell Rep*. 2020;31(13):107827.

255. Keir ME, et al. Tissue expression of PD-L1 mediates peripheral T cell tolerance. *J Exp Med*. 2006;203(4):883–895.

256. Hurrell BP, et al. PD-L2 controls peripherally induced regulatory T cells by maintaining metabolic activity and Foxp3 stability. *Nat Commun*. 2022;13(1):5118.

257. Fanelli G, et al. PD-L1 signaling on human memory CD4+ T cells induces a regulatory phenotype. *PLOS Biology*. 2021;19(4):e3001199.

258. Kelley TW, et al. Helios Is Not a Reliable Marker to Distinguish Thymus-Derived Natural Regulatory T Cells From Induced Regulatory T Cells: Stimulation Conditions Influence Helios Expression. *Blood*. 2011;118(21):2177.

259. Hastings W, Dranoff G, Cao A. Abstract 3210: An in vitro approach to study T cell exhaustion. *Cancer Res*. 2016;76(14 Supplement):3210–3210.

260. Dunsford L, et al. A Human In Vitro T Cell Exhaustion Model for Assessing Immuno-Oncology Therapies. 2020:89–101.

261. Long SA, et al. Defects in IL-2R Signaling Contribute to Diminished Maintenance of FOXP3 Expression in CD4+CD25+ Regulatory T-Cells of Type 1 Diabetic Subjects. *Diabetes*. 2010;59(2):407–415.

262. Tang Q, et al. Central Role of Defective Interleukin-2 Production in the Triggering of Islet Autoimmune Destruction. *Immunity*. 2008;28(5):687–697.

263. Franceschini D, et al. PD-L1 negatively regulates CD4+CD25+Foxp3+ Tregs by limiting STAT-5 phosphorylation in patients chronically infected with HCV. *J Clin Invest*. 2009;119(3):551–564.

264. Asano T, et al. PD-1 modulates regulatory T-cell homeostasis during low-dose interleukin-2 therapy. *Blood*. 2017;129(15):2186–2197.

265. Lowther DE, et al. PD-1 marks dysfunctional regulatory T cells in malignant gliomas. *JCI Insight*. 2019;1(5). https://doi.org/10.1172/jci.insight.85935.

266. Yang B-H, et al. TCF1 and LEF1 Control Treg Competitive Survival and Tfr Development to Prevent Autoimmune Diseases. *Cell Rep*. 2019;27(12):3629-3645.e6.

267. Osman A, et al. TCF-1 controls Treg cell functions that regulate inflammation, CD8+ T cell cytotoxicity and severity of colon cancer. *Nat Immunol*. 2021;22(9):1152–1162.

268. Kim HR, et al. Tumor microenvironment dictates regulatory T cell phenotype: Upregulated immune checkpoints reinforce suppressive function. *J Immunother Cancer*. 2019;7(1):339.

269. Kornete M, et al. KLRG1 expression identifies short-lived Foxp3+ Treg effector cells with functional plasticity in islets of NOD mice. *Autoimmunity*. 2017;50(6):354–362.

270. Cheng G, et al. IL-2 receptor signaling is essential for the development of Klrg1+ terminally differentiated T regulatory cells. *J Immunol*. 2012;189(4):1780–1791.

271. Sojka DK, et al. Early kinetic window of target T cell susceptibility to CD25+ regulatory T cell activity. *J Immunol*. 2005;175(11):7274–7280.

272. Rubtsov YP, et al. Stability of the regulatory T cell lineage in vivo. *Science*. 2010;329(5999):1667–1671.

273. Higashi AY, et al. Direct hematological toxicity and illegitimate chromosomal recombination caused by the systemic activation of CreERT2. *J Immunol*. 2009;182(9):5633–5640.

274. Behjati S, Frank MH. The Effects of Tamoxifen on Immunity. *Curr Med Chem*. 2009;16(24):3076–3080.

275. Bettini ML, et al. Loss of Epigenetic Modification Driven by the Foxp3 Transcription Factor Leads to Regulatory T Cell Insufficiency. *Immunity*. 2012;36(5):717–730.

276. Krueger J, Rudd CE, Taylor A. Glycogen synthase 3 (GSK-3) regulation of PD-1 expression and and its therapeutic implications. *Semin Immunol*. 2019;42:101295.

277. Hettich M, et al. High-Resolution PET Imaging with Therapeutic Antibody-based PD-1/PD-L1 Checkpoint Tracers. *Theranostics*. 2016;6(10):1629–1640.

278. England CG, et al. Preclinical Pharmacokinetics and Biodistribution Studies of 89Zr-Labeled Pembrolizumab. *J Nucl Med*. 2017;58(1):162–168.

279. Zemek RM, et al. Bilateral murine tumor models for characterizing the response to immune checkpoint blockade. *Nat Protoc*. 2020;15(5):1628–1648.

280. Chen IX, et al. A bilateral tumor model identifies transcriptional programs associated with patient response to immune checkpoint blockade. *PNAS*. 2020;117(38):23684–23694.

281. Snell LM, et al. Dynamic CD4+ T cell heterogeneity defines subset-specific suppression and PD-L1-blockade-driven functional restoration in chronic infection. *Nat Immunol*. 2021;22(12):1524–1537.

282. Grotz TE, et al. Evidence of Th2 polarization of the sentinel lymph node (SLN) in melanoma. *Oncoimmunology*. 2015;4(8):e1026504.

283. Kharkevitch DD, et al. Characterization of autologous tumor-specific T-helper 2 cells in tumor-infiltrating lymphocytes from a patient with metastatic melanoma. *Int J Cancer*. 1994;58(3):317–323.

284. Muranski P, et al. Tumor-specific Th17-polarized cells eradicate large established melanoma. *Blood*. 2008;112(2):362–373.

285. Jacenik D, Karagiannidis I, Beswick EJ. Th2 cells inhibit growth of colon and pancreas cancers by promoting anti-tumorigenic responses from macrophages and eosinophils. *Br J Cancer*. 2023;128(2):387–397.

286. Kryczek I, et al. Endogenous IL-17 contributes to reduced tumor growth and metastasis. *Blood*. 2009;114(2):357–359.

287. Eschweiler S, et al. Intratumoral follicular regulatory T cells curtail anti-PD-1 treatment efficacy. *Nat Immunol*. 2021;22(8):1052–1063.

288. Ritvo P-GG, et al. Tfr cells lack IL-2Rα but express decoy IL-1R2 and IL-1Ra and suppress the IL-1–dependent activation of Tfh cells. *Science Immunology*. 2017;2(15):eaan0368.

289. Ghosh N, et al. Autoantibodies in Patients With Immune-Related Adverse Events From Checkpoint Inhibitors: A Systematic Literature Review. *J Clin Rheumatol*. 2022;28(2):e498–e505.

290. Santinon F, et al. Direct AKT activation in tumor-infiltrating lymphocytes markedly increases interferon-γ (IFN-γ) for the regression of tumors resistant to PD-1 checkpoint blockade. *Sci Rep*. 2022;12(1):18509.

291. Taylor A, et al. Glycogen Synthase Kinase 3 Inactivation Drives T-bet-Mediated Downregulation of Co-receptor PD-1 to Enhance CD8+ Cytolytic T Cell Responses. *Immunity*. 2016;44(2):274–286.

292. Zhou T, et al. IL-18BP is a secreted immune checkpoint and barrier to IL-18 immunotherapy. *Nature*. 2020;583(7817):609–614.

293. Carmenate T, et al. Blocking IL-2 Signal In Vivo with an IL-2 Antagonist Reduces Tumor Growth through the Control of Regulatory T Cells. *The Journal of Immunology*. 2018;200(10):3475–3484.

294. Mehdi A, et al. S-adenosylmethionine blocks tumorigenesis and with immune checkpoint inhibitor enhances anti-cancer efficacy against BRAF mutant and wildtype melanomas. *Neoplasia*. 2023;36:100874.

295. Wiedemann GM, et al. Cancer cell-derived IL-1α induces CCL22 and the recruitment of regulatory T cells. *Oncoimmunology*. 2016;5(9):e1175794.

296. Whiteside SK, et al. CCR8 marks highly suppressive Treg cells within tumours but is dispensable for their accumulation and suppressive function. *Immunology*. 2021;163(4):512–520.

297. Kidani Y, et al. CCR8-targeted specific depletion of clonally expanded Treg cells in tumor tissues evokes potent tumor immunity with long-lasting memory. *Proceedings of the National Academy of Sciences*. 2022;119(7):e2114282119.

298. Haruna M, et al. The impact of CCR8+ regulatory T cells on cytotoxic T cell function in human lung cancer. *Sci Rep*. 2022;12(1):5377.

299. Dyck L, et al. Anti-PD-1 inhibits Foxp3+ Treg cell conversion and unleashes intratumoural effector T cells thereby enhancing the efficacy of a cancer vaccine in a mouse model. *Cancer Immunol Immunother*. 2016;65(12):1491–1498.